Stochastic Modelling of Space-Time Rainfall and the Significance of Spatial Data for Flood Runoff Generation

A thesis submitted for the degree of Doctor of Philosophy
of the University of London

by

Marie-Laure Segond

Department of Civil and Environmental Engineering
Imperial College London

March 2006

I hereby certify that this submission is my own work. Any quotation from, or description of, the work of others is acknowledged herein by reference to the sources, whether published or unpublished.

Marie-Laure Segond

Abstract

In the context of flood management, this thesis investigates the relationship between spatial rainfall and runoff production, for a range of scales and catchment types. A methodology for the spatial-temporal rainfall simulation of hourly rainfall is developed and the sensitivity of simulated flood runoff to the representation of observed and simulated spatial rainfall is evaluated. The study is based on 15 years of radar data, 21 raingauges and 12 flow stations from the 1400 km^2 Lee catchment, UK.

A Generalized Linear Model, which can represent spatial and temporal non-stationarities of daily rainfall fields, is combined with a single-site disaggregation model based on Poisson-cluster processes. As a first approach, complete spatial dependence is assumed and a spatially uniform temporal disaggregation scheme is applied. The proposed model preserves standard statistics but has some limitations in the representation of extreme rainfall and the correlation structure. The method can be extended to sites within the modelled region not used in model calibration.

Event-based, semi-distributed rainfall-runoff modelling is undertaken. Alternative rainfall descriptors (raingauge networks of various density, radar data and disaggregated data) are considered and their effects on simulated runoff evaluated as a function of rainfall type, catchment type and catchment scale. An index of spatial variability is defined, based on the difference between the reference rainfall (defined by the full raingauge network) and alternative rainfall descriptors. A modified Nash-Sutcliffe Efficiency criterion measures the performance of the simulated runoff with respect to reference simulated runoff.

Results show a complex picture. The dominant effect is the spatial variability of the rainfall. No clear pattern emerges as a function of catchment scale, or response time, except that the impact of spatial variability is damped at the whole catchment scale. The sensitivity to spatial rainfall is enhanced on urbanised catchments. In conclusion, the thesis provides specific guidance concerning the importance of spatial rainfall for flood estimation.

Acknowledgements

I would like to thank my two supervisors, Prof. Howard Wheater and Dr. Christian Onof for their guidance throughout the three years of my project. I would also like to thank Dr. Richard Chandler and Prof. Valerie Isham for valuable discussions on the rainfall modelling. I am also grateful to Dr. Demetris Lekkas, Dr. Enrica Bellone and Dr. Chi Yang for their technical assistance in the implementation of the rainfall models. I also thank Prof. Russell Mein for answering my many queries from the other hemisphere about the use of the RORB model and Prof. Demetris Koutsoyiannis for his help with the use of HYETOS. I am grateful to Shanmuga-Ratnam Ponnampalam and Mathilde Stoskopf for liaising with the Environment Agency of England and Wales which I would like to acknowledge for providing the Lee catchment dataset. I would also like to thank Wasim Quasem for his contribution to the rainfall-runoff calibration of the Lee catchment.

My thanks go to the third floor members of the EWRE section for their friendship, help and support, in particular to Bethanna Jackson, Barbara Orellana, Hyosang Lee, Simon Mathias and Andrew Frost. I would also like to thank Judith Barritt and Angela Frederick for being great facilitators.

Special thanks go to my friends Sarah Bluhme, Karim Lekadir, Laura Welbon, Sebastian Mueller, Tamara Hale, Natalia Papalouca, Fleur Strasser and David Allgayer and to the members of the London School of Samba for providing me with the fun and the energy that kept me going.

I am extremely grateful to my parents, Bich Lan Nguyen and Jean-Pierre Segond for their trust and continuous support and to my cousin, Florence Mondon for her encouragements, especially in the last stage of my PhD studies.

Finally I would like to acknowledge the financial contribution received from the UK National Environmental Research Council and the UK Department for Environment Food and Rural Affairs under DEFRA project FD2105.

Contents

1 Introduction **18**

1.1 Stochastic Modelling of Space-Time rainfall 18

1.2 The Significance of Spatial Data for Flood Runoff Estimation 19

1.3 Research Aims and Objectives 20

1.4 Thesis Outline 21

2 Literature Review **23**

2.1 Structure of the Review 23

2.2 Urban Catchments 24

2.2.1 Effect of Storm Movement 24

2.2.2 Spatial Rainfall 25

2.2.3 Conclusions 27

2.3 Semi-Arid Regions with Convective Rainfall 27

2.3.1 Small Catchments (< 100 km^2) 28

2.3.2 Medium Size Catchments (100-2000 km^2) 30

2.3.3 Large Catchments (> 2000 km^2) 31

2.3.4 Conclusions 32

2.4 Temperate Climate 32

2.4.1 Small Catchments (< 100 km^2) 33

2.4.2 Medium to Large Catchments (100-2000 km^2) 35

2.4.3 Large Catchments (> 2000 km^2) 43

2.4.4 Conclusions 47

2.5 Conclusions 50

2.5.1 Summary 50

2.5.2 Direction of Research for Modelling of Space-Time Rainfall . . . 52

2.5.3 Direction of Research for Rainfall-Runoff Investigation 53

3 Introduction to the Lee Catchment **55**

3.1 The Lee catchment 55
3.2 Radar Archive 60
3.2.1 Observation of the radar archive 60
3.2.2 Problems Associated with Radar Data 61
3.2.3 Calibration of the Chenies Radar Dataset 62
3.3 Raingauge Records 65
3.4 Flow Data 66

4 Spatial-Temporal Disaggregation of a Daily GLM 70
4.1 Review of the Literature 70
4.2 Methodology 73
4.3 Simulation of Daily Rainfall 73
4.3.1 Treatment of "Trace Values" 76
4.3.2 Occurrence Model 76
4.3.3 Amounts Model 77
4.3.4 Model Checks 81
4.3.5 Simulation 82
4.4 Single-site Disaggregation 87
4.4.1 Fitting of the BLRPM 88
4.4.2 Disaggregation using HYETOS 90
4.4.3 Preliminary Results 93
4.5 Multisite Disaggregation 95
4.6 Testing the Combined Scheme 98
4.6.1 Application of a Single Temporal Profile at All Gauges 98
4.6.2 Effect of Single-Site Disaggregation 98
4.6.3 Effect of GLM Simulations 99
4.6.4 Analysis of Extremes 103
4.7 Discussion 105

5 Rainfall-Runoff Model Calibration 107
5.1 RORB Rainfall-Runoff Model 107
5.2 Modelling Strategy 111
5.2.1 Model Configuration 111
5.2.2 Catchment Subdivisions 112
5.2.3 Event Selection 113
5.2.4 Baseflow Separation 113

5.2.5 Performance Criteria 114
5.2.6 Calibration Strategy 115
5.3 Calibration and Validation 115
5.3.1 Modelling the Individual Subcatchments 116
5.3.2 Modelling the Integrated Lee Catchment 131

6 The Significance of Spatial Data 134
6.1 Measure of Rainfall Variability and Basin Damping 134
6.1.1 Rainfall Estimators 134
6.1.2 Spatial Deviation Index 136
6.1.3 Catchment Response Time 137
6.2 Rural Catchment Results 138
6.2.1 Impact of Spatial Variability of Rainfall 152
6.2.2 Influence of Catchment Response Time 155
6.2.3 Effect of Scale 160
6.2.4 Rainfall Variability, Catchment Characteristics and Model Performance 161
6.2.5 Conclusion 161
6.3 Urban Catchment Results 163
6.3.1 Impact of Spatial Variability of Rainfall 175
6.3.2 Influence of Catchment Response Time and Catchment Scale . . 176
6.3.3 Conclusion 178
6.4 Disaggregation Scheme Results 178
6.4.1 Rural Catchments 178
6.4.2 Urban Catchments 185
6.4.3 Conclusion 186
6.5 Conclusion and Discussion 192

7 Conclusions and Recommendations 194
7.1 Observed Data 194
7.2 Stochastic Modelling of Space-Time Rainfall and Disaggregation 195
7.3 The Significance of Spatial Rainfall Data for Runoff Estimation 196
7.4 Conclusions 198

References 200

A Catchment descriptors 210

B Spatial Extent of Selected Events **212**

C Averaged rainfall time-series **218**

List of Figures

3.1 Map of the Lee catchment (British National Grid Coordinate System) . 56

3.2 Hydrogeological characteristics of the Upper Catchment of the Lee (top map). The lower map shows the drift deposit on top of the hydrogeological properties. 57

3.3 Anomaly map applied to the radar data in 1994. The area is bordered by National Grid Coordinates (km): top left (4240, 2760) and bottom right (5760, 1240). The white areas represent the dubious pixels set to missing values. The location of the Lee catchment is roughly represented by the region enclosed in black. 63

3.4 Daily mean flow characteristics 68

3.5 Autocorrelation function of the streamflow times-series 69

4.1 Schematic of the proposed disaggregation scheme. (1) Simulation of multisite daily rainfall, (2) Single-site disaggregation, (3) Multisite disaggregation 74

4.2 Bubble map showing mean Pearson residuals from fitted occurrence model at each site, prior to incorporation of site effects. Positive and negative mean residuals are represented in blue and white respectively. The diameter on the bubble map is proportional to the mean Pearson residuals. 79

4.3 Bubble map showing mean Pearson residuals from fitted amounts model at each site, prior to incorporation of site effects. Positive and negative mean residuals are represented in blue and white respectively. The diameter on the bubble map is proportional to the mean Pearson residuals. 79

4.4 Bubble map showing mean residuals from fitted occurrence model at each site, after incorporation of site effects. Positive and negative mean residuals are represented in blue and white respectively. The diameter on the bubble map is proportional to the mean Pearson residuals. 80

4.5 Bubble map showing mean Pearson residuals from fitted amounts model at each site, after incorporation of site effects. Positive and negative mean residuals are represented in blue and white respectively. The diameter on the bubble map is proportional to the mean Pearson residuals. 80
4.6 Anscombe residuals from amount models 81
4.7 Mean Pearson residuals from occurrence and amount models 83
4.8 Observed and simulated monthly statistics for site 0160 at daily time-step 84
4.9 Observed frequency distribution of number of wet sites in the Lee catchment, together with distribution simulated by GLMs with a beta-binomial model for spatial dependence in rainfall occurrence. 85
4.10 Pairwise correlation between rain gauges for the Lee catchment. White box-plots are observed daily (top) and hourly (bottom) correlations, Grey box-plots are the results from simulations with observed inter-site Anscombe residual correlations in rainfall amounts. The box-plots represent the median, 25 and 75% quantiles, the whiskers extend to the extreme values 86
4.11 Daily pairwise correlation between rain gauges for the Lee catchment. White are observed and Grey are the results from simulations with constant inter-site Anscombe residual correlation in rainfall amounts. 86
4.12 Schematic of the BLRPM (Adapted from Wheater et al. (2005a)) 87
4.13 Flow diagram of the repetition scheme used in Hyetos, BL stands for Bartlett-Lewis model. (Source: Koutsoyiannis and Onof, 2001) 92
4.14 Impact of the disaggregation scheme on properties of hourly rainfall at the master gauge. In each plot the blue line represents observed properties; the dashed red line represents the theoretical properties from a BLRPM fitted to the data (Expected); and the solid red line represents the properties after applying the HYETOS disaggregation scheme (Hyetos). 94
4.15 Event of 03/02/90 - Applying the observed profile of the master gauge to the satellite gauges 96
4.16 Event of 23/07/96 - Applying the observed profile of the master gauge to the satellite gauges 97
4.17 Observed sub-daily temporal profile of the master gauge applied to observed daily data at a typical site on the catchment 100

4.18 Properties of hourly sequences at site 0160, 1991-2002. Solid lines show the observed hourly properties; dashed lines show the envelopes from 20 disaggregations obtained by applying temporal profiles from the master gauge to all sites in the catchment. The profile were obtained by applying the HYETOS single-site disaggregation technique to the observed daily sequence at the master gauge. 101
4.19 Single-site disaggregation at the master gauge conditioned on simulated daily rainfall from GLMs and sub-daily temporal profile applied at a typical site on the catchment. The plot compares the observed series with the envelope of 20 simulations at a gauge used (Sim 1) and not used (Sim 2) in the calibration of the model. 102
4.20 Gumbel plots of daily (left) and hourly (right) annual maxima. The plots compare the observed series with the envelope generated by 20 simulations at a gauge used (Sim 1) and not used (Sim 2) in the calibration of the combined multisite disaggregation model. 103
4.21 Gumbel plots of daily (left) and hourly (right) annual maxima of the average for all gauges. The circles represent the individual simulations. . 104

5.1 RORB structural diagram of the model (Source: Laurenson and Mein, 1988) 108
5.2 Types of run. (Source: Laurenson and Mein (1988)) 110
5.3 Baseflow separation (Adapted from Chow et al. (1988)) 114
5.4 Subcatchment subdivisions 117
5.5 Calibration (FIT) and Validation (TEST) results for the Upper Lee. . . 122
5.6 Calibration (FIT) and Validation (TEST) results for the Mimram, adapted from Quasem (2004b). 123
5.7 Calibration (FIT) and Validation (TEST) results for the Beane. 124
5.8 Calibration (FIT) and Validation (TEST) results for the Rib. 125
5.9 Calibration (FIT) and Validation (TEST) results for the Rib, adapted from Quasem (2004b). 126
5.10 Calibration (FIT) and Validation (TEST) results for the Stort, adapted from Quasem (2004b). 127
5.11 Calibration (FIT) and Validation (TEST) results for the Middle Lee . . 128
5.12 Variability of the event of 30/07/02 at two sites 132

6.1 Observed, reference and simulated flows at catchment outlets on 11/10/93142
6.2 Observed, reference and simulated flows at catchment outlets on 03/02/94143
6.3 Observed, reference and simulated flows at catchment outlets on 08/01/96144

6.4 Observed, reference and simulated flows at catchment outlets on 16/05/95 145
6.5 Observed, reference and simulated flows at catchment outlets on 30/07/02 146
6.6 Percentage change in peak flow, time to peak and volume in comparison to the reference flow for the event of 11/10/93 147
6.7 Percentage change in peak flow, time to peak and volume in comparison to the reference flow for the event of 03/02/94 148
6.8 Percentage change in peak flow, time to peak and volume in comparison to the reference flow for the event of 08/01/96 149
6.9 Percentage change in peak flow, time to peak and volume in comparison to the reference flow for the event of 16/05/95 150
6.10 Percentage change in peak flow, time to peak and volume in comparison to the reference flow for the event of 30/07/02 151
6.11 Impact of rainfall spatial variability on NSE_{ref}. Influence of rainfall estimators (Top) and type of rainfall events (Bottom). 153
6.12 Impact of rainfall spatial variability on peak flow. Influence of rainfall estimators (Top) and type of rainfall events (Bottom). 154
6.13 Catchment response time versus area 156
6.14 Boxplots of NSE criteria for each subcatchment ranked according to their catchment response time (expressed in hours on the upper axis) 159
6.15 Boxplots of NSE_{ref} criteria for each subcatchment ranked according to their size 160
6.16 Model performance vs rainfall variability highlighting the effect of catchment scale (Top) and catchment response time (Bottom) for SG1 representation 162
6.17 Reference and simulated flow at urban catchment outlets on 11/10/93 . 165
6.18 Reference and simulated flow at urban catchment outlets on 03/02/94 . 166
6.19 Reference and simulated flow at urban catchment outlets on 08/01/96 . 167
6.20 Reference and simulated flow at urban catchment outlets on 16/05/95 . 168
6.21 Reference and simulated flow at urban catchment outlets on 30/07/02 . 169
6.22 Relative change (%) in peak flow, time to peak and volume in comparison to the reference flow for the event of 11/10/93 170
6.23 Relative change (%) in peak flow, time to peak and volume in comparison to the reference flow for the event of 03/02/94 171
6.24 Relative change (%) in peak flow, time to peak and volume in comparison to the reference flow for the event of 08/01/96 172
6.25 Relative change (%) in peak flow, time to peak and volume in comparison to the reference flow for the event of 16/05/95 173

6.26 Relative change (%) in peak flow, time to peak and volume in comparison to the reference flow for the event of 30/07/02 174
6.27 Impact of rainfall spatial variability on NSE_{ref}. Influence of rainfall estimators (Top) and type of rainfall events (Bottom). 175
6.28 Response time of existing and urbanised basins against catchment area . 176
6.29 Model performance for rural and urban catchments ranked according to their catchment characteristic response time 177
6.30 Boxplots of NSE_ref criteria for each urban subcatchment ranked according to catchment scale 177
6.31 Simulated flow using disaggregated rainfall for the event of 11/10/93 (observed daily rainfall at all sites and hourly rainfall at master gauge, simulated hourly rainfall at other sites). 180
6.32 Simulated flow using disaggregated rainfall for the event of 03/02/94 . . 181
6.33 Simulated flow using disaggregated rainfall for the event of 08/01/96 . . 182
6.34 Simulated flow using disaggregated rainfall for the event of 16/05/95 . . 183
6.35 Simulated flow using disaggregated rainfall for the event of 30/07/02 . . 184
6.36 Simulated flow using disaggregated rainfall on urbanised catchments for the event of 11/10/93 187
6.37 Simulated flow using disaggregated rainfall on urbanised catchments for the event of 03/02/94 188
6.38 Simulated flow using disaggregated rainfall on urbanised catchments for the event of 08/01/96 189
6.39 Simulated flow using disaggregated rainfall on urbanised catchments for the event of 16/05/95 190
6.40 Simulated flow using disaggregated rainfall on urbanised catchments for the event of 30/07/02 191

B.1 Radar images for the event of 11th October 1993 213
B.2 Radar images foe the event of 3rd February 1994 214
B.3 Radar images for the event of 8th January 1996 215
B.4 Radar images for the event of 16th May 1995 216
B.5 Radar images for the event of 30th July 2002 217

C.1 Hourly averaged rainfall time-series for the even of 11th October 1993 . 219
C.2 Hourly veraged rainfall time-series for the event of 3rd February 1994 . 220
C.3 Hourly averaged rainfall time-series for the event of 8th January 1996 . 221
C.4 Hourly averaged rainfall time-series for the event of 16th May 1995 . . . 222

C.5 Hourly averaged rainfall time-series for the event of 30th July 2002 . . . 223

List of Tables

3.1 % Distribution of hydrogeological characteristics of the Upper Catchment of the Lee 59
3.2 % Distribution of the main components of drift 59
3.3 Urbanisation 59
3.4 Raingauge records for the Lee catchment 65
3.5 Flow gauging data on the Upper Catchment of the Lee 66

4.1 Covariates used in occurrence model for daily rainfall in the Lee catchment 78
4.2 Covariates used in amounts model for daily rainfall in the Lee catchment 78
4.3 Relationship between model and mechanistic parameters 88
4.4 Constraints imposed on parameters for fitting to data from site 0163 . . 90
4.5 Estimated BLRPM parameters for site 0163 (OF: value of the objective function) 91

5.1 Events used for calibration 113
5.2 Individual subcatchment calibration summary table 118
5.3 Calibrated parameters results 118
5.4 Calibration results of the Upper Lee 129
5.5 Calibration results of the Mimram 129
5.6 Calibration results of the Beane 129
5.7 Calibration results of the Rib 129
5.8 Calibration results of the Ash 130
5.9 Calibration results of the Stort 130
5.10 Calibration results of the Middle Lee 130
5.11 Characteristics of selected events 131
5.12 Runoff coefficient (RC) calibrated for the 5 selected events 132
5.13 Calibration results in terms of NSE_{obs} 133

6.1 SDI (%) values for the five selected events for each (sub)catchment. . . . 136

6.2 SDIR (%) values for Radar, SG7 and SG1 representations for the five selected events for each (sub)catchment. 137
6.3 Average percentage change in peak flow, time to peak and hydrograph volume 140
6.4 NSE_{ref} rural catchments 140
6.5 NSE_{obs} rural catchments 141
6.6 Mean lag time (t_c) for natural catchments 155
6.7 NSE_{ref} for urban catchments 164
6.8 Percentage change of peak flow, time to peak and hydrograph volume . 164
6.9 Mean lag time (t_c) for urban and natural (predominantly rural) catchments 176
6.10 NSE_{ref} for the disaggregation scheme 178
6.11 Summary performance on rural catchments 179
6.12 NSE_{ref} for the disaggregation scheme 185
6.13 Summary performance on urban catchments 185

A.1 Lee Catchment descriptors 211

"Begin at the beginning," the king said "and then go on till you come to the end, then stop".

Lewis Carroll - Alice in Wonderland

Chapter 1

Introduction

Flooding is the most widely distributed of all natural hazards across Europe where floods from rivers, estuaries and the sea threaten many millions of people as well as causing significant economic impacts (FLOODSITE, 2005). For England and Wales, the value of assets at risk of river and coastal flooding was estimated to be £214 billion in 1998 (Burgess et al., 2000). Recent research has focused on the need to improve flood defence, mapping of risk areas, forecasts and warnings for flood mitigation in practice (Rogers, 2005). However in order to address problems associated with flood and risk management, it is desirable to simulate catchment processes over extended periods of time. This thesis aims to develop techniques to provide continuous spatial-temporal rainfall data and to gain further knowledge of catchment behaviour to support integrated flood risk management.

1.1 Stochastic Modelling of Space-Time rainfall

Recent developments in the stochastic modelling of rainfall have been reported in the literature (Wheater et al., 2005a; Foufoula-Georgiou and Krajewski, 1995). One family of models based on Poisson-cluster processes (Cox and Isham, 1980; Rodriguez-Iturbe et al., 1987), represents the main observable features of rainfall processes, such as the clustering of rain cells within a storm, in continuous time using simple stochastic assumptions and a few physically interpretable parameters. Such models are becoming widely used for single site, or areal average, rainfall generation (Onof et al., 2000; Cowpertwait, 1994; Cameron et al., 2000; Faulkner and Wass, 2005).

More generally, for example for distributed hydrological modelling, it is desirable to represent the spatial distribution of rainfall. Radar data are required to represent the full cluster structure of rainfall but their availability, particularly of long records, is currently extremely limited. In addition, the quantitative measurements of precipitation from radar data are less accurate than what can be obtained by raingauges for the

same location and calibration issues remain problematic. This is an impediment for continuous space-time models (Northrop, 1998; Mellor, 1996; De Lannoy et al., 2005) which are not sufficiently developed for immediate application in engineering practice (Wheater et al., 2005b).

Commonly, reasonably long raingauge records are available at daily level, while there are greater limitations on the number of sites and record lengths at the sub-daily scales. However the catchment response time of most basins studied in Europe is of the order of several hours: therefore subdaily rainfall data are more appropriate for runoff estimation. Hence there is a need for simulation methods that can generate spatial subdaily rainfall sequences based on the typical availability of rainfall data. The development of techniques for rainfall disaggregation is currently of considerable appeal due to their ability to provide rainfall data of higher temporal or spatial resolution than a given coarse scale while simultaneously providing a multiple scale preservation of the stochastic structure of rainfall (Koutsoyiannis et al., 2003). One such approach based on downscaling of simulated daily rainfall sequences from a Generalized Linear Model is introduced and evaluated in this thesis. The problem tackled is crucial for modern engineering hydrology, especially the continuous time simulation of floods for design and management purposes.

1.2 The Significance of Spatial Data for Flood Runoff Estimation

A key issue for the application of methods to simulate spatial-temporal rainfall fields as input to rainfall-runoff models is the importance of the spatial structure of rainfall and its representation for flood runoff generation. The literature on the relationship between spatial rainfall and runoff response is extensive yet contrasting. A major review was carried out by Singh (1997). The author concluded that the spatial and temporal variability of rainfall can significantly influence the flood hydrograph and shape, and that the importance varies as a function of catchment rainfall properties. However from this review, no overall conclusion on the importance of spatial rainfall emerges since there is no explicit connection between the papers reviewed. This highlights a lack of clear conclusions in most studies assessing the impact of spatial rainfall on runoff generation and illustrates the complexity of the problem.

The importance of the representation of spatial rainfall on runoff generation can be expected to depend on complex interactions between the type of event, the nature of the catchment and the spatial scale (i.e. catchment area) of the problem. Further, this relationship is usually assessed indirectly via the use of a watershed model that uses the rainfall data in prediction of the hydrological behaviour of the catchment. Those

hydrological models provide a powerful tool to test the sensitivity of the catchment to various rainfall patterns (Grayson and Blöschl, 2000) but their calibration is done at a fixed spatial scale and this introduces uncertainties in relating the rainfall input to the simulated flow (Morin et al., 2001; Koren et al., 1999). In addition, there is no specific guidance to support the use of spatial rainfall data as input to rainfall-runoff models. The terminology used is unclear, the expression 'spatial variability of rainfall' includes investigations on the impact of the variability within a rainfall event and the impact of the variability captured by different representations of rainfall on the river flow and the findings from the literature are often subjective.

Given that there is a lack of current guidance, this thesis explores the importance of spatial rainfall representation for rainfall-runoff modelling as a function of rainfall type, catchment type and catchment scale, with particular reference to humid temperate regions. The results from this investigation are of practical relevance to the design of raingauge and radar networks for hydrological use where the accuracy of flood estimations from rainfall-runoff models is of primary concern. In addition, the thesis provides guidance to the spatial resolution requirements for rainfall at different catchment scales.

1.3 Research Aims and Objectives

The purpose of this thesis is to employ a dataset encompassing information from a dense raingauge network and a weather radar, on the Lee catchment, north of London, UK, to:

- Develop a procedure to obtain subdaily spatial-temporal rainfall by disaggregation.
- Investigate the significance of spatial rainfall properties to estimate the runoff in the context of flood management.

This leads to the following objectives:

- Develop and test a procedure for temporal disaggregation of multisite daily rainfall and include a spatial extension to the current development of stochastic models to obtain multisite sequences of subdaily rainfall.
- Analyse selected radar rainfall events and long-term raingauge data, together with disaggregated observed daily rainfall data, using a semi-distributed rainfall-runoff model for different catchment types and scales.

- Provide guidance to users on the relative importance of spatial rainfall properties and appropriateness of disaggregation method as a function of rainfall type, catchment type and catchment scale.
- Provide recommendations on the spatial resolution requirements for rainfall at different catchment scales, with particular reference to UK conditions.

1.4 Thesis Outline

Chapter 2 presents a review of the significance of spatial data for flood runoff generation based on the international research literature. Particular emphasis is directed at catchments in temperate humid conditions. This chapter provides guidance for a numerical investigation carried out on the Lee catchment.

Chapter 3 describes the Lee catchment, a relatively large catchment in the UK (1400 km^2) which is representative of the characteristics of the Thames basin, and presents the substantial dataset of radar, raingauge and flow data that are used in this investigation.

Chapter 4 develops a methodology for rainfall generation and disaggregation to obtain hourly rainfall at multiple sites. This involves combining two existing models to obtain multisite sequences of daily rainfall and an hourly temporal profile of rainfall at a single site. A simple disaggregation procedure is proposed: the hourly temporal profile is extended in space to downscale the daily rainfall to an hourly time-step. The methodology is tested on 21 raingauges covering a large area of 1400 km^2 and is evaluated with respect to the reproduction of standard statistics and the representation of extreme rainfall.

Calibration of an event-based semi-distributed rainfall-runoff model fitted to 7 individual sub-catchments, and to the catchment as a whole is addressed in Chapter 5. 2 km resolution radar data, records from 16 raingauges and 12 flow stations on the Upper Catchment of the Lee are used in this study.

Results of the rainfall-runoff investigation are presented in Chapter 6. Alternative rainfall estimators based on radar data and subsets of the raingauge network are considered and their effects on simulated runoff are evaluated as a function of rainfall type, catchment type and catchment scale. The impact of the spatial-temporal disaggregation procedure of Chapter 4, conditioned on observed daily rainfall, on runoff is also evaluated.

Finally, a summary of the conclusions is presented in Chapter 7 and future directions of research are discussed.

Chapter 2

Review of the Significance of Spatial Data for Runoff Generation

A review of the literature is presented in this chapter to gain insights into the significance of spatial rainfall for runoff generation for a range of rainfall types, catchment types and catchment scales. A practical objective is to provide recommendations on the spatial resolution of precipitation input needed to model catchments in medium temperature climatic regions. This review also sets the direction of research for the rainfall and rainfall-runoff modelling investigations presented in this thesis.

2.1 Structure of the Review

The sensitivity of the hydrological response to the variability of rainfall is usually the result of a nonlinear interaction between the rainfall and some other component of the system (Over, 1995). When studying the runoff response of a given catchment, the modeller takes into account (a) the storm characteristics, (b) the catchment properties, (c) the effect of scale and (d) the interactions between these three components. Assuming a moderate impact of the model structure, a rainfall-runoff model can be used to test various rainfall representations and the generated streamflow is compared with the observed one. However, the calibration of hydrological models is done at a fixed spatial scale and their use as a tool to determine the impact of spatial rainfall at various scales is therefore questionable (Morin, et al. 2001, Koren et al. 1999). A review of the significance of spatial data for runoff generation for different conditions, focusing on the impact of these three interactions in association with the modelling needs is presented in this Chapter.

On impervious areas, a high proportion of the rain becomes effective and produces runoff whereas on pervious areas, rainfall variations are damped by the integrating reaction of the catchment. The review is structured such that we consider different catchment types ranging from fast to slow flow response. Similarly, the effect of rainfall

type is introduced ranging from localised highly variable convective rainfall to relatively more homogeneous large scale frontal structures. The effect of catchment scale is also included. In order to get a coherent view of the controls, three catchments types are selected.

Fast-responding, usually small, urban catchments are presented in Section 2.2. As a natural extension, the impact of highly spatially variable rainfall on fast-responding natural basins is assessed. To illustrate these conditions, the focus is on semi-arid areas characterised by a dominance of Hortonian overland flow and associated with convectively-dominated rainfall. The findings are presented in Section 2.3 for a range of scale, from small (<100 km^2), medium (100-2000 km^2) to large (>2000 km^2) catchments. The review at this stage does not aim to be comprehensive; articles are selected so that key points are highlighted. A more extensive review for humid temperate regions is undertaken as more complexity is encountered when modelling this type of catchment and because ultimately the aim is to apply the findings to catchments under these climatic conditions. Section 2.4 presents the findings for the dominantly large-scale frontal rainfall in humid temperate climatic regions, as a function of catchment scale, again ranging from small (<100 km^2), medium (100-2000 km^2) to large (>2000 km^2) catchments. The main conclusions for urban, semi-arid and natural basins are presented in Section 2.2.3, 2.3.4 and 2.4.4. Overall conclusions and proposed extensions to future work can be found in Section 2.5.

2.2 Urban Catchments

2.2.1 Effect of Storm Movement

Singh (1997) observed that the effect of storm movement is significant for urban basins. From his review of the literature, he suggested that on an urban catchment a rain storm moving in the direction of flow produces a higher peak than it would if it were moving in the opposite direction. The effect of storm speed on peak discharge is much less for rapidly moving storms than for storms moving at about the same speed as the flow velocity.

Using synthetic urban catchments, represented by a hydrologic, semi-distributed non-linear rainfall-runoff model, Ngirane-Katashaya and Wheater (1985) showed that the hydrograph is sensitive to the velocity and direction of the storm. Different storms were used, designed with uniform intensity in time and space, passing at 30 degree intervals over 3 synthetic catchments of 0.31, 2.5 and 20 km^2. Eight storm speeds in the range 0.156-20.0 ms^{-1} were tested under fast and slow responding catchment con-

ditions. Results were compared with equivalent stationary storms. Peak discharge for a downstream-moving storm was greater than for the corresponding upstream-moving storm over the whole range of storm speeds, and with the exception of the 5 ms^{-1} storm speed, a consistent variation with storm direction was observed. The peak discharge owing to the downstream-moving storm increased initially with increasing storm speed, reached a maximum and then decreased. However, for the upstream-moving storms the peak discharge increased, although at a decreasing rate, throughout the range of storm speeds. Identical patterns were seen for all catchments. However, the variation of magnitude of discharge between different catchment areas was masked by the effect of the response characteristic of the catchment. Discharge rates for the 2.5 km^2 catchment with high response were greater than for the 20 km^2 catchment with low response. The smaller catchments gave similar results, with a maximum increase in peak discharge, in comparison with the one obtained from a uniform rainfall, of 45% and a maximum reduction of 23-24%. For the larger catchments a maximum reduction of 24% was also observed, but the maximum enhancement is slightly less than for the other catchments (41%). For fast storm movement and a rapidly responding catchment, at resonance conditions, the peak discharge downstream was on average 87% greater than upstream. The resonance speed was lower for slow response conditions and for the largest catchment area.

de Lima and Singh (2002) conducted a study for a synthetic impervious plane surface of 100m$\times$1m using a hydraulic model of overland flow, based on the nonlinear kinematic wave. The results for hypothetical storms with varying temporal pattern (uniform, intermediate, advanced and delayed), length, speed (0.5 to 2 ms^{-1}) and direction (upstream and downstream) were compared. They found that peak discharges and hydrograph shapes depend strongly on the storm temporal pattern; two distinct hydrologic responses were observed for storms moving upstream and downstream. Storms moving upstream are normally characterised by hydrographs with early rise, low peak discharge, not so steep rising limb, and long base time. They observed that the sensitivity of runoff to storm patterns decreases at high storm speeds. Finally, when comparing equivalent storms, downstream storm movement presents larger differences in the hydrograph shapes for different rainfall patterns than does upstream movement.

2.2.2 Spatial Rainfall

Aronica and Cannarozzo (2000) developed a conceptual, hydraulic, semi-distributed rainfall-runoff model and assessed the impact on the modelled hydrograph due to changes in the spatial representation of rainfall and in the spatial discretisation of the sub-catchments. The urban, 12.8 ha Parco d'Orleans catchment was used as a

case-study. Four events were selected and recorded by two raingauges. Three rainfall scenarios were tested, a uniform rainfall for each subcatchment based on raingauge 1; a uniform rainfall for each subcatchment based on raingauge 2 and a spatially variable hyetograph based on both raingauges. Then using the spatially variable rainfall as input to the model, the catchment was subdivided into 32, 18, and 10 subareas with a mean subarea of 0.40, 0.71 and 1.28 ha respectively. Results showed no influence on the time to peak but both spatial representation of the rainfall and spatial discretisation of the subcatchments had a significant effect on the outlet hydrograph peak (between 0.3 and 44.5% change depending on the rainfall representation) and volume (0.9-19.4% change), especially for high intensity events.

Berne et al. (2004) provided recommendations on the temporal and spatial resolution of rainfall measurements required for urban hydrological applications, based on a high resolution precipitation data set from the HYDROMET Integrated Radar Experiment 98 (HIRE 98). Rainfall data came from a network of 25 rain gauges and from 2 radar networks covering 6 sub-basins of 38 ha to 105 km^2 around Marseilles, France. The three most intense events during autumn 1998 in terms of rainfall intensity and total rain amount were selected as representative of the Mediterranean precipitation.

The characteristic time of the catchment, taken as the lag time, i.e. the time difference between the centroid of the catchment-averaged rainfall and the centroid of the modelled hydrograph, was calculated for each of the six catchments and plotted versus surface area (in ha). A power law relation between the lag time t_c (min) and surface area A (ha) was established. The required time resolution of rainfall Δt (defined as $t_c/4$) was estimated as a function of the surface area of the catchments according to:

$$\Delta t = 0.75A^{0.3} \tag{2.1}$$

Using geostatistics, a simple relation between the range of the variogram of the spatial rainfall field (r km) and the required time resolution of measurement (Δt min) was fitted (both using raingauges and radar data at 1, 2, 3, 6, 12 min resolutions). Finally, the required space resolution of the rainfall measurement Δr (defined as $r/3$) for urban hydrology in Mediterranean regions was estimated as:

$$\Delta r = 1.5\sqrt{\Delta t} \tag{2.2}$$

They concluded that hydrological applications for urban catchments in the Mediterranean region of the order of 1000 ha require a temporal resolution of about 6 min and a spatial resolution of about 3.7 km. Modelling urban catchments of the order of 100

ha requires a resolution of about 3 min and 2 km.

Jensen and Pedersen (2005) examined the variability in accumulated rainfall within a 500m grid single radar pixel (as part of the Local Area Weather Radar, 15 km south of Arhus, Denmark) using nine high-resolution rain gauges. The spatial variability of rainfall was measured by the coefficient of variation. Results were presented for 7 events over a 65 days period. The mean of the rainfall events varied between 1.2 and 33.8 mm, the coefficient of variation ranged from 13.9 to 80.4%. The magnitude of variation in the accumulated rainfall at the nine points within this small area was found to be high with a variation from the mean ranging from 4 to 200%. This confirms that a high density raingauge network is required for runoff modelling of fast-responding urban catchments.

2.2.3 Conclusions

The studies show that the runoff response on urban catchments is sensitive to storm variability in space and time and is also affected by storm movement. More variability in the runoff hydrograph is introduced when the storm moves in the direction of flow and at low speed. Hydrological modelling requires fine spatial and temporal rainfall resolution. Smaller catchments require a higher resolution (Berne et al., 2004) and are more sensitive to storm movement (Ngirane-Katashaya and Wheater, 1985).

2.3 Semi-Arid Regions with Convective Rainfall

This section concerns semi-arid regions characterised by Hortonian overland flow and affected by convective storm systems; i.e. combining rapid runoff response with high spatial variability of precipitation.

A large number of investigations were carried out on the semi-arid experimental Walnut Gulch basin in Arizona across a range of scales from 4.4 ha to 150 km^2. The summer weather of this region is strongly affected by the North American monsoon, which results in frequent air mass thunderstorms that are highly convective, intense, localised and of short duration. These are complemented by studies in semi-arid areas also subject to convective thunderstorms and conducted in other part of the US and in Israel. An attempt to summarise the main findings is undertaken below.

The last study discussed here was conducted in Mexico City (Arnaud et al., 2002). This is not exactly a semi-arid area, possessing an average annual rainfall between 600 and 1000 mm. However it has pronounced dry and wet seasons associated with heavy

convective rainfall, and the catchment is fast-responding. The findings are therefore presented here to illustrate effects at the large catchment scale.

2.3.1 Small Catchments (< 100 km^2)

Faurès et al. (1995) found that accurately estimating the spatial variability of rainfall in small catchments experiencing convective thunderstorms is of fundamental importance for runoff simulation. The study was conducted on a 4.4 ha catchment as part of the 150 km^2 semi-arid Walnut Gulch experimental basin using a distributed model applied to 8 events. Results show that simulation errors are halved as the number of raingauges is increased from one to five, and that at a small scale of 4.4 ha, at least 4 raingauges are required to model appropriately the runoff.

Lopes (1996) examined the effect of uncertainty in spatial estimates of rainfall in predictions of runoff volume, peak runoff and sediment yield using a distributed, event-based runoff-erosion model on a 6.73 km^2 catchment as part of Walnut Gulch. The best areal rainfall estimate was given by applying Thiessen method based on the 10 gauges available on the catchment and served to calibrate the model. Three storm rainfall events, representative of the localised, convective rainfall in the area were selected. This includes one large event (areal mean of 32.01 mm with a standard deviation of 10.84 mm) and two medium-sized events (areal mean of 24.51 mm with a standard deviation of 8.71 mm, and areal mean of 23.45 mm with a standard deviation of 6.11 mm). Results demonstrated that the density of the raingauge network, the spatial arrangement of individual raingauges, and the spatio-temporal characteristics of storm events had a significant effect on catchment response prediction. The relative error of prediction with reference to the case of 10 rain gauges was computed. Considering the largest storm, when the rain gauge density was decreased (randomly) from 10 to 6 rain gauges, prediction errors of the order of 30% were observed. As the network density was further reduced to 1 rain gauge, prediction errors in runoff volume increased to about 130%. However, errors in areal estimates of rainfall at the catchment scale increased by only 30% when computed from one raingauge in comparison to the 10 gauges case. These results emphasise that the catchment response to rainfall input is nonlinear. Overall it seems that a network density of 5 raingauges ensures good modelling at the 6.7km ^{2} scale.

Morin et al. (2001) used radar data to determine a characteristic temporal scale for the hydrological response of a basin. The response time scale is defined as the time resolution at which the radar data should be aggregated so that the rainfall hyetograph is most similar to the pattern of the measured outlet runoff hydrograph and represents

the integrative properties of the drainage basin in transforming rainfall into runoff. One approach to study this scale is to test the effect of spatial and temporal variability of rainfall and basin properties on the streamflow using a specific rainfall-runoff model. However the authors argue that hydrological models and their parameters are scale-dependent and their use as a tool for determining characteristic scale is therefore questionable. Radar data with spatial resolution of 0.5 to 4 km^2 and a temporal resolution of 5 minutes were used together with discharge data from 4 small basins (10-100 km^2) in Israel. Spatially, the radar rainfall was averaged over the entire basin so that the temporal scale could be studied independently of the spatial scale. The response time scale was objectively identified using a heuristic method based on matching rainfall and runoff peaks and finding the minimum number of unmatched peaks for different time resolutions. They found a similarity between radar rainfall and outlet runoff at a specific temporal scale which was stable over several storms and therefore could be considered as an intrinsic property of the catchment. Relatively short time scales were found when applying the method to arid areas, especially for the urban and arid catchments (15-30 min) while for the rural catchments larger time scale were identified (90-180 min). Hence, the study confirms that arid catchments are fast-responding and this suggests that the runoff response is highly affected by the storm variability.

Ogden and Julien (1993) explored two-dimensional catchment sensitivity to the spatial and temporal variability of rainfall using a physically-based rainfall-runoff model. The rainfall-runoff model was applied to two basins in Idaho and Colorado, covering areas of 32 km^2 and 121 km^2, respectively. Spatially-variable precipitation fields of identical statistics were generated using a rainfall model (Rodriguez-Iturbe and Eagleson, 1987). A total of 50 spatially-variable rainfall fields were applied to each basin using a Monte-Carlo methodology. Defining t_r and t_e as rainfall duration and time to equilibrium, respectively, they found that spatial variability dominates at large scale when $t_r < t_e$, while the temporal variability dominates at small scales when $t_r > t_e$.

Ogden and Julien (1994) examined the sensitivity of a physically-based rainfall-runoff model to the spatial resolution of radar rainfall input data with consideration of length scales. Based on a 2 hour convective rainfall event recorded by the NEXRAD radar, a set of 50 and 40 independent rainfall realisations at 1, 2, 3, 4, 6, 8 km resolution were analysed on two semi-arid basins of 32 and 121 km^2 (model grid size of 125 and 200 m respectively). A rainfall realisation is obtained by taking a subset of the pixels corresponding to the location of the basin, which is artificially moved within the large radar domain of 6400 km^2. The results from simulations with the finest rainfall resolution (1km) were the best available outflow calculations and were used as reference outflow

hydrographs. They defined two parameters:

$$\frac{L_R}{L_S} \tag{2.3}$$

which is an indication of "storm smearing".

$$\frac{L_R}{L_W} \tag{2.4}$$

which is an indication of "catchment smearing".

L_S is the correlation length of the rainfall, L_R the grid size of the rainfall data, L_W the characteristic length of the catchment taken as the square root of the area. They considered the standard deviation of peak discharge, runoff volume and rainfall volume versus the two parameters defined above. Results from simulations without infiltration showed storm smearing occurring as $L_R \rightarrow L_S$. Catchment smearing caused more significant deviations from simulations using the finest resolution data when L_R/L_W exceeded 0.4. The deviations are larger in the case of the smallest basin. The first set of simulations assumed impervious basins (no infiltration) and every storm produced runoff. In the case of pervious basins, for dry conditions, not all rainfall subsets generated runoff (11 and 18 events out of 40 and 50 storms for the 32 and 121 km^2 basins, respectively). Results with infiltration revealed that excess rainfall volumes decrease with increasing L_R/L_W, i.e. due solely to rainfall data aggregation.

2.3.2 Medium Size Catchments (100-2000 km^2)

Michaud and Sorooshian (1994) examined the effect of rainfall sampling errors on simulation of flash floods using a distributed model on the 150 km^2 Walnut Gulch basin. They studied 10 storms triggering large runoff events, using rainfall fields based on kriging interpolation from 58 raingauges, and a subset of 8 raingauges. Rainfall-sampling errors and their effects on hydrologic simulations were inferred by comparing the peak runoff from the eight-gauge and areal cases (defined below) to the peak runoff from the 58-gauge case. Total errors represent the sum of errors associated with rainfall-sampling and errors between the peak runoff from the 58-gauge case to observed peak runoff. Errors are expressed as percentage bias of the mean observed peak on average for the 10 storms.

Results showed that inadequate raingauge density (1 gauge per 20 km^2 compared to 1 gauge per 2.5 km^2) gave total errors in simulated peak of 13.7% of the observed peak flow. Rainfall sampling errors accounted for approximately -10% of errors between ob-

served and simulated peaks. Degradation of the rainfall field from the 58 raingauges and spatial averaging over a 4-km grid resulted in total errors of -24% of the observed peak. Rainfall sampling errors accounted for -47% of errors between observed and simulated peaks. The 4-km pixels were too coarse to preserve the small cells of high rainfall intensity. Although the catchment average rainfall volume was preserved, the distribution of rainfall intensity was modified in a manner that reduced Hortonian runoff. Decreasing the temporal resolution from 2 min to 1 hour also resulted in a marked reduction of simulated runoff. The authors concluded that at least 2-km spatial resolution is required for 50-500 km^2 semi-arid catchments subjected to convective thunderstorms.

2.3.3 Large Catchments (> 2000 km^2)

Arnaud et al. (2002) studied the sensitivity of distributed hydrological models to different patterns that represent the spatial distribution of rainfall: spatially averaged (i.e. a synthetic hyetograph obtained by a weighted average of the different observations) or rainfall field (represented by the different hyetographs observed in space). The rainfall data came from a network of 44 rain gauges that covers about 2000 km^2 around Mexico City. The 50 most significant events were selected for the period 1988-1998 and events were classified as extreme or more frequent events. The mean duration was approximately 10 hours and the maximum point depth reached 170 mm for a 126-hour storm with cumulative basin precipitation of 81 mm. Each event was separated by at least 1 hour dry at all stations. Four fictitious basins ranging from 20 to 1500 km^2 were defined. The tests were undertaken for a distributed model allowing three different rainfall-runoff processes and different basin size to avoid conclusions based on runoff-generation mechanisms and catchment size. For the 50 events, the relative difference between the empirical distribution of the peak flow and runoff volumes was calculated according to the two patterns of rainfall input (uniform basin rainfall and non uniform rainfall field).

They concluded that runoff volumes and peak flows can vary considerably between spatially uniform and spatially distributed rainfall patterns. Differences in flows range from 10 to 80% depending on the type of runoff production model used, the size of the basin and the return period of the event. The differences were generally moderate for extreme events (10 to 30%) and more significant for more frequent events (20 to 80%). A possible explanation is that highest flows are generally obtained for rain events that affect the whole basin and have lower spatial heterogeneity of cumulative rainfall. This seems to be a particular feature of Mexico City. Higher relative errors were observed for the largest basins in comparison to the smallest ones, which suggest that the runoff sensitivity to rainfall spatial variability increases with catchment scale,

again a particular feature of Mexico City.

2.3.4 Conclusions

The studies conducted in semi-arid environments associated with localised convective rainstorms confirm the importance of spatial rainfall for runoff generation. Studies conducted on the Walnut Gulch basin in Arizona across a range of catchment size reveal that spatial rainfall is important at all scales and the importance increases as the scale decreases. This is also confirmed by Ogden and Julien (1994) who observe larger deviations due to rainfall aggregation in the case of the smallest basin. It seems that the basin response is more sensitive to larger events.

Based on the studies reviewed, it is concluded that a density of 4 raingauges is required to model adequately a 4.4 ha catchment (Faurès et al., 1995), at least 5 raingauges are necessary at the 6.7 km^2 scale (Lopes, 1996). Michaud and Sorooshian (1994) use rainfall input from 58 raingauges at the 150 km^2 scale and suggest 2 km resolution to model 50-500 km^2 catchments (Michaud and Sorooshian, 1994). Ogden and Julien (1994) recommend a spatial resolution of less than 0.4 times the square root of the basin area (i.e., 1 km resolution for a 10 km^2 basin, 4 km resolution for a 100 km^2 basin).

Conversely, in the study conducted at the large catchment scale in Mexico City, higher differences in the flow were observed for more frequent events compared to extreme events. Higher relative errors were observed for the largest basins in comparison to the smallest ones, which suggest that the sensitivity of the runoff on spatial variability of rainfall increases with catchment size. This seems to be a particular feature of Mexico City and may highlight the complexity introduced when mixed weather and catchment conditions are considered.

2.4 Temperate Climate

In the temperate mid-latitudes, frontal low-pressure systems dominate in winter, and rainfall tends to be higher. During the summer, the subtropical high-pressure anticyclones expand to influence the weather patterns. Consequently, precipitation is somewhat lower, and most that falls is convective in nature, arising from the uplift of air during elevated daytime heating and the generation of heavy short-lived showers and thunderstoms (EAE, 2005).

2.4.1 Small Catchments (< 100 km^2)

Shah et al. (1996a) developed a stochastic rainfall field model and studied the effects of spatial variability of rainfall on catchment response on the 10.5 km^2 Upper Wye catchment, UK, using the Systme Hydrologique Europeen (SHE), a physically based, distributed rainfall-runoff model. Conditioned on ten storms from three raingauges, the rainfall model, which uses the Turning Bands Method and a fractionally differenced line process, generates Gaussian random fields with a specified space-time correlation structure. The model has 7 parameters, the rate of decay of the space-time correlation function of the Gaussian field which is assumed isotropic and defined by the lag-one correlation space-time coefficient, the mean and standard deviation of the transformed Gaussian field, two parameters controlling the duration and the spread of the storm, and two components for the storm velocity (see details Shah et al. (1996b)).

Antecedent soil moisture conditions are described by the depth of the phreatic surface component of the rainfall-runoff model. Provided that there is at least one gauge available, results revealed that under "wet" conditions, good prediction of runoff could be obtained with a spatially averaged rainfall input. However, for "dry" conditions, the errors were considerably higher if spatially averaged rainfall is used. In comparison to the reference flow (driven by the full rainfall field, i.e. an equivalent of 169 raingauges), the mean absolute error in peak flow and volume were of the order of 6 and 3% for wet conditions and 14 and 8% for dry conditions. They related this to the interaction between the spatial variability in rainfall and the spatial distribution of soil moisture. Results also showed the nonlinearity of the runoff response with higher errors in runoff compared to errors in rainfall depth. By decreasing the lag-one space-time correlation parameter of the model (i.e. assuming more spatially variable rainfall regime or larger catchment areas with the same number of raingauges), they observed that the errors increase with decreasing correlation and are again larger for dry conditions. They also found that larger errors in runoff prediction arise when applying a lumped model to the catchment compared to averaging the rainfall using distributed modelling.

Corral et al. (2000) presented a semi-distributed version of TOPMODEL and applied it to Ample, a mediterranean 48 km^2 basin in France. 30 min radar rainfall estimates averaged on 1 km^2 grid served as input to the hydrological model at the same spatial resolution. Based on a set of 13 events, they compared the performance of the semi-distributed model with two lumped models: SCS and the original TOPMODEL run using spatially uniform rainfall. They found that the semi-distributed model, which is able to incorporate the spatial variability of rainfall, outperformed the lumped models in terms of reproduction of the peak flow, recession curve and NSE. The NSE for the

semi-distributed model was 0.90 in optimisation mode compared to 0.80 for the lumped models, in validation mode a NSE of 0.72 was compared to 0.55. However it is not possible to distinguish the effect of spatial rainfall from the effect of the model discretisation.

Obled et al. (1994) used a semi-distributed rainfall-runoff model on a 71 km^2 rural catchment in the south-east of France containing a network of 21 rain gauges. They studied the sensitivity of this hydrological model to spatial rainfall patterns. Three spatial representations of rainfall were tested: spatially uniform rainfall from a network of 5 (PU5) and 21 (PU21) rain gauges, and a spatially variable rainfall field based on the 21 (PS21) rain gauges, distributed over subcatchment areas of 6-8 km^2. Calibration and validation of the model was undertaken, based on a set of 19 events, for each rainfall representation. The NSE increased from 0.76 for PU5 to 0.80 for PU21, suggesting that a better estimate of the volume of rainfall (a difference of 3% was observed) improves the model performance.

The results also showed that the optimised parameters vary quite strongly according to the type of uniform rainfall used. However when using input from the spatially variable rainfall PS21, the NSE was 0.78 compared to 0.76 with PU5 and shows lower performance than PU21. This is because the main peaks were better represented than with PU5 but the model also responded to a rainfall event that the catchment ignored or dampened. This evidenced the sensitivity of the particular rainfall-runoff model rather than the sensitivity of the basin to spatial rainfall. These secondary peaks were not dampened enough by the isochrone routing of the model to fit the observed discharge. With the isochrone assumption, the routing of the runoff generated over contributing areas has been ignored and all the surface water is immediately available to the closest channel reach.

An extension of the model was implemented to allow for a specific hillslope unit hydrograph. It preserved the isochrone concept but allowed some spreading in time by assuming that a transfer function, working at the land-unit scale, routes the water to the river. This was defined in terms of a parameterised Gamma function to route the surface water down to the channel only. Compared to the previous case, the NSE increased from 0.78 to 0.82. Hence the results with distributed information remain similar to the case of PU21. Further minor improvement from PU5 to PU21 was observed, which suggests that a spatial average of 5 raingauges is appropriate to model this 71km^2 catchment.

They concluded that the spatial variability of rainfall, although important, was not

sufficiently organised in time and space to overcome the effects of smoothing and dampening of the catchment. The authors reasoned that the dampening behaviour may be due to the mechanism of runoff generation. In this case, it is of the Dunne type where most of the water infiltrates and local variations in input are smoothed as the water is stored and delayed within the soil. They suggest that the catchment is characterised by small contributing areas which makes the catchment less sensitive to rainfall patterns. Woods and Sivapalan (1999) reached similar conclusions in a study conducted in New-Zealand (see following Section).

2.4.2 Medium to Large Catchments (100-2000 km^2)

This section concerns the impact of spatial rainfall on medium to large catchments of the order of 100-2000 km^2. In comparison to the previous section, more studies have benefited from the use of radar data. A number of errors can be observed in radar measurements and long records of continuous data are still lacking. Nevertheless, provided that a simple correction is applied, radar data represent an important source of information, which allows the continuous spatial distribution to be studied. An example of this is presented below.

Borga (2002) analysed the impact of errors in radar rainfall estimates on rainfall-runoff modelling using a lumped, continuous simulation, model on the 135 km^2 Brue catchment in Southwest England. Adjustment of the radar estimates include correction for range-related bias due to vertical profile of reflectivity (VPR) (Cluckie et al., 2000); orographic enhancement of precipitation (Kitchen et al., 1994); anomalous propagation; uncertainty in Z-R calibration (Illingworth et al., 2000); mean field bias adjustment against raingauges (Borga et al., 2002).

5 minute radar rainfall estimates were available at 4 elevation scans, together with a high density network of 49 raingauges, for a 2.5 year period. Spatially-uniform areal rainfall, given by an average of the raingauges, was used for the calibration (Dec 97 -July 99) and validation (Nov 93 - Aug 96) of the model. Good agreement in terms of Mean Relative Error (MRE) and NSE between the calibration (0.043 and 0.82 for MRE and NSE, respectively) and validation (0.054 and 0.83) period were obtained. Next, the model was run over the validation period using both unadjusted and adjusted radar rainfall estimates, and estimates from the four elevation scans.

Results showed that adjustment of the radar rainfall significantly improved the model performance. In comparison to the reference flow driven by the raingauges, the NSE for the adjusted radar data ranged from 0.92 at 0.5° scan (0.82 for unadjusted data)

to 0.84 at 2.5° scan (0.58 for unadjusted data). In comparison to the observed flow, the NSE ranged from 0.75 at 0.5° (0.69 for unadjusted data, 0.83 for the raingauge-driven simulation) to 0.5 at the higher elevation scan of 2.5°. The low value of NSE at the higher scan may be attributed to an effect of residual bright band remaining after VPR adjustment. It may also be expected that the use of radar rainfall estimates for calibration purposes could force model parameters to compensate for the biases and sampling characteristics of radar areal precipitation estimates, thus leading to different simulation results during validation.

Bell and Moore (2000) investigated the sensitivity of catchment runoff models, lumped and distributed, to rainfall at a variety of spatial scales using data from a dense raingauge network and weather radar on the 135 km^2 Brue catchment. 49 raingauges were available, together with radar data at 2 and 5 km grid resolution. The sensitivity of the catchment runoff models was evaluated for two representative periods of stratiform and convective rainfall events that triggered peak flows of about 15 m^3s^{-1} and 10 m^3s^{-1}, respectively.

The distributed model was calibrated twice, using catchment average rainfall from the raingauges and radar data. To determine the effect of rainfall variability on flow response at the catchment scale, rainfall estimates for each of the 28, 2 km pixel containing raingauges were used as alternative inputs to rainfall-runoff models to obtain an ensemble of 28 hydrographs. It was found that the distributed model is sensitive to the location within the catchment of the grid-square raingauge data. As expected, the greater spatial variability in rainfall for the predominantly convective period is reflected in the wide variation in modelled hydrographs. The generated peak flow ranged from 1 to 45 m^3s^{-1} for the convective event compared to 7-22 m^3s^{-1} for stratiform rainfall.

Sensitivity to rainfall (both radar and raingauge data) and distributed model resolution was explored at 2, 5 and 10 km grid resolution. Model recalibration returned the model performance to that obtained from catchment average rainfall data. Best performance was obtained using a lower resolution of rainfall data and model (5 and 10 km than for the 2 km scale). The improvement in performance of the distributed model over the lumped one was marginal in case of the stratiform event (NSE of 0.922 compared to 0.911) but enhanced for the convective event (NSE of 0.953 compared to 0.909).

Using raingauge data, sensitivity to rainfall resolutions at 2, 4, 6, 8, 10 and 16 km was explored with the 2 km grid distributed model. Results show that provided the

model is recalibrated for each rainfall resolution, equivalent performance is observed for the convective event. However if the model is not recalibrated, the simulation accuracy decreases with the rainfall resolution and drops to 0.4 above 10 km. For the more spatially homogeneous stratiform event, there is little change in simulation accuracy with resolution of rainfall data.

In conclusion, the runoff response is sensitive to the type of rainfall event and the particular model used. The modelling of the Brue catchment benefits from using a distributed approach over a lumped one. Results show that recalibration of the model parameters compensate for bias in rainfall. Using a model discretisation of 2 km, the adequate modelling of the runoff response during convective events requires a rainfall resolution of 2 km.

Chaubey et al. (1999) used a distributed-model on a 148 km^2 catchment in Oklahoma and a network of 17 rain gauges, to simulate surface runoff, sediment nutrients and pesticide transport. The model was calibrated on five events using rainfall input obtained from the Thiessen Polygon method. The four calibrated model parameters served as reference. Applying one rain gauge at a time uniformly across the catchment, results showed that a large uncertainty in model parameters is introduced due to the spatial variability of rainfall. The smallest parameter uncertainty resulted from the rainfall that was the most homogeneous in nature. The correlation analysis between the parameters and the input rainfall revealed that for a particular event, the model parameters are highly correlated. One question that still needs to be answered is the number of raingauges required to estimate appropriately the model parameters.

In the context of real time flood forecasting, Maskey et al. (2004) designed a method based on fuzzy set theory combined with a genetic algorithm to propagate and assess rainfall uncertainty in rainfall-runoff modelling. It used the temporal disaggregation of the precipitation over a period into sub-periods and allowed the uncertainty in both the temporal and spatial distributions of the rainfall to be accounted for. The method consisted of division of the temporal period over which the accumulated rainfall is known into a fixed number of sub-periods and random disaggregation of the accumulated sum over sub-periods. The disaggregated rainfall sums up to the accumulated rainfall. The disaggregated precipitation signal is then used as input to the rainfall-runoff routing model. Further details and implementation of the methodology can be found in Maskey et al. (2004). The results, based on 60 hours forecast on a 1744 km^2 catchment in Poland with 9 sub-catchments ranging in size from 64 to 280 km^2, showed that the output uncertainty due to the uncertain temporal distribution of precipitation

dominates the uncertainty due to the magnitude of the precipitation (a maximum difference of 80% in forecast discharge is observed when introducing temporal uncertainty). Marginal differences were observed when varying the temporal pattern over sub-basins, which accounts for the spatial variations of the rainfall field, and when disaggregating into 6 sub-periods instead of 3.

Woods and Sivapalan (1999) proposed an analytical method to identify the importance of different components of the hydrological cycle during storm events in a humid temperate catchment of 420 km^2 in New Zealand. In particular, the relative importance of the spatial or temporal distribution of rainfall, and the interaction between the rainfall variability and the flow routing can be assessed. For a single event, they assume that the space-time variability in rainfall and runoff generation can be separated into independent multiplicative time and space components, according to:

$$P(x, y, t) = P_{x,y}(t) P_t(x, y) \tag{2.5}$$

where $P(x, y, t)$ is the space-time rainfall field, $P_{x,y}(t)$ is the time-series of spatially averaged rainfall rates for the study-area delimited by x and y, $P_t(x, y)$ is the dimensionless rainfall space pattern for the duration of the storm event. A similar expression for the runoff generation function is assumed.

Implicitly, in Equation 2.5, a spatially-uniform temporal profile conditioned on storm-averaged totals at each pixel is assumed, which may be a suitable approximation in practice (see Chapter 4) for predominantly frontal rainfall in humid areas. However this scheme may not be appropriate for rapidly moving storms, more spatially variable (and intermittent) rainfall in summer or for larger catchments.

The model of rainfall, runoff generation, and routing can be summarised as follows: rain falls on the catchment and either becomes rainfall excess through the action of a runoff generation process or is stored. Rainfall excess is routed to the base of hillslopes (where it enters the channel) via a time-invariant hillslope unit hydrograph, which is assumed to be the same throughout the catchment. Hillslope discharges are then routed through the channel network to a river basin outlet (where they become catchment runoff) by a time-invariant channel network unit hydrograph with constant velocity. Only the runoff generation mechanism in this theory can provide a nonlinear hydrological response. This simple model has the advantage of accounting for the main interactions between rainfall and catchment properties. Apart from the storm movement, storm variability is directly incorporated. Catchment properties are included in the mechanism of runoff generation, the hillslope routing and the channel routing.

The spatial organisation of rainfall is taken into account via the distribution of rainfall-excess with flow distance to the outlet. The effect of scale can be studied by applying the methodology at various scales.

To treat these interactions analytically, two sets of equations are derived and the method is illustrated on a 10-hour storm using hourly radar rainfall data. The first set deals with understanding controls on rainfall excess and runoff for a single catchment. For instance, expressions for the mean and variance of runoff duration can be derived. For this event, the mean catchment runoff time (i.e. a characteristic time of the catchment defined here as the lag time between the start of the rainfall event and the centroid of the runoff hydrograph) is dominated by the storm duration and the flow distance, whereas the storm duration, temporal variability and flow distance govern the variance of runoff duration. In both cases spatial variability has little importance. The authors argue that the extreme values of rainfall excess occur at flow distances representing only a small fraction of the catchment area.

The second set of equations shows the effects of between-catchment variability on variability between hydrographs. To test these expressions, sub-catchments were created by applying thresholds of 0.0625, 0.2, 0.625, 2, 6.25, 20 and 62.5 km^2. Results show that for small catchments, the mean runoff time is dominated by the storm duration, and for larger catchments the mean travel time in the network gradually becomes more important. The variance of runoff time is dominated by the duration of the rain event and the temporal variability of rainfall excess; for larger catchments the variability of network travel time exerts greater influence. Considering variability among catchments of similar size, results suggest, for both the mean and variance of runoff time, that differences in the temporal spread of rainfall excess dominate between-catchment variability for small catchments, and differences in the distribution of flow distance become more important. Although the example is purely illustrative, it seems that the apparently substantial spatial variations in rainfall fail to exert any significant influence on the timing of catchment response. For this event, at each flow distance, there is a wide range of rainfall depths so the distance-averaged rainfall excess is relatively uniform (see also Naden (1992); Obled et al. (1994)).

Carpenter et al. (2001) analysed the sensitivity of a distributed hydrologic model to change in parameter and radar rainfall input. Rainfall estimates came from the NEXRAD radar (4 km^2) and were applied to 4 basins ranging in size from 285 to 2483 km^2 in Oklahoma and Arkansas. Mean areal precipitation over 80 km^2 was used as input to the rainfall-runoff model for a set of 13 events. They allowed for a 50% change

in precipitation and model parameters. Results show that the relative variability in flow increases as basin size decreases and the authors conclude that the sensitivity of flow statistics to parameters and rainfall-input is scale-dependent. For the larger sub-catchments (>800 km^2), the 5-95% uncertainty range in simulated flow is between 10-15% of the median of simulated flows for a 50% radar rainfall error magnitude.

When independent parametric and radar rainfall uncertainties are combined, the flow uncertainties remain in the range of 25-40% of median flow for the larger basins. Increasing the scale of model spatial discretisation from 80 to 160 km^2 increases the range to 38-100% of median flow, while the median flow itself varied substantially. The analyses show that in 60% of the events examined, the spatially lumped model response driven by raingauge data was outside the 5-95% uncertainty boundaries of the flow simulated by the spatially-distributed model indicating that a distributed approach is preferred in this case. In conclusion, the modelling of the runoff response benefits from a distributed approach even though the sensitivity of flow statistics to parameters and rainfall-input is scale-dependent. It seems that for basins larger than 800 km^2, a mean areal rainfall over 80 km^2 (i.e. 9 km grid) is adequate. For the smallest basin of 280 km^2, larger variability in flow is observed when uncertainties in the rainfall and in the parameters are introduced.

In the USA, the Distributed Model Intercomparison Project (DMIP) was defined as a general comparison between 12 distributed rainfall-runoff models with reference to the Sacramento Soil Moisture Accounting Model (SAC-SMA), a lumped model used for operational river forecasting. Three main objectives were defined. First, to assess the benefit of using distributed modelling in an operational forecasting environment. Second, to investigate the dominant form of rainfall spatial variability and to refine the understanding of the effect of rainfall spatial variability on simulated basin outlet hydrograph; and finally, to evaluate the performance of using distributed model to produce hydrologic simulations at interior points (Smith et al., 2003).

7 years of hourly, 4 km resolution data from the Next Generation Radar (NEXRAD) were made available to each participant. The study was conducted on one small basin of 65 km^2 and 7 medium to large basins ranging in size from 285 km^2 to 2485 km^2 in Oklahoma, Arkansas and Missouri. Comparison from DMIP simulations to observed streamflow and to simulation from the SAC-SMA model was based on 12 statistics (see Appendix A (Smith et al., 2003)). These include measures of relative improvement to evaluate the gain in simulation accuracy realised by using distributed versus lumped models and calibrated versus uncalibrated models. Uncalibrated models were

derived with parameters that were estimated without the benefit of using the available discharge time-series. For statistical analysis, 16 to 24 events per basin were selected. Model performance was studied across a range of event sizes: all largest events, several moderately sized storms and few small storms.

Results (Reed et al., 2004) showed improvement in average model performance after calibration for distributed modelling. Although for the majority of catchment configurations, the lumped model performed better than distributed models, some distributed models showed comparable results to lumped models in many basins, and clear improvements in one or more basins. Noteworthy improvements in predicting flood peaks were demonstrated in a basin distinguishable from other basins studied in its shape, orientation, and soil characteristics. Greater uncertainties in modelling the smallest basin were observed. Two articles from the DMIP project are introduced below.

Smith et al. (2004) observed that catchments characterised by marked spatial variability in precipitation, and less of a filtering effect of the rainfall input signal, present improved outlet simulations from distributed versus lumped models. Both a lumped and distributed model were used on three catchments in Oklahoma: Eldon (795 km^2), Blue (1233 km^2) and Watts (1645 km^2). They defined two indices to measure the spatial variability of rainfall for specific events. The locational index I_L describes the variability of rainfall in comparison with channel flow distance and investigates the spatial organisation of rainfall (i.e. where the heavy rainfall lies in the basin), the general variability index I_σ quantifies the intrastorm variability (including terms for the standard deviation of the hourly gridded radar rainfall estimate covering the entire basin). These indexes, in particular I_L , express similar concepts to those developed by Woods and Sivapalan.

An index of outflow hydrograph variability is defined in terms of filtering performed on the input signal. They seek the use of wavelet transforms to derive a composite measure of rainfall signal dampening for an event and used the Mexican Hat wavelet to analyse the hourly streamflow. Consequently, an index R_d of outlet hydrograph variability in terms of the amount of filtering or dampening on the input rainfall signal was defined. Next, an analysis to assess the benefit of using distributed modelling was carried out by plotting the modified correlation coefficient R_{mod} statistics (correlation coefficient between the simulated and observed flow time-series weighted by the standard deviations of the simulated and observed hydrographs) against I_σ and I_L .

Results show that for the Blue basin, the distributed model on average provides im-

provements over the entire range of I_σ values (R_{mod} in [0-0.4]). The distributed model shows more gains as the I_L statistic varies from a value of 1 in both directions. The rainfall for the Blue is the most spatially variable with I_L in the range [0.5-13]. These results suggest that the spatial variability of rainfall is large enough so that distributed modelling is necessary to improve the results. Besides, the Blue basin is characterised by low levels of filtering of the input signal with a narrow range of dampening ratio R_d in [2-25] (compared to [2-47] for the Watts). The results show that distributed modelling presents improvement for about half of the events for Eldon and only marginal improvement for Watts. Overall, distributed modelling does not provide improvements for the most dampened events. These events have I_L value around 1.1 and I_σ values in the range 3-5, indicating that the distance-averaged rainfall and the rainfall itself are fairly uniform. In this case, a lumped model performs well.

In conclusion, this article proposes indices which give inferences about whether spatial variability of rainfall overcomes the filtering of the basin so that distributed modelling is required. Knowledge of spatial rainfall is important when (a) the rainfall is variable, (b) the catchment is responsive and (c) the distance-averaged rainfall excess is also relatively variable. This approach is analogous to the analytical framework proposed by Woods and Sivapalan (1999), in which the relative importance of the spatial and temporal distribution of rainfall, and the interaction between the rainfall variability and the flow routing can be assessed. It would be interesting to apply the methodology of Woods and Sivapalan (1999) and check whether the space-time covariance between rainfall and runoff generation is negligible in the Watts basin and significant in the Blue basin.

Ajami et al. (2004) compared lumped and semi-distributed versions of the SAC-SMA model based on NEXRAD radar data, also for the 1645 km^2 Watts basin in Arkansas. For the semi-distributed model, they developed a multi-step automatic calibration scheme using the Shuffled Complex Evolution optimization algorithm (Duan et al., 1992) for model calibration and use rainfall averaging over 9 sub-basins between 20 and 500 km^2. For this homogeneous basin, analysis of the overall performance at the outlet showed that there is no improvement when moving from the manually calibrated lumped model (DMIP reference) to a semi-distributed structure. NSE is 0.77 and 0.91 for the reference lumped model in calibration and validation, respectively, compared to 0.68 and 0.78 for the semi-distributed model. A closer inspection indicates a better performance for the distributed model during specific periods, especially during the summer and early autumn, when the basin response is dominated by baseflow and also provides better simulations for high flows. In terms of rainfall spatial variability, this

suggests that knowledge of spatial rainfall during convective events in summer and extreme events is required in order to improve the model performance. Also this indicates that the usual measures of efficiency (such as NSE), while giving a general indication of the model performance, may not be able to capture the details of the fit.

Next the results were compared for three model calibration strategies defined as follows: lumped, semi-lumped and semi-distributed. The calibration results showed that moving from a lumped calibration strategy to a semi-distributed approach while keeping the model parameters constant over each sub-catchment (semi-lumped), improved the simulation results. However, varying the parameters between sub-basins (semi-distributed) did not further improve the simulations results, either at the outlet or at an interior point. Hence when a semi-distributed model structure is adopted, information of spatial rainfall (averaged over each sub-basin) improves the model performance.

2.4.3 Large Catchments (> 2000 km^2)

Andréassian et al. (2001) analysed the link between the performance of a rainfall-runoff model and the representativeness of the areal rainfall estimate used to run the model. To this end, they defined two indexes to compare the rainfall estimates given by different raingauge combinations to the reference rainfall (defined below). The GORE index compares the sum of squared errors in the rainfall estimate to the temporal variance of the reference areal precipitation. The BALANCE index assesses the quality of rainfall total depth by quantifying the overestimation or underestimation of the reference rainfall by a given raingauge subset.

These indices were compared with model efficiency (NSE) and model parameters for three French catchments of increasing size 71 (same catchment studied by Obled et al. (1994)), 1120 and 10700 km^2, and different climate conditions (Mediterranean climate for the smallest basin and temperate oceanic climate for the two larger catchments); and three continuous, lumped, daily rainfall-runoff models. The reference areal rainfall estimate was taken as the spatial average of all (or the best positioned) rain gauges. 33, 8 and 20 rain gauges were used for reference areal rainfall estimation for the 10700, 1120 and 71 km^2 catchments, respectively.

The sensitivity of model performance to the rain gauge network quality was assessed by plotting the NSE criteria against the GORE or BALANCE index. Results show that there is an overall increase in model efficiency with the GORE index. For all three catchments, GORE values above 0.9 lead to maximum NSE criteria above 80%. Similarly, the model performance is maximum (NSE >80%) for BALANCE values between

0.9 and 1.1, i.e. when the estimate of total precipitation is within 10% the reference value. However this feature is necessary but not sufficient to achieve good performance (cases where the balance index is 1 and the corresponding NSE value is around 50%). The models proved to be robust and reliable due to their ability to cope with imperfect rainfall input estimates. For instance, a single raingauge for the 10700 km^2 basin, with a GORE index of 0.74, achieves a NSE criterion of 81%. Bias in basin rainfall estimates may, at least partially, be compensated by model parameter adjustment. However, the conclusions may be affected by the lumped nature of the model, which is less sensitive to the spatial variability of rainfall. Further the three models showed improved performance and reduced variability of efficiency with more accurate rainfall input. The smaller basins require more precise areal rainfall estimates (a higher concentration of rain gauges) to ensure good modelling results. Poor modelling results are obtained when a single gauge is used to model the 71 km^2 basin even though it provides a greater density per unit area than the 33 and 8 raingauges used for the 10700 and the 1120 km^2 basins.

In this study, the catchment is considered as a lumped unit even at the 10700 km^2 scale. This article gives an indication of the raingauge network density required to model the streamflow at the outlet for a range of scales. They used 20 raingauges at the 71 km^2 scale, it seems that 8 and 33 raingauges are suitable to model the 1120 km^2 (i.e. 1 gauge per 140 km^2), and 10700 km^2 (i.e. 1 gauge per 324 km^2) catchment, respectively. Combined with the study by Obled et al. (1994) a density of five raingauges may be appropriate to model the 71 km^2 catchment. Overall the findings suggest that the importance of spatial rainfall decreases with scale. As in Smith et al. (2004), the rainfall variability is described in terms of two indices accounting for spatial and temporal variability.

In her study of the Thames catchment, Naden (1992) observed that the slow component of the hillslope response was dominant over the channel routing response and masked any impact of the spatial variability of rainfall. It seemed that the hillslope dominance was due to the large proportion of limestone and chalk in this catchment. Runoff moving through the catchment had a much longer residence time in the hillslope component than in the channel system. Naden (1992) obtained very similar catchment response functions for seven events despite the observed spatial variability in precipitation. Hence, she concluded that a semi-distributed modelling approach over a lumped model was not justified when applied to this 7000 km^2 basin. However her methodology that incorporates the spatial distribution of rainfall in the form of a weighted network function into a unit hydrograph type flood estimation procedure, showed improved per-

formance compare to the traditional unit hydrograph method used in the UK Flood Studies Report (NERC, 1975). In comparison with the observed flow, an efficiency of fit of about 80% on average is obtained, compared with 60% with the traditional method. The weighted width functions could be expressed in terms of the distribution of (relative) rainfall excess with flow distance and in terms of the probability density function for flow distance in the channel network to the catchment outlet, two components developed by Woods and Sivapalan (1999).

Koren et al. (1999) examined the scale dependencies of hydrologic models to spatial variability of precipitation using four lumped rainfall-runoff models. The 4km grid, hourly rainfall estimates for the three year period May 93 - July 96 from the NEXRAD radar were used in this study. The test area was the 256×256 km Arkansas-Red river basin. Results from different resolutions of spatial averaging of hourly data (4, 8, 16, 32, 64, 128 and 256 km grid) over sub-basins defined by the grid scale, revealed that all models were scale-dependent but the level of dependency varied with the type of rainfall-runoff partitioning mechanisms. It was found that each model produced less surface runoff with increasing scale. Surface runoff was gradually reduced within the range of 20% (relative to cumulated surface runoff at the finest scale) up to the scale of 32 km. At higher scales, there was a faster reduction in surface runoff with a wide range of variability from one model to the other (between 25 and 100% depending on the model). They deduced that the main factor governing runoff reduction at the smaller scales was rainfall variability over a rainfall averaging area. At the largest scales, the rainfall coverage became the major factor controlling runoff reduction. In this case, the event covered about 50% of the area at the largest scale. Total runoff was less sensitive to scale than surface runoff (reduction at largest scale is 10-25%). Defining the runoff coefficient as the ratio of accumulated runoff to accumulated precipitation, it was observed that the runoff coefficient was rather stable at the beginning of the event before the rainfall became effective. Afterwards, the runoff coefficient varied significantly over different scales with the highest values at the finest scale and this also depended on the runoff partition mechanism. Infiltration-excess type models were the most sensitive whereas saturation excess models were less scale-dependent. They observed that scale dependency was reduced when the spatial variability of rainfall was taken into account in the rainfall-runoff model structure. This paper shows that there is a need to improve the hydrological lumped model structure.

In the context of nonlinear dynamical systems (Wiggins, 1999) applied to nonparametric streamflow prediction (Porporato and Ridolfi, 2001), Dodov and Foufoula-Georgiou (2005) proposed a methodology which combines the spatial and temporal distribu-

tion of rainfall and basin geomorphology into nonlinear analyses of streamflow dynamics. The methodology is based on optimal phase-space reconstruction of the coupled rainfall-runoff process. The (multi-variate) time-series of rainfall and the corresponding (univariate) time-series of streamflow are independently reconstructed in their optimal phase-space by using Takens's 1981 delay time method so that two state vectors or rainfall and runoff states are obtained.

A brief summary of the methodology is given here; further details can be found in Dodov and Foufoula-Georgiou (2005). Catchment geomorphology is accounted for by two criteria, firstly by spatially aggregating the rainfall information according to the (sub)catchment topology. Various aggregation levels of rainfall have been investigated: pixel size, catchment scale, and sub-catchment scale. A geomorphologically derived response function (Unit Hydrograph) is used to assign weights to the elements of the rainfall state-vector according to their contribution to the discharge. The streamflow of a reference state can be predicted by coupling the rainfall and runoff information in a distance space. In this distance space, the reference state represents the origin, the x-axis corresponds to streamflow distances (i.e. the Euclidean distance between the reference streamflow and all other observed streamflow states) and the y-axis corresponds to rainfall distances. The similarity between the reference rainfall and all other rainfall states is evaluated by means of root mean square error, multiscale root mean square error and Hausdorff distance (see Appendix A-C in Dodov and Foufoula-Georgiou (2005) at pixel level, weighted (using the geomorphologically derived response function mentioned above) and non-weighted Euclidean distances otherwise. First, the rainfall distances are plotted against the corresponding streamflow distances. Then a kernel function is defined so that it captures a neighbourhood of points around the reference state. Finally, the average of the points within the neighbourhood gives the streamflow prediction at the time horizon defined.

The methodology is applied to two basins in Missouri and Oklahoma with contrasting geology: deep limestone aquifer underlying the Gasconade River basin (7352.4 km^2) and in absence of dominating aquifer in the case of the Chikaskia River basin (4813.7 km^2). This study was based on 6-hour streamflow time-series and radar data available for a period of 5 years.

Here is a summary of the findings:

- Including information about rainfall in the phase-space approach improves the streamflow prediction by up to 18% for the Chiskakia basin and 6% for the Gasconade catchment, compared to prediction based on streamflow only.

- Including information of rainfall spatial distribution increases the prediction accuracy (up to 12% and 5% for the Chikaskia and Gasconade basins, respectively), compared to the results based on averaged rainfall over the catchment.

- Best performances are obtained using a crude catchment discretisation of 3 or 10 subcatchments. Despite the damping effect of the catchment and the uncertainty in the data, the results suggest that rainfall averaging at the subcatchment scale captures enough information on rainfall spatial and temporal variability to predict the runoff response.

- Including information about (sub)catchment's response based on a geomorphologically-derived unit hydrograph, additionally improves the accuracy of streamflow prediction by 2-5%.

- The difference in prediction accuracy due to the information about the spatial distribution of rainfall depends on the geological characteristics of the basin. More improvement is achieved in the case of the Chikaskia River (10-15%), while in the case of the Gasconade River the prediction accuracy is significantly affected by the smoothing effect of the underlying limestone aquifer (improvement of 3-8%).

2.4.4 Conclusions

Contrasting observations arise from the studies conducted in temperate areas. The catchment response is a trade-off between the impact of spatial variability of rainfall and the smoothing effect due to the heterogeneity of the catchment. The importance of spatial rainfall depends on how variable the rainfall is and whether there is enough variability to overcome the damping and filtering effect of the basins (Smith et al., 2004; Obled et al., 1994)

The rainfall variability depends on the type of event. Bell and Moore (2000) observed lower variability in rainfall and runoff response during a stratiform event as opposed to a convective event in a study on the 135 km^2 Brue catchment in the UK. On the 1645 km^2 Watts basin in North America, Ajami et al. (2004) concluded that knowledge of spatial rainfall is important when modelling extreme events and convective events in summer.

When there is not enough variability in rainfall to overcome the damping effect of the catchment, detailed knowledge of rainfall spatial variability is not required to model the catchment response. Rather reliable information of catchment averaged rainfall is important (Woods and Sivapalan, 1999; Smith et al., 2004; Andréassian et al., 2001;

Naden, 1992). For instance, Smith et al. (2004) observed that improvement in model efficiency using a distributed model is observed when spatial variability of rainfall is included to model the 795 km^2 Blue catchment whereas a lumped approach using catchment-averaged rainfall is suitable to model the 1645 km^2 Watts basin. The Blue basin is characterised by variable precipitation and low level of basin filtering whereas the Watts show higher level of filtering and more uniform precipitation.

The flow routing and the distribution of rainfall-excess with flow distance control the catchment response. Woods and Sivapalan (1999) proposed an analytical method to identify the importance of different components of the hydrological cycle during storm events in a 420 km^2 catchment in New Zealand. The method is illustrated on a 10-hour storm using hourly radar rainfall data at 1 km grid resolution and a lumped rainfall-runoff model. The authors conclude that if the space and time covariance between rainfall and runoff generation are negligible then methods for estimating catchment average rainfall and runoff generation may be more important than methods for estimating their variability. The apparently substantial spatial variations in rainfall do not seem to have any significant influence on the timing of catchment response. For the small sub-catchments the space pattern of excess rainfall is unimportant because it only influences channel routing, and the timescale of channel routing in those catchments is small compared to storm duration. For larger catchments, spatial variability of rainfall has little influence because rainfall does not vary significantly with flow distance in spite of its spatial variability in (x,y) coordinates. For this event, at each flow distance, there is a wide range of rainfall depths so the distance-averaged rainfall excess is relatively uniform.

Obled et al. (1994) reached similar conclusions. In a study conducted on a 71 km^2 catchment in France, they found that a spatially-uniform rainfall from five raingauges was enough to estimate the streamflow hydrograph because of the large dampening behaviour of the basin. In this area, the runoff generation mechanism is predominantly of the Dunne type, the water infiltrates and local variation of the rainfall input is smoothed and delayed within the soil.

The underlying geology is important and can mask the impact of spatial rainfall as in the case of Naden (1992) where the runoff had a much longer residence time in the hillslope component due to the large proportion of limestone and chalk in the 7000 km^2 Thames catchment. She concludes that a lumped approach is appropriate to model the 7000 km^2 Thames catchment. In the context of nonlinear analyses of streamflow dynamics, Dodov and Foufoula-Georgiou (2005) find that including information

of rainfall spatial distribution improves the prediction performance of streamflow but the improvement is less in the case of a 7300 km^2 catchment in central North America with presence of limestone aquifer (3-8%).

The antecedent catchment condition controls the catchment response to the spatial variability of rainfall. Based on results from a 10 km^2 catchment in the UK, Shah et al. (1996a) observed that under dry conditions, higher error prediction of runoff (14 and 8% in peak flow and volume) are obtained with a spatially averaged rainfall input compared to the case with wet conditions (6 and 3%).

The importance of spatial rainfall on runoff generation is also a function of catchment scale. More precise areal rainfall estimates are required at small scales (Shah et al., 1996a; Andréassian et al., 2001; Carpenter et al., 2001). Obled et al. (1994) recommend 5 raingauges for a 71 km^2 basin in the South of France. The study from Bell and Moore (2000) suggests a 2 km grid rainfall resolution to model the 132 km^2 Brue catchment. As the scale increases, in the case where knowledge of spatial rainfall improves the runoff prediction, a crude resolution of rainfall is adequate. Smith et al. (2004) use 4km rainfall grid resolution to model a 800 km^2 basin. Carpenter et al. (2001) suggest a rainfall resolution of 80 km^2 (i.e. about 9km grid) for catchment scales greater than 800 km^2 and recommend a smaller one for the 280 km^2 catchment. At the larger scale, Dodov and Foufoula-Georgiou (2005) suggest that aggregation of rainfall at the sub-catchment scale captures enough spatial information that improves the prediction performance of streamflow by about 10-15% and 3-8% for two catchments of 4800 and 7300 km^2, respectively. They use catchment-averaged rainfall over subcatchments of 530 km^2 (9 subdivisions scheme) and 1600 km^2 (3 subdivisions scheme) for the 4800 km^2 basin, and subcatchments of 735 km^2 (10 subdivisions scheme) and 2450 km^2 (3 subdivisions scheme) for the 7300 km^2 basin.

Further complexity in unscrambling the effect of spatial rainfall on runoff is added when using a rainfall-runoff model. Obled et al. (1994) observed the sensitivity of a particular model to the spatial variability of precipitation, and not the sensitivity of the actual basin. Koren et al. (1999) concluded that lumped hydrologic models are scale-dependent and that scale-dependency decreases when spatial variation of rainfall is accounted for in the model structure. Using a semi-distributed model Chaubey et al. (1999) showed that large uncertainties in model parameters are introduced due to the spatial variability of rainfall. Shah et al. (1996a) found that larger errors in runoff prediction arise when a lumped instead of a distributed model is applied on the catchment, compared to using a distributed model with averaged or spatially variable

rainfall. One reason for moving from the lumped to the distributed approach is the potential to simulate streamflow at interior points of the catchment.

To conclude, the runoff response is the result of a complex interaction between the rainfall spatial variability and the heterogeneous catchment properties such as the flow routing, the soil moisture and the geology. The spatial organisation of rainfall (i.e. the distribution of rainfall excess with flow distance) also controls the runoff response. The importance of spatial rainfall decreases with catchment scale. The relative importance of spatial rainfall is dependent upon the modelling strategy, hence the impact of the model should be quantified and kept to a minimum. For instance a small catchment discretisation is preferable to avoid smearing of rainfall information due to spatial averaging. The impact or rainfall errors only can be assessed by defining a reference rainfall and comparing the errors between the reference flow and the flow triggered by an alternative rainfall scenario. Modelling errors can be estimated by computing the difference between the reference and the observed flow. Appropriate calibration is required to keep them to a minimum.

2.5 Conclusions

2.5.1 Summary

A review of the literature on the importance of spatial rainfall for runoff generation has been conducted for three conditions: (a) urban areas where most rainfall events contribute to runoff, (b) semi-arid areas associated with localised thunderstorms and (c) temperate regions where storms are the results of frontal and convective activities, or a combination of both, and the catchment is more heterogeneous in nature.

Across all catchment types, the review stresses the nonlinearity of the runoff response to rainfall input (Lopes, 1996; Shah et al., 1996a) and highlights three main interactions: (a) rainfall, (b) catchment properties and (c) scale. The effect of rainfall includes variability in space and time, storm movement and spatial organisation. The responding or damping effect of the basin is an intrinsic property of the catchment and can be characterised by the lag time (sometimes referred to as the time of concentration, characteristic time scale, mean runoff time, catchment response time). It is a measure of the catchment response time and expresses the average travel time from all points on the catchment to the outlet (Lekkas and Onof, 2005). As the scale increases, the importance of spatial rainfall decreases and there is a transfer from spatial variability of rainfall to catchment response time distribution as the dominant factor governing the runoff generation. Hence these three interactions control principally the runoff re-

sponse; however their relative contributions differ depending on the type of catchment considered.

Small urban catchments are fast-responding and sensitive to storm movement, storm variability and event magnitude. Their hydrological modelling requires fine spatial and temporal rainfall resolution of the order of minutes and kilometres. Since the damage as a result of flooding can be important in urban areas, there is a strong incentive to use radar data or develop disaggregation techniques (Onof et al., 2005) to meet the requirement of urban hydrological modelling. Berne et al. (2004) show that finer spatial and temporal resolutions are required at smaller scale.

In semi-arid areas dominated by convective thunderstorms, the catchment response is also very rapid and a detailed representation of the rainfall distribution is necessary to reproduce the outflow accurately. The findings from this review highlight the importance of spatial rainfall at the small scale and suggest a spatial resolution of 1 km below 50 km^2, 2 km between 50 and 500 km^2. This is a hard recommendation to implement in practice as common operational networks are usually not as extensively instrumented as the catchments reviewed (Reefsgaard and Knudsen, 1996).

Contrasting observations arise from the studies in sub-humid areas where more complex interactions between spatial rainfall and catchment characteristics exist. A key paper is presented by Woods and Sivapalan (1999). Their analytical framework includes the main components of the hydrological cycle and quantifies the effects of rainfall and catchment response. The distribution of rainfall-excess with flow distance to the outlet was found to be a dominant factor influencing the runoff response. This finding was also corroborated by other authors (Smith et al., 2004; Naden, 1992; Dodov and Foufoula-Georgiou, 2005). In the event examined, although substantial variation in rainfall distribution was observed, the distribution of rainfall-excess with flow distance was relatively uniform so that knowledge of catchment-averaged rainfall was sufficient to model the runoff response. Obled et al. (1994); Naden (1992) and Smith et al. (2004) reached similar conclusions. Woods and Sivapalan (1999) conclude that the mean runoff time is dominated by storm duration at small scale and for larger catchments the mean travel time gradually becomes more important. Smith et al. (2004) suggest that when catchments are characterised by marked spatial variability in precipitation and less of a filtering effect of the rainfall input signal, they present improved outlet simulations from distributed versus lumped models. In this case, spatially-variable rainfall input is required but a detailed spatial representation is not necessary. The raingauge network density proposed by Obled et al. (1994) and Andréassian et al. (2001) seems adequate

to model the behaviour of humid catchments, i.e. 5, 8 and 33 raingauges at scale of 71, 1120 and 10700 km^2. At the large catchment scale, daily data are adequate for lumped modelling, when distributed (or semi-distributed) modelling is undertaken, subdaily data are recommended.

In rainfall-runoff modelling, a simulated hydrograph is derived from a transformation of the rainfall input via the use of parameters that are the results of a calibration procedure at a fixed spatial scale. The modelling strategy adds another level of complexity and can mask the effect of spatial rainfall, therefore its impact should be quantified independently from the effect of rainfall (see discussion in 2.4.4). The main advantage of catchment modelling is that it provides a framework to use rainfall patterns to test hypothesis about the behaviour of the catchment.

2.5.2 Direction of Research for Modelling of Space-Time Rainfall

The literature on the significance of spatial rainfall is complex and sometimes contradictory for catchments in temperate humid areas. Overall it seems that knowledge of the spatial structure of rainfall improved runoff estimation but a detailed representation is not necessary due to the integrating effects of the catchment. The rainfall-runoff investigation of Woods and Sivapalan (1999) suggests that a rainfall representation described by a spatially-uniform temporal profile conditioned on storm averaged totals is appropriate for runoff production in humid temperate areas. In their model, the space-time rainfall field can be determined from a temporal profile of rainfall defined as the storm (space) averaged rainfall time-series and scaled at any pixel location using a dimensionless rainfall space pattern.

An analogous methodology is presented in this thesis, in which spatial variations of multisite daily rainfall are directly incorporated in the modelling framework. This is similar to the space pattern component of Woods and Sivapalan (1999). The reason for choosing a daily time-step is because it captures the duration of the storm. Then a single profile can be obtained using a temporal disaggregation procedure from daily to hourly time steps at a representative site on the catchment. The resulting temporal profile is then applied linearly to the spatially-varying daily rainfall totals to obtain multi-site sequences of hourly rainfall.

This scheme may not reproduce adequately rapidly moving storms but a visual inspection of the Chenies radar dataset (see Chapter 3) reveals that the storm speed is relatively constant in this region. Further, the review suggests that at the large catchment scale, although the rainfall variability may increase, so is the integrating

effect of the catchment. This scheme is probably too simple to model the behaviour of convective rainfall, but in the context of flood management, as a first approach focus is on winter rainfall and wet antecedent catchment conditions. In this investigation, two existing models are combined in which simulation at the daily scale is performed by GLMs and the subdaily profile is obtained using a single-site temporal disaggregation scheme based on Poisson-cluster processes.

2.5.3 Direction of Research for Rainfall-Runoff Investigation

This review has identified a number of open problems on the importance of spatial rainfall representation for rainfall-runoff modelling in temperate humid areas. It is not clear whether an explicit rainfall representation is required. The findings are usually subjective and there is a need to quantify the effect of rainfall, catchment response and catchment scale independently. It is also difficult to distinguish between the effect of spatial rainfall and the impact of the model spatial discretisation. Further guidance is required. A numerical investigation on the Lee catchment is undertaken to explore some of the following issues (a) to test whether spatial rainfall is important to model medium to large scale catchments in humid areas, (b) assuming that it is important, to investigate the rainfall spatial resolution required at catchment scale, for a range of scales and catchment types (c) to identify the modelling needs.

The findings from the literature emphasise the non-linearity of the runoff response to rainfall input. Taking into account the spatial variability of rainfall is important in some cases. Therefore the catchment is selected for its heterogeneity to assess the impact of spatial rainfall as a function of catchment properties. A distributed approach is applied to test various rainfall representations and assess the impact on the flow. The importance of spatial rainfall data seems to decrease as the catchment scale increases. Therefore the experiment is carried out for different sizes of catchment. There is a need to reduce the impact of the modelling issues so an event-based structure is chosen rather than a more complex continuous approach. This has the main advantage of allowing some simplifications, fewer model parameters need to be identified, and losses (such as evapotranspiration and soil infiltration) can be neglected. In addition, given that there is a lack of clear guidance, an understanding of the impact of spatial rainfall on illustrative events is required before moving onto continuous simulations. The findings from the review highlight the effect of the type of basins, so the experiment is designed such that spatial rainfall is tested for natural catchments and artificially urbanised basins. From the literature, it is concluded that the impact of the spatial variability rainfall is moderated by the travel flow distance to the outlet. Therefore a model incorporating this variable is preferred.

The event-based, semi-distributed hydrological model RORB is selected to carry out the investigation. A semi-distributed model provides a compromise between the complexity of distributed models and the simplicity of lumped models to account for the spatial variations of rainfall input. The RORB model satisfies the requirements stated above. It incorporates nonlinear routing and has the capability of accepting a large number of distributed rainfall input data to assess the importance of rainfall representation. It has an event-based structure and a small number of parameters, which facilitates parameter identification of catchment response. It takes into account the travel flow distance from the outlet and urbanisation can easily be incorporated. Further, the RORB model has been used extensively in practice to model the Lee catchment (Lotufo Conejo, 1979; Flynn & Rothwell, 1991a,b; Hawnt, 1987a,b) and some model configuration files have been made available.

The experimental design is constructed so that spatial rainfall is tested according to rainfall representation and the type of rainfall events. To address this issue, data for selected events from the period 1987-2002 are used. These data comprise 2km grid radar data, subdaily data from a network of 16 raingauges and subsets of the raingauges are used. A reference rainfall field is defined, based on the full set of subdaily raingauge data, and compared with alternative rainfall estimators based on subsets of the gauges and radar data. In the case where only daily data are available, the disaggregation scheme (defined above), conditioned on observed daily data at all sites and observed subdaily data at one site, is also evaluated. The use of this rainfall estimator will serve to validate the hypothesis of applying a single temporal profile of rainfall on a catchment for hydrological applications.

The Lee is divided into six subcatchments, representing the main tributaries. Each subcatchment is first modelled independently and the simulated runoff is then routed to obtain the total flow at the catchment outlet. Hence the relationship between the spatial structure of observed rainfall and runoff production for a range of catchments can be analysed. To investigate the sensitivity to catchment type, the existing (sub)catchments are then artificially turned into fast-responding urban basins. To assess the impact of catchment properties and following guidance from the literature, the catchment response time is taken as an independent variable of catchment response (Woods and Sivapalan, 1999; Berne et al., 2004; Lekkas and Onof, 2005). The impact of catchment scale is investigated by analysing the spatial structure of catchment-scale rainfall at scales ranging from 80 to 1000 km^2.

Chapter 3

Introduction to the Lee Catchment

The review reveals that in humid temperate climatic regions, contrasting messages arise on the importance of spatial rainfall for runoff generation, especially for medium to large scale catchments where there is a need to quantify the impact of the rainfall spatial variability and the integrating effect of the basin. Hence, the findings from the review provide the motivation for a study on the 1400 km^2 Lee catchment, in the Thames region, UK. This chapter introduces the Lee catchment and its main tributaries before focusing on the spatial data that will serve the analysis. The radar, raingauge and flow records have been obtained from the Environment Agency of England and Wales.

3.1 The Lee catchment

The Lee Catchment, which can be seen in Figure 3.1, is selected as it encompasses a range of contrasting geologies, i.e London Clay, Chalk and quaternary deposit. Moreover an extensive dataset of raingauge and flow data is available. In addition, it is overseen by the Chenies radar, for which a long record of re-calibrated data is also available. The River Lee drains a relatively large catchment of 1416 km^2 and is the principal tributary of the River Thames within Greater London. The catchment is characterised as humid-temperate with a mean annual rainfall of 632 mm. With a maximum length (east-west) and width (north-south) of 56 km, its elevation ranges from 20 to 250 m. The River Lee essentially flows in a southerly direction from its source in Bedfordshire through North London before joining the River Thames on the east side of London, near Bow Creek (Halcrow, 2001). It is convenient to divide the catchment into two parts: the Upper Catchment comprising the part of the basin upstream of Feildes Weir and the Lower Lee, defining the area below it.

The solid geology of the Upper Catchment is relatively simple and can be divided along a NE-SW line (See Figure 3.2), being largely Chalk of the Cretaceous period, overlain in the south and east by London Clay (Sumbler, 1996).

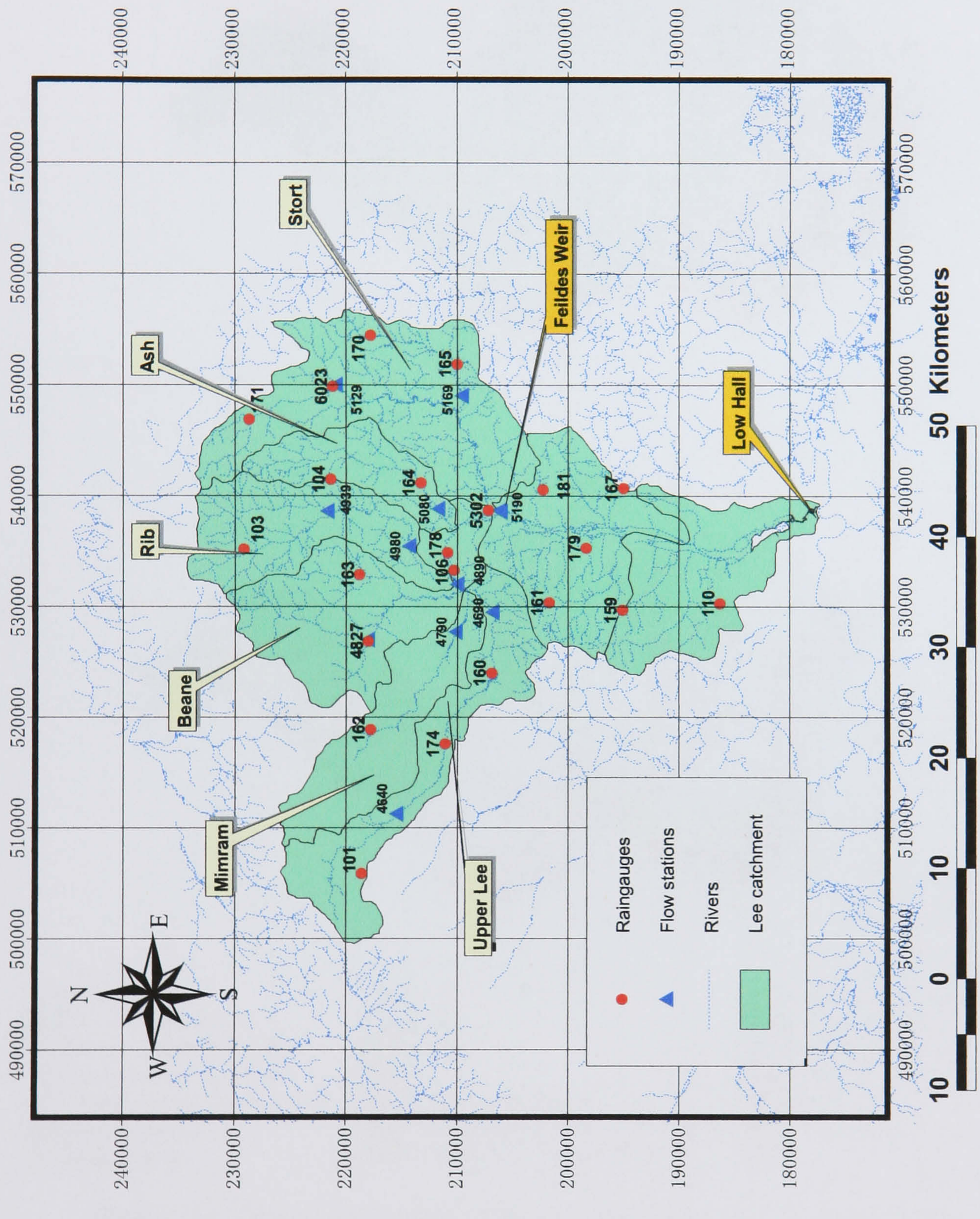

Figure 3.1 Map of the Lee catchment (British National Grid Coordinate System)

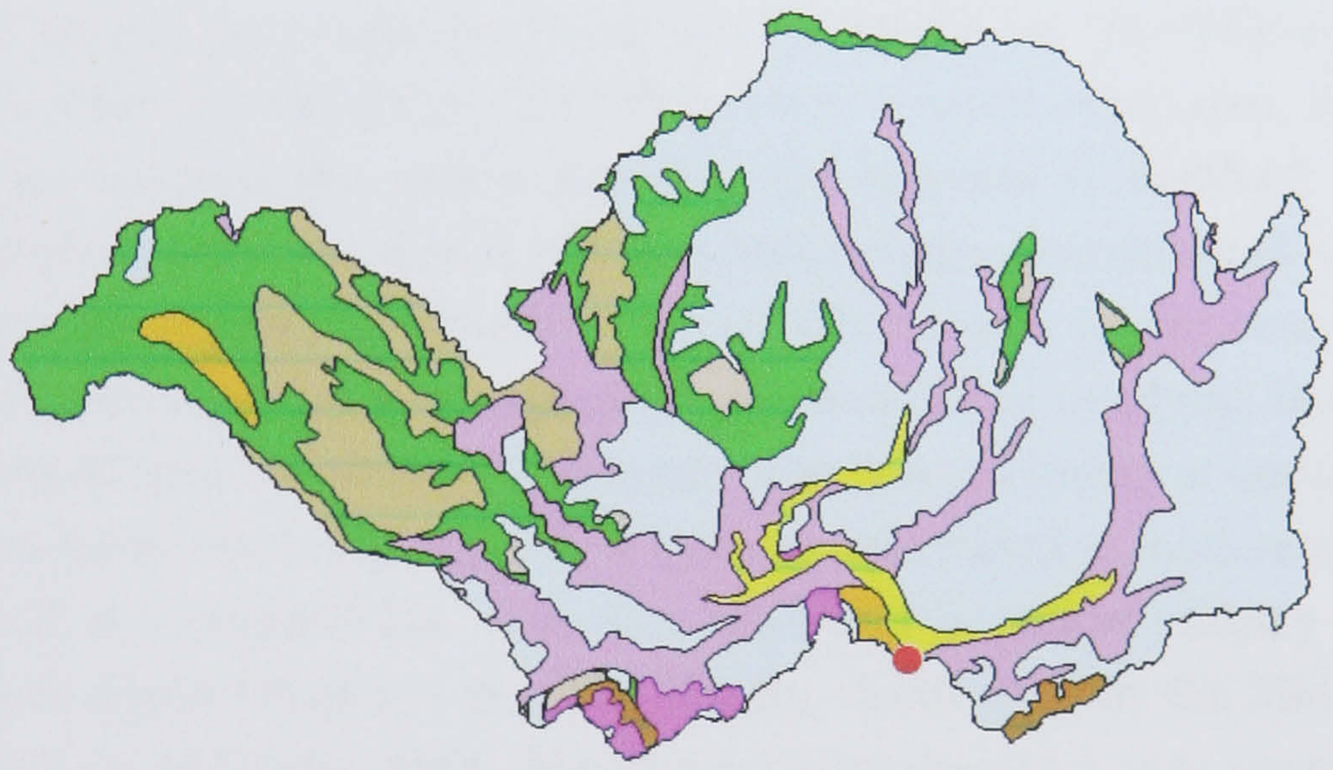

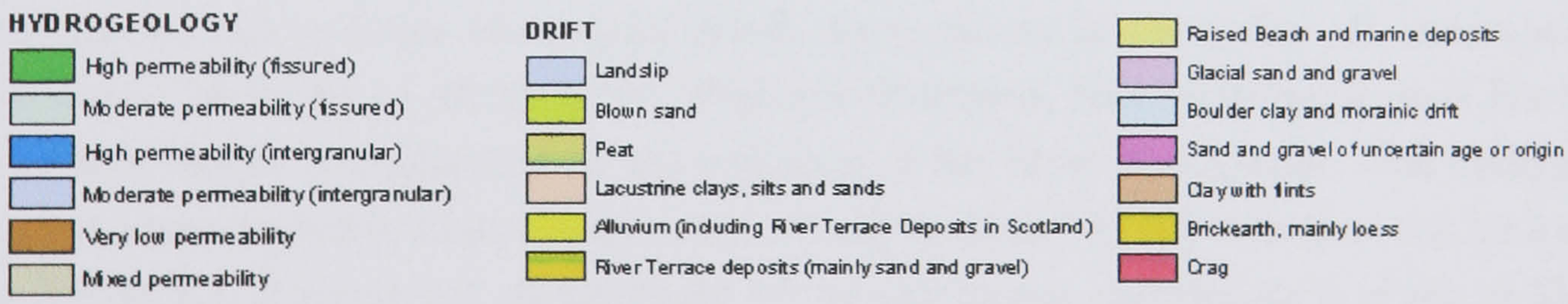

Figure 3.2 Hydrogeological characteristics of the Upper Catchment of the Lee (top map). The lower map shows the drift deposit on top of the hydrogeological properties.

Source:http://www.nwl.ac.uk/ih/nrfa/spatialinfo/Geology/geology038001.html

Throughout much of the basin, the superficial deposits which overlay the solid geology complicate the picture. These include the predominant boulder clay of central and east Hertfordshire, the Clay-with-flints of much of west Hertfordshire, and the gravels of the river valleys. The Chalk is the most important aquifer of the region. The Chalk has complex hydraulic properties. It has a porous matrix providing groundwater storage but, because the pores and their interconnections are so small, the matrix permeability and thus the speed with which water can be taken up or released, is low. Chalk has also a second porosity, due to the presence of joints and fissures. These fissures can provide rapid groundwater transport and contain the most mobile water. Because of these properties, the level of the water table changes rapidly in response to winter rains or summer droughts (Sumbler, 1996).

The Upper Catchment to Feildes Weir is mainly rural, characterised by arable farming. The area has seen significant growth in housing since the 1950s, with urban areas covering 15% (see Table 3.3) of the total Upper Catchment area. From West to East, the main tributaries of the upper catchment are the Upper Lee, the Mimram, the Beane, the Ash, the Rib and the Stort. The Upper Lee, a chalk catchment, is substantially urbanised up to Luton Hoo and is joined by the Mimram at Hertford. The Mimram drains a mostly rural area and is predominantly chalk, characterised by low natural runoff. The Beane joins the Middle Lee just downstream in the centre of Hertford. Low runoff from chalk areas is augmented by runoff from overlying boulder clay and by urban runoff from the town of Stevenage. The Rib catchment is underlain by chalk, but with extensive overlying deposits of boulder clay, runoff is moderately high, albeit characterised by a marked lag. The Ash catchment is almost entirely rural and has similar runoff characteristics to the Rib. Finally, the Stort joins the Middle Lee immediately upstream of Feildes Weir. Runoff rates from the Stort vary considerably, being high on the clay and much lower on the chalk. The Stort presents a mainly rural upper catchment, but includes substantial urban development in the valley. It encompasses the towns of Stansted Mountfichet, Bishop's Stortford, Sawbridgeworth and Harlow. The flow regime is dominated by the influence of the Stort Navigation. The hydrogeological characteristics, main components of drift and level of urbanisation can be found in Tables 3.1, 3.2 and 3.3. A summary of the catchment descriptors is given in Table A.1, Appendix A.

The upstream limit of the Lower Lee Catchment is at Feildes Weir. The lower limit of the Lower Lee Catchment is the point at which it joins the Thames River on the Thames Estuary in the south, giving it a length of approximately 34 km. For 25 km of its length, the Lower River Lee gets divided into the main channel and the River

Lee Flood Relief Channel (RLFRC) before rejoining again, 9 km from the confluence with the Thames. For most of its length, the RLFRC runs parallel to the River Lee Navigation Channel and the old River Lee system of channels (Halcrow, 2001). The Lower Lee is geologically more homogeneous, comprising London clay, with deposits of alluvium and river gravels, overlying chalk. The catchment area of the Lower Lee from Feildes Weir to its confluence with the Thames is 367.4 km^2 with significant sub-catchments, which vary in size from approximately 20 to 40 km^2. The catchment is heavily urbanised in the lower reaches.

	High permeability (fissured)	Very low permeability	Mixed permeability
Upper Lee	90.1	6.0	3.9
Mimram	97.0	-	3.0
Beane	96.1	-	3.9
Rib	93.9	-	6.1
Ash	63.9	10.5	25.5
Stort	24.1	70.8	5.1
Feildes Weir	71.4	22.1	6.4

Table 3.1 % Distribution of hydrogeological characteristics of the Upper Catchment of the Lee

	Sand and gravel	Boulder clay and morainic drift	Clay with flints
Upper Lee	22.3	13.5	9.8
Mimram	14.9	9.3	35.6
Beane	14.9	41.8	7.5
Rib	12.5	81.3	-
Ash	14.9	77.2	-
Stort	18.4	76.2	-
Feildes Weir	18.4	50.8	7.2

Table 3.2 % Distribution of the main components of drift

	Built-up areas (%)	Main towns
Upper Lee	34.7	Luton, Hatfield
Mimram	12.7	Welwyn
Beane	12.7	Stevenage
Rib	3.5	-
Ash	3.5	-
Stort	12.9	Bishops, Harlow
Feildes Weir	14.9	Hertford

Table 3.3 Urbanisation

Source of Tables 3.1, 3.2 and 3.3:
http://www.nerc-wallingford.ac.uk/ih/nrfa/spatialinfo/Index/indexEAThames.html

3.2 Radar Archive

The Chenies radar is one of a network of the UK Meteorological Office (Met. Office) C band weather radars and is located at Chenies, north-west of London. It provides high-resolution estimates of precipitation intensity and extent over the south-east of England. The data archive used in this study have a spatial resolution of 2 and 5 km Cartesian grid and a time resolution of 5 and 15 minutes, respectively. The Chenies radar is partly funded by the Environment Agency of England and Wales who provided the raw radar data together with records from a network of 122 supporting raingauges for the period 1987-2002. The 2 and 5 km resolution data cover a 152 by 152 km and a 420 by 420 km square centred at the Chenies radar, respectively. The raingauge data are recorded every 15 minutes and represent rainfall amount.

3.2.1 Observation of the radar archive

Observation of the radar archive is undertaken in order to gain a better understanding of the rainfall spatial distribution in the area and for events identification. These events are then classified according to their spatial patterns before defining some more extreme events. Some events were then selected to be used as input to a semi-distributed rainfall-runoff model in Chapter 6.

The visual inspection of the uncalibrated Chenies radar dataset between January 1988 and December 2002 at 2 and 5 km resolution showed the following points:

- Showers were identified, which could be scattered or widespread.
- Bands of different widths passing across the radar window were observed.
- Widespread events covering the whole radar window which could either be stationary or traversing as they form and disappear were also identified. These events were characterised by a high coverage, the intensity was usually uniform in space and time but could also include areas of very high intensities.

The directions observed were usually from Northwest or Southwest, with few events coming from the East. A few changes of directions were noticed: for example a storm forming from the Northwest, spreading to cover the whole radar window, then dissolving in the Southwest direction. Sometimes, no clear direction could be identified. The velocity within an event seemed constant. At first a visualisation of the 5 km data was undertaken. The duration of an event is defined as the time elapsed between the event starting and ending. The events selected were then observed at 2km resolution. The maximum and mean depths (i.e. cumulative intensities) over the duration of an

event served as a first indicator to identify some more extreme events. Based on this selection, it can be seen that two types of events lead to high mean and maximum depths:

- Long-duration widespread events showing occasional areas of high intensity.
- Short-duration high intensity rainbands.

The display of the radar archive revealed a number of anomalies; for instance some pixels repeatedly recorded rainfall even though they were surrounded by dry pixels and some scattering originating at the centre of the radar images were observed. Further some intensities seemed particularly high (> 124 mm/h). Hence a calibration procedure was implemented to improve the accuracy of the radar rainfall estimates.

3.2.2 Problems Associated with Radar Data

Errors in estimates of surface precipitation arise from the difficulty of converting radar measurements to rainfall falling at the ground. Some of the main causes of significant errors in relation to the Chenies radar are outlined here; for a more comprehensive description see Austin (2001).

First, the relationship between measured radar reflectivity of the targets (Z) and precipitation rate (R) depends upon the nature of the drop size distribution (since Z is proportional to the sum of the sixth powers of the particle diameters). Empirical relationships of the form $Z = aR^b$ (Marshall and Palmer, 1948) are used, but the most appropriate values of parameters a and b depend on the type of precipitation being sampled (Collier, 1996). A fixed $Z - R$ relationship (which is the case for the Chenies radar) for all precipitation types may introduce uncertainty in the derived rainfall rate. Further, the radar beam measures a reflected signal at a height in the atmosphere that increases with distance from the radar site and may overshoot shallow precipitation at long range. In addition, obstacles (e.g. buildings) may intercept the radar beam causing anomalies that are permanent; thus techniques which utilise a map of ground clutter locations to discard the coincident pixels are relatively successful. However, returns from ground targets which occur under conditions of anomalous radar beam propagation (anaprop) are more unpredictable in terms of location (Harrison et al., 2000). Both contaminations by clutter and anaprop were observed on the Chenies images. This led to operational attempts to overcome these problems using raingauge adjustment techniques.

3.2.3 Calibration of the Chenies Radar Dataset

A review of the literature revealed the potential of two main techniques for radar calibration. One technique is based on Kalman filter estimator. Its application to radar calibration (Todini, 2001; Lord, 1998) combines a mathematical model for the behaviour of the bias, and an observation model for the radar and raingauge measurement behaviour. It is extensively used in the USA as part of the Next Generation Weather Radar (NEXRAD) system. Another traditionally used method is based on calibration factor values defined as the ratio of raingauge to coincident radar pixel estimates of rainfall (Moore et al., 1994; Wood et al., 2000). This is then applied to the whole catchment using a surface fitting method.

The methodology developed by Moore et al. (1994) has been applied operationally to the Chenies radar by the Thames Region. The scheme was finalised in 1989 and occasionally readjusted to account for the increased network of raingauges. Reliable rainfall estimates have been obtained for real-time flood forecasting. The method is simple, which is important when dealing with an archive of 15 years of data. It was then decided to implement this scheme first and examine, from a trial sample, the goodness of fit of the radar estimates with the raingauge data before selecting a calibration method. Data from years preceding 1990, and one month (August) in 1992, had been calibrated at site by the Met. Office. Since the effect of this on site calibration could not be entirely removed, these data are not used in this investigation.

The first step of procedure involves deriving a "clutter" map for each year in order to remove the systematic anomalies present in the radar images and this was undertaken by Bellone (2003). As a first approach, these pixels are set to missing data. Interpolation across permanent clutter areas could be considered. Clutter is also removed from each radar image by setting to zero any isolated pixel that appears to be 'wet'. An example of the 2km resolution anomaly map which is applied to each radar image in 1994 is presented in Figure 3.3. It can be seen that the Lee catchment is conveniently located in a region free from systematic anomalies.

As part of this thesis, the calibration procedure developed by Moore et al. (1994) was carried out following guidance and codes supplied by Crees (2003). Changes were made to this original calibration code by Bellone (2003), based on issues identified with application to the Chenies radar dataset and which are also reported in Wheater et al. (2005b).

Taking notations from Wheater et al. (2005b), the methodology of Moore et al. (1994)

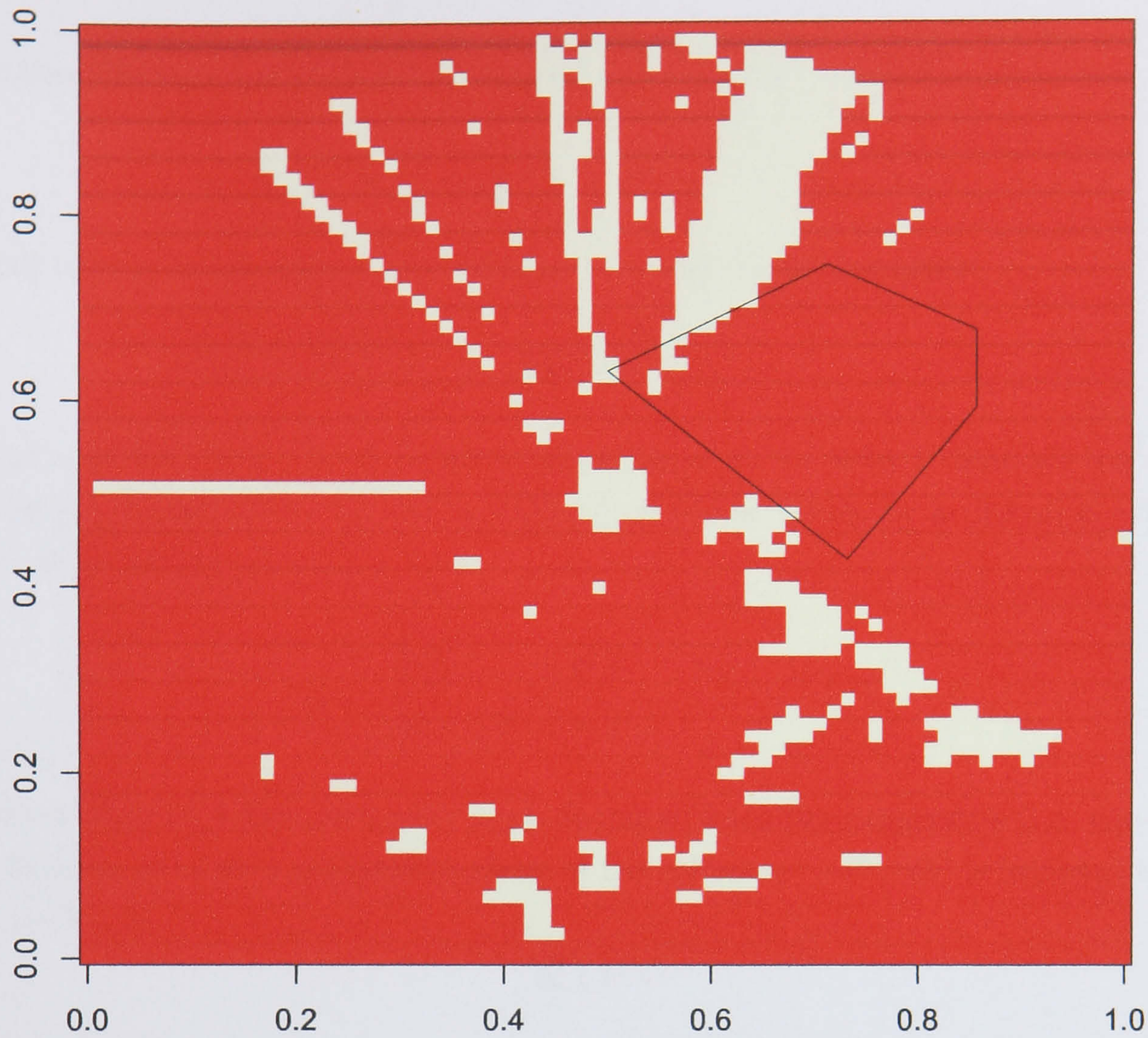

Figure 3.3 Anomaly map applied to the radar data in 1994. The area is bordered by National Grid Coordinates (km): top left (4240, 2760) and bottom right (5760, 1240). The white areas represent the dubious pixels set to missing values. The location of the Lee catchment is roughly represented by the region enclosed in black.

is summarised below. The calibration factor corresponding to the j-th gauge, at pixel i, is defined as:

$$z_j = \frac{R_G^j + \epsilon_G}{R_R^i + \epsilon_R} \tag{3.1}$$

R_G^j and R_R^i are respectively the hourly intensity recorded at raingauge j and the corresponding hourly intensity at pixel i containing raingauge j. ϵ_G and ϵ_R are small constant values which ensure the calibration factor is defined for radar values equal to zero. Then a mathematical surface is computed as:

$$\underline{s} = G\underline{a} + \underline{a_0} \tag{3.2}$$

where $\underline{s}$ is the vector of scaling factors to be applied to the raw radar data. $\underline{a}$ is the vector of weights that are to be estimated. The elements of the matrix G represent the

Euclidean distance between the m pixel centres and the n gauges:

$$G_{ij} = d_{ij}, \qquad i = 1, \ldots, m, \qquad j = 1, \ldots, n. \tag{3.3}$$

Setting $s_i = z_j$ in the case where the pixel contains the gauge gives

$$\underline{a} = G^{*-1}(\underline{z} - \underline{a_0}) \tag{3.4}$$

where G^* is the $n \times n$ matrix of inter-gauge distances. In order to smooth the surface, the surface departs from the actual calibration factor values by a distance $-K$ (km). Hence G is defined by

$$G^*_{ij} = \begin{cases} d_{ij} & i \neq j \qquad i, j = 1, \ldots, n \\ K \leq 0 & i = j \end{cases} \tag{3.5}$$

A requirement for a flat surface at large distances from the raingauges (i.e. the surface has slope equal to zero outside the range of the raingauge network) is imposed through the constraint:

$$\underline{a^T 1} = 0 \tag{3.6}$$

which results in

$$a_0 = a_0 \underline{1} = \frac{\underline{1}^T G^{*-1} \underline{z}}{\underline{1}^T G^{*-1} \underline{1}} \underline{1} \tag{3.7}$$

The recommended values by Moore et al. (1994) for $\{K, \epsilon_G, \epsilon_R\}$ vary in time. However since the calibration procedure affects the spatial properties of the radar rainfall estimates (Bellone, 2003), for consistency a unique parameter set, $\{K = 0, \epsilon_G = 0.1, \epsilon_R = 0.1\}$, was selected to be applied to the whole period of records (Bellone, 2003). This set gave a better agreement in terms of annual totals between the gauge and radar spatially averaged rainfall with a relative difference in annual totals between calibrated radar and gauges ranging from -2% (1996) to -12% (1991) (Wheater et al., 2005b). Further, over all available years, this parameter set best reproduced the hourly spatially averaged rainfall values observed at the gauges (Bellone, 2003). For details of changes and modifications made on the calibration procedure, see Wheater et al. (2005b) and Bellone (2003). This calibration procedure, although not optimal, mitigates some of the errors in radar estimates of precipitation. The use of calibrated radar data as input to rainfall-runoff modelling is evaluated in Chapter 6.

3.3 Raingauge Records

15 minutes data from a network of 21 raingauges are available for the Lee catchment. Their location can be found in Figure 3.1 and their characteristics are given in Table 3.4. The raingauge elevations vary between 20 and 150m. Data from the full raingauge network will be used to assess a methodology for continuous simulation of hourly rainfall fields. First, daily data will serve to evaluate the use of GLMs to simulate daily sequences of rainfall at multiple sites. In addition, hourly data will serve to test a scheme for spatial-temporal disaggregation of the simulated daily rainfall into hourly time-series. 17 raingauges (marked with a × in Table 3.4) on the Upper catchment will be used a input to a semi-distributed rainfall-runoff model in Chapter 5 and 6. Due to the proximity of sites 106 and 178 (1.7 km distance) and the fact that their period of record is complementary, they are taken as a single gauge for the rainfall-runoff investigation.

Site ID	Name	Easting m	Northing m	Altitude m	Start	End	
0101	Runley Wood	506400	221700	137	1988	2002	×
0103	Chipping	535700	232300	104	1988	2002	×
0104	Braughing Friars	542000	224500	116	1988	2002	×
0106	Hertford	533800	213400	37	1988	1994	×
0110	Hornsey	530800	189400	33	1988	2002	
0159	Hadley Road	530200	198200	49	1990	2002	
0160	Mill Green	524500	210000	68	1989	2002	×
0161	Darnicle Hill	530900	204800	73	1990	2002	×
0162	Whitwell	519400	220900	90	1989	2002	×
0163	Dane End	533400	221900	70	1989	2002	×
0164	Widford	541700	216400	60	1990	2002	×
0165	Hatfield Heath	552400	213100	67	1990	2002	×
0167	Epping	541200	198100	110	1989	2002	
0170	Takeley	555000	220900	94	1990	2002	×
0171	Clavering	547400	231800	84	1990	2002	×
0174	Wheathampstead	518100	214200	86	1991	2002	×
0178	Broadmeads	535400	214000	35	1994	2002	×
0181	Nazeing	541100	205400	47	1997	2002	
4827	Bragbury Park	527400	221100	69	1988	2002	×
5302	Rye Meads	539200	210300	30	1990	2002	×
6023	Stansted Argus	550400	224300	70	1987	2002	×

Table 3.4 Raingauge records for the Lee catchment

3.4 Flow Data

The flow data were provided at an hourly time resolution. Data from 12 stations on the Upper Lee catchment are used in the rainfall-runoff modelling of the Upper Lee catchment in Chapter 5 and 6. The location of the flow gauging stations can be found in Figure 3.1 and their characteristics are given in Table 3.5. Figure 3.4 shows the mean daily discharge series and the relative contribution from each tributary to the total runoff at Feildes Weir for the period January 1987 - December 2002. It can be seen that the Stort, the Beane and the Rib contribute to most of the runoff at Feildes Weir whereas the Mimram has a minor contribution.

The (hourly) temporal autocorrelation function of the streamflow time-series plotted in Figure 3.5, reveals different behaviour according to the geology of the catchment. The two predominantly chalk subcatchments, the Upper Lee and especially the Mimram show a high persistence in the flow compared to the watersheds with a higher proportion of clay.

Station	Location	River	Grid reference	Start	End
4640	Luton Hoo	Upper Lee	TL11791860	1987	2002
4690	Water Hall	Upper Lee	TL29990995	1987	2002
4790	Panshanger	Mimram	TL28241328	1987	2002
4827	Stevenage (Bragbury)	Beane	TL27492116	1987	2002
4890	Hertford (Hartham)	Beane	TL32511314	1987	2002
4939	Griggs bridge	Rib	TL39142480	1987	2002
4980	Wadesmill	Rib	TL3597144	1987	2002
5080	Mardock	Ash	TL39361484	1987	2002
5129	Gypsy Lane	Stort	TL50532403	1987	2002
5169	Sheering	Stort	TL49531270	1987	2002
5190	Glen Faba	Stort	TL39180931	1988	2002
5290	Feildes Weir	Middle Lee	TL39070920	1987	2002

Table 3.5 Flow gauging data on the Upper Catchment of the Lee

This chapter introduced the Lee catchment, which is representative of southern England and evidenced the heterogeneity of the Upper Lee watershed to Feildes Weir. Further, this catchment benefits from a large amount of rainfall and flow data. These data will serve to (a) develop a multi-site disaggregation methodology of daily rainfall, which can be either simulated or observed, (b) implement a hydrological model of the Upper Lee catchment to test the importance of spatial data including the disaggregation scheme above. The findings of this investigation should be transferable to other sub-humid areas associated with temperate climate. The flow data are provided at an hourly

time-step and this sets the time resolution used for this study. Besides the findings from the literature imply that daily (Andréassian et al., 2001) , 6 hours (Dodov and Foufoula-Georgiou, 2005), or hourly data (Obled et al., 1994) are appropriate to model the streamflow in humid temperate regions. In addition, the hourly time-scale permits to minimise the effects of time inconsistencies between the different raingauges (Obled et al., 1994). Further a disaggregation methodology is presented in this thesis, which downscales daily rainfall to hourly time-series. Hence, to be able to compare the impact of various rainfall representations on the streamflow, the same time-scale (hourly) is used for each estimator.

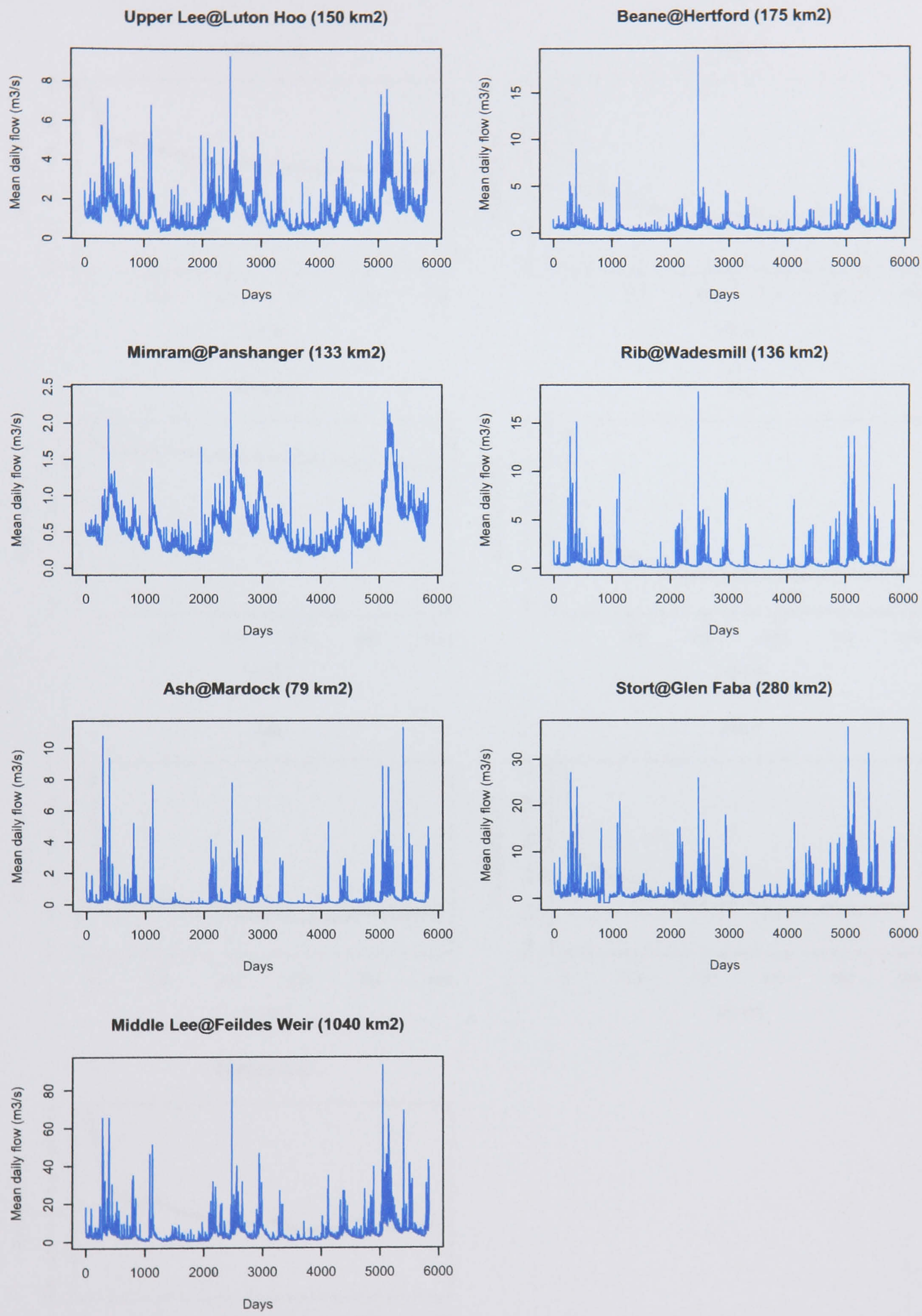

Figure 3.4 Daily mean flow characteristics

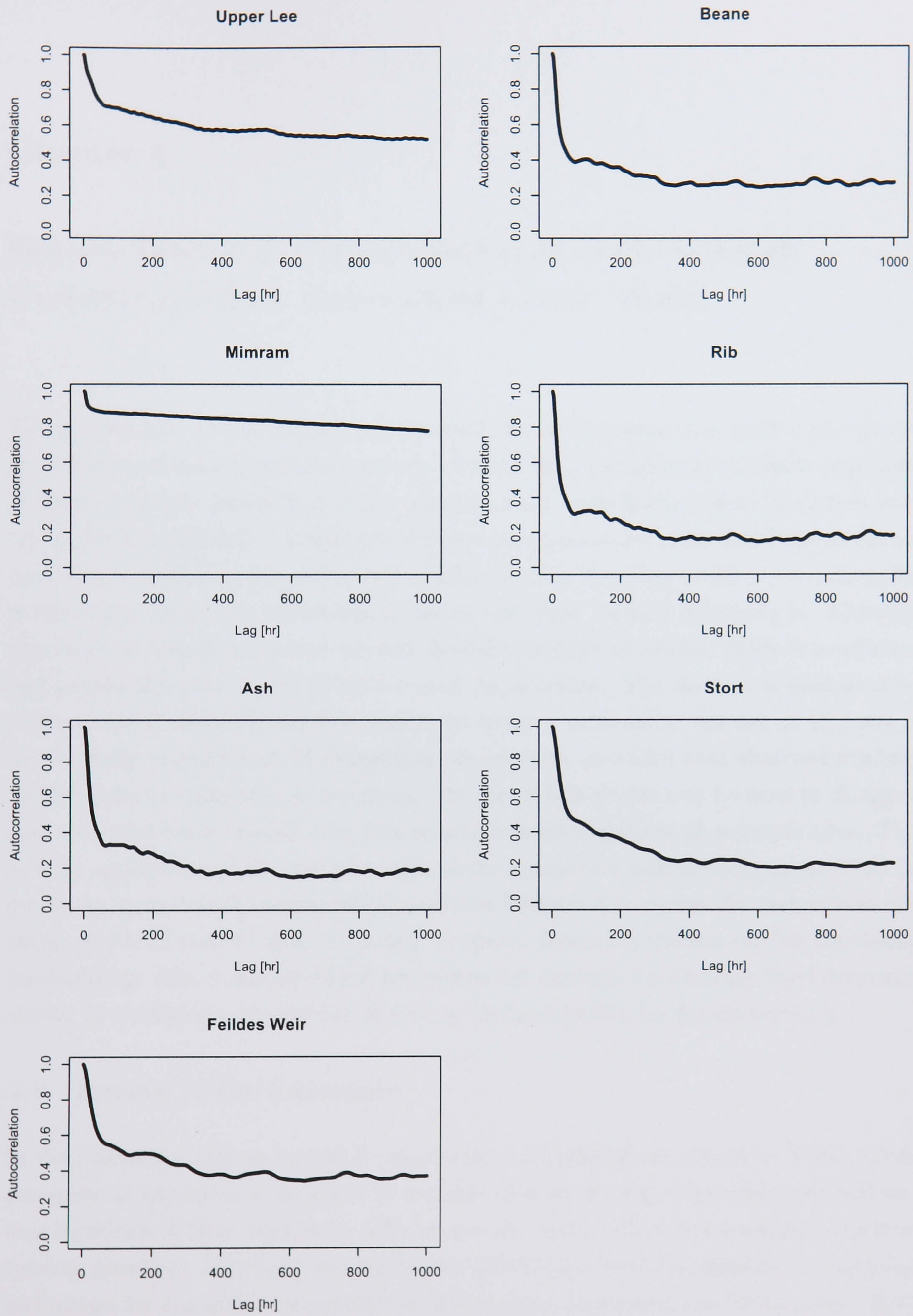

Figure 3.5 Autocorrelation function of the streamflow times-series

Chapter 4

Spatial-Temporal Disaggregation of Daily Rainfall Generated from a Generalized Linear Model

The general aim of this chapter is to present the development and testing of a procedure that combines two existing models with the aim of simulating multisite sequences of hourly rainfall. Simulation at the multisite daily scale is performed by Generalized Linear Models (GLMs). A single-site disaggregation procedure based on Poisson cluster processes is applied at one of the sites of interest. The resulting profile is then extended to the other sites on a catchment to rescale the daily rainfall information. Although this method cannot represent the full spatial structure of rainfall fields it is efficient and potentially very useful in hydrological applications. The method is evaluated on a large area (1400km^2), the Lee catchment using a substantial dataset of 15 years of hourly/daily rainfall from 21 raingauges. In addition, provided that observed subdaily rainfall data are available at one gauge, the use of this profile can be used to disaggregate observed daily rainfall data into hourly rainfall sequences at multiple sites. This simpler application of the spatial-temporal disaggregation methodology is tested as input to an event-based rainfall-runoff model in Chapter 6 to assess the assumption of a single profile of rainfall applied linearly in space. Assessing the full rainfall simulation methodology with a rainfall-runoff procedure, for example for deriving flood frequency curves by continuous simulation, is seen as an opportunity for future research.

4.1 Review of the Literature

In the literature, various models for multi-site daily rainfall are available. Wilks (1998) proposed an extension from single to multiple sites by driving single-site models at various locations in New York state with temporally independent but spatially-correlated random numbers. Buishand and Brandsma (2001) used nearest-neighbour re-sampling techniques for simultaneous simulation of daily precipitation in the Rhine basin. However historical days are reshuffled without consideration of temporal trends in rainfall sequences, so this is not appropriate if, for instance, climate change is to be incorpo-

rated.

GLMs are statistical tools based on an extension of linear regression models and were first developed in a hydrological context by Coe and Stern (1982) and Stern and Coe (1984). Chandler and Wheater (2002) illustrated the use of GLMs to account for spatial and temporal structures in modelling rainfall in Western Ireland, and Yang et al. (2005) also used GLMs for the generation of multisite rainfall series in Southern England. In both cases, good performance was obtained so that GLMs are an appropriate tool to model multisite sequences of daily rainfall and is used in this investigation. If the daily level simulations could be downscaled, for example to generate hourly sequences, these models would have high potential for use in hydrological applications.

Several authors have investigated the issue of temporally disaggregating rainfall amount at a coarser scale into shorter time-steps, such as hourly precipitation obtained from daily totals at a single-site. Disaggregation methods based on point process theory (e.g., the Bartlett Lewis or Neyman Scott rectangular pulse models, Rodriguez-Iturbe and Eagleson, 1987) can be found in the literature. Bo et al. (1994) used a modified version of the Bartlett-Lewis rectangular pulses model to disaggregate rainfall statistics from daily data with satisfactory results at a site in Italy and in the United States. Koutsoyiannis and Onof (2001) also used a modified version of the Bartlett-Lewis model coupled with an empirical procedure so that the hourly rainfall sequence is consistent with the daily totals. Gyasi-Agyei (2005) extended the methodology and successfully validated a rainfall disaggregation scheme combining the latter model with a regionalised hybrid model to disaggregate Australian daily rainfall into hourly values. Hence the relative success of disaggregation models based on Poisson process is confirmed in the literature and this approach is adopted in this investigation.

Other approaches for rainfall disaggregation include methods based on scale invariance theory (Schertzer and Lovejoy, 1987; Over and Gupta, 1996). So called multiplicative random cascades models distribute rainfall mass on successive regular subdivisions of an interval in a multiplicative manner. Using a simple random cascade model, Molnar and Burlando (2005) disaggregated rainfall at scale 1280 minutes into 10 minutes data for a 20-year period at a site in Zurich, Switzerland. The canonical model, which preserved the mass of rainfall in the average, proved to be successful in preserving the distribution and the intermittency of rainfall across scales. However it showed some limitations in reproducing rainfall extremes for aggregation of rainfall above 20 minutes. A simple-scaling based cascade model was also proposed by Olsson and Berndtsson (1998) to disaggregate a daily seasonal (April-June; 3years) rainfall time-series to 45

minutes data in southern Sweden. The model was able to reproduce the distribution of the rainfall distribution, the intermittency and the scaling behaviour of rainfall. Yet there is a need to assess the ability of the model to accommodate the extreme behaviour of rainfall and to extend it to a wider range of seasons. Hence these techniques are promising for the disaggregation problem but the performance also needs to be evaluated for other properties of rainfall such as variance and autocorrelations.

Another approach was presented by Sivakumar et al. (2001) who developed a chaotic model to disaggregate rainfall using the correlation dimension technique to verify the assumption of chaos and obtained encouraging results from the Leaf River (Mississippi, US) rainfall data. However the presence of deterministic chaotic process in the temporal evolution of rainfall is a controversial issue (Koutsoyiannis and Pachakis, 1996; Schertzer et al., 2002).

The literature on multisite disaggregation is more limited. Socolofsky et al. (2001) proposed a methodology for multisite disaggregation from daily to hourly rainfall. The method breaks down observed daily precipitation at several sites into storm intensity patterns by selecting samples of historical event statistics under the same climate from a nearby hourly gauge. A technique for spatial-temporal disaggregation of daily rainfall was proposed by Koutsoyiannis et al. (2003). They combined a simplified multivariate model of hourly rainfall based on autoregressive time-series modelling with a transformation model so that the hourly rainfall sequences sum to the daily observed totals. Using this scheme, the hourly spatial correlation in rainfall is preserved but the method is relatively complex as it involves fitting a spatial-temporal rainfall model to infer the spatial correlation between the gauges.

A simpler methodology that simulates daily rainfall and obtains hourly values by disaggregation was presented by Kottegoda et al. (2002). They proposed a multisite approach for daily rainfall using a two-station model at a key gauge and a satellite gauge. The daily occurrence of rainfall is predicted at the key station using a geometric distribution and is assumed to be the same at all stations. Next the daily rainfall amount is simulated at the key gauge and is used to predict the daily rainfall at the satellite stations. Disaggregation of daily rainfall into hourly rainfall is done, using a beta distribution, independently at each gauge but conditioned on the total daily amounts. They obtained satisfactory results on a catchment in Italy; however the assumption that the occurrence of daily rainfall is identical at all stations is questionable for large size catchments. Further independent disaggregation into hourly rainfall at various raingauges is questionable for small scale catchments. In this chapter, the de-

velopment and testing of an alternative procedure that combines two existing models with the aim of simulating hourly rainfall at multiple sites on a catchment is presented.

4.2 Methodology

A methodology to generate hourly rainfall using a GLM (Chandler and Wheater, 2002) combined with the HYETOS single-site disaggregation model (Koutsoyiannis and Onof, 2001) is reported. The single site generator produces hourly totals that are consistent with the daily amounts. In the implementation described here, the single-site model is applied at one of the sites of interest, and the resulting subdaily temporal pattern is then applied uniformly in space to daily rainfall simulated from a GLM. An important reason for selecting a spatially-uniform temporal disaggregation procedure is based on an analysis of observed raingauge data which confirmed this hypothesis (see discussion in Section 4.5, Figure 4.15 to Figure 4.17). In particular, based on 16 events, it was observed that the hourly profile of gauge 0163 and gauge 0104 best fitted the hourly profile of rainfall at the other sites. The main steps of the algorithm are summarised as follows and can be seen in Figure 4.1:

1. Generate a sequence of daily rainfall across a network of sites using a GLM.
2. Taking a cluster of wet days, defined as a series of consecutive wet days delimited by at least one dry day, use the single-site model to simulate the hourly rainfall at one gauge, referred to as the master gauge, and disaggregate using an adjusting procedure, so that the hourly totals sum up to the daily totals.
3. Use the hourly pattern generated at the master gauge to disaggregate the daily information to sub-daily rainfall at the other gauges. If the master gauge records zero rainfall, the previous day's temporal profile is applied.

The method is assessed using rainfall records from a network of 21 raingauges (see Table 3.4) from the 1400 km^2 Lee catchment in the Thames region, UK, for the period 1987-2002. Daily data for the raingauge network and sub-daily data from the master gauge are used to develop the model. The simulated hourly rainfall fields are then compared with the observed sub-daily data from the other gauges to test the model.

4.3 Simulation of Daily Rainfall

The application of GLMs was undertaken using the GLIMCLIM software package (Chandler, 2002). GLMs are an extension of normal linear regression and are used by Chandler and Wheater (2002) to predict a probability distribution for daily rainfall at a site based on observations of various other related quantities. Taking similar

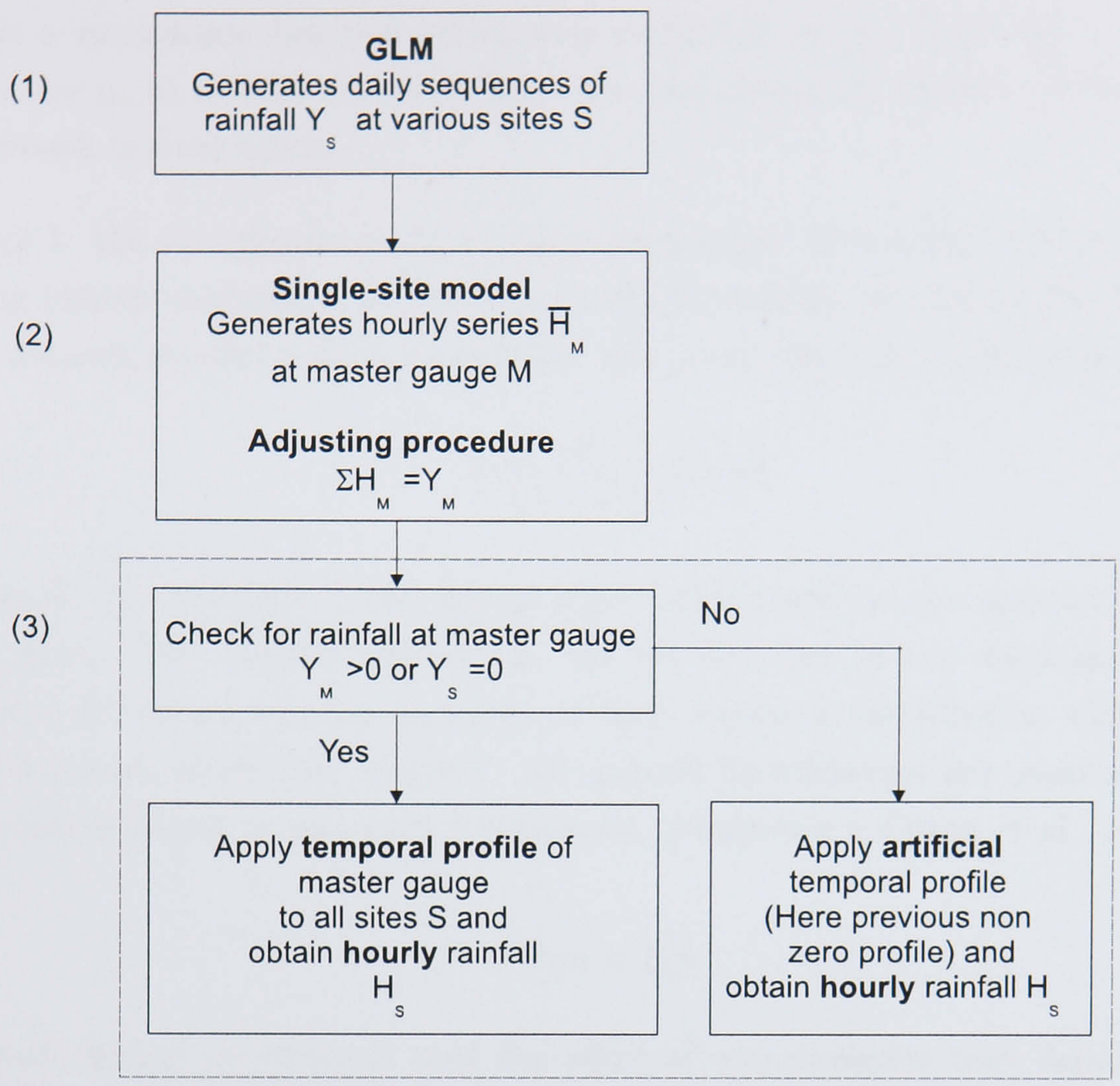

Figure 4.1 Schematic of the proposed disaggregation scheme. (1) Simulation of multisite daily rainfall, (2) Single-site disaggregation, (3) Multisite disaggregation

notations as the authors, let $\mathbf{Y} = (Y_1 \ldots, Y_n)'$ be a $n \times 1$ vector of random variables, each dependent on p predictors (also called covariates). The p predictor values can be grouped into an $n \times p$ matrix $\mathbf{Z}$ whose (i, j)th element is the value of the jth predictor for Y_i. In the linear case, a normal distribution is assumed for $\mathbf{Y}$, with vector mean $\boldsymbol{\mu} = (\mu_1, \ldots, \mu_n)'$ such that:

$$\boldsymbol{\mu} = \mathbf{Z}\boldsymbol{\theta} \tag{4.1}$$

In some cases, linearity does not hold because the Y_i and μ_i are bounded. For instance, if $\mathbf{Y}$ represents the amount of rainfall, we have $Y_i \geq 0$ and $\mu_i \geq 0$. Another example is when Y_i takes binary values (on a particular day either it rains or not) then $0 < \mu_i < 1$. Further the distribution for $\mathbf{Y}$ may not be normal (e.g. logistic distribution for the occurrence of rainfall, gamma distribution for the amount of rainfall). GLMs can be used to specify a non-normal probability distribution for $\mathbf{Y}$ and assume a *link linear* relationship of the form:

$$g(\boldsymbol{\mu}) = \mathbf{Z}\boldsymbol{\theta} \tag{4.2}$$

where g is a monotonic function which acts pointwise on $\boldsymbol{\mu}$. Typically g is used to transform the μ_i to a scale on which they are unconstrained (Smyth, 2006). A two-stage approach is then taken:

- Stage 1: the occurrence model predicts the pattern of wet and dry days at a site using logistic regression. Defining p_i as the probability of rain for the ith case in the dataset, conditional on a predictor vector $\boldsymbol{x_i}$, then the model is given by:

$$ln\left[\frac{p_i}{1-p_i}\right] = \boldsymbol{x_i'}\boldsymbol{\beta} \tag{4.3}$$

- Stage 2: the amounts model fits gamma distributions to the amount of rain on wet days. The rainfall amount for the ith wet day in the database is taken, conditional on a predictor vector $\boldsymbol{\xi_i}$, to have a gamma distribution with mean μ_i and for some coefficient vector $\boldsymbol{\gamma}$. All gamma distributions are assumed to have a common shape, or also called dispersion, parameter ν (Yang et al., 2005).

$$ln\mu_i = \boldsymbol{\xi_i'}\boldsymbol{\gamma} \tag{4.4}$$

A feature of climate processes is that the effect of one predictor may depend on the values of others, for instance the temporal dependence on the previous days' rainfall (persistence) may vary with seasonality components and exhibit different trends in winter and summer. Such interactions can be incorporated by representing the coefficients as linear combinations of other predictors. Formally, this is achieved by adding an extra predictor defined as the product of the interacting covariates. Non-linearities, i.e. when the response of rainfall occurrence or amount is associated with a nonlinear transformation of the predictor, can be represented.

Fitting of the GLM is achieved by choosing an appropriate set of predictors "$\boldsymbol{x}$" in equation 4.3 or "$\boldsymbol{\xi}$" in equation 5.4 and estimating the corresponding parameters "$\boldsymbol{\beta}$" and "$\boldsymbol{\gamma}$". The estimation and selection of the coefficient vectors $\boldsymbol{\beta}$ and $\boldsymbol{\gamma}$ is carried out using likelihood methods. ν is a function of the mean and the variance of the gamma distribution and is estimated from a method of moment once γ is determined (McCullagh and Nelder, 1989). Models are checked through simple residual plots.

Temporal dependence can be directly built in the model using appropriate predictors whereas spatial dependence between the sites needs to be included separately. A joint distribution for the next day's rainfall at all sites is obtained by construction of a model for spatial dependence which respects the marginal distributions from the GLM. A brief description of the spatial dependence structure in the occurrence and amount models

is given in Section 4.3.2 and Section 4.3.3; more details can be found in Chandler and Wheater (2002) and Yang et al. (2005)

4.3.1 Treatment of "Trace Values"

In order to remove apparent inconsistencies, mainly related to the recording of small amounts of rainfall, a threshold is applied to the data before modelling, i.e. the GLM is fitted to:

$$Y_{st}^{*} = max(Y_{st} - \tau, 0) \tag{4.5}$$

for some threshold τ (in our case 0.45 mm) and where Y_{st} represents the daily rainfall on day t at site s. When simulating daily sequences, the thresholding is removed by computing:

$$\tilde{Y}_{st} = \begin{cases} Y_{st}^{*} + \tau & Y_{st}^{*} > 0 \\ 0 & \text{otherwise} \end{cases} \tag{4.6}$$

The simulated output will contain no values between 0 and τ. However for practical applications this is acceptable providing the threshold is small enough (Yang et al., 2005).

4.3.2 Occurrence Model

The GLM is fitted to 21 raingauges for the 1987-2002 period. Few gauges have records starting in 1987 (See Table 3.4, Appendix A) and most of them were introduced during 1990, hence most of the comparisons thereafter are run for the 1991-2002 period. A simple model structure is expected when fitting the model to this relatively short time-scale. 14 predictors are used for the occurrence model. A summary of the covariates composing the occurrence model can be found in Table 4.1.

Prior to including any systematic regional effects, the bubble map in Figure 4.2 shows the mean Pearson residuals (which are defined in Section 4.3.4) at each site, where positive residuals are represented in blue, negative in white. The plot suggests a possible variation along the x-coordinate which is then introduced in the model by a Fourier representation of site Eastings. Site altitude is also included to account for spatial variation. The map for the final model in Figure 4.4 indicates that the residuals are more randomly distributed in space, which suggests that the site effects incorporated in the model have captured most of the patterns in the area (Yang et al., 2005). The model contains a linear trend to improve the performance by year. Seasonality is represented via sine and cosine components, temporal persistence is taken into account using indicators, averaged over all available sites, for the 3 previous days' rainfall. In

addition, seasonal variation in coefficients associated with previous days' rainfall is also represented (interaction terms).

Generating rainfall occurrence sequences with the correct spatial properties is more difficult than in the case of continuous variables. At the typical scale of hydrological interest, all sites tend to be influenced by the same weather systems on particular days. It can thus be assumed that inter-site dependence is strong and sites tend to be either mostly wet or mostly dry. The distribution of the number of wet sites is modelled via the flexible beta-binomial distribution which takes integer values and can be U-shaped (see mathematical details in (Yang et al., 2005)). Parameterising this distribution involves two terms: θ_t can be seen as a mean value parameter, which varies in time and is estimated from the probabilities derived from the occurrence model. ϕ controls the shape of the distribution, it is assumed constant for all days and is estimated from the method of moments. In this case-study, a small value of ϕ (0.3059, see Table 4.1) is obtained which corresponds to strong inter-site dependence (Yang et al., 2005). In simulation mode, a (non-unique) joint distribution specifies the conditional probability that a site is wet given the total number of wet sites on day t.

4.3.3 Amounts Model

The gamma model is fitted to the same dataset in order to predict the rainfall amount distribution. A summary of the covariates for the amounts model is provided in Table 4.2. The predictors are similar to those in the occurrence model, but fewer in number (7 covariates). The reduction is mainly due to simpler site effects, implying that rainfall amounts are less affected by spatial variations within the region than rainfall occurrence (Yang et al., 2005). Additionally, the amounts model contains only one term for temporal persistence (predictor for the previous day rainfall only). Prior to including any systematic regional effects, the mean Pearson residuals at each site (Figure 4.3) suggest a possible southwest-northeast gradient, which can be represented as a planar surface. Legendre polynomials of degree 1 in each direction are introduced to represent this pattern. A map for the final model is given in Figure 4.5; as with the occurrence model, the residuals now seem more randomly distributed in space.

In order to specify a joint distribution for the amounts model, a transformation to marginal normality is applied so that the spatial dependence is characterised by the inter-site correlation structure of the transformed values. If Y_i is the observed amount for the ith wet day in the database, and μ_i is the mean of the gamma distribution fitted

Components	Values	
Constant	-2.3966	
Fourier sine component 1 for Eastings	0.0274	1
Fourier cosine component 1 for Eastings	-0.0591	2
Fourier sine component 1 for Eastings	-0.0152	3
Fourier cosine component 1 for Eastings	-0.0521	4
Altitude(km)	0.8810	5
Trend 1 - Linear (0.1 per year)	0.1972	6
Daily seasonal effect, cosine component	0.2738	7
Daily seasonal effect, sine component	-0.0789	8
Mean of I(Y[t-1]>0)	1.6663	9
Mean of I(Y[t-2]>0)	0.7848	10
Mean of I(Y[t-3]>0)	0.2343	11
Mean of I(Y[t-k]>0: k=1 to 2)	-0.7973	12
2-way interaction: covariates 7 and 9	-0.2502	13
2-way interaction: covariates 8 and 9	0.1991	14
'Soft' threshold for +ve values	0.4500	
Shape parameter of beta-binomial distribution	0.3059	

Table 4.1 Covariates used in occurrence model for daily rainfall in the Lee catchment

Components	Values	
Constant	1.3175	
Legendre polynomial 1 for Eastings	-0.0918	1
Legendre polynomial 1 for Northings	-0.0779	2
Daily seasonal effect, cosine component	-0.1720	3
Daily seasonal effect, sine component	-0.1558	4
Mean of I(Y[t-1]>0)	0.2737	5
2-way interaction: covariates 3 and 5	0.1413	6
2-way interaction: covariates 4 and 5	-0.0439	7
'Soft' threshold for +ve values	0.4500	
Dispersion parameter	0.7528	
Observed residual correlation structure		

Table 4.2 Covariates used in amounts model for daily rainfall in the Lee catchment

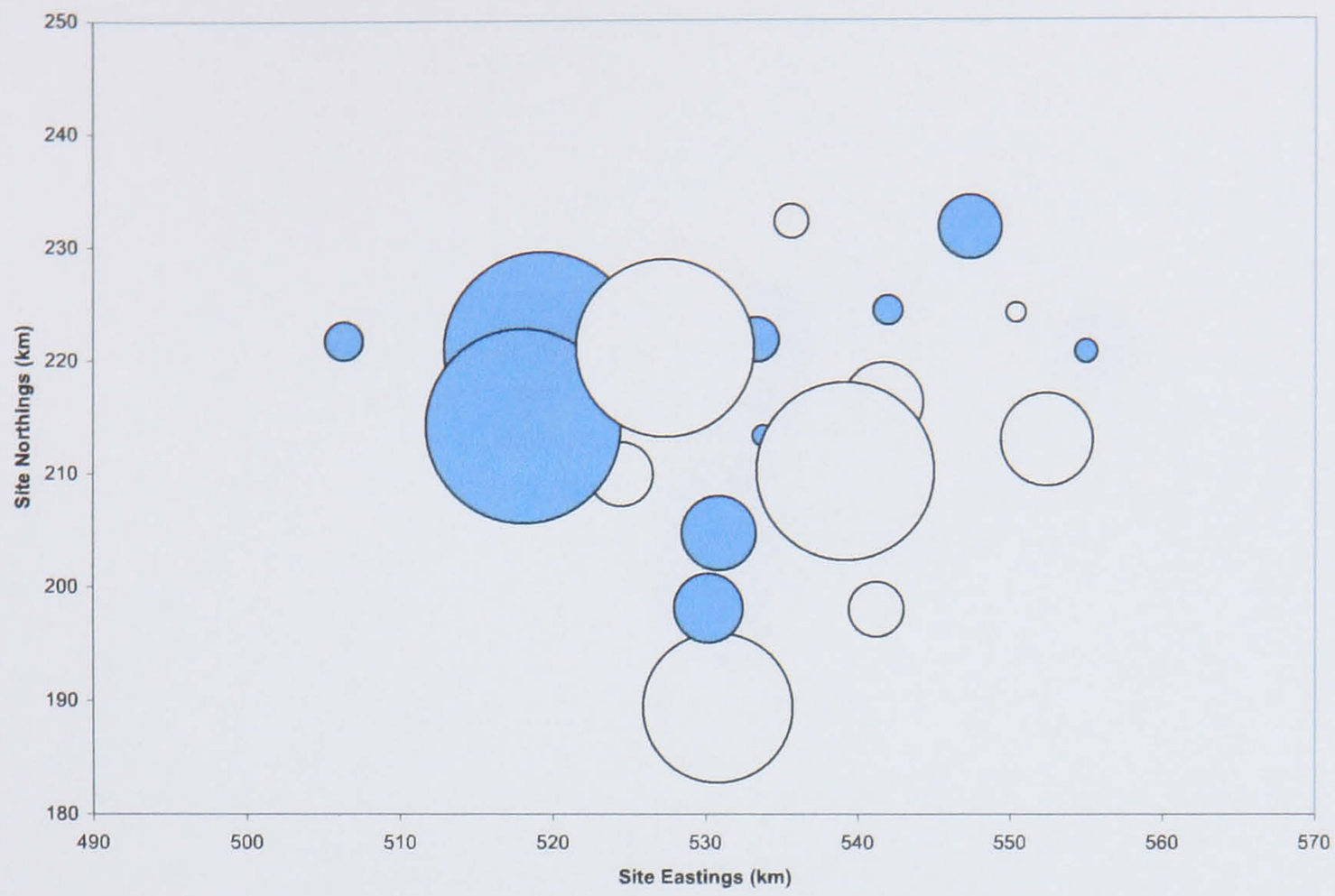

Figure 4.2 Bubble map showing mean Pearson residuals from fitted occurrence model at each site, prior to incorporation of site effects. Positive and negative mean residuals are represented in blue and white respectively. The diameter on the bubble map is proportional to the mean Pearson residuals.

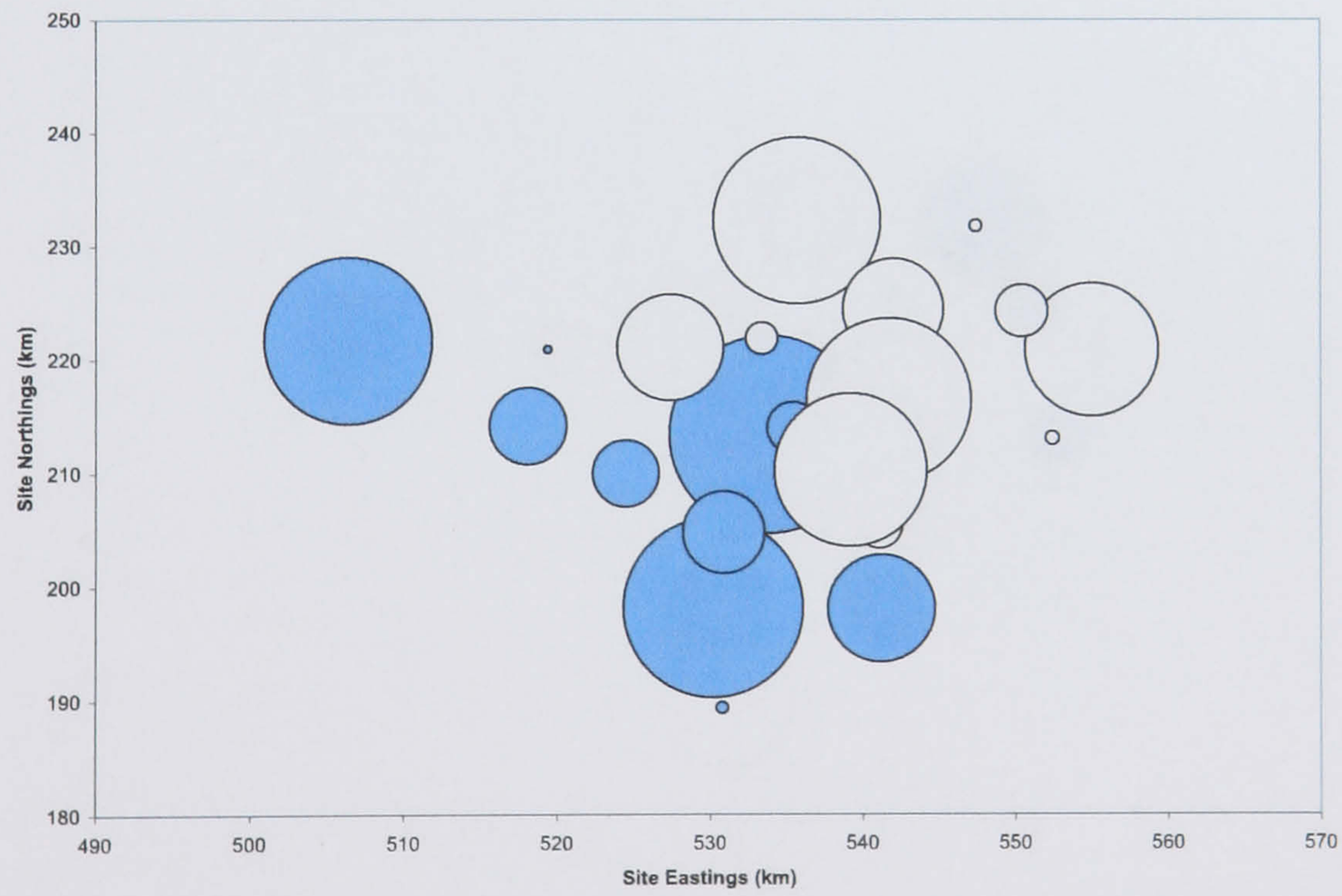

Figure 4.3 Bubble map showing mean Pearson residuals from fitted amounts model at each site, prior to incorporation of site effects. Positive and negative mean residuals are represented in blue and white respectively. The diameter on the bubble map is proportional to the mean Pearson residuals.

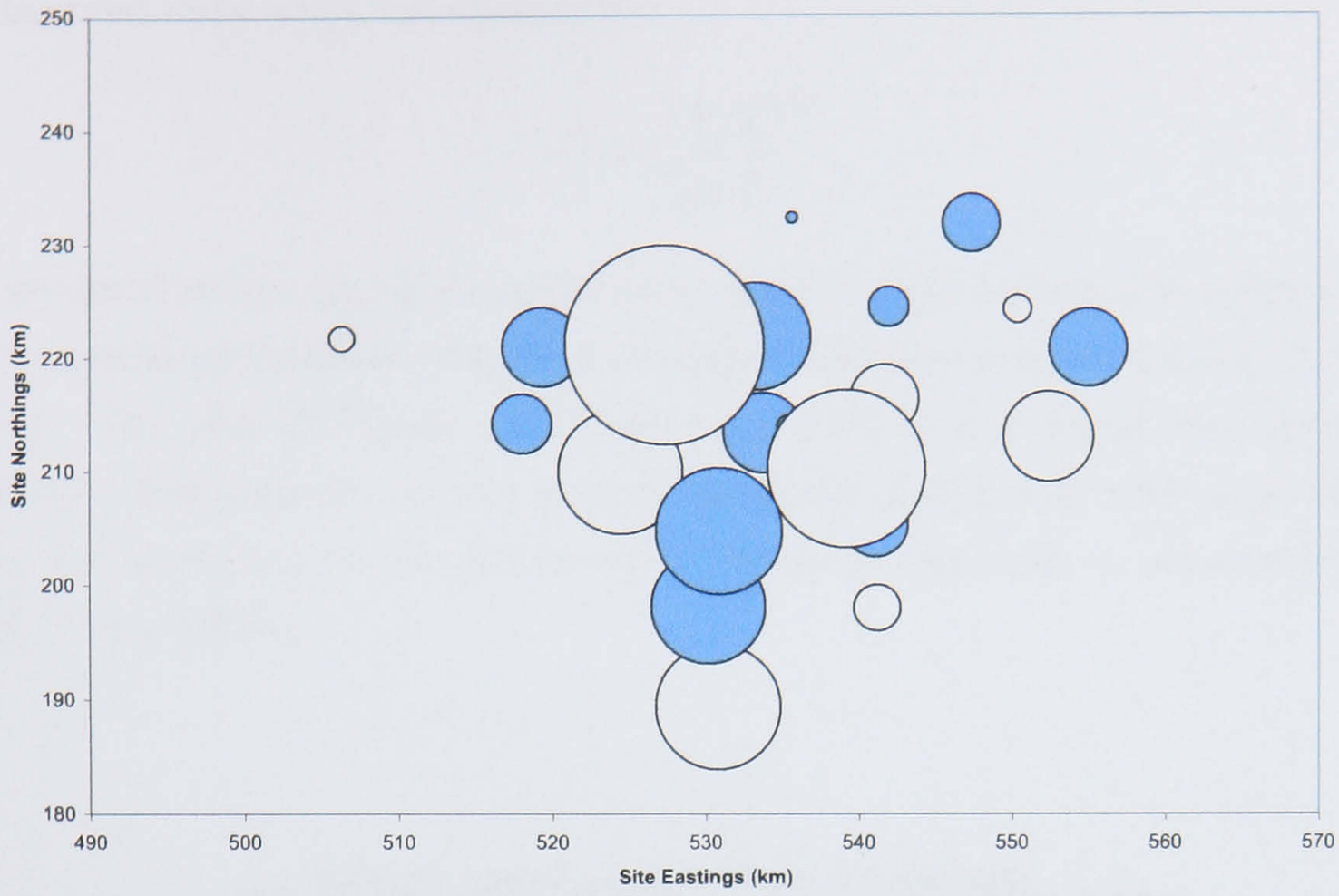

Figure 4.4 Bubble map showing mean residuals from fitted occurrence model at each site, after incorporation of site effects. Positive and negative mean residuals are represented in blue and white respectively. The diameter on the bubble map is proportional to the mean Pearson residuals.

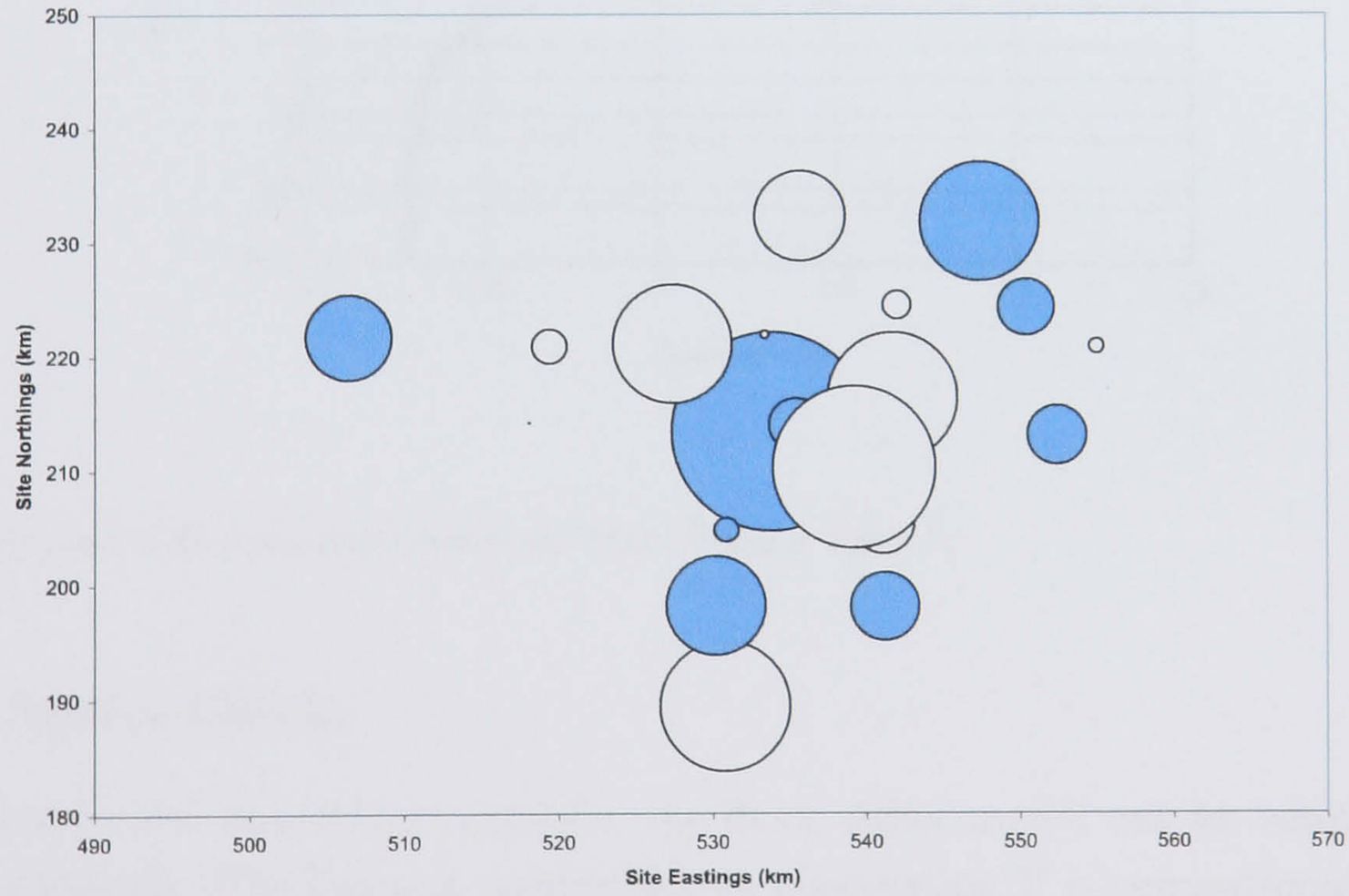

Figure 4.5 Bubble map showing mean Pearson residuals from fitted amounts model at each site, after incorporation of site effects. Positive and negative mean residuals are represented in blue and white respectively. The diameter on the bubble map is proportional to the mean Pearson residuals.

to the observed data, then the quantities:

$$r_i^A = \left(\frac{Y_i}{\mu_i}\right)^{1/3}, \tag{4.7}$$

called Anscombe residuals, all share the same normal distribution (Chandler and Wheater, 2002). A normal probability plot of Anscombe residuals can be used to check this assumptions. The plot in Figure 4.6 shows a good fit to a straight line, implying that the Anscombe residuals are almost exactly normally distributed over most of the range except in the lower tail of the distribution which corresponds to small rainfall values (Wheater et al., 2005b).

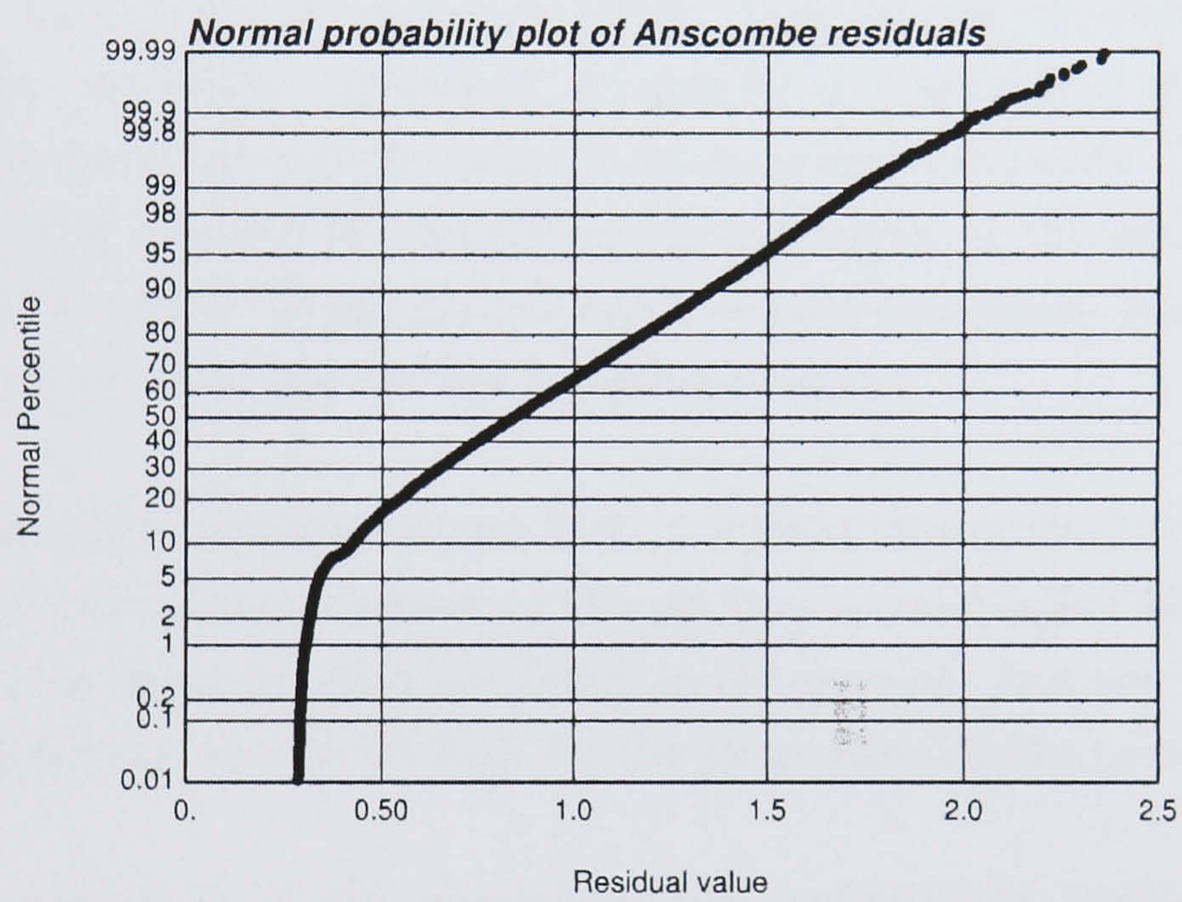

Figure 4.6 Anscombe residuals from amount models

4.3.4 Model Checks

In addition to the Anscombe residuals, the fit of either model can be assessed using Pearson residuals. The Pearson residual for an observation Y is proportional to:

$$\frac{Y - \mu}{\sigma} \tag{4.8}$$

where μ and σ are respectively the mean and standard deviation of Y under the fitted model. If the occurrence or amount model is correct, the Pearson residuals all come from distributions with zero mean and constant variance (Yang et al., 2005). The fit of

the model can be assessed by plotting summary statistics for mean residual measures over subgroups of observations. The 95% limits for this mean μ_ϵ are at $\mu_\epsilon \pm 1.96 s.e.(\overline{r})$, where $s.e.(\overline{r})$ is the standard error of the mean residuals (See expression of $s.e.(\overline{r})$ in Appendix D, Chandler (2002)). Figure 4.7 shows the residual plots calculated for each month, site and year for the occurrence and amounts models. The mean Pearson residuals lie within the 95% confidence interval (dashed lines) under the assumption that the model is correct. We conclude that the fitted models succeed in reproducing the seasonal and regional structure, along with trends in the rainfall sequences.

4.3.5 Simulation

The calibrated occurrence and amounts models are used simultaneously to produce rainfall sequences at multiple sites. One gauge (0106) has records stopping in 1994 and this site is not used in the simulation exercise. Conditioned on data from December 1990 to initialise the model, 40 sets of simulations are generated at 20 sites for the 1991-2002 period as these capture most of the sampling variability. The performance of the simulation is assessed by comparing the properties of the simulated sequences with the historical series. Summary statistics include the mean, standard deviation, proportion of dry periods, and the lag 1 autocorrelation.

At a typical site on the catchment (site 0160, 5 missing days), the results in Figure 4.8 shows that the observed series behave as though they were sampled from the simulated distributions. This indicates that the fitted model provides realistic simulations even though the simulations seem a bit high for the proportion of dry periods.

The multi-site properties of the simulations are evaluated by comparing the reproduction of the distribution of wet sites and the inter-site correlations between the GLM simulations and the observed series. Results are displayed for a subset of 20 (randomly chosen) simulations since this subset size is found to be representative of the sampling variability for these properties. Figure 4.9 shows that a spatial dependence structure defined by a beta-binomial distribution reproduces well the frequency distribution of number of wet sites.

Spatial dependence in rainfall amounts is modelled through the inter-site correlations between Anscombe residuals. Figure 4.10 presents some boxplots of pairwise correlations between raingauges versus distance (binned in 5 km intervals), both for observed and simulated at daily and hourly time-steps. There is a clear decay of the correlations with distance here; therefore the observed inter-site correlations have been used to drive the GLM simulations rather than using a constant correlation. To illustrate

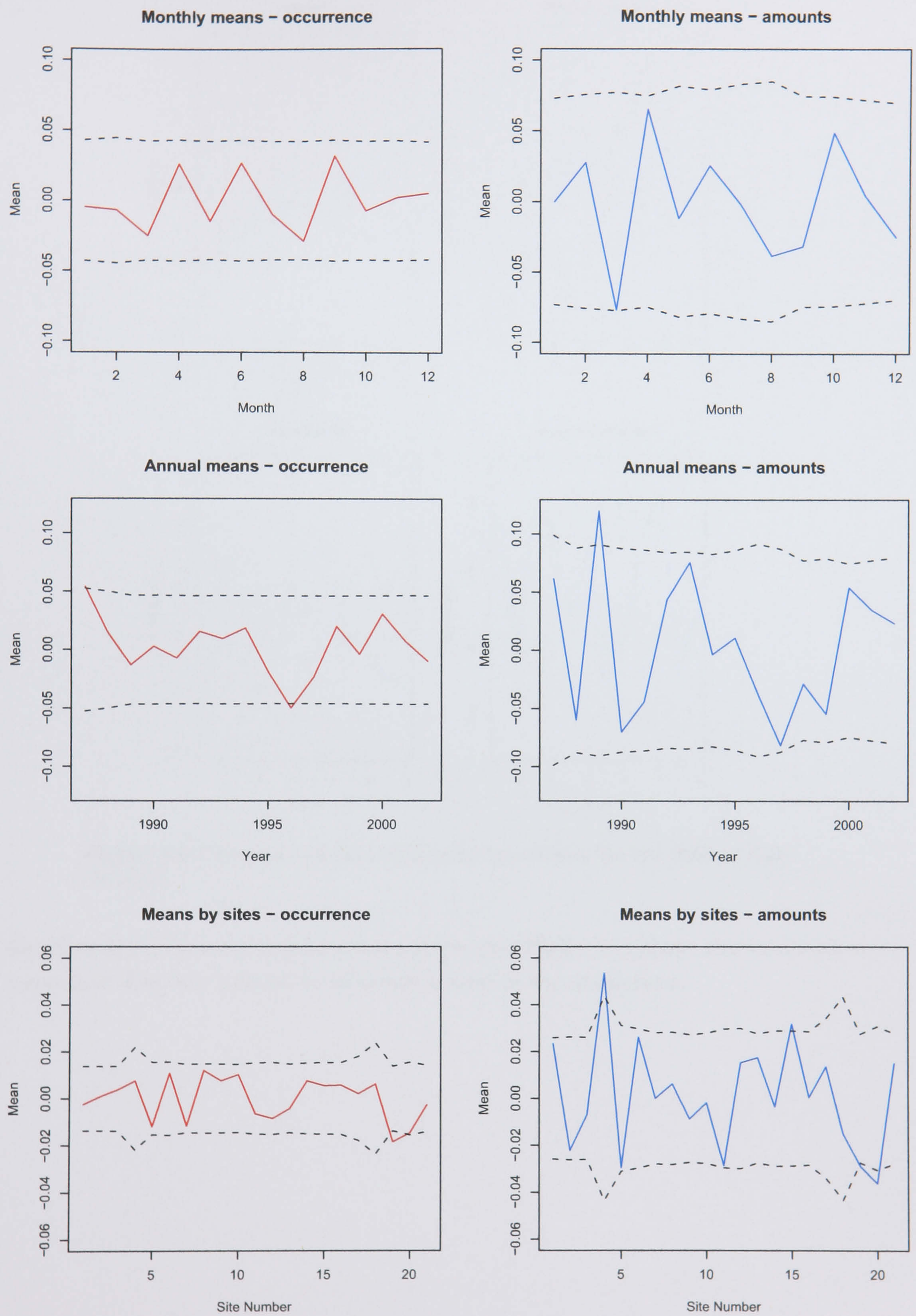

Figure 4.7 Mean Pearson residuals from occurrence and amount models

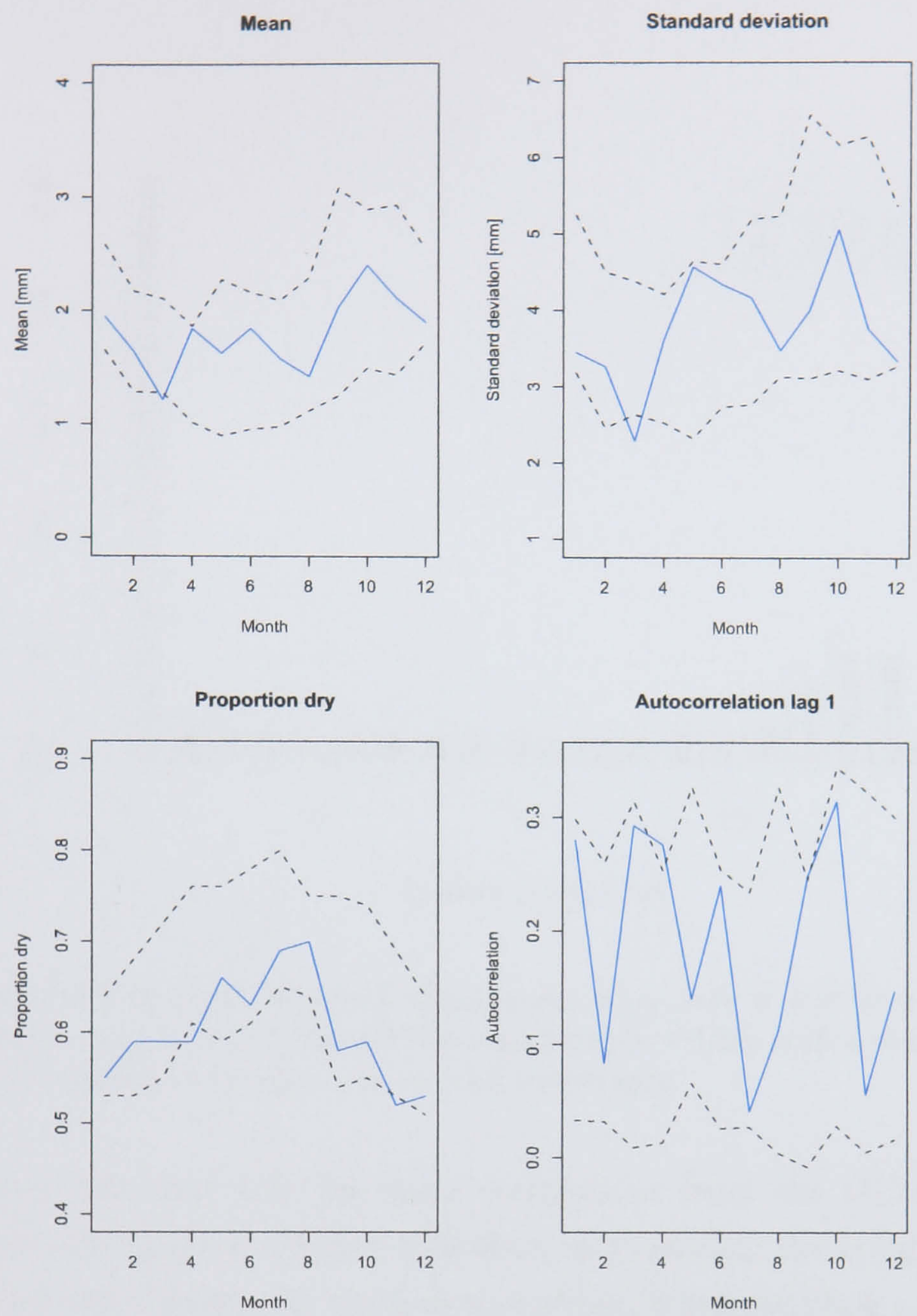

Figure 4.8 Observed and simulated monthly statistics for site 0160 at daily time-step

the effect of the choice of correlation structure here, Figure 4.11 shows the results when a constant inter-site correlation structure is used in the simulations.

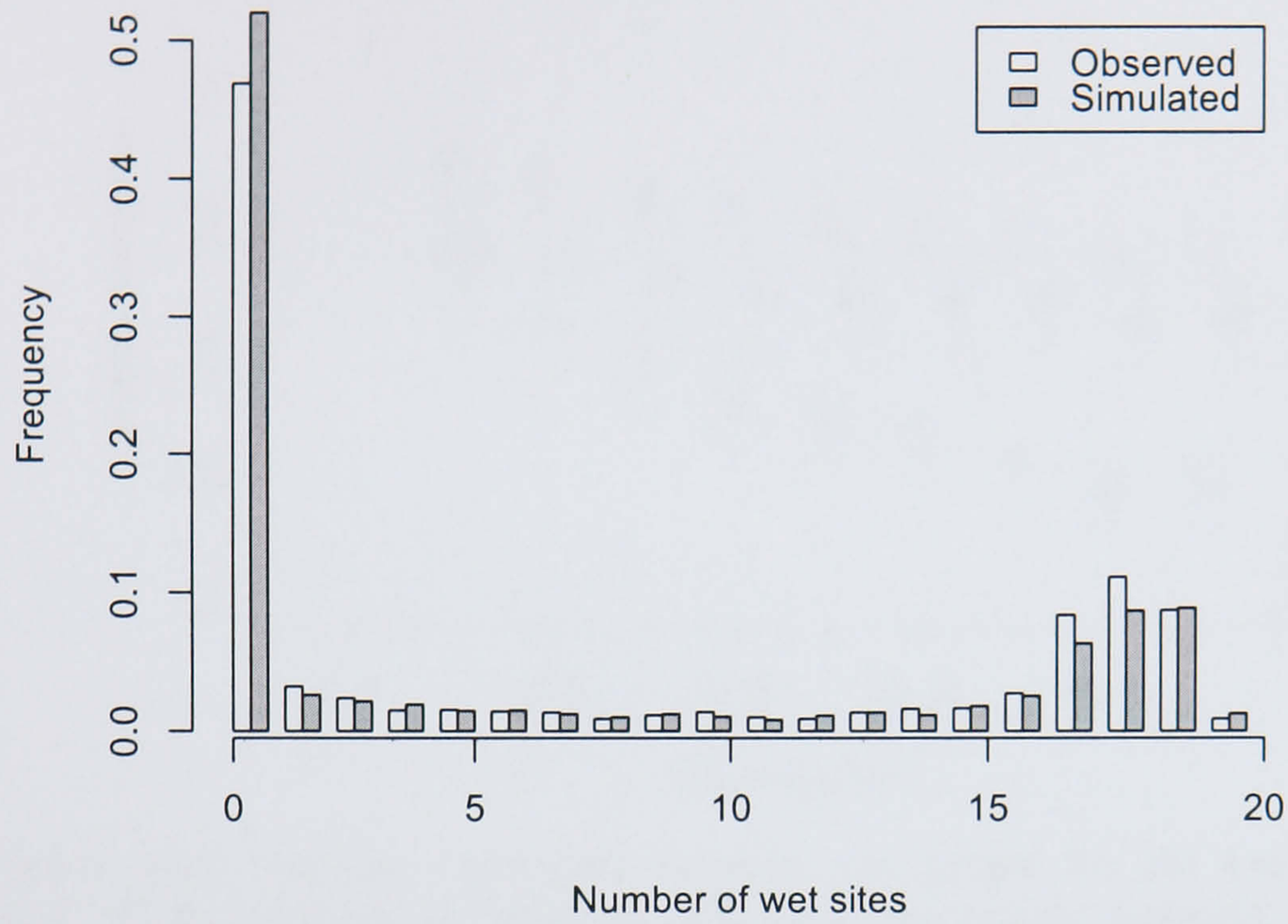

Figure 4.9 Observed frequency distribution of number of wet sites in the Lee catchment, together with distribution simulated by GLMs with a beta-binomial model for spatial dependence in rainfall occurrence.

In both Figures 4.10 and 4.11 the daily correlations from the GLM simulations are underestimated but those in Figure 4.10 show very similar decaying structure to the observed spatial correlations. As we shall see further, when applying a spatially uniform temporal disaggregation, the simulated daily correlation is transferred directly to the hourly level and overestimates the observed hourly correlations. This is one of the limitations of the proposed scheme; the extent to which this is important with respect to the extremal behaviour is evaluated further below.

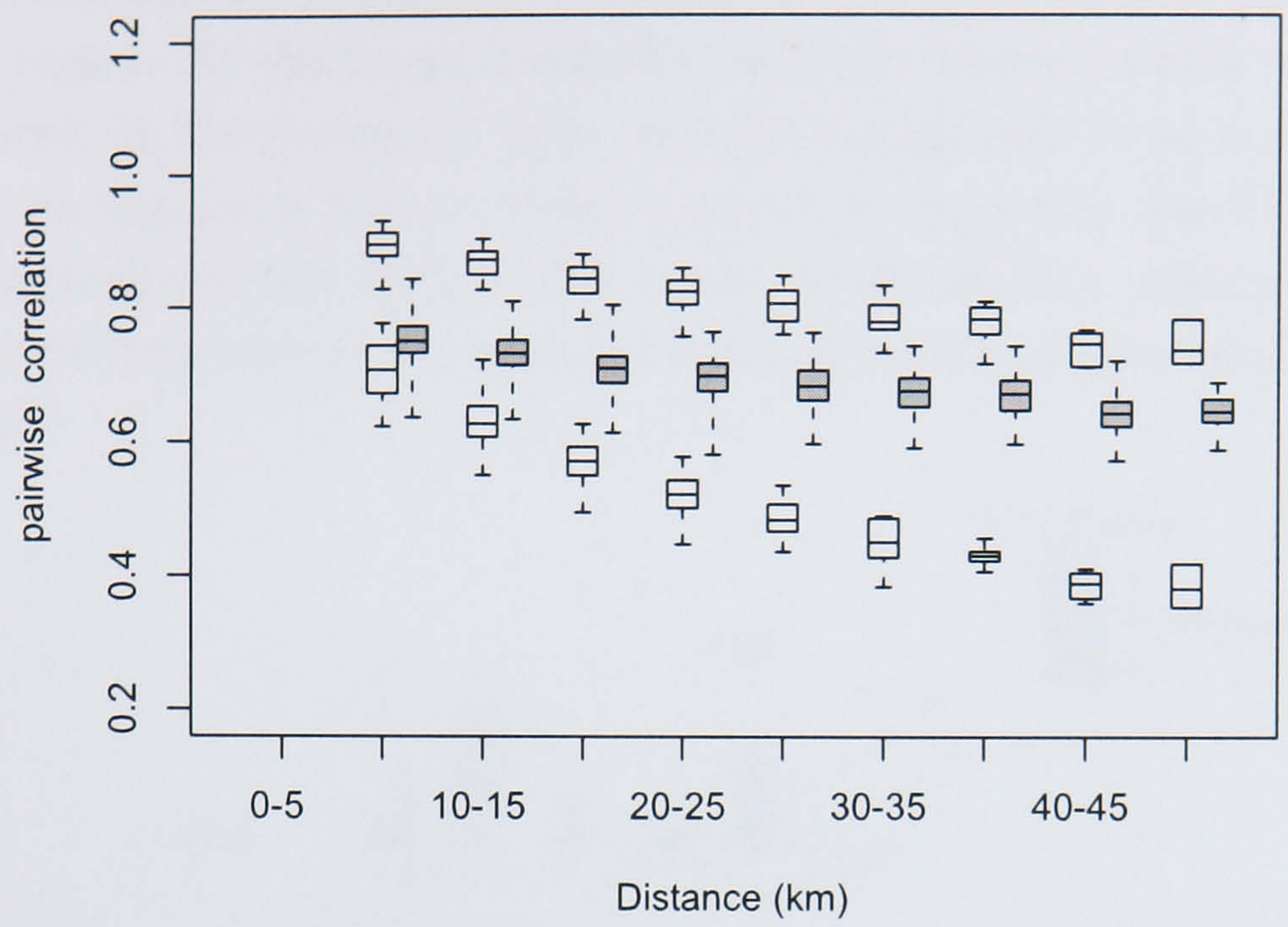

Figure 4.10 Pairwise correlation between rain gauges for the Lee catchment. White box-plots are observed daily (top) and hourly (bottom) correlations, Grey box-plots are the results from simulations with observed inter-site Anscombe residual correlations in rainfall amounts. The box-plots represent the median, 25 and 75% quantiles, the whiskers extend to the extreme values

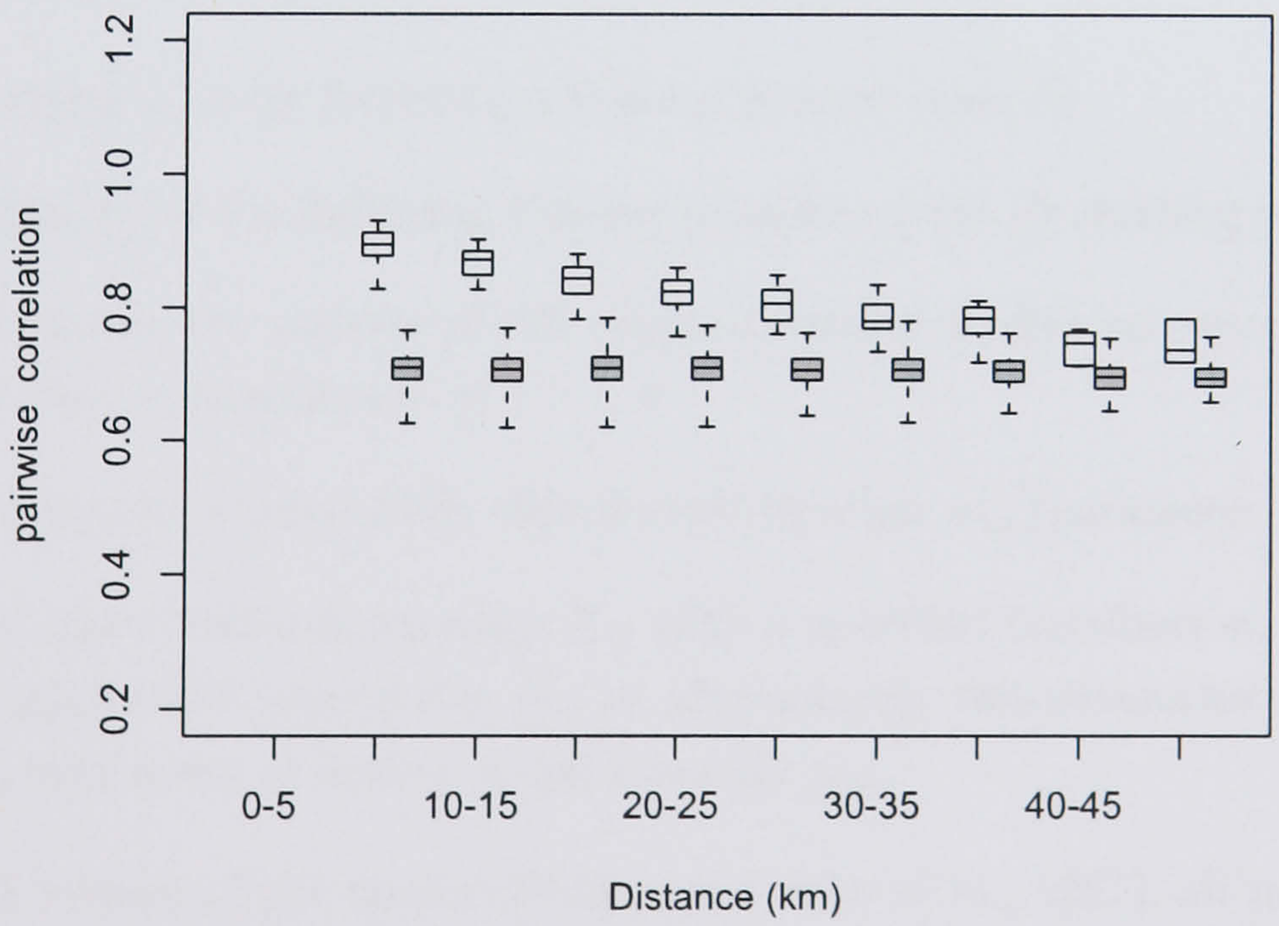

Figure 4.11 Daily pairwise correlation between rain gauges for the Lee catchment. White are observed and Grey are the results from simulations with constant inter-site Anscombe residual correlation in rainfall amounts.

4.4 Single-site Disaggregation

The GLM can simulate daily rainfall at various sites, or indeed at any location within the modelled region. At this stage, a model to generate hourly rainfall at the master gauge is required. In the literature, many variants of single-site Poisson cluster model are presented; an important feature is their capacity to generate rainfall in *continuous time*. The single-site model used in this study, is the random parameter Bartlett-Lewis model with 2-parameter cell intensity distribution whose schematic can be seen in Figure 4.12.

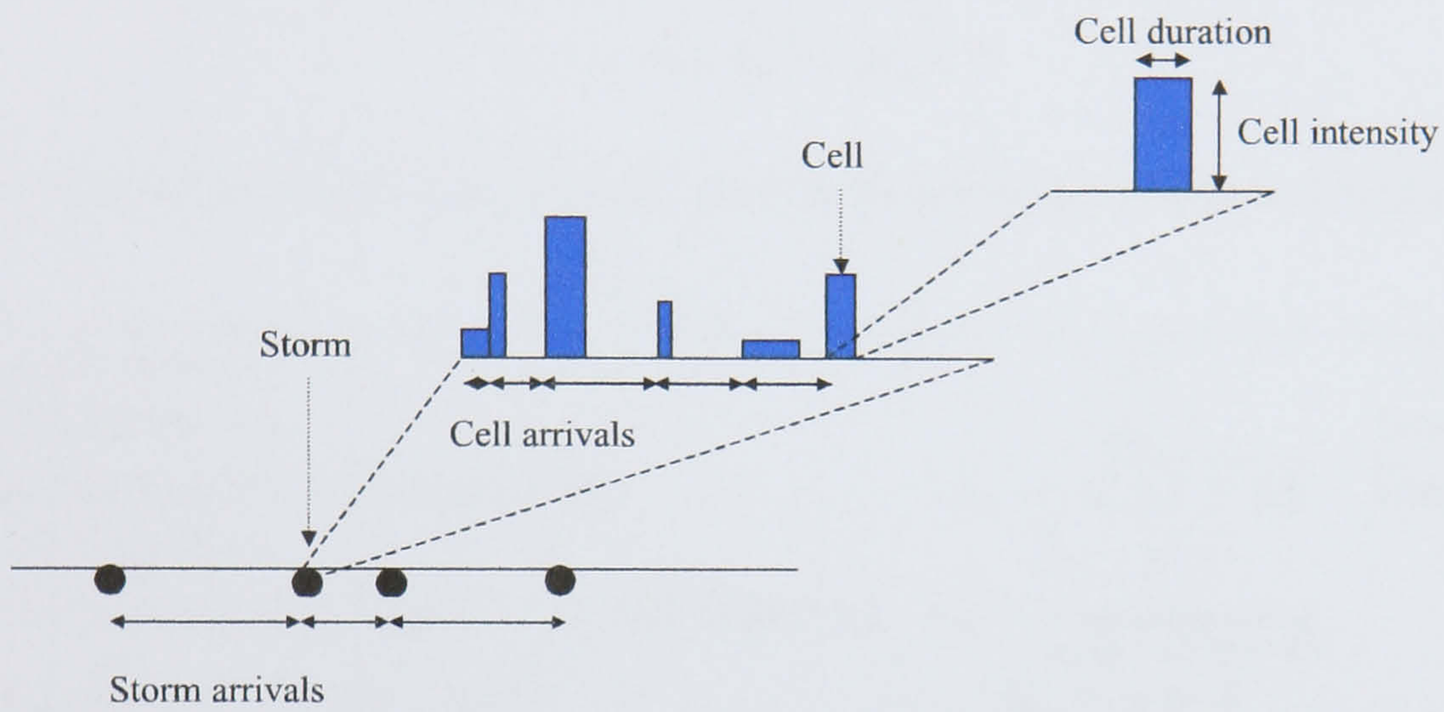

Figure 4.12 Schematic of the BLRPM (Adapted from Wheater et al. (2005a))

The general assumptions of the Bartlett-Lewis Rectangular Pulse Model (BLRPM) are (Onof et al., 2000):

- Storm origins t_i occur following a Poisson process (rate λ)
- Cell origins t_{ij} arrive following Poisson processes (rate β) starting at each t_i
- For each storm, the process of cell origins terminates after an exponentially distributed time v_i (parameter γ)
- Each cell has an exponentially distributed duration w_{ij} (parameter η)
- Each cell has a uniform intensity X_{ij} with a specified distribution, typically assumed exponential (parameter $\frac{1}{\mu_x}$) or alternatively two-parameter gamma with mean μ_x and mean of square of cell intensity μ_{x^2}.

In the original version of the model (Rodriguez-Iturbe et al., 1987), all model parameters are assumed constant. However it has been observed that the model does not provide a satisfactory reproduction of dry periods. Therefore a greater diversity of the internal wet-dry structures of storms was introduced (Rodriguez-Iturbe et al., 1988).

The cell duration parameter η is randomly varied from storm to storm with a gamma distribution with shape parameter α and scale parameter ν. Hence, parameters β and γ also vary so that the ratios $\kappa = \frac{\beta}{\eta}$ and $\phi = \frac{\gamma}{\eta}$ are constant. Subsequently a 7 parameter model (Onof, 2003) is obtained, characterised by the following set of parameters:

$$\{\lambda, \mu_x, \mu_{x^2}, \alpha, \nu, \kappa, \phi\}$$

or using more physically meaningful (mechanistic) parameters:

$$\{\lambda, \mu_x, \sigma_x, \delta_c, \sigma_c, \mu_c, \delta_s\}$$

where the relationships between original and mechanistic parameters are given in table 4.3.

Storm arrival rate	λ	(hr^{-1})
Mean cell intensity	μ_x	$(mm.hr^{-1})$
Standard deviation of cell intensity	$\sigma_x = \sqrt{\mu_{x^2} - \mu_x^2}$	$(mm.hr^{-1})$
Mean cell duration	$\delta_c = \frac{\nu}{\alpha-1}$	(hr)
Inter-storm standard deviation of cell duration	$\sigma_c = \frac{\nu}{\sqrt{(\alpha-1)^2(\alpha-2)}}$	(hr)
Mean number of cells per storm	$\mu_c = 1 + \frac{\kappa}{\phi}$	
Mean duration of storm activity	$\delta_s = \frac{\nu}{(\alpha-1)\phi}$	(hr)

Table 4.3 Relationship between model and mechanistic parameters

4.4.1 Fitting of the BLRPM

Calibrating the BLRPM model is an essential part of the modelling process and affects the performance of the resulting model. The single-site model is continuous in time; however to account for seasonality, the fitting is performed for each month separately. Standard statistical techniques such as Maximum Likelihood estimation cannot be used here, because the complex dependencies in the model prohibit the formulation of a likelihood function.

Fitting is therefore carried out using a Generalised Method of Moments. Weights are introduced so that more importance can be given to certain features. This involves minimising an objective function (Lekkas, 2002) given in equation 4.9:

$$g(\theta) = \sum_{i=1}^{n} w_i(\Phi_i(\theta) - M_i)^2 \tag{4.9}$$

where $\theta = (\theta_1, \theta_2, ..., \theta_7)$ is the set of unknown parameters, w_i represents the weights, M_i the historical statistics of the data, and Φ_i the theoretical model properties as a function of θ.

In this investigation the Shuffled Complex Evolutionary (SCE-UA) algorithm is used as an optimisation tool for parameter estimation. First applied by Duan et al. (1992), it has been widely applied in the hydrological literature (e.g. Ajami et al. (2004); Brath et al. (2004)). The main steps of the algorithm can be summarised as follows:

1. A population of s parameter sets is sampled randomly from the n-dimensional feasible parameter space

2. The population is ranked from best to worst using an objective function (in this case Equation (8)), and then partitioned into p communities referred to as "complexes", each containing m ($m = 2n + 1$) parameter sets

3. Each complex is evolved independently using the deterministic downhill simplex method of Nelder and Mead (1965).The Nelder-Mead method is a direct optimisation search based on evaluating a function at the vertices of a simplex (a geometrical figure in n dimension with $n + 1$ vertices). The selection of the simplex parameter sets is selected based on a probability distribution which favours parameter sets producing a better value of the objective function.

4. Shuffling step: the parameters of each evolved complex are regrouped, to ensure information is shared

5. The population of parameter sets is then ranked again and new complexes are formed. The evolution step or iteration, is repeated and this continues until convergence criteria are satisfied

By incorparating elements of global search, the method is less prone to converge towards a local optimum than methods based on deterministic searches alone (eg. Newton-Raphson). However, the parameter set to which the algorithm converges may still be sensitive to the choice of the initial parameter values.

The combination of statistics to be included in the objective function is an open-ended problem. The standard statistics usually incorporated are the mean, variance and lag 1 autocovariance of rainfall intensities at time-scale of 1 hour and multiples thereof (Onof and Lekkas, 2003). The reproduction of the wet-dry structure of the rainfall (i.e. intermittency of precipitation) suggests the inclusion of the proportion of dry periods at the same scales. Other statistics that have been included successfully in the estimation procedure involve the variance function which describes the variance of rainfall

intensity as a function of scale (Bo et al., 1994); and the skewness of rainfall intensities (Cowpertwait, 1998).

The master gauge is chosen to run the disaggregation scheme because of its central location in the Lee catchment and its continuous record length for the period 1990-2002 with few missing values. Several combinations were tested. The statistics that gave best results in terms of minimising the fit between the expected and observed properties are the Mean; 1-hour Variance; 6-hour Variance; 24-hour Variance; 1-hour Autocovariance; 1-hour Proportion of dry periods and 24-hour Proportion of dry periods. Best results were obtained using the inverse of the squared historical values as weights.

Initially, for a few months, storms with only one cell were repeatedly generated. In order to obtain more realistic storms, some boundaries constraining the range of model parameters were defined as shown in Table 4.4. In particular to ensure that storms with more than one cell are produced (i.e. $\mu_c = 1 + \frac{\kappa}{\phi} > 1$), the lower boundary for κ was set to 0.01 so that κ does not become too small, and the upper boundary for ϕ was set to 1 to prevent too large a value of ϕ. An upper boundary on λ was set so that up to five storms per hour could be generated. Finally, the monthly parameters selected are given in Table 4.5.

Parameter	Lower bound	Upper bound
λ	0.00001	0.18
μ_x	0.00010	20.00
α	2.00001	20.00
ν	0.00001	20.00
κ	0.01000	10.00
ϕ	0.00001	1.00
σ_x	0.00001	10.00

Table 4.4 Constraints imposed on parameters for fitting to data from site 0163

4.4.2 Disaggregation using HYETOS

Once the single-site parameters are obtained they can be input to the HYETOS single-site disaggregation model (Koutsoyiannis and Onof, 2000). Given a sequence of daily rainfall from the GLMs, several runs from the Bartlett-Lewis model are performed separately for each cluster of wet days. This continues until the sequence of simulated daily depths matches the sequence of daily totals from the GLM within a tolerance

Month	λ (hr^{-1})	μ_x (mm/hr)	α	ν (hr)	κ	ϕ	σ_x (mm/hr)	OF
1	0.03180	1.44480	6.45502	3.48998	0.24764	0.15963	0.66352	6.48E-09
2	0.03088	0.97155	3.70047	1.59769	0.65262	0.21727	0.67948	6.43E-07
3	0.02114	1.25618	4.59485	2.43372	0.22869	0.12865	0.35678	9.44E-07
4	0.02374	1.27010	7.29332	1.26043	0.59964	0.04839	1.34963	2.04E-06
5	0.01829	1.72448	6.38034	0.28931	0.69754	0.02120	4.20670	1.31E-05
6	0.01915	6.58788	3.95294	0.34049	0.14794	0.03947	2.31878	4.53E-06
7	0.01752	1.92690	7.72351	1.20251	1.08564	0.11288	4.45936	7.81E-06
8	0.01666	4.98179	10.60813	1.54685	0.35758	0.10102	3.06124	2.60E-06
9	0.02385	1.14486	10.00757	2.89612	0.88906	0.09982	1.67808	3.83E-06
10	0.02591	1.72476	2.98359	0.22083	0.65200	0.03766	2.21018	2.77E-05
11	0.03227	0.94980	3.74207	0.53414	0.68891	0.04996	1.39419	1.59E-05
12	0.03686	0.95697	4.21056	0.97753	0.74226	0.12601	0.73860	7.46E-11

Table 4.5 Estimated BLRPM parameters for site 0163 (OF: value of the objective function)

distance d, defined as

$$d = \left[\sum_{i=1}^{L} ln^2 \left(\frac{Y_{Mi} + c}{\widetilde{Y}_{Mi} + c} \right) \right]^{\frac{1}{2}} \tag{4.10}$$

where Y_{Mi} and $\widetilde{Y}_{Mi}$ are respectively the original and simulated daily totals at the master gauge, L the sequence of wet days, c is a small constant (set to 0.1 mm). An empirical correction procedure referred to as "adjustment" (Koutsoyiannis and Onof, 2001) is then performed so that the hourly synthetic series generated by the Bartlett-Lewis model is modified for consistency with the given daily series. Koutsoyiannis and Onof (2001) used the proportional adjusting procedure to modify the initially generated hourly series $\widetilde{H_M}$ to obtain the hourly series H_M according to:

$$H_{Mj} = \widetilde{H}_{Mj} \times \frac{Y_M}{\widetilde{Y}_M}, \; j = 1, \ldots, 24 \tag{4.11}$$

Four levels of repetition are incorporated to minimise the error in the cumulative hourly rainfall with respect to the given daily totals so that the bias is minimised in all statistics that are to be preserved. The details of the scheme can be found in Figure 4.13.

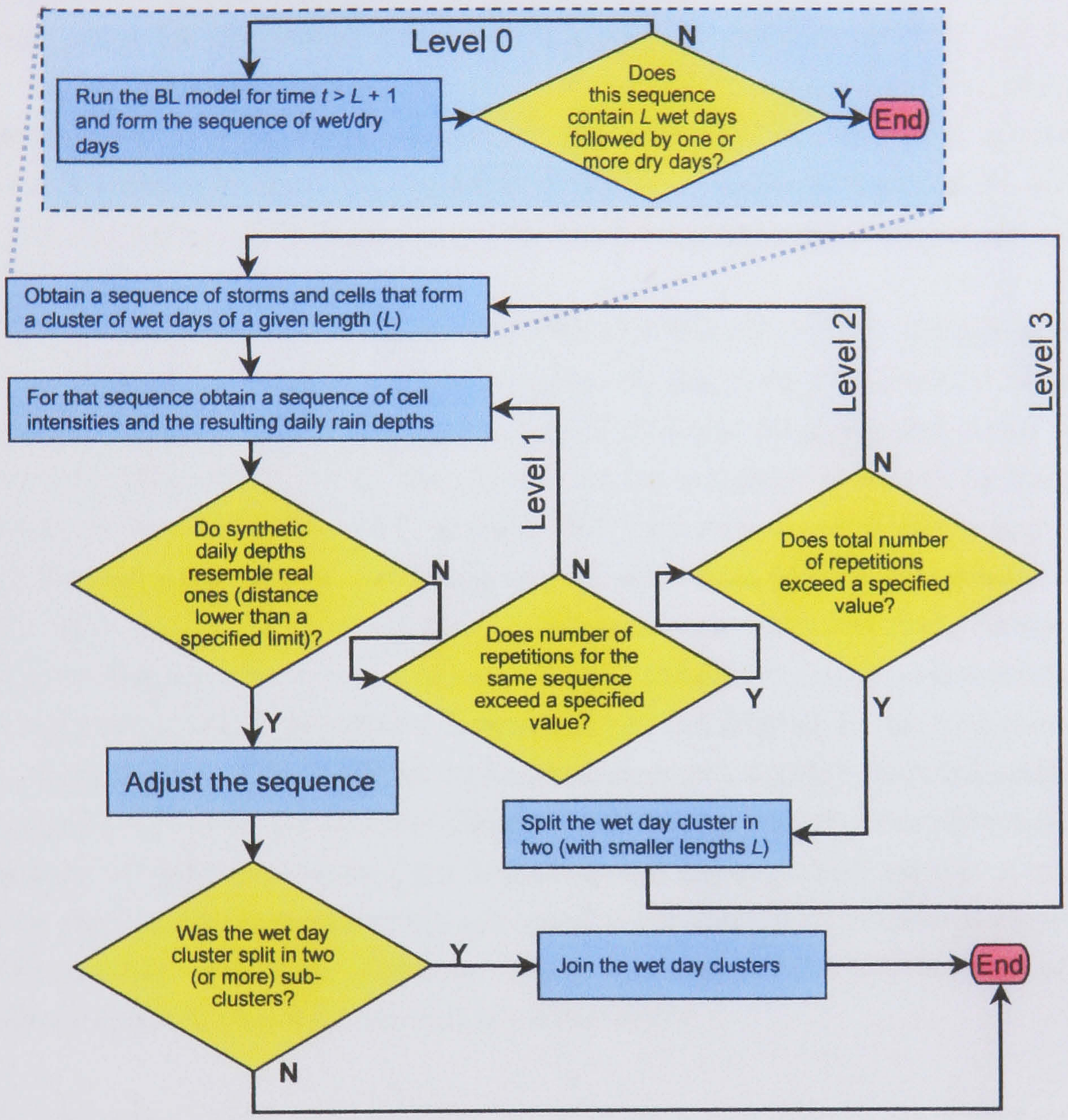

Figure 4.13 Flow diagram of the repetition scheme used in Hyetos, BL stands for Bartlett-Lewis model. (Source: Koutsoyiannis and Onof, 2001)

4.4.3 Preliminary Results

To investigate the performance of the single-site disaggregation scheme, the theoretical values of various summary statistics were calculated under the fitted BLRPM (the analytical expressions of the properties can be found in Onof, 2003) and compared with the values obtained by applying the disaggregation procedure to real daily data from the master gauge for the period 1990-2002. A sensitivity analysis was conducted to assess the impact of the convergence criterion on the iterative sampling procedure. Koutsoyiannis and Onof (2001) recommend a value of 0.1 for the tolerance. Various values around 0.1 were tested, but no significant difference could be observed when changing the allowed distance between 0.01 and 0.5; hence the suggested tolerance of 0.1 was kept.

Figure 4.14 compares the historical, BLRPM fitted (expected) and disaggregated values of some hourly statistics at the master gauge for the period 1990-2002. A reasonable agreement is observed between the historical and the disaggregated series using the previously fitted parameters. An increase in the standard deviation by 0.04 mm on average for the whole year (i.e. around 10%) is however noted and is partly due to the adjusting procedure in the disaggregation algorithm. Indeed, the simulated hourly series from the BLRPM is modified to be consistent with the daily totals but this also increases the bias in the variance. The optimal set of parameters overestimates the proportion of dry periods in January, June and August by an increment of 0.02 (i.e. around 2%). The temporal autocorrelations are slightly underestimated with a discrepancy of 0.035 between the historical and disaggregated series; about half of this difference is observed between the historical and the expected values. A refinement can be obtained in retaining single-site parameters that fit better the autocorrelations in October and November where the largest discrepancy of 0.1 (i.e. around 20%) is observed between the expected and historical series.

Only 13 years of data were available to calibrate the model at the master gauge and the fitting showed some sensitivity when recalibrating the model to 12 years of data. Therefore it seems that provided the model were calibrated to a longer time period (Wheater et al. (2005b) suggest at least 15 years to calibrate the single-site model), the reproduction of the statistics would improve. Therefore given that only 13 years of data are available, the results are considered as satisfactory and the optimal parameter set is selected to pursue this investigation.

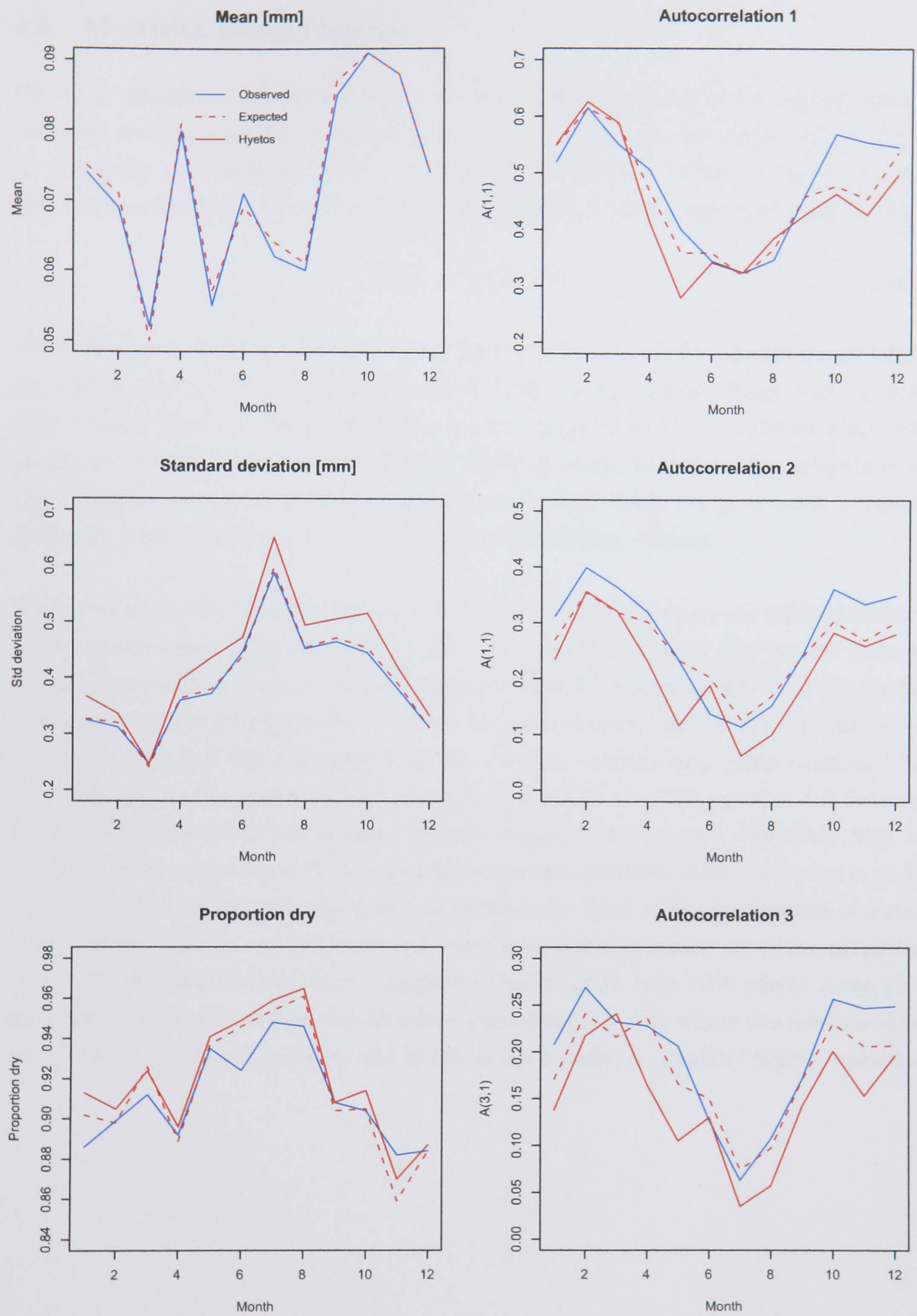

Figure 4.14 Impact of the disaggregation scheme on properties of hourly rainfall at the master gauge. In each plot the blue line represents observed properties; the dashed red line represents the theoretical properties from a BLRPM fitted to the data (Expected); and the solid red line represents the properties after applying the HYETOS disaggregation scheme (Hyetos).

4.5 Multisite Disaggregation

Once the disaggregation model is run to obtain sub-daily data at the master gauge, a standard temporal profile is defined as the hourly rainfall at the master gauge divided by the daily total rainfall. The temporal profile is then applied to each gauge by multiplying the standard profile by the total rainfall at that gauge according to (4.12).

$$H_{Sj} = \frac{H_{Mj}}{Y_M} \times Y_S \tag{4.12}$$

where H_{Sj} is the hourly profile at hour j for gauge S, H_{Mj} is the master gauge rainfall amount at hour j, Y_M is the daily rainfall depth at the master gauge and Y_S is the daily rainfall depth for gauge S. If the master gauge records zero rainfall while other gauges record non-zero daily intensity, an artificial profile is used to disaggregate at the other gauges. So far the analysis has been carried out using the previously computed profile at a site, but there is scope for refinement of this strategy.

A data analysis of 16 events, taken at different times of the year and representative of most rainfall types, was undertaken. For the majority of them, the results from applying a spatially-uniform temporal disaggregation are encouraging. Two contrasting events are used to illustrate the method. Using real data, the standard profile of the master gauge (site 0163) is applied to the satellite stations and some simulated and observed profiles are presented in Figures 4.15 and 4.16. For the event of 3rd February 1990 (daily mean of 13 raingauges: 24 mm, range: 17.8-28.6 mm, duration: 9h), the modelled data reproduce well the observed series except at site 0101. This site is on the edge of the Lee catchment, and this may indicate the limit of the application of a standard profile. This is representative of usual model performance: however exceptions exist. An example is the intense summer event of 23rd July 1996 (daily mean of 19 raingauges: 20.8 mm, range: 1.4-53.2 mm, core duration: 4h) where the method shows some limitations (see sites 0101 and 0110) as the rainfall is spatially highly variable.

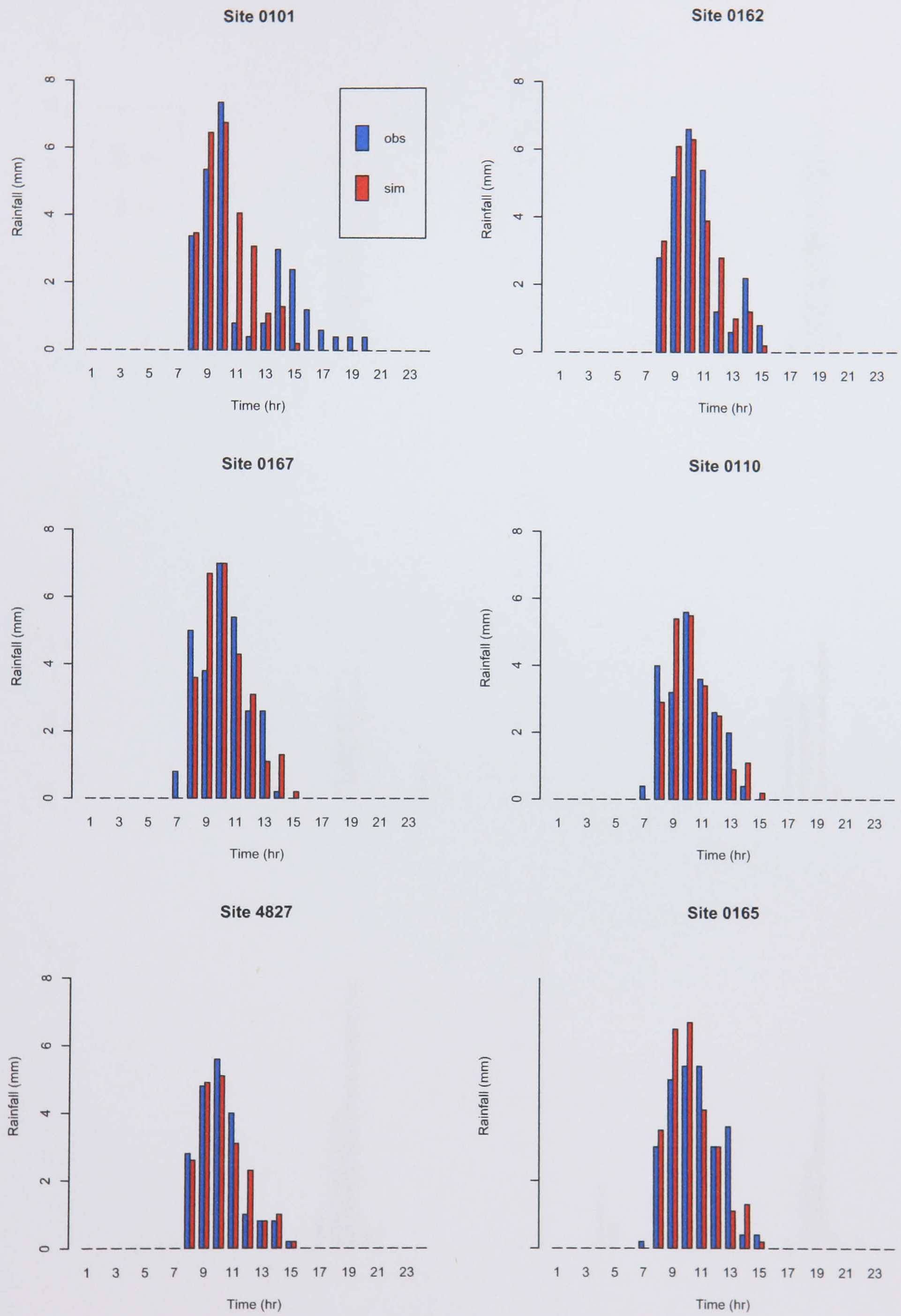

Figure 4.15 Event of 03/02/90 - Applying the observed profile of the master gauge to the satellite gauges

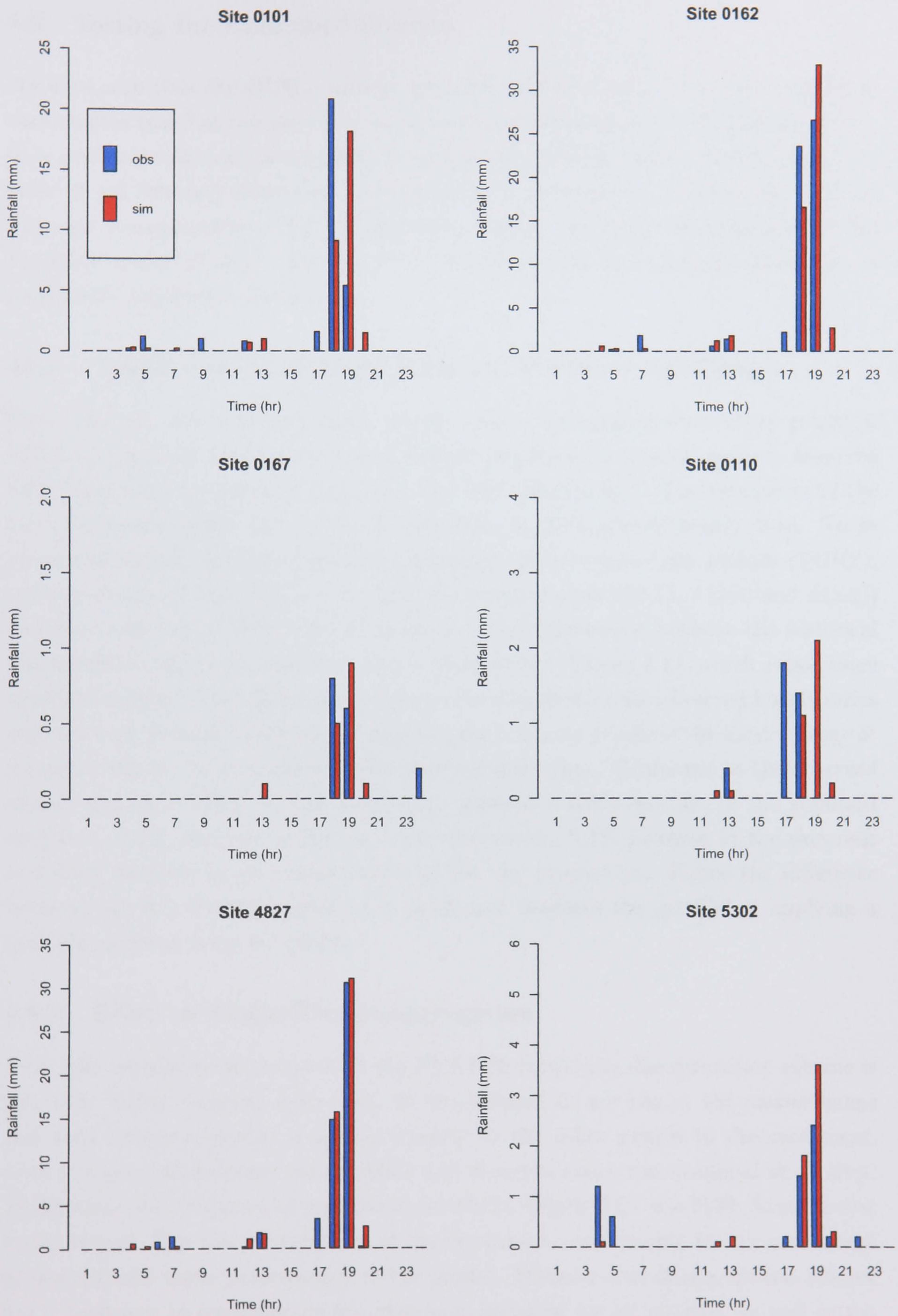

Figure 4.16 Event of 23/07/96 - Applying the observed profile of the master gauge to the satellite gauges

4.6 Testing the Combined Scheme

We have seen that the GLM is able to generate realistic sequences of daily rainfall at various sites and that the joint Poisson-cluster model together with the adjusting procedure performs well in simulating hourly rainfall at the master gauge. The representative event of 3rd February illustrates successfully the implementation of a spatially-uniform temporal disaggregation. The next step is to evaluate the temporal disaggregation for the whole period of study. Further, these models need to be tested in combination to assess their simulation performance.

4.6.1 Application of a Single Temporal Profile at All Gauges

First, the use of a temporal profile at one gauge to disaggregate at other gauges is tested by applying the observed hourly profile data from the master gauge to observed daily data from the satellite gauges for the 1991-2002 period. The properties of the resulting hourly series are compared with those of the observed hourly data. These properties include the mean, standard deviation, proportion of dry periods (PDRY), autocorrelation at lags 1, 2 and 3 hours (also referred to as A(1,1), A(2,1) and A(3,1)) and the coefficient of skewness. At all sites, a close agreement between the historical and modelled series was observed. This is illustrated in Figure 4.17, which shows some specimen results for site 0160 and compares the statistics for the observed hourly series with the ones obtained when simply applying the temporal profile of the master gauge at a typical site on the catchment to the observed daily data. Compared to the observed values, and on average for the whole year, there is a 0.4% increase in the standard deviation, 3.4% decrease in the lag 1 autocorrelation, 1.1% increase in the skewness and 0.2% decrease in the reproduction of the dry proportion. Hence the difference between the two series of statistics is small and validates the method of applying a spatially-uniform temporal profile.

4.6.2 Effect of Single-Site Disaggregation

Next, the variability introduced by the HYETOS single-site disaggregation scheme is assessed. Using observed daily data, 20 disaggregations are run at the master gauge and each temporal profile is applied linearly to the other gauges in the catchment. Overall a good fit between the modelled and observed series was obtained at all sites. To illustrate this, Figure 4.18 presents the statistics obtained for site 0160. In particular it can be seen that the reproduction of the skewness is encouraging for the assessment of the extreme value performance of the model. However the disaggregation scheme has a tendency to overestimate the standard deviation for all months, as well as the proportion of dry periods for the summer months and to underestimate the autocor-

relations. These features were already in evidence when fitting the BLRPM. Taking the mean statistics from the 20 disaggregations, we have a 14% increase in standard deviation, 15% decrease in lag 1 autocorrelation, 5.6% increase in skewness and 1.4% increase in the proportion of dry periods. Hence the disaggregation scheme compares well with the observed statistics even though it introduces some bias.

4.6.3 Effect of GLM Simulations

To assess the effect of using GLM simulations instead of actual daily sequences, 20 GLM simulations are generated for the period 1991-2002 at 20 sites and combined with the disaggregation scheme. The results show good agreement between the observed and modelled series, although the overestimation of the standard deviation and proportion of dry periods is still present. The envelope generated from the 20 simulations is represented in Figure 4.19. On average for the 20 simulations, the mean is well represented throughout the year with a 0.3% increase compared to the historical values. In total, we also observe a 24% increase in the standard deviation, 18% decrease in the lag 1 autocorrelation, 1.5% decrease in skewness and 2.6% increase in the proportion of dry periods.

Finally, the effect of using the GLM-disaggregation method at sites not used in the model fitting is also displayed in Figure 4.19 (dotted lines). In this case, the GLM model is recalibrated to 19 gauges on the catchment (exclusion of sites 0160 and 0106), daily data are simulated at site 0160 and the combined scheme is run. Similar features in the reproduction of the statistics are observed compared to the case where all gauges were used to fit the GLM. The results are promising and, provided that a site is surrounded by a few rain gauges, the combined scheme has the potential to simulate hourly rainfall information at a location where no data are available.

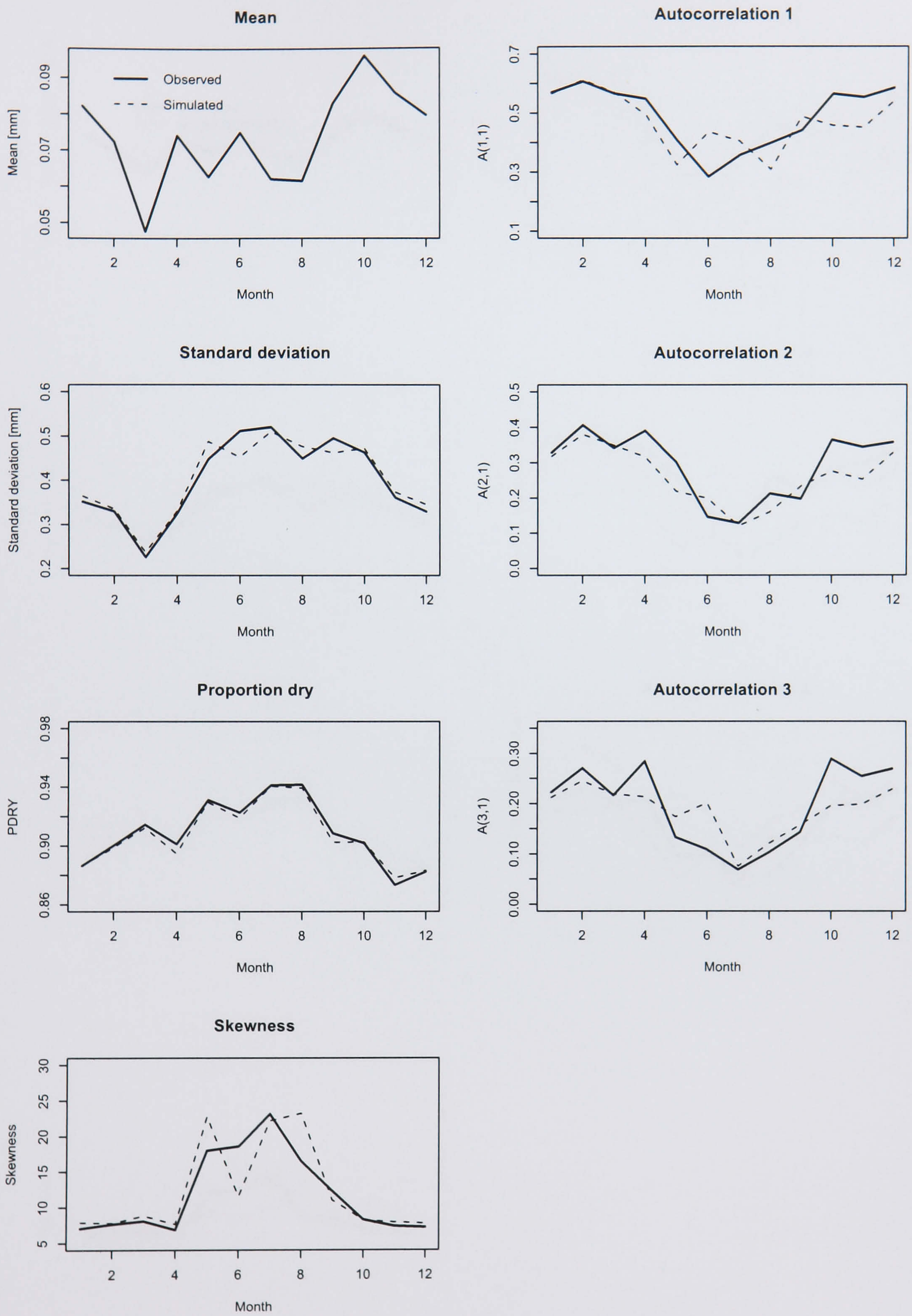

Figure 4.17 Observed sub-daily temporal profile of the master gauge applied to observed daily data at a typical site on the catchment

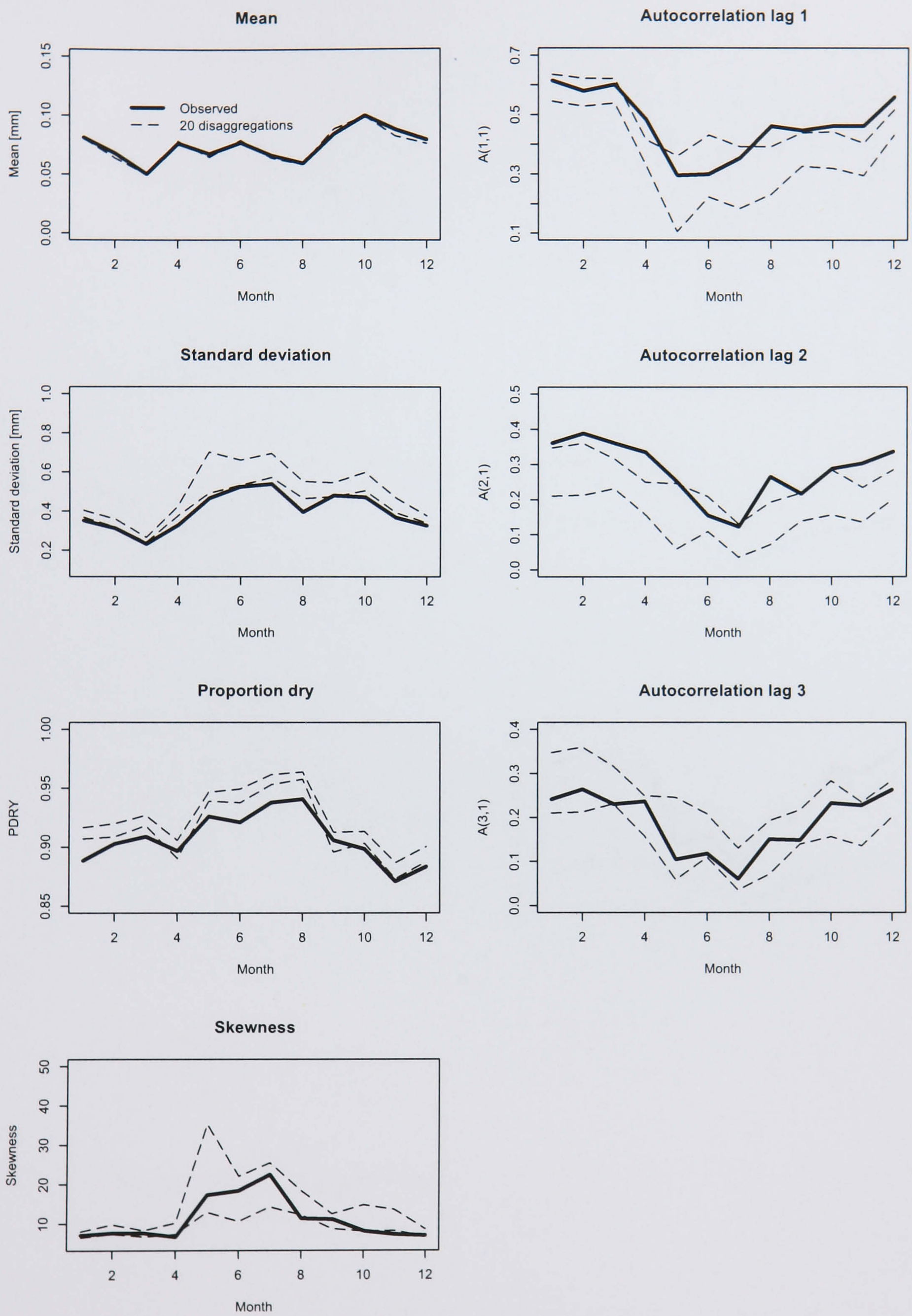

Figure 4.18 Properties of hourly sequences at site 0160, 1991-2002. Solid lines show the observed hourly properties; dashed lines show the envelopes from 20 disaggregations obtained by applying temporal profiles from the master gauge to all sites in the catchment. The profile were obtained by applying the HYETOS single-site disaggregation technique to the observed daily sequence at the master gauge.

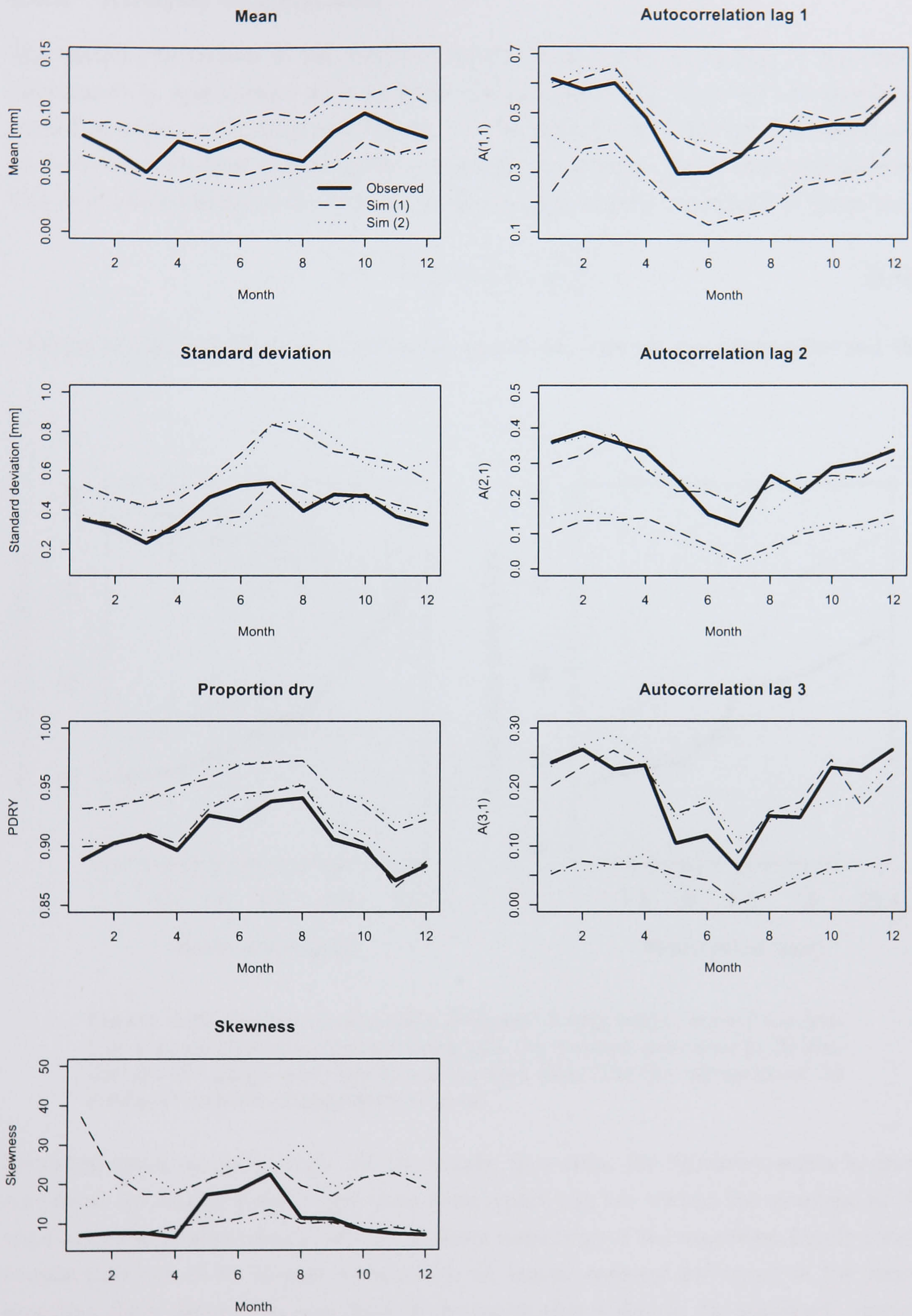

Figure 4.19 Single-site disaggregation at the master gauge conditioned on simulated daily rainfall from GLMs and sub-daily temporal profile applied at a typical site on the catchment. The plot compares the observed series with the envelope of 20 simulations at a gauge used (Sim 1) and not used (Sim 2) in the calibration of the model.

4.6.4 Analysis of Extremes

The extreme behaviour of the modelled rainfall is inspected since this is of primary importance in applications such as flood management. The observed and simulated annual maxima, both daily and hourly, for the period 1991-2002 are considered and displayed on a Gumbel plot using the Gringorten formulae to assign rank probabilities. The relationship between the reduced variate y and the return period T is given by:

$$y = -ln\left[-ln\left(1 - \frac{1}{T}\right)\right] \tag{4.13}$$

Results in Figure 4.20 show a reasonable agreement between the simulations and the

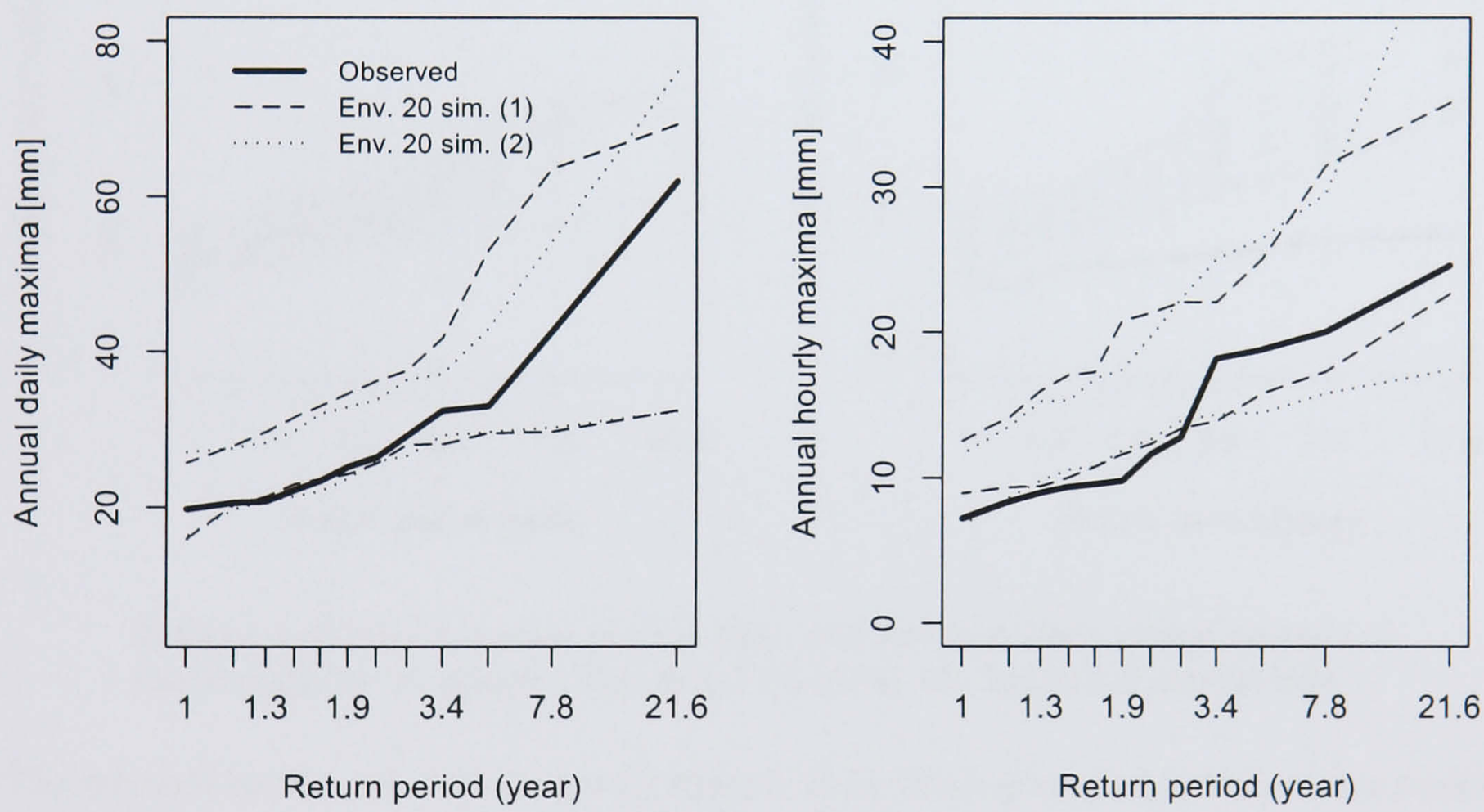

Figure 4.20 Gumbel plots of daily (left) and hourly (right) annual maxima. The plots compare the observed series with the envelope generated by 20 simulations at a gauge used (Sim 1) and not used (Sim 2) in the calibration of the combined multisite disaggregation model.

historical series at daily level. At the hourly time-step, the historical series is overestimated for return periods less than three years but lies within the envelope of 20 simulations for higher return periods. A closer inspection of the maximum hourly totals reveals that out of 20 12-year simulations, 31 annual maxima are equal to the corresponding daily depths. In one third of the cases, this is due to the single-site model, the other two thirds arise when the master gauge records zero rainfall and the previous profile applied corresponds to a day where the total rainfall falls in an hour. An analy-

sis of the empirical data indicates two occurrence of an hourly extreme corresponding to the total daily rainfall over the 1991-2002 period; but on average the observed daily total is lower than for the simulations (11.3 mm observed compared to 18 mm on average for the simulations). A refinement could be obtained, for instance by capping the maximum hourly rainfall that can be generated by the artificial profile or defining a more appropriate artificial profile when the master gauge records zero rainfall.

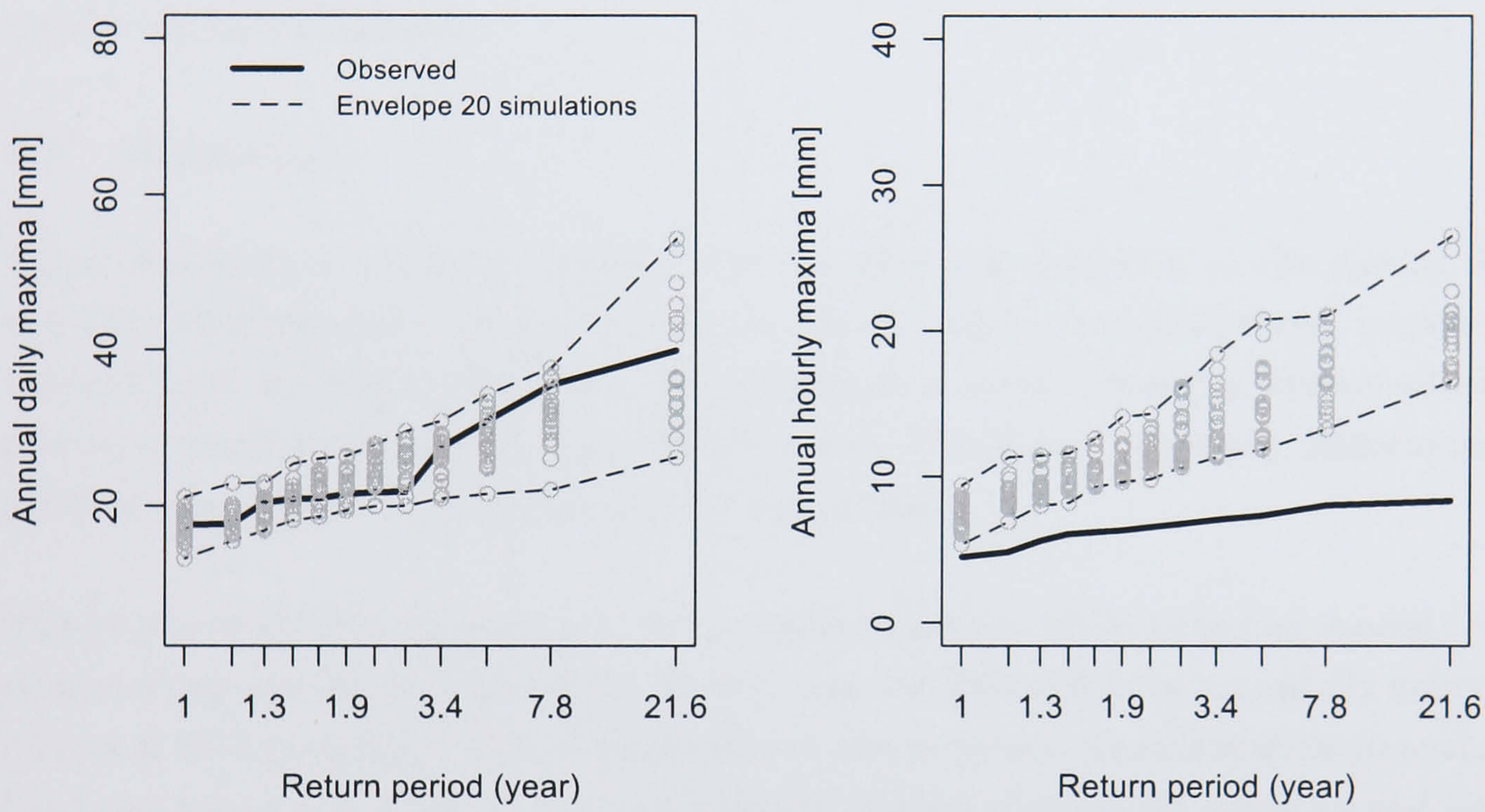

Figure 4.21 Gumbel plots of daily (left) and hourly (right) annual maxima of the average for all gauges. The circles represent the individual simulations.

The overestimation can also be partly explained by the higher proportion of dry periods obtained from the combined scheme, which suggests that more intense short duration rainfall intensities are produced, leading to higher hourly maxima. Furthermore, the mixed performance of the RPBLM in reproducing the extreme values was already evidenced (Onof and Wheater, 1993; Onof et al., 2000). To improve the extremal behaviour of the simulations, as in Wheater et al. (2005a), a two-stage fitting procedure of the single-site model parameters could be adopted. In the first stage the objective function in Equation (4.9) is minimised to locate sets of "almost optimal" parameters. The second stage selects, among these sets, the one that yields the best extreme value performance.

Similar conclusions can be reached considering performance when the site is not used in the fitting of the GLM (Figure 4.20, dotted lines). Compare to the previous case,

this is encouraging as the model is able to preserve the hourly extreme properties of rainfall at a site within the modelled region where no data are available.

Examining spatial extremes, return level plots of observed values versus simulated average rainfall from all gauges (Figure 4.21) reveal that the model performs well with respect to the daily extreme values but clearly overestimates the hourly series for all return periods. This is expected since a single temporal profile is applied at all sites and therefore the hourly peak is reproduced at the same time for all gauges. The importance of this overestimation will depend on the sensitivity of a catchment to individual hourly rainfall intensities.

4.7 Discussion

There is a need to construct models that represent the evolution of the spatial distribution of rainfall over time, which can be used as input to rainfall-runoff models to support flood and risk management. A disaggregation method based on Poisson-cluster processes conditioned on daily data simulated from a GLM and a spatially uniform temporal profile applied to all gauges has been presented.

The proposed scheme retains a relatively simple structure, while including spatial non-stationary properties on a daily basis, hourly data are obtained using a spatially uniform temporal disaggregation. The performance of the proposed disaggregation procedure has been assessed in terms of the reproduction of a set of standard statistics and with regard to extremes. Results from a network of 21 raingauges over the River Lee are promising. The simulated rainfall present properties that match the empirical statistics to an acceptable level for practical purposes. Although the model overestimates the extreme rainfalls, the larger observed maxima fall within an approximate 95% confidence interval of simulated extremes. Additionally, the combined scheme has the potential to transfer information from sites included in the calibration of the GLM to nearby locations which are not used to calibrate the model.

Further research is required to improve the reproduction of the proportion of dry periods, which in turn will benefit the simulation of extreme values. The performance of the Bartlett-Lewis model is conditional on the finding of suitable parameters to run the model. The first step would be to identify some single-site parameters that provide a better fit to the proportion of dry periods for the months of January, June and August; and also the lag 1 autocorrelation in October and November. It is also recommended to ensure at least 15 years of data to fit the single-site model at the master gauge (Wheater et al., 2005b). A second direction where development can take place involves

further investigation on the impact of the adjusting procedure on the overestimation of the standard deviation. Improvement in the reproduction of the proportion of dry periods and the standard deviation would lead to data that are more temporally correlated.

The major limitation of this scheme is the overestimation of the spatial correlation due to a unique temporal profile applied at all gauges. In order to decrease this correlation, the temporal profile could be shifted in time for some of the gauges (either randomly or taking into account the distance away from the master gauge). More generally, when applying the temporal profile, complete spatial dependence between sites is assumed, which does not hold beyond a certain distance. It will be important to identify at what scale allowance for spatial heterogeneity must be made. To address this issue, evaluation of the methodology could be extended to a larger region. Various options could be pursued for more complex procedures. One possible development would be to run independent disaggregation procedures for discrete sub-areas, another would be to build in spatial correlation to a multi-site procedure. More generally, continuous space-time models could be used for subdaily data, conditioned on daily GLM simulation.

The scheme proposed here has the advantage of simplicity and can readily be implemented. Software for the GLMs (Chandler, 2002) and the single-site disaggregation model (Koutsoyiannis and Onof, 2000) is already available; then a single profile of hourly rainfall is simply used for multisite disaggregation. Areas where the disaggregation method need improving have been identified, but overall the performance is sufficiently good to take forward for joint testing with the rainfall-runoff model to assess the impact of the simulated rainfall on runoff generation in the context of flood management. A first study of this aspect, using semi-distributed modelling applied to the Lee catchment is presented in Chapter 6. Recommendations for improvement would follow that evaluation.

Chapter 5

Rainfall-Runoff Model Calibration for the Lee Catchment

Event-based, semi-distributed hydrological rainfall-runoff modelling of the Upper Catchment of the Lee is undertaken to analyse the effects of the spatial structure of catchment-scale rainfall at scales ranging from 80 to 1000 km^2. In this chapter, the calibration of the Upper Catchment of the Lee and its tributaries is discussed. This includes a description of the rainfall-runoff model and a presentation of the modelling strategy. The modelling of each individual subcatchment is then presented before modelling the integrated basin to Feildes Weir. Calibration is done using data from 16 raingauges and this constitutes a basis to compare the impact of various rainfall estimators based on radar data, subsets of the gauges and disaggregation of observed daily data, for runoff generation.

5.1 RORB Rainfall-Runoff Model

A semi-distributed rainfall-runoff modelling approach is applied to account for the catchment heterogeneity. The semi-distributed model permits exploration of the catchment response sensitivity to spatial variations of rainfall without entering the level of complexity of fully distributed models. Preference is given to an event-based modelling procedure for its simplicity as it excludes components describing losses such as evapotranspiration and soil infiltration. The catchment response sensitivity is assessed for specific events and therefore as a function of rainfall type. Trends as a function of rainfall type can be derived. In addition, due to the large dataset being tested and the amount of missing data occurring at different times for each rainfall estimator, an event-based procedure is preferred over a continuous approach. The RORB model is selected as it satisfies these requirements. It provides non-linear routing and has only a small number of model parameters (3 or 4 depending on the type of run) to be identified. Moreover it has been extensively used in practice to represent the hydrological routing of this particular area (Lotufo Conejo, 1979; Flynn & Rothwell, 1991b).

RORB is a hydrologic simulation model designed to estimate the flood hydrograph by routing rainfall excess through the catchment. Its general concept is illustrated in Figure 5.1. From the total rainfall over a subcatchment, losses are deducted through the loss model in such a way that the volume of the generated hyetograph of rainfall excess equals the volume of the observed surface runoff hydrograph (hydrograph less baseflow).

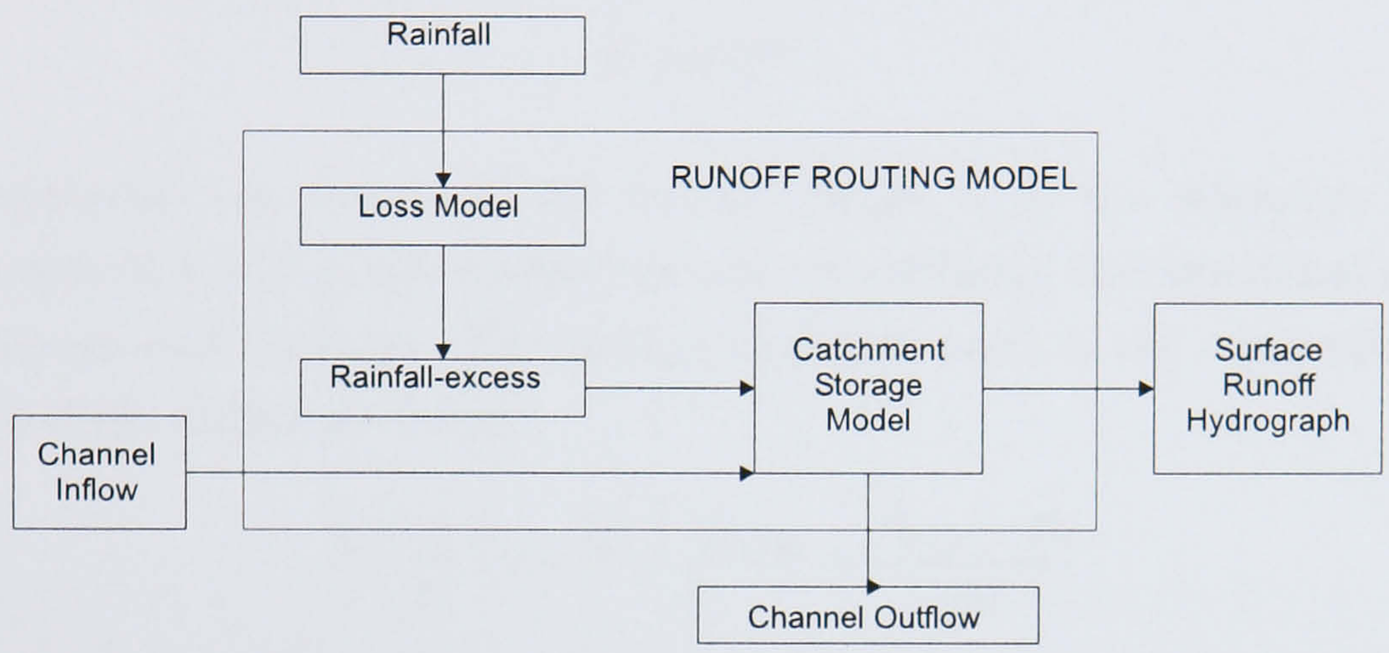

Figure 5.1 RORB structural diagram of the model (Source: Laurenson and Mein, 1988)

The user can choose two loss models:

- Model 0 is based on an initial loss which must be satisfied before rainfall excess is generated, followed by a constant proportional rate of loss and hence of runoff (runoff coefficient)
- Model 1 is composed of an initial loss followed by a constant (continuing) loss rate

In this study, Model 0 is selected. The excess hyetograph is converted to an input hydrograph which is then routed through the subcatchment storage model and the result is a surface runoff hydrograph at the outlet of the subcatchment. The model can include several subareas and allows for different rainfall depths and patterns over the catchment. Areal variability of loss parameters over sub-areas is taken into account via the fraction imperviousness for urban areas or runoff capacity index for rural areas. The parameters for each sub-area are then calculated as follows:

$$IL_i = (1 - F_i)IL_{perv} \tag{5.1}$$

$$C_i = F_i C_{imp} + (1 - F_i)C_{perv} \tag{5.2}$$

$$CL_i = (1 - F_i)CL_{perv} \tag{5.3}$$

where IL, C and CL are respectively the initial loss, runoff coefficient and continuing loss rate, F is the fraction imperviousness (or relative runoff capacity), and subscripts i, imp, and $perv$ indicate the ith sub-area, the impervious area and the pervious area. C_{imp} is set to 0.9 by the program (Laurenson and Mein, 1988).

The storage-discharge relation is represented by a non-linear element:

$$S = kQ^m \tag{5.4}$$

where S represents the storage in the subcatchment, Q is the discharge leaving the subcatchment and k and m are constant parameters defining the functional relationship between storage and outflow. The second equation used is the continuity equation expressed in finite difference form:

$$\frac{I_t + I_{t+1}}{2} - \frac{Q_t + Q_{t+1}}{2} = \frac{S_{t+1} - S_t}{\Delta t} \tag{5.5}$$

where I relates to the ordinate of the hydrograph obtained from the rainfall excess, Q to the ordinate of the outflow hydrograph, S to the model storage, t and t+1 are time indices referring the variables in the equation to successive time steps and Δt is the time interval used. Equations 5.4 and 5.5 require the use of an iterative technique to solve the non-linear system (the Newton Raphson method is used in the model which is described in the appendix of the user manual (Laurenson and Mein, 1988)).
k is the product of two factors:

$$k = k_c \times k_r \tag{5.6}$$

k_r is a dimensionless ratio called the relative delay time for a given model storage, determined from physical characteristics of the stream channel. k_c is an empirical parameter, which is calibrated by fitting the model to recorded rainfall and streamflow data. For a given storage i, the relative delay time is calculated as

$$k_{ri} = F\frac{L_i}{d_{av}} \tag{5.7}$$

where L_i is the length of reach represented by storage i (km), d_{av} is the average flow distance in the channel network of subarea inflows (km) and F is a factor depending on the type of reach. For instance, F is 1 when the reach is in natural condition or can be computed as:

$$F = \frac{1}{9S^{0.5}} \tag{5.8}$$

for lined or piped reaches (typically applied to urban catchments), where S is the slope of the channel reach.

For a particular catchment divided into n subareas, d_{av} is computed as:

$$d_{av} = \frac{\sum_{i=1}^{n}(a_i di)}{A} \tag{5.9}$$

where A is the total catchment area (km^2), a_i is the subarea area (km^2) at a travel distance to the catchment outlet d_i.

Hence the program has four main parameters to be calibrated: the initial loss (IL), the runoff coefficient (or constant loss rate) and the parameters m and k_c. The parameters m and k_c influence the shape of the hydrograph, regulating the attenuation and delay caused to the input hydrograph by the storage of water in the model storage. The runoff coefficient defines the volume of water in the input hydrograph.

The model provides three types of run: FIT, TEST and DESIGN, the characteristics of which are given in Figure 5.2. On gauged catchments, a FIT run is used first with data for one or more of the available recorded floods to evaluate the model parameters. When the initial loss has been entered as input by the user, the program calculates the pervious area runoff coefficient or continuing loss rate by iteratively achieving a volume balance of rainfall-excess with measured surface runoff. The TEST run is used next with data for the remainder of the recorded floods to test the model. Assuming that the results of the TEST run are satisfactory, a DESIGN run is then used to predict the catchment behaviour under various hypothetical design conditions. Model parameters should all be entered as input in a DESIGN run.

TYPE OF STUDY	ITEM		TYPE OF RUN		
			FIT	TEST	DESIGN
CATCH-MENT STUDIES & FLOOD ROUTING STUDIES	HYDROGRAPH		Known	Known	Unknown
	MODEL PARAMETERS		Unknown	Known	Known or assumed
	PURPOSE OF RUN		To determine model parameters	To test model	To determine design hydrograph
	OUTPUT LABELED:		FIT RUN	TEST RUN	DESIGN RUN
	SPECIAL STORAGES		Existing only	Existing only	Existing or to be designed
CATCH-MENT STUDIES ONLY	TRIAL ROUTING PARAMETERS		Suggested by program	Not suggested	Suggested, but k_c only if $m = 0.8$
	LOSS PARA-METER	GAUGING STN.	Calculated	Calculated	Input
		NO GAUGING STATION	Input from terminal	Input from terminal	Input from terminal

Figure 5.2 Types of run. (Source: Laurenson and Mein (1988))

In order to run the model, the following steps are taken:

- The catchment is divided into sub-areas to provide for areal variation of rainfall and losses and the fact that runoff from different parts of the catchment travels different distances to the outlet. Rainfall and losses are averaged over each sub-area.
- Normal (model) storages are placed in each river reach located between the centroid of the subcatchment and the outlet. Special storages such as storage reservoirs, lakes and retarding basins, can also be defined. They are modelled differently from the normal channel reach storage.
- To derive the surface runoff hydrographs for input to the model the baseflow contribution needs to be removed from the observed hydrographs
- The model calibration requires the determination of the initial loss (IL), m, k_c and depending on the type of run, the runoff coefficient (RC). m, k_c are constant parameters, IL and RC vary depending on the event.

5.2 Modelling Strategy

5.2.1 Model Configuration

Previous studies were undertaken using the RORB model on the Lee catchment. Lotufo Conejo (1979) designed a configuration for the whole Lee catchment. The aim was to develop a flood prediction method to route flood flows in the River Lee from Feildes Weir to Low Hall (Wheater and Lotufo Conejo, 1979). RORB was used to estimate inputs to the Lower Lee, both from the Upper Catchment tributaries and from the subcatchments below Feildes Weir.

Flynn & Rothwell (1991b) focused on the upper part of the catchment and modelled various tributaries independently (Hawnt, 1987a,b). Their aim was to integrate all tributary RORB models in order to cover the whole Upper Catchment of the Lee and estimate design floods at Feildes Weir (Flynn & Rothwell, 1991b). Ideally, previous and new RORB models for all tributaries would be combined to create a single model. However, a large number of sub-areas would have been needed to be modelled and this would have required too much time due to the computer memory constraints within RORB. Instead, the existing RORB models were run independently for each tributary to provide tributary inflows to a new model combining all flow to Feildes Weir (Middle Lee model). Due to data inaccuracy of the Stort at Glen Faba, the Middle Lee model of Flynn & Rothwell (1991a) incorporated the Upper Lee, the Mimram, the Beane, the Rib and the Ash but excluded the Stort contribution, which was modelled independently.

The Upper Catchment of the Lee is heterogeneous and a single model would result in a loss of accuracy at the subcatchment scale and extra "special storages" would be needed to locally modify the global routing parameters "m" and "k_c". Following Flynn & Rothwell (1991b), the Lee catchment is subdivided into 6 subcatchments, of zones assumed internally homogeneous, and the rainfall-runoff model is applied to each of these regions. The flow from each tributary, including the Stort configuration, is then added and routed to the outlet of the catchment at Feildes Weir. This option allows for spatial variation of the model parameters. Further it was perceived essential to keep the same model discretisation at subcatchment and catchment scale. The impact of spatial rainfall can be studied as a function of subcatchment type, subcatchment scale (80-280 km^2) and catchment scale (1000 km^2). One drawback is that it is not easy to run the combined model under design conditions. Design runs have to be made for each tributary model, predicted flood hydrographs abstracted from output files and then combined in a datafile as concentrated inflows.

5.2.2 Catchment Subdivisions

In order to minimise the impact of model discretisation, a relatively small subdivision of the catchment is required. Apart for the Mimram, each subcatchment is subdivided into subareas of about 10 km^2 based on the stream network and the drainage divides of the catchment. The very low response of the Mimram, which is baseflow dominated due to the chalk geology, does not justify detailed subdivision (Flynn & Rothwell, 1991b). This size was chosen on the basis of previous studies (Hawnt, 1987a; Flynn & Rothwell, 1991b). This scale is small enough so that the impact of various rainfall representations leads to variation in sub-areal rainfall estimates and to satisfactory computations in terms of running time of the programme. Moreover, for this catchment a raingauge influences on average 60 km^2, so a smaller subdivision does not seem justified.

For calibration purposes, spatially variable rainfall from the full raingauge network is used as input and this representation is referred to as the reference rainfall. Since we have available a relatively dense network of representative raingauges, a simple method to derive the sub-areal precipitation is selected. Spatial interpolation of the point raingauges using Thiessen Polygons methods is used to estimate the areal rainfall. One of the drawbacks is the inflexibility of this method as a new Thiessen network needs to be constructed each time there is a change in the raingauge network, such as when data are missing from one of the gauges (Shaw, 1994). The temporal pattern applied to each subarea is given by the nearest raingauge. The simulated flow driven by the reference rainfall is referred to as the reference flow.

5.2.3 Event Selection

The calibration of the rainfall-runoff model is based on events taking at different times of the year from the dataset. The events are selected so that they are preceded by periods when there is no rainfall intensity recorded at all gauges for several hours (usually about 24 hours) and their characteristics in terms of event duration, arithmetic average of available gauges, return period (T), determined using the methodology in Faulkner (1999), and coefficient of variation of rainfall (CV) are given in Table 5.1. "Common" refers to events with return period less than a month (NERC, 1999).

Event	Rainfall duration (hr)	Average rainfall depth (mm)	No. RG	Return period T (Year)	CV(%)
11-Nov-91	19	22	15	1.2	13.6
18-Nov-91	20	22.4	15	1.2	13.4
08-Jan-92	25	11.6	16	common	49.1
28-May-92	56	55.2	16	7.5	33.9
13-Aug-92	13	20.9	15	1.4	13.5
19-Oct-92	34	30.7	16	1.56	38.1
09-Apr-93	21	14.4	16	common	12.2
12-Aug-93	10	16.1	16	1.1	26.6
11-Oct-93	65	62.7	16	11.2	16.9
03-Feb-94	8	12.1	16	1.01	16.5
15-Sep-94	24	15.4	16	common	28.6
07-Dec-94	47	21.9	16	1	27.9
16-May-95	25	17.1	16	common	11.1
22-Dec-95	45	27.4	16	1.08	14.6
08-Jan-96	19	20.3	16	1.09	14.3
12-Feb-96	41	18	16	common	18.9
23-Jul-96	4	20.6	16	4.6	81
22-Aug-96	18	17.3	16	1.01	23.1
24-Feb-97	39	21.2	16	1	22.6
14-Apr-98	33	26.3	15	1.17	16.3
02-Apr-00	49	35.7	14	1.69	38.6
27-May-00	20	22.2	15	1.19	12.8
10-Nov-00	32	13.8	14	common	19.6
03-Jan-01	44	20	16	common	20
26-Jan-01	14	14	16	1.02	28.6
21-Oct-01	24	40.7	15	5.8	32.7
30-Jul-02	30	21.4	16	1.03	42.7
09-Sep-02	16	20.5	16	1.19	39.3

Table 5.1 Events used for calibration

5.2.4 Baseflow Separation

Direct runoff is required for calibration of RORB and as a first approach a simple straight line method is applied (Chow et al., 1988) to each flow event to remove the

baseflow component. The basic principles are illustrated in Figure 5.3 where AB and DE represent the baseflow recession, BC the rising limb, CD the falling limb. A straight line from the point at which surface runoff begins (B) to the intersection with the recession limb (E) is drawn to produce the direct runoff storm hydrograph. The point of inflection from the logarithm of the discharge time-series determines the point (E) at which the straight line and the hydrograph recession limb intersect.

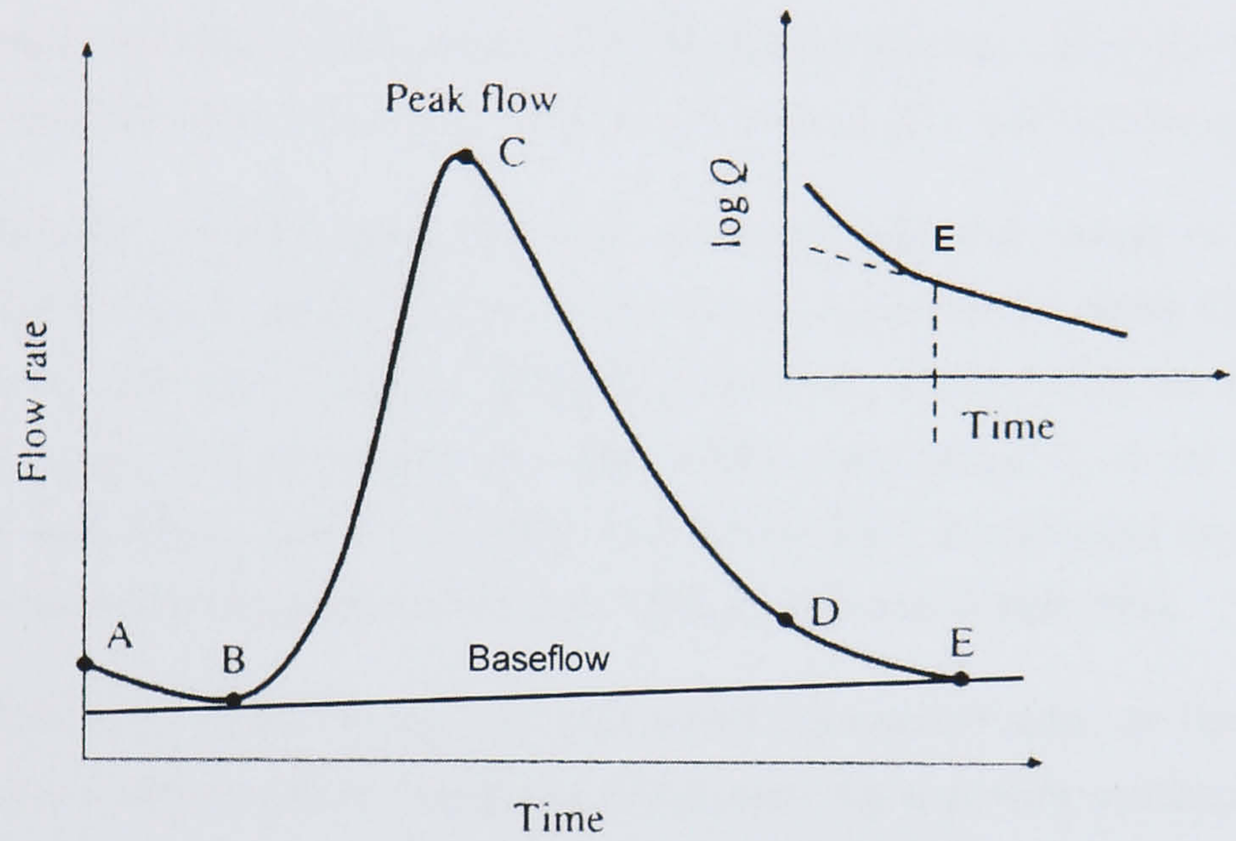

Figure 5.3 Baseflow separation (Adapted from Chow et al. (1988))

5.2.5 Performance Criteria

Model parameter calibration and validation is based on the reproduction of the peak outflow (Q_p) and the time to peak (T_p), which is defined as the lag time between the start time and the peak time of the runoff hydrograph. This is complemented by a non-dimensional form of the time-series least squares error, the well-known Nash-Sutcliffe efficiency (NSE), which is also sensitive to hydrograph peak error.

$$NSE_{obs} = 1 - \frac{\sum_{i=1}^{M}(C_i - O_i)^2}{\sum_{i=1}^{M}(O_i - \overline{O})^2} \tag{5.10}$$

where C_i and O_i are the calculated and observed discharge at hour i, $\overline{O}$ the mean discharge over the event duration, M the number of time steps.

More generally, there are some issues associated with the accuracy of flow measurements, which is a factor affecting differences between models over the catchments. However some quality control have been carried out by the Environment Agency of England and Wales, where dubious data have been flagged in the datafiles provided.

5.2.6 Calibration Strategy

The aim of the calibration is to identify model parameters which provide a suitable basis for analysis of model sensitivity to precipitation inputs. An exhaustive calibration exercise was therefore not justified. Manual calibration is undertaken, varying the model parameters m, k_c and IL for a range of events to achieve a close match between the observed and calculated hydrograph. The procedure is as follows:

- Several events covering a wide range of peak discharge and taken at different time of the year are selected (typically four to six events per subcatchment).
- In the calibration or FIT runs, for each event, a selected range of m, typically $\{0.6, 0.7, 0.8, 0.9\}$, is used. For each m value, k_c is varied until the best fit in terms of peak flow and time to peak is obtained. Decreasing kc increases the hydrograph peak and decreases the lag, while increasing k_c does the opposite (Laurenson and Mein, 1988). Finally, the initial loss is adjusted to improve the fit. The parameter set maximising the NSE_{obs} criteria is selected.
- In the validation or TEST runs, the calibrated parameter sets are tested on a few (typically two to four) other events to determine an *a priori* optimum set.
- A sensitivity analysis is conducted, applying each calibrated parameter set to all events in the FIT runs and computing the resulting NSE_{obs} criteria. This indicates a standard parameter set reproducing best all events and either confirms the results from the TEST run, or highlights the need to use an alternative set in addition to the standard one to fit specific types of flow.

5.3 Calibration and Validation

Example datafiles were provided for the Upper Lee, the Mimram, the Ash, the Stort and the Middle Lee. Documentation on the Mimram, the Ash and the Middle Lee are given in Flynn & Rothwell (1991b). Documentation on the Stort can be found in Flynn & Rothwell (1991a). Some description of the model of the Beane and the Rib structure can be found in Hawnt (1987a) and Hawnt (1987b). The Mimram, the Ash and the Stort were calibrated by Quasem (2004b).

In the first instance, seven RORB models are calibrated independently and the results for the individual subcatchments are presented in Section 5.3.1. The calibration of the Feildes Weir outlet using observed tributary inflows is referred to as the Middle Lee model. Second the integrated Lee calibration is presented by choosing a set of

events common for all tributaries in Section 5.3.2. The simulated flow from each tributary is routed to Feildes Weir outlet. The integrated modelling of the Upper Catchment of the Lee is referred to as the Feildes model.

5.3.1 Modelling the Individual Subcatchments

A map showing the discretisation of each subcatchment is included in Figure 5.4. The reader is also referred to the map of the Lee catchment in Figure 3.1 representing the raingauge and flow station locations. A summary of the subcatchment configurations can be found in Table 5.2. This refers to the number (N) of subareas, the number of raingauges used for each tributary, the intermediate and main flow gauging stations (FGS), the type of reaches, the number of special storages and whether a coefficient of imperviousness is included in the modelling configuration.

Calibration results for each subcatchment is described below. For a particular subcatchment, it was not possible to determine a unique parameter set. The fitted k_c generally increased with the size of the flow event. A summary of the calibrated model parameters $\{m, k_c\}$ for each subcatchment is presented in Table 5.3. "Standard" refers to the default parameter set fitting most events, "Low" and "Large" refer to the parameter set required to represent low or large flows determined by a peak flow above the threshold given in Table 5.3. Even though the initial loss is defined as an event parameter, a suggested value fitting most events on a particular subcatchment is included in Table 5.3. Overall a good fit was achieved for all tributaries with NSE_{obs} on average for all subcatchments and events of 0.88 and 0.89 in calibration and validation mode, respectively.

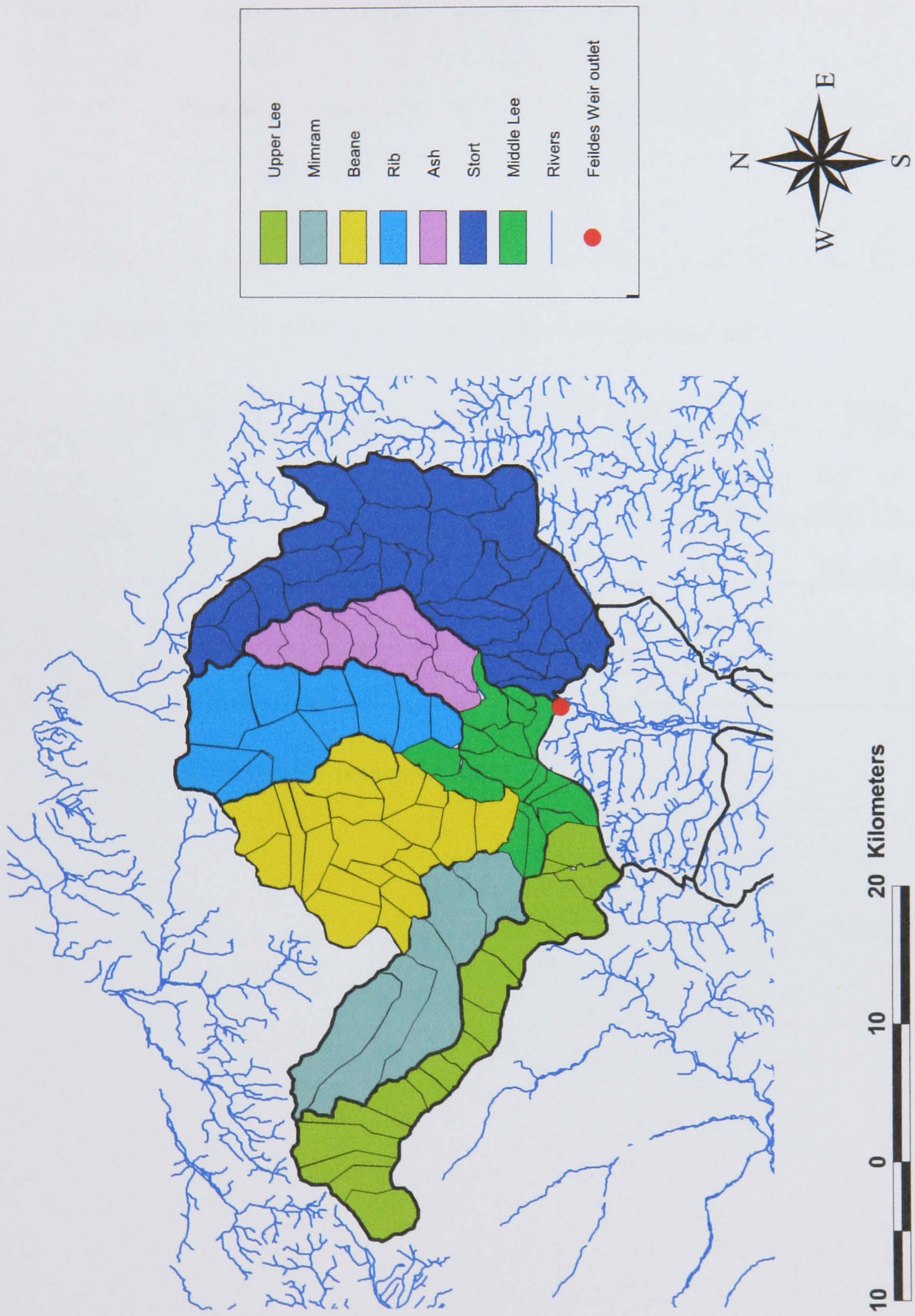

Figure 5.4 Subcatchment subdivisions

Catchment	Upper Lee	Mimram	Ash	Beane	Rib	Stort	Middle Lee
Area (km^2)	156	132	79	176	134	278	78
No. Sub-areas	16	5	8	21	11	32	15
Range (km^2)	1.5-19.2	18.5-31	6.8-13.3	2.5-14.8	6.8-19.7	2-18.6	2.2-10
No. RG	5	5	4	5	6	7	6
Centroid RG	174	162	104	163	104	170	106/178
Inter. FGS	1	0	0	1	1	2	6 (inflow)
Main FGS	Water Hall	Panshanger	Mardock	Hartham	Wadesmill	Glen Faba	Feildes Weir
Reaches							
-Natural	21	9	14	33	18	50	15
-Drowned	9						1
N. Special Storage	4	0	0	0	0	4	0
Coeff. imp.	Yes	No	No	Yes	No	No	Yes

Table 5.2 Individual subcatchment calibration summary table

	Upper Lee	Mimram	Beane	Rib	Ash	Stort	Middle Lee
Low							
m - k_c	-	-	0.8 -7	-	0.8-7	0.8 - 17	0.6 - 7
Flow			<1 m^3/s		<1 m^3/s	<3 m^3/s	<10 m^3/s
Standard							
m - k_c	0.8 - 21	0.8 - 7	0.8 - 21	0.8 - 16	0.8 - 15	0.8 - 37	0.6 - 21
Large							
m - k_c	0.8 - 33	0.8 - 17	-	0.8 - 21	0.8 - 21	-	0.6 - 35
Flow	> 5 m^3/s	> 3 m^3/s		>15 m^3/s	>7 m^3/s		>50 m^3/s
IL (mm)	3	0	5	9	7	0	0

Table 5.3 Calibrated parameters results

The Upper Lee

The 156 km^2 Upper Lee subcatchment until Water Hall was subdivided into 16 subareas and 4 special storages accounting for three lakes and a storm tank were included. 21 reaches were of standard type, 9 were drowned (by reservoir). A fraction of imperviousness of 10% the urban proportion was applied to the 6 sub-areas accounting for the town of Luton. Flow from Luton Hoo (4640) and Water Hall (4690) flow gauging stations were available. Simulated hydrographs at Water Hall outlet are displayed in Figures 5.5 and in Figures 6.2 and 6.1 for the events of 3rd February 1994 and 11th October 1993, respectively. Table 5.4 presents the calibration and validation results at Water Hall in terms of Q_p, T_p and NSE$_{obs}$. The parameter set $\{0.8, 21\}$ representing $\{m, k_c\}$ was selected to fit the majority of events. For large events (i.e. peak flow at Water Hall above 5 m^{3}s^{-1}), the parameter set $\{0.8, 33\}$ was used instead. Initial loss ranged from 0 to 4 mm and runoff coefficient varied from 0.03 to 0.24, with lower values in summer.

The Mimram

The calibration of the Mimram catchment upstream of Panshanger flow gauging station (4790), which has a catchment area of 132 km^2, did not show much sensitivity to subdivision area. Hence a larger subdivision was taken (between 18.5 and 31 km^2) and was divided into 5 sub-areas. All reaches were in natural condition. The catchment is mainly rural even though it contains the town of Welwyn Garden City. However calibration resulted in predicted runoff peak being too high due to the high storage in the underlying chalk, therefore the fraction imperviousness was set to zero. Hydrographs at Panshanger outlet are displayed in Figures 5.6 and in Figure 6.1 for the event 11th October 1993. Results from calibration can be found in Table 5.5. Preliminary calibration runs used $\{0.8, 7\}$ for standard events and $\{0.8, 17\}$ for large events triggering a peak flow above 3 m^{3}s^{-1}. Initial loss varied between 0 and 7 mm and runoff coefficient between 0.01 and 0.04.

The Beane

The 176 km^2 Beane catchment is mainly rural with the subcatchment of Stevenage Brook draining the new town of Stevenage. The influence of urbanisation on the hydrology of the catchment and the assumed variable spatial distribution of runoff from the mixed chalk and clay catchment, were the main factors influencing the selection of the RORB modelling approach for analysing the rainfall-runoff response of the Beane (Hawnt, 1987a). Two major subcatchments, separating the urban area (Stevenage, 7 sub-areas) from the rural catchment (14 sub-areas) were jointly calibrated as opposed

to the strategy of Hawnt (1987a) where the two catchments were calibrated separately. A fraction of imperviousness of 10% the urban proportion was applied to the 7 sub-areas accounting for the town of Stevenage. Flow data from Bragbury Park (4827) and Hartham (4890) stations were used for calibration. Simulated hydrographs at Hartham outlet are displayed in Figures 5.7 and in Figures 6.3 and 6.5 for the events of 8th January 1996 and 30th July 2002, respectively. Results in Table 5.6 suggest values of $\{0.8, 21\}$ to be applied to the majority of events and the parameter set $\{0.8, 7\}$ to low flows (i.e. peak flow below 1 m^3s^{-1}). Initial loss ranged between 0 and 9 mm, the corresponding runoff coefficient ranged between 0.02 and 0.12 with lower values associated with summer events.

The Rib

The predominantly rural Rib subcatchment was divided into 11 subareas and calibrated using data from Griggs Bridge (4939) and Wadesmill (4980) stations. The calibration of the Rib was more difficult as the response at Wadesmill (4980) was lagged and resulted in a simulated peak flow often in advanced of the observed one. Simulated hydrographs at Wadesmill outlet are displayed in Figures 5.8 and in Figures 6.2, 6.3 and 6.1 for the events of 3rd February 1994, 8th January 1996 and 11th October 1993, respectively. Results from calibration can be found in Table 5.7 and suggest the parameter set $\{0.8, 16\}$ to fit standard events and $\{0.8, 21\}$ for larger events. Relatively high values of initial loss were calibrated ranging between 6 and 9 mm and with corresponding runoff coefficient between 0.18 and 0.32 mm.

The Ash

The 79 km^2 Ash catchment upstream of Mardock flow gauging station (5080), was divided into 8 sub-areas. The catchment contains no significant urban areas. Therefore the impervious area flag was set to zero and all reach types were assumed to be natural. Simulated hydrographs at Mardock outlet are displayed in Figures 5.9 and in Figures 6.1, 6.4, 6.3 and 6.5 for the events of 11th October 1993, 16 May 1995, 8th January 1996 and 30th July 2002, respectively. The calibration of the Ash was sensitive to the size of the events. Results in Table 5.8 led to $\{0.8, 7\}$, $\{0.8, 15\}$, $\{0.8, 21\}$ to fit low (peak flow < 1 m^3s^{-1}), medium and large (peak flow $> 7m^3s^{-1}$) flows. Initial losses ranged from 0 to 5 mm and runoff coefficient from 0.01 to 0.39.

The Stort

The river network of the Stort is a complex inter-relationship of an historically constructed navigation canal, ancient water driven mills and the original natural course

of the rivers, its backwaters, tributaries and floodplains (Flynn & Rothwell, 1991a). The 278 km^2 Stort subcatchment was difficult to calibrate since the data at Glen Faba station were of poor quality with discontinuous records and presence of negative flow values. The Stort is dominated by the Stort navigation system, the river is relatively slow flowing and when the lock is in use by the boats it creates a reverse flow or "backwater" (Flynn & Rothwell, 1991a) which influences the gauging station record. The datafiles were therefore simplified, the fraction imperviousness was set to zero even though about 13% of the catchment is urbanised (see Table 3.3). All reaches were in natural conditions and four special storages accounted for the Stort navigation channel, the reservoir at Mountfitchet, Spellbrook Lagoon and Cannon Brook were included (Quasem, 2004b).

The catchment to Glen Faba was divided into 32 sub-areas, data from two intermediate flow stations were available at Gypsy Lane and Sheering Hall. However it was difficult to match the hydrographs simultaneously at the three stations so the parameter set which provided a good fit in terms of time to peak and peak flow at Glen Faba and one of the intermediate station was selected (Quasem, 2004a). Simulated hydrographs at Glen Faba outlet are displayed in Figures 5.10 and in Figures 6.1, 6.3 and 6.2 for the events of 11th October 1993, 8th January 1996 and 3rd February 1994, respectively. Results in Table 5.9 highlight the parameter set {0.8,37} fitting the majority of events and the parameter set {0.8,17} fitting low events (peak flow <1 m^{3}s^{-1}). Initial loss ranged between 0 and 8 mm, the runoff coefficient varied between 0.03 and 0.45.

The Middle Lee

The Middle Lee model routes the above tributary flows to Feildes Weir. 15 sub-areas are included. At this stage the calibration is undertaken using observed tributary inflow and the configuration is referred to as the Middle Lee. Hydrograph inflows from the Lee at Waterhall, the Mimram at Panshanger, the Beane at Hartham, the Rib at Wadesmill, the Ash at Mardock and the Stort at Glen Faba are then routed to Feildes Weir. A fraction of imperviousness of 10% the urban proportion was applied to 10 sub-areas. Simulated hydrographs at Feildes Weir outlet are displayed in Figures 5.11. Results in Table 5.10 suggest the parameter sets $\{0.8, 7\}$, $\{0.8, 21\}$,$\{0.8, 35\}$ to fit low (peak flow < 10 m^{3}s^{-1}), medium and large (peak flow > 50m^{3}s^{-1}) flows. Initial losses ranged from 0 to 6 mm and runoff coefficient from 0.02 to 0.92. The integrated response at Feildes Weir using simulated tributary inflows is tested in the following Section and the configuration is referred to as the Feildes catchment.

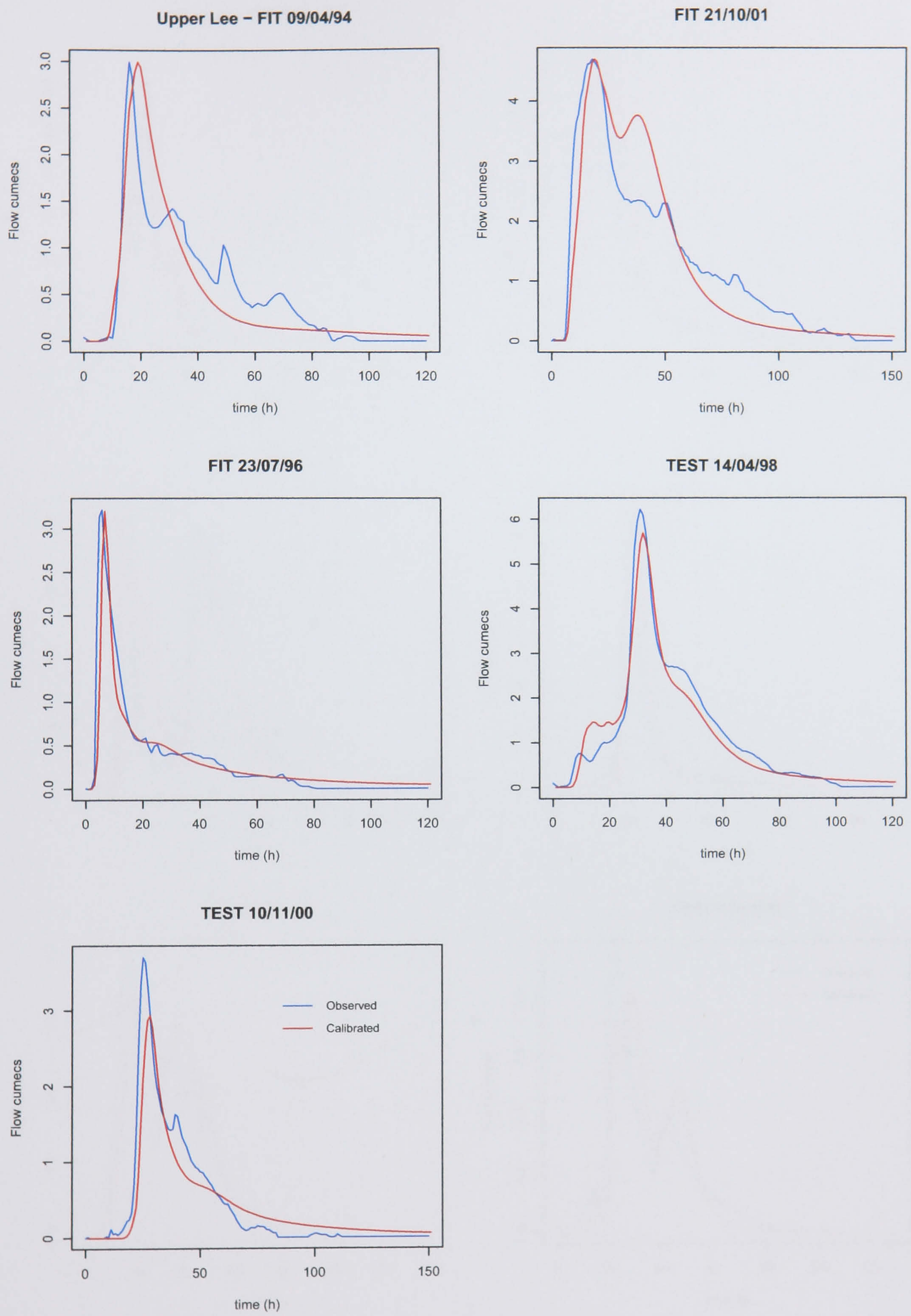

Figure 5.5 Calibration (FIT) and Validation (TEST) results for the Upper Lee.

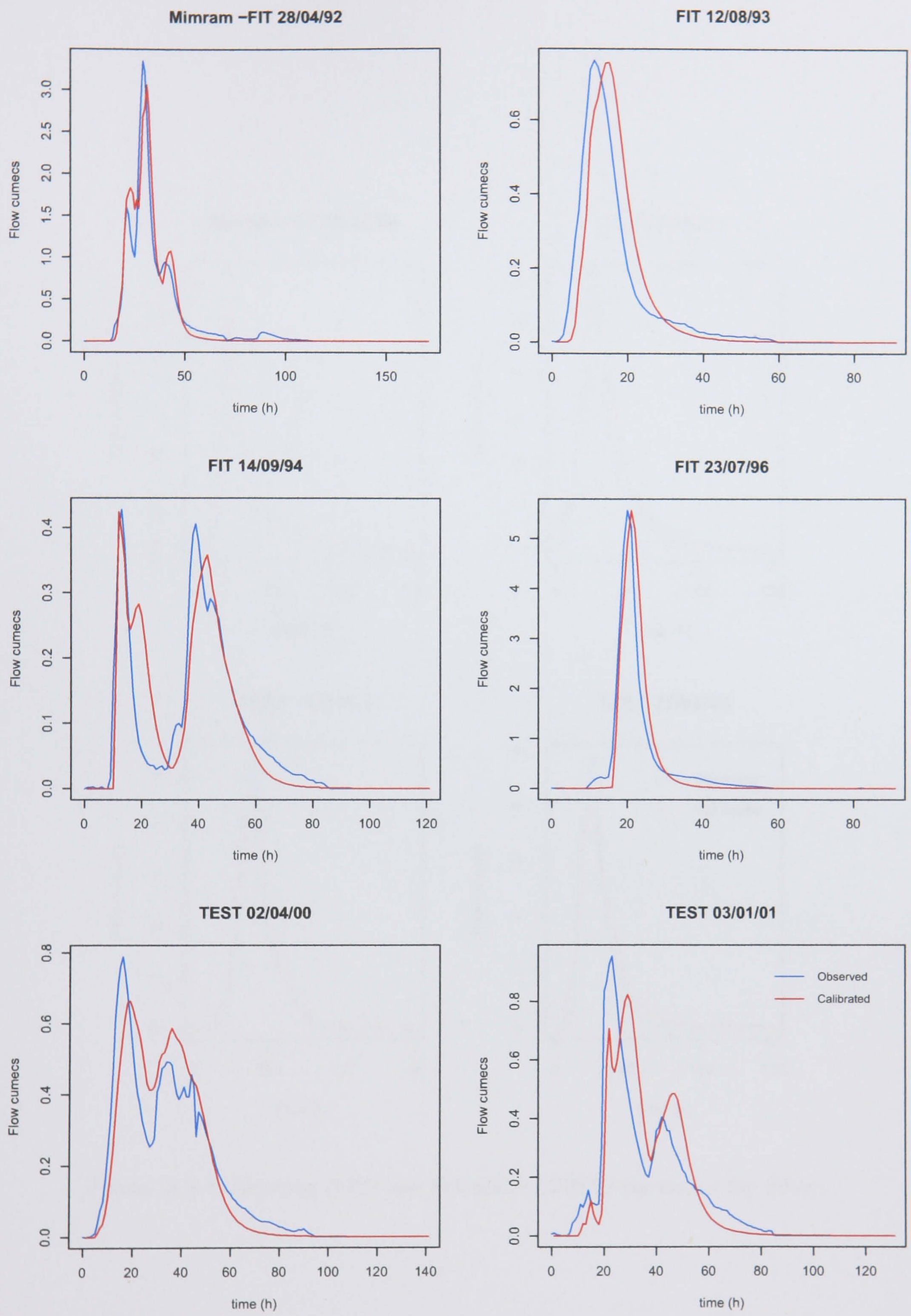

Figure 5.6 Calibration (FIT) and Validation (TEST) results for the Mimram, adapted from Quasem (2004b).

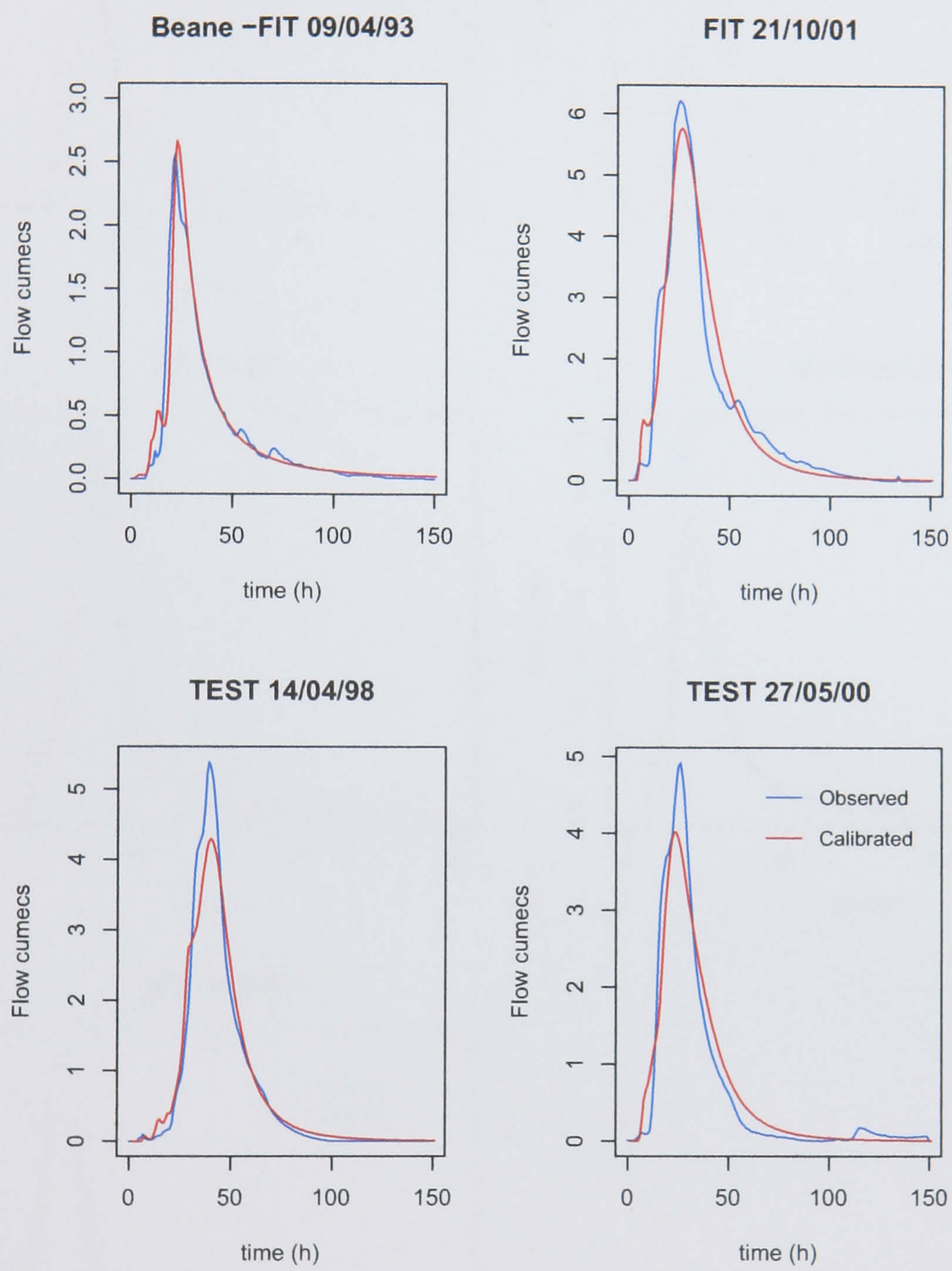

Figure 5.7 Calibration (FIT) and Validation (TEST) results for the Beane.

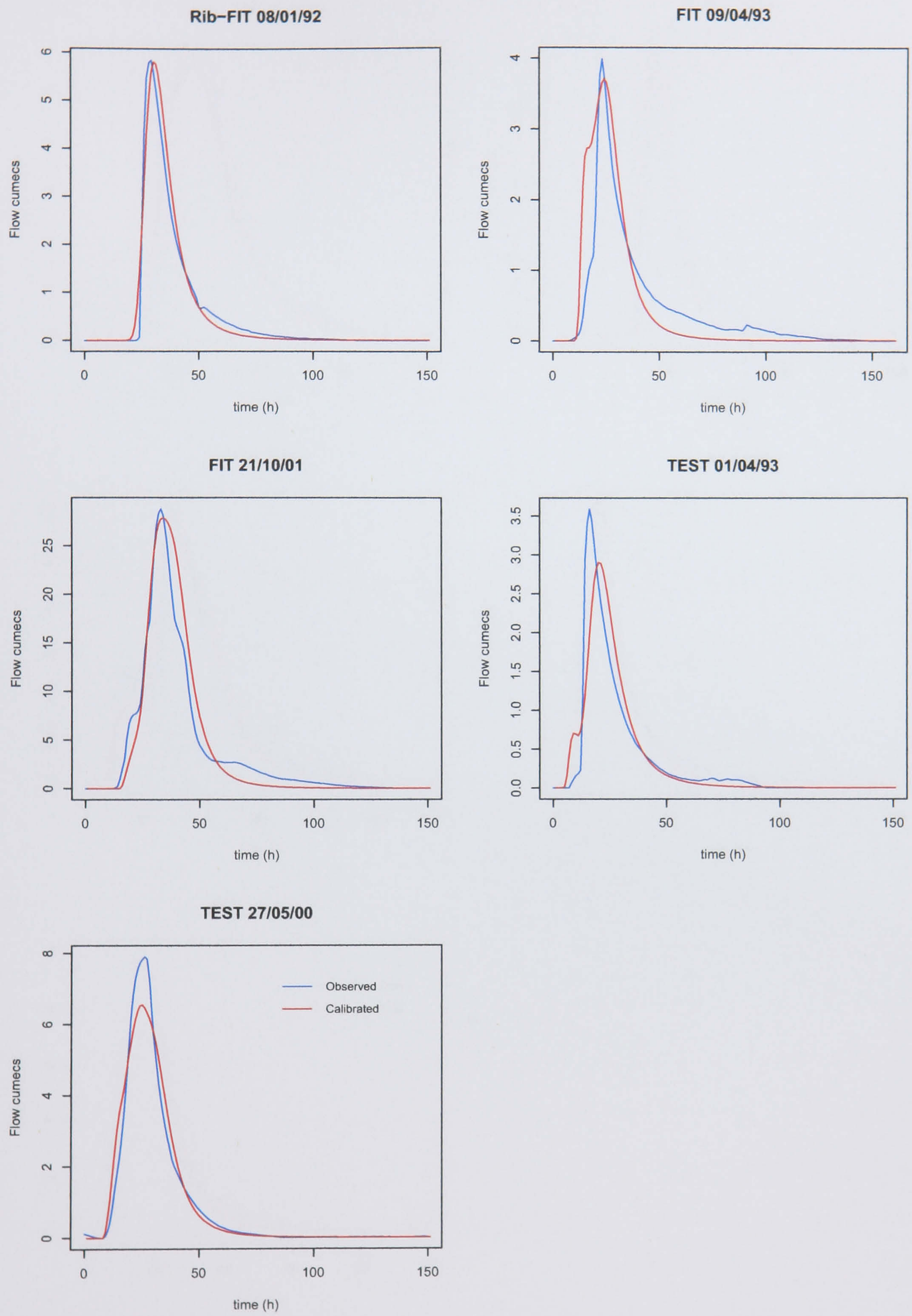

Figure 5.8 Calibration (FIT) and Validation (TEST) results for the Rib.

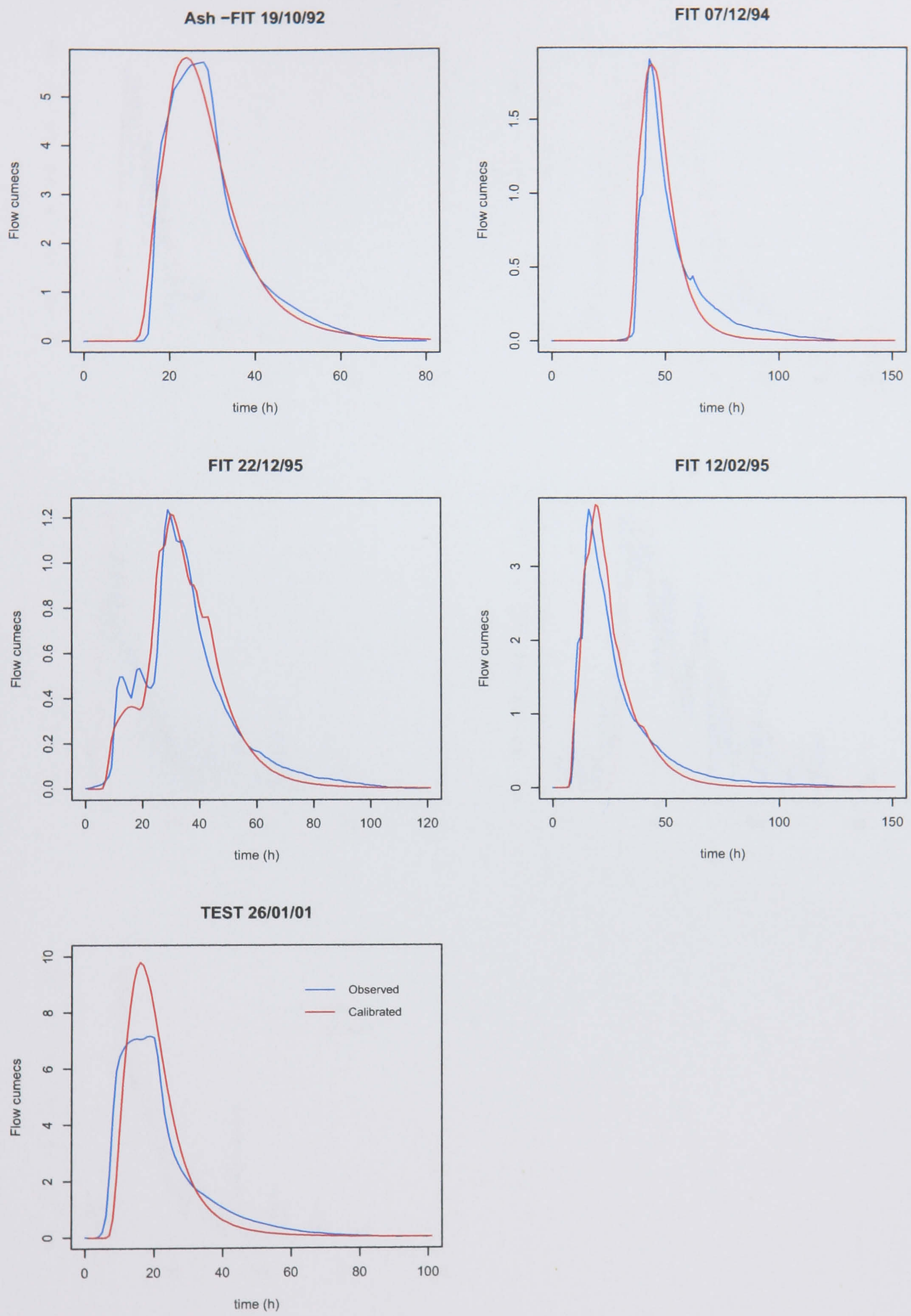

Figure 5.9 Calibration (FIT) and Validation (TEST) results for the Rib, adapted from Quasem (2004b).

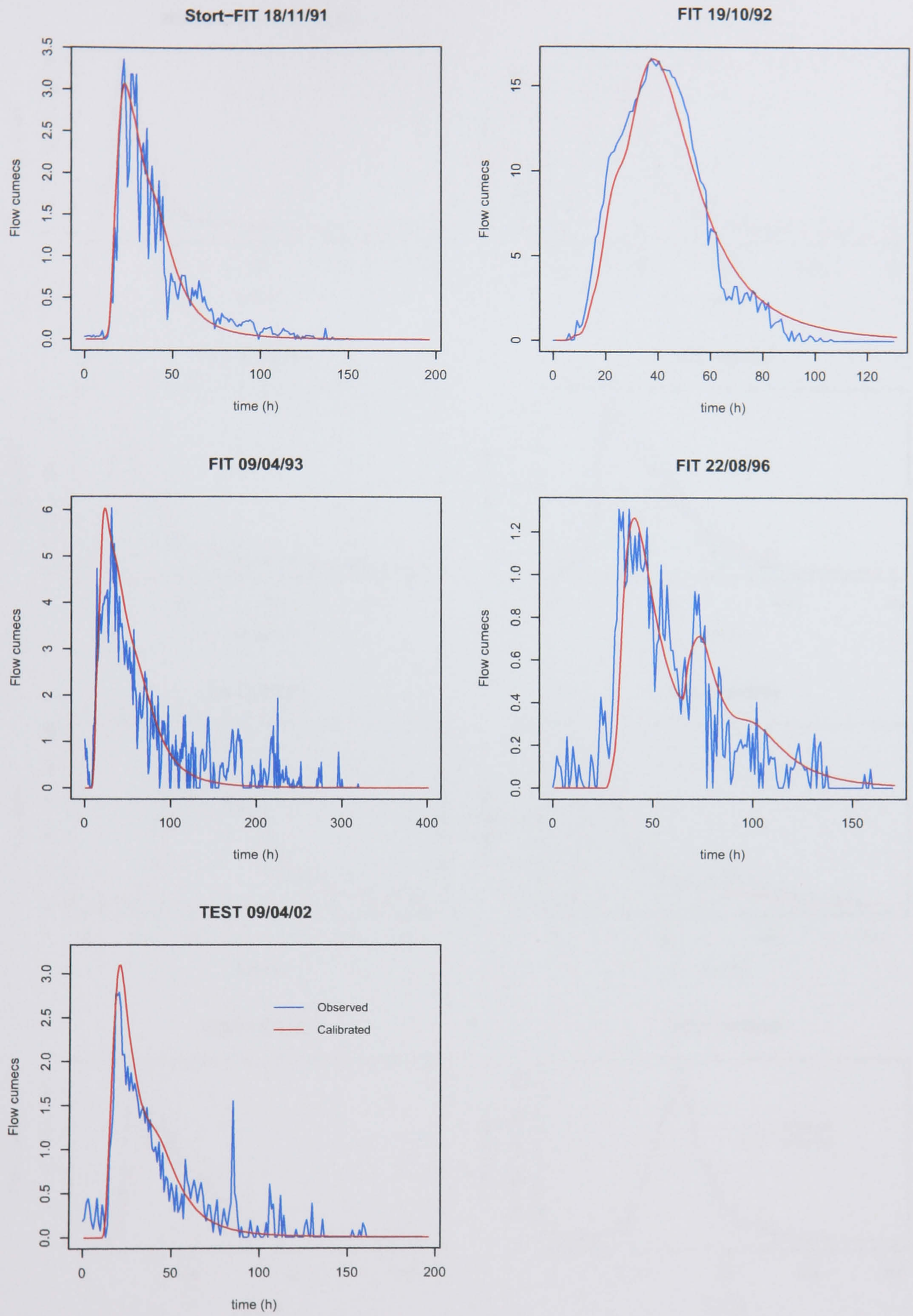

Figure 5.10 Calibration (FIT) and Validation (TEST) results for the Stort, adapted from Quasem (2004b).

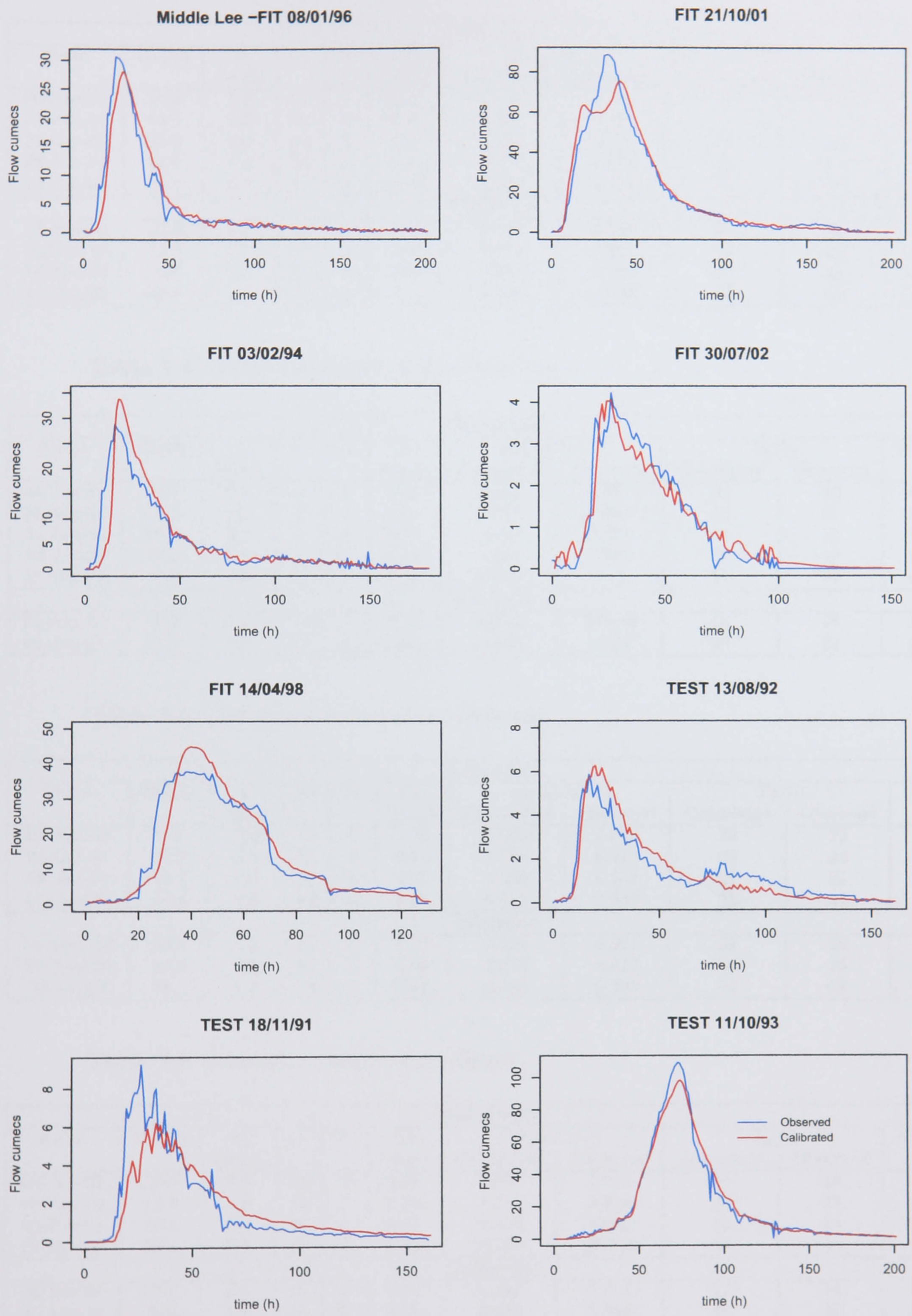

Figure 5.11 Calibration (FIT) and Validation (TEST) results for the Middle Lee

Calibration										
Event	Depth	m (mm)	kc	IL	RC (mm)	Qp (m^3s^{-1}) Calculated	Qp (m^3s^{-1}) Observed	Tp(h) Calculated	Tp(h) Observed	NSE_{obs}
09-Apr-93	15.0	0.8	27	1	0.18	3.000	3.004	18	16	0.78
03-Feb-94	14.5	0.8	21	3	0.23	4.481	4.407	8	8	0.92
21-Oct-01	30.5	0.8	33	4	0.17	4.693	4.696	18	18	0.84
08-Jan-96	21.6	0.8	24	3	0.18	4.294	4.274	12	13	0.94
23-Jul-96	32.1	0.8	11	0	0.03	3.204	3.221	6	6	0.93
Validation										
14-Apr-98	23.9	0.8	21	3	0.21	5.691	6.223	31	31	0.95
16-May-95	17.4	0.8	21	3	0.07	0.942	1.267	23	20	0.95
10-Nov-00	12.6	0.8	21	3	0.24	2.931	3.707	27	25	0.92
11-Oct-93	69.0	0.8	33	3	0.14	9.390	11.580	66	61	0.92

Table 5.4 Calibration results of the Upper Lee

Calibration										
Event	Depth	m (mm)	kc	IL	RC (mm)	Qp (m^3s^{-1}) Calculated	Qp (m^3s^{-1}) Observed	Tp(h) Calculated	Tp(h) Observed	NSE_{obs}
28-Apr-92	80.5	0.8	5	7	0.02	3.063	3.352	30	29	0.96
12-Aug-93	18.3	0.8	7	2	0.02	0.753	0.760	14	11	0.92
14-Sep-94	29.2	0.8	5	1	0.01	0.424	0.428	11	13	0.82
23-Jul-96	48.2	0.8	6	3	0.02	5.564	5.571	20	20	0.97
11-Oct-93	71.0	0.8	17	0	0.04	3.722	3.16	57	51	0.64
Validation										
02-Apr-00	42.8	0.8	7	2	0.01	0.664	0.7893	18	16	0.90
03-Jan-01	16.0	0.8	7	2	0.04	0.823	0.955	28	23	0.81

Table 5.5 Calibration results of the Mimram

Calibration										
Event	Depth	m (mm)	kc	IL	RC (mm)	Qp (m^3s^{-1}) Calculated	Qp (m^3s^{-1}) Observed	Tp(h) Calculated	Tp(h) Observed	NSE_{obs}
09-Apr-93	13.9	0.6	19	0	0.06	2.666	2.563	22	22	0.97
21-Oct-01	33.9	0.8	25	9	0.11	5.766	6.219	25	24	0.96
08-Jan-96	20.8	0.8	21	5	0.09	4.180	4.152	21	21	0.97
16-May-95	16.6	0.8	12	5	0.03	0.812	0.840	28	27	0.78
Validation										
14-April-98	20.6	0.8	21	5	0.12	4.299	5.387	39	39	0.95
27-May-00	23.6	0.8	21	5	0.09	4.016	4.917	22	26	0.94
30-Jul-02	18.5	0.8	12	5	0.02	0.736	0.709	28	29	0.92

Table 5.6 Calibration results of the Beane

Calibration										
Event	Depth	m (mm)	kc	IL	RC (mm)	Qp (m^3s^{-1}) Calculated	Qp (m^3s^{-1}) Observed	Tp(h) Calculated	Tp(h) Observed	NSE_{obs}
08-Jan-92	20.9	0.8	16	9	0.24	5.808	5.849	29	29	0.96
09-Apr-93	13.8	0.8	15	7	0.28	3.704	3.989	23	23	0.62
03-Feb-94	10.0	0.8	14	4	0.47	8.104	8.082	15	15	0.72
21-Oct-01	53.4	0.8	21	6	0.22	27.330	28.710	33	33	0.95
Validation										
08-Jan-96	17.8	0.8	16	9	0.35	6.443	7.883	17	19	0.74
01-Apr-93	18.5	0.8	16	9	0.18	2.902	3.588	19	16	0.88
27-May-00	26.8	0.8	16	9	0.23	6.546	7.901	24	26	0.95
11-Oct-93	63.0	0.8	21	9	0.32	21.180	23.510	68	70	0.95

Table 5.7 Calibration results of the Rib

Calibration										
Event	Depth	m (mm)	kc	IL	RC (mm)	Qp (m^3s^{-1}) Calculated	Qp (m^3s^{-1}) Observed	Tp(h) Calculated	Tp(h) Observed	NSE_{obs}
19-Oct-92	35.4	0.8	15	9	0.20	5.834	5.739	23	28	0.95
11-Oct-93	56.0	0.8	21	5	0.29	9.826	9.900	57	63	0.94
07-Dec-94	17.0	0.8	9	8	0.13	1.866	1.906	43	43	0.86
22-Dec-95	25.0	0.8	10	7	0.08	1.216	1.238	29	29	0.92
12-Feb-96	18.5	0.8	10	7	0.31	3.832	3.773	18	16	0.96
16-May-95	15.7	0.8	7	4	0.01	0.060	0.088	27	27	0.83
Validation										
26-Jan-01	17.4	0.8	15	9	0.83	9.979	7.164	15	19	0.95
08-Jan-96	20.0	0.8	15	1	0.21	4.283	4.733	18	18	0.97
30-Jul-02	22.4	0.8	7	0	0.01	0.079	0.137	34	18	0.73

Table 5.8 Calibration results of the Ash

Calibration										
Event	Depth	m (mm)	kc	IL	RC (mm)	Qp (m^3s^{-1}) Calculated	Qp (m^3s^{-1}) Observed	Tp(h) Calculated	Tp(h) Observed	NSE_{obs}
18-Nov-91	21.0	0.8	17	8	0.07	3.070	3.368	21	22	0.87
19-Oct-92	44.5	0.8	37	8	0.16	16.580	16.630	37	37	0.97
09-Apr-93	13.7	0.8	39	8	0.45	6.033	6.040	22	31	0.77
22-Aug-96	27.5	0.8	17	8	0.03	1.266	1.300	40	38	0.79
Validation										
09-Sep-02	20.6	0.8	17	8	0.06	3.099	2.790	20	20	0.80
11-Oct-93	55.0	0.8	37	0	0.33	28.160	27.630	53	74	0.75
08-Jan-96	19.0	0.8	37	8	0.41	7.396	8.883	20	20	0.87
03-Feb-94	11.0	0.8	37	0	0.43	7.218	8.764	29	28	0.88

Table 5.9 Calibration results of the Stort

Calibration										
Event	Depth	m (mm)	kc	IL	RC (mm)	Qp (m^3s^{-1}) Calculated	Qp (m^3s^{-1}) Observed	Tp(h) Calculated	Tp(h) Observed	NSE_{obs}
08-Jan-96	12.7	0.6	11	6	0.11	28.060	30.700	22	19	0.95
21-Oct-01	39.5	0.6	35	0	0.92	75.360	88.640	39	33	0.94
03-Feb-94	22.4	0.6	21	0	0.68	33.810	28.820	17	16	0.87
30-Jul-02	21.9	0.6	7	0	0.02	4.050	4.225	25	26	0.92
14-Apr-98	28.6	0.6	30	0	0.52	44.810	37.720	39	39	0.92
Validation										
13-Aug-92	21.2	0.6	21	0	0.13	6.264	5.863	19	17	0.87
18-Nov-91	24.3	0.6	21	0	0.06	6.184	9.266	32	26	0.80
11-Oct-93	59.0	0.6	35	0	0.46	98.000	109.100	73	73	0.98

Table 5.10 Calibration results of the Middle Lee

5.3.2 Modelling the Integrated Lee Catchment

Following validation of the individual tributaries, the subcatchments are incorporated into an integrated modelling strategy to achieve the catchment hydrological routing. Each subcatchment is first modelled independently and the simulated runoff is then used as inflow to the Middle Lee model and routed into the total runoff generated at Feildes Weir to represent the behaviour of the basin at the 1033 km^2 catchment scale (Feildes model). A common set of events is defined in order to test the combined calibration at Feildes Weir. This task is more difficult to undertake as radar images, rainfall and discharge data are not always available at all 16 raingauges and 7 main flow stations.

Selected events

Due to data availability and the manual calibration procedure, the study is limited to five individual storm events. In the context of flood management, these events are of medium to large size. They are taken at different times of the year, representative of frontal and convective activities and associated with high, medium and low flows. Hence the largest rainfall event in the database, 11th October 1993, leading to the highest peak plow in the database, is selected to represent an extreme event. This is complemented with two medium, more frequent events in winter, on 03rd February 94 and 08th January 1996, and two frequent events in summer on 16th May 1995 and 30th July 2002. Summer events are difficult to calibrate since they generate low flow values. Hence the above events are selected so that a minimum peak flow of 5 m^3/s is recorded at Feildes Weir (including baseflow). The characteristics of the selected events are provided in Table 5.11 and their spatial extent captured by the Chenies radar can be found in Appendix B. The coefficient of variation is large for the event of 30th July 2002. This event is characterised by a high temporal and spatial variability as illustrated in Figure 5.12, representing two contrasting temporal profiles at two raingauges relatively close in space (10 km apart).

Events	Duration hr	Mean mm	CV. %	Direct runoff cumecs
11 Oct 1993	65	62.7	16.9	109.1
03 Feb 1994	8	12.1	16.5	28.8
08 Jan 1996	19	20.3	14.3	30.7
16 May 1995	25	17.1	11.1	4.3
30 Jul 2002	30	21.4	42.7	4.2

Table 5.11 Characteristics of selected events

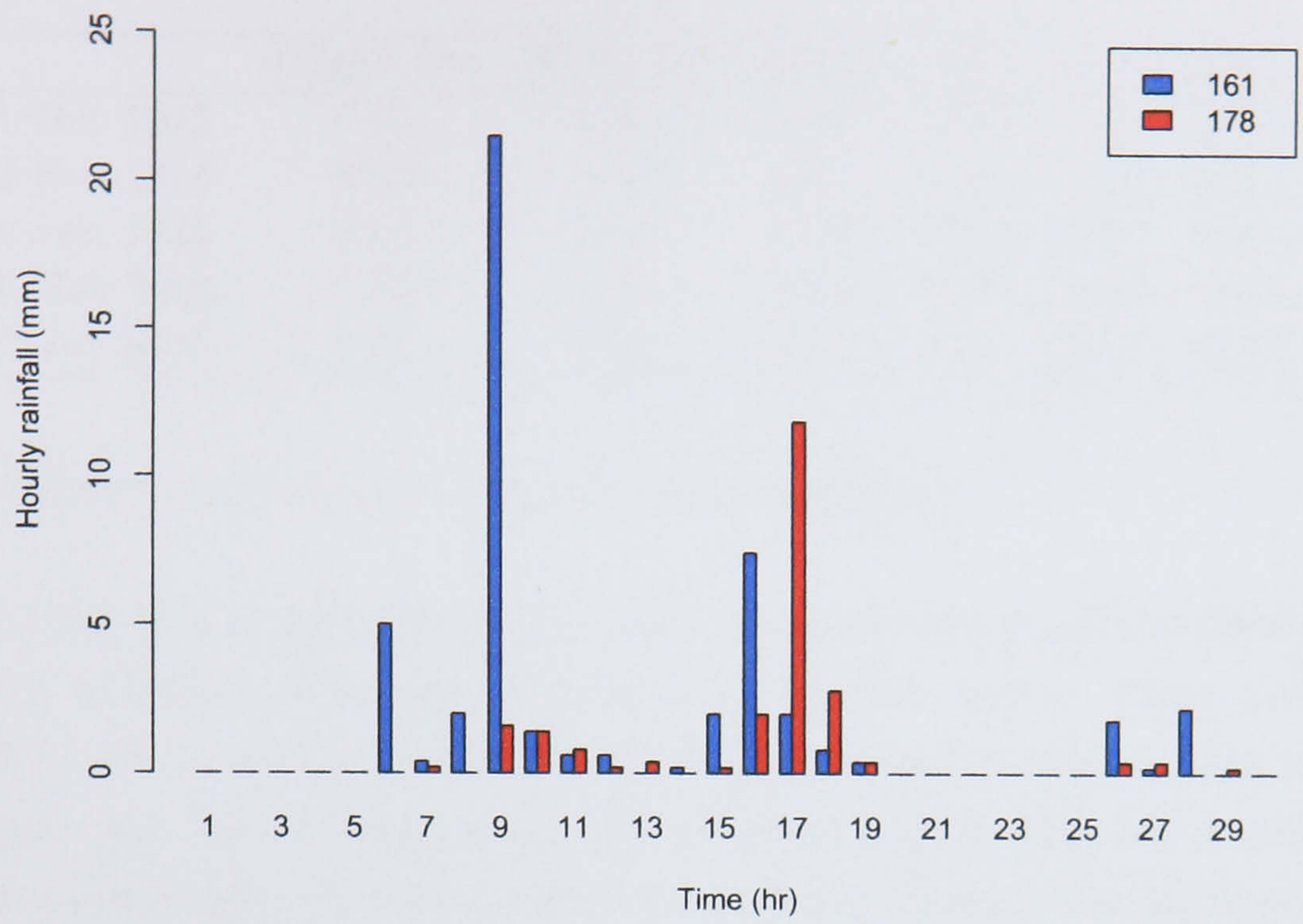

Figure 5.12 Variability of the event of 30/07/02 at two sites

Model Performance

The range in runoff coefficient calibrated to the five selected events is given in Table 5.12. For most subcatchments, it can be seen that the runoff coefficient is higher in winter than in summer, which reflects the wetter/drier antecedent catchment condition in winter/summer. Compared to the other subcatchments, the Mimram is characterised by a low value of the runoff coefficient, which is in agreement with the observed damped behaviour of this catchment.

	Upper Lee	Mimram	Beane	Rib	Ash	Stort	Feildes
RC winter	0.14-0.23	0.03-0.04	0.09-0.29	0.32-0.74	0.21-0.39	0.33-0.43	0.15-0.69
RC summer	0.07-0.08	0.01-0.02	0.02-0.03	0.01-0.02	0.01	0.02-0.03	0.03

Table 5.12 Runoff coefficient (RC) calibrated for the 5 selected events

Using the calibrated parameters, the results in terms of NSE_{obs} for the 5 selected events are displayed in Table 5.13. A reasonable fit is achieved with NSE_{obs} of 0.77 on average for all subcatchments and events. The performance at interior points is lower in the case of extreme and summer events. The observed and reference flow at each (sub)catchment outlet are plotted in Figure 6.1 to 6.5.

	Upper Lee	Mimram	Beane	Rib	Ash	Stort	Feildes
11 Oct 1993	0.92	0.55	0.54	0.96	0.94	0.75	0.84
03 Feb 1994	0.92	0.65	0.83	0.86	0.84	0.88	0.95
08 Jan 1996	0.94	0.64	0.97	0.85	0.97	0.88	0.87
16 May 1995	0.73	0.61	0.78	0.78	0.22	0.59	0.92
30 Jul 2002	0.61	0.84	0.92	0.51	0.73	0.23	0.88

Table 5.13 Calibration results in terms of NSE_{obs}

Hence, calibration of the individual subcatchments has been achieved and the integrated modelling to Feildes Weir has been validated on five events. These events constitute a reference set to which rainfall representations based on radar data, subsets of the raingauges and the disaggregation scheme presented in Chapter 4 will be tested to assess the significance of spatial data for runoff generation. The findings are presented in the following chapter.

Chapter 6

The Significance of Spatial Rainfall Data for Flood Runoff Modelling

In this chapter the significance of rainfall spatial data for flood generation is analysed by comparing the impact of various rainfall representations on the reference flow at the (sub)catchment scale. An index of rainfall spatial variability is defined to quantify this and results are analysed as a function of rainfall type, catchment properties and catchment scale.

6.1 Measure of Rainfall Variability and Basin Damping

6.1.1 Rainfall Estimators

As mentioned previously, the reference rainfall consists of spatially variable areal estimates determined from the Thiessen polygons method using all available raingauges. The hourly temporal pattern applied to each sub-area is given by the nearest raingauge. In this study, in order to analyse the effects of various rainfall representations, the subcatchments are also run with the following rainfall inputs at an hourly time-step:

- Raingauge network:
  - Single raingauge per subcatchment with uniform rainfall over the subcatchment. The raingauge which is nearest to the centroid of the subcatchment is selected (See 'Centroid RG' in Table 5.2). Hence at the catchment scale, the flow at Feildes Weir is driven by seven raingauges (SG7).
  - Single raingauge with uniform rainfall over the catchment. The raingauge which is nearest to the centroid of the Feildes Weir catchment is selected (SG1).
- Spatially variable rainfall from radar data calibrated using the network of supporting raingauges (Bellone, 2003). The areal rainfall on each sub-area is estimated

from the average of the pixels included in the subarea. The hourly temporal pattern applied to each subarea is given by the hourly averaged radar rainfall estimate for the sub-area.

- Spatially variable rainfall from spatially-uniform temporal disaggregation (presented in Chapter 4) conditioned on real daily data at the raingauge locations (Dis). The observed hourly temporal profile of the raingauge in the centroid of the catchment (0163) is selected to disaggregate the daily totals to hourly rainfall at the other sites on the catchment.

For the practitioner, a central question is to assess the importance of the spatial structure of rainfall in rainfall-runoff modelling and evaluate what is necessary to characterise this in terms of observational (and simulated) data. Hence one objective of this investigation is to determine the requirements in terms of type of data and raingauge density for rainfall-runoff applications. SG7 and SG1 represent a degradation of spatial information in comparison to the reference rainfall and lower model performance is expected. Note that, the aim of this comparison is to examine the sensitivity of runoff to the number of raingauges used. Therefore a single rainfall input is used (for a subcatchment or the whole catchment), it represents the modelled or observed rainfall at the raingauge site and *not* the areal average over that subcatchment or catchment. The use of radar data represents an improvement in terms of spatial information but since the model is calibrated using the reference rainfall, similar model performance is expected. The disaggregation scheme preserves the areal rainfall variability in comparison to the reference rainfall but tests the hypothesis of a single temporal profile applied at all sites. In addition, the rainfall estimators are selected because they give an insight to the requirements in terms of modelling of spatial rainfall for hydrological applications (i.e. a full spatial-temporal rainfall model based on radar data, a multisite model based on a raingauge network, a point model at one gauge).

Due to time constraint, the analysis is restricted to these four rainfall representations in addition to the reference rainfall. It could be argued that a different volume of rainfall is used and that might be a factor affecting the sensitivity of the model. However, the volume of rainfall is preserved when using the disaggregation rainfall estimator. In addition, the parameters derived for calibration of the radar data ensured that on the average, the discrepancies between the gauge and radar estimates are minimised (see Chapter 3). Therefore the difference in volume is small and the runoff sensitivity to the rainfall estimators is assessed.

6.1.2 Spatial Deviation Index

The Spatial Deviation Index (SDI) (Quasem, 2004b) is defined for each storm and (sub)catchment as a measure of spatial variability over a (sub)catchment. It measures the deviation between the sub-areal reference rainfall to the (sub)catchment averaged areal rainfall and is defined as follows:

$$SDI = \frac{1}{N}\sum_{i=1}^{N}\frac{|P_{ri} - P_T|}{P_T} \tag{6.1}$$

where P_{ri} represents the reference areal precipitation (i.e. as defined by the full rain-gauge network) for sub-area i in mm, P_T the (sub)catchment Thiessen averaged areal precipitation in mm, and N the number of sub-areas for a given (sub)catchment.

A Reference Spatial Deviation Index (SDIR) compares the rainfall spatial deviation between the sub-areal estimates from the tested rainfall representations to the reference sub-areal precipitation estimates.

$$SDIR = \frac{1}{N}\sum_{i=1}^{N}\frac{|P_i - P_{ri}|}{P_{ri}} \tag{6.2}$$

where P_i represents the areal precipitation from either radar data or subsets of the gauges for sub-area i in mm, P_{ri} the reference areal precipitation in mm for sub-area i, and N the number of sub-areas.

For each subcatchment, the events defined in Table 5.11 are used to test the model sensitivity to the rainfall representation defined above. The model is run using the parameters selected from the calibration stage. The rainfall variability in terms of SDI (%) and SDIR (%) is presented in Tables 6.1 and 6.2. Results in Table 6.1 show that

	Upper Lee	Mimram	Beane	Rib	Ash	Stort	Feildes
11 Oct 1993	11.3	5.5	10.0	7.9	2.3	9.1	8.1
03 Feb 1994	6.6	5.2	8.3	9.7	7.2	5.9	7.3
08 Jan 1996	6.9	8.3	8.6	13.1	4.6	10.6	8.3
16 May 1995	4.4	4.1	5.2	3.2	2.6	3.8	4.6
30 Jul 2002	19.6	11.6	11.2	11.7	25.3	25	19

Table 6.1 SDI (%) values for the five selected events for each (sub)catchment.

across all events and all subcatchments, the SDI ranges between 2.3% and 25.3%. As expected, larger discrepancies are introduced for the more variable event of 30th July 2002. Results from Table 6.2 show that SDIR ranges between 2% and 42%. Radar data

	Upper Lee	Mimram	Beane	Rib	Ash	Stort	Feildes
11-Oct-93							
Radar	11.5	18.6	11.6	18.6	10.8	18.9	15.9
SG7	18.0	9.3	12.9	10.0	2.2	12.5	10.9
SG1	14.6	17.5	18.4	8.7	4.7	9.1	10.8
03-Feb-94							
Radar	7.8	11.3	7.9	8.2	6.8	5.0	6.8
SG7	4.0	5.5	12.5	15.6	9.2	5.0	8.3
SG1	8.5	6.3	22.8	33.5	24.8	22.9	19.3
08-Jan-96							
Radar	7.4	2.8	7.2	10.4	4.2	10.3	8.2
SG7	9.0	10.6	9.1	20.7	4.8	21.9	12.9
SG1	7.2	10.4	9.3	26.4	11.3	19.2	13.0
16-May-95							
Radar	10.8	15.6	7.8	12.7	8.2	10.4	9.8
SG7	8.8	9.2	5.2	4.0	3.3	4.1	6.1
SG1	22.6	13.4	30.1	33.5	36.5	33.7	27.4
30-Jul-02							
Radar	30.0	34.6	28.5	22.0	16.2	27.1	25.0
SG7	39.9	15.4	20.8	11.8	17.3	32.8	26.3
SG1	21.2	21.2	27.1	19.0	24.8	42.3	29.2

Table 6.2 SDIR (%) values for Radar, SG7 and SG1 representations for the five selected events for each (sub)catchment.

lead to the largest deviation in areal rainfall, compared to SG7 and SG1 for the event of 11th October 1993 but in general, a closer agreement is seen between the reference rainfall and radar data, and the discrepancies are worse when SG1 is used. The event of 30th July 2002 leads to the highest deviations of the order of 30% for all rainfall representations.

6.1.3 Catchment Response Time

Indices have been derived to measure the runoff variability in relation to rainfall (Woods and Sivapalan, 1999; Ogden and Julien, 1993; Smith et al., 2004; Morin et al., 2001). A common descriptor is the lag time which represents an intrinsic property of the catchment. It is a measure of the catchment response time and expresses the average travel time from all points on the catchment to the outlet (Lekkas and Onof, 2005). Following NERC (1975), the time from the centroid of total rainfall to the peak flow is taken as a measure of the lag times. In case of multipeaked events, the definition is widened to be the time from the centroid of total rainfall to the "centroid of peaks". For each subcatchment, a rainfall time-series is obtained as the arithmetic average of

the raingauges. The lag time between the centroid of the averaged rainfall time-series and the reference flow peak is calculated. It varies between events according to the spatial and temporal distribution of the rainfall and to the antecedent condition of the catchment. Therefore, for each subcatchment, an average of the lag time over the five events is taken as the catchment response time.

6.2 Rural Catchment Results

In order to assess which level of spatial representation of rainfall is required to adequately reproduce the streamflow at the outlet, radar data, SG7 and SG1 are used as input to the rainfall-runoff model with the parameters calibrated to the reference rainfall. The simulated runoff is compared to the reference streamflow as illustrated in Figure 6.1 to 6.5.

A modified definition of NSE is introduced at this stage to measure the performance of the simulated runoff in comparison to the reference flow according to:

$$NSE_{ref} = 1 - \frac{\sum_{i=1}^{M}(C_i - R_i)^2}{\sum_{i=1}^{M}(R_i - \overline{R})^2} \tag{6.3}$$

where C_i and R_i are the calculated and reference discharge at hour i. The results in terms of NSE_{ref} and NSE_{obs} can be found in Table 6.4 and Table 6.5.

On average for all subcatchments and events, NSE_{ref} values of 0.95, 0.91 and 0.80 are observed for Radar, SG7 and SG1, respectively. In terms of NSE_{obs}, values of 0.73, 0.73 and 0.60 are observed for Radar, SG7 and SG1, respectively. It is difficult to interpret the results in terms of NSE_{obs} since the calibration is not perfect. The average value of NSE_{obs} between the reference and observed flow is 0.77 and the difference to a value of 1 (perfect fit) should be seen as a model error. The results in terms of NSE_{ref} express the errors introduced by the rainfall representation.

Radar data always lead to high performance at both catchment and subcatchment scale ($\mathrm{NSE}_{ref} > 0.95$). Considering the variation over all events, lower performance is observed for the extreme event on the Rib and the Ash (NSE_{ref} of 0.86 and 0.83, respectively) and during summer events (NSE_{ref} of 0.78 on the Upper Lee on 16th May 1995 and NSE_{ref} of 0.74 and 0.73 on the Upper Lee and the Beane on 30th July 2002). This suggests that the rainfall information captured by the radar data differs from that of the network of 16 raingauges in the case of the extreme and summer events studied.

SG7 also generally gives high values of NSE_{ref} at catchment scale, with somewhat lower performance on the Rib on 3rd February 1994 (NSE_{ref} of 0.88) and 8th January 1996 (NSE_{ref} of 0.82), the Stort on 8th January 1996 (NSE_{ref} of 0.72) and 30th July 2002 (NSE_{ref} of 0.78), the Upper Lee on 16th May 1995 (NSE_{ref} of 0.72) and on 30th July 2002 (NSE_{ref} of -0.06) and the Beane on 30th July 2002 (NSE_{ref} of 0.75). The performance is always high for the Mimram, the Ash and the Beane. This suggests that one gauge per tributary may be adequate for the Mimram, a medium size Chalk basin and the Ash, an entirely rural small basin. A network of seven raingauges may be suitable to model the more heterogeneous large scale catchment (i.e. the flow at the catchment outlet only, no interior point).

SG1 gives lower results for all events at both catchment and subcatchment scale, except for the Mimram. Hence this confirms that the Mimram does not show much sensitivity to spatial rainfall and can be modelled using rainfall from one raingauge.

The graphs in Figures 6.6 to 6.10 display the percentage change in peak discharge (Q_p), peak time (T_p) and runoff volume (V) in comparison to the reference flow. The catchments are ranked by size. T_p is usually well reproduced (less than 8% error on average) but depending on the rainfall representation, larger errors are introduced with a percentage change ranging between [-40,80], [-20,60] for Q_p and V, respectively. Results in Table 6.3 show that the relative error in Q_p T_p and V is less with radar data and increases with SG7 and SG1. However there is no obvious trend between the percentage change in Q_p, T_p, V and the scale of the catchment.

In conclusion, radar data lead to high values of NSE_{ref} at all scales and to the smallest variations in Q_p, T_p, V. SG7 lead to high NSE_{ref} values at the catchment scale but occasionally lower performances at subcatchment scale. This representation does not seem to affect the average T_p but compared to radar data, increases the errors in Q_p and V. Lower performances in terms of NSE_{ref}, Q_p, T_p and V are observed at subcatchment and catchment scales with SG1. Lower performance are observed for the extreme event and the summer events. The relative importance of spatial rainfall, basin damping and basin scale is assessed in the following sections.

	Radar	SG7	SG1
Q_p (%)	12.6	15.3	28.1
T_p (%)	5.6	5.8	8.0
V (%)	7.4	12.4	21.6

Table 6.3 Average percentage change in peak flow, time to peak and hydrograph volume

	Upper Lee	Mimram	Beane	Rib	Ash	Stort	Feildes
11-Oct-93							
Radar	0.98	0.97	0.99	0.86	0.83	0.94	0.97
SG7	0.91	1	0.96	0.95	0.97	0.96	0.98
SG1	0.97	0.89	0.96	0.96	0.96	0.95	0.96
03-Feb-94							
Radar	0.92	1	0.99	0.99	0.98	1	0.99
SG7	0.93	0.99	0.93	0.88	0.99	1	0.99
SG1	0.97	1	0.73	0.36	0.74	0.89	0.86
08-Jan-96							
Radar	0.99	1	1	0.98	0.99	0.99	1
SG7	0.97	0.99	0.98	0.82	1	0.72	0.98
SG1	0.98	0.96	0.99	0.69	0.99	0.79	0.92
16-May-95							
Radar	0.90	0.97	0.94	0.97	0.99	0.99	1
SG7	0.82	0.98	0.98	0.99	1	0.99	0.94
SG1	0.42	0.92	0.54	0.69	0.54	0.74	0.65
30-Jul-02							
Radar	0.74	0.98	0.73	0.97	0.98	0.9	0.95
SG7	−0.06	0.97	0.75	0.96	0.97	0.78	0.98
SG1	0.35	0.93	0.53	0.99	0.77	0.61	0.85

Table 6.4 NSE_{ref} rural catchments

	Upper Lee	Mimram	Beane	Rib	Ash	Stort	Feildes
11-Oct-93							
Radar	0.93	0.71	0.55	0.83	0.68	0.55	0.78
SG7	0.80	0.58	0.65	0.97	0.92	0.72	0.90
SG1	0.90	0.74	0.51	0.97	0.97	0.87	0.92
03-Feb-94							
Radar	0.87	0.65	0.78	0.88	0.74	0.89	0.92
SG7	0.90	0.58	0.78	0.62	0.81	0.89	0.92
SG1	0.90	0.61	0.57	<0	0.08	0.73	0.75
08-Jan-96							
Radar	0.91	0.63	0.96	0.82	0.97	0.87	0.86
SG7	0.94	0.71	0.93	0.68	0.98	0.57	0.91
SG1	0.94	0.41	0.98	0.36	0.95	0.76	0.83
16-May-95							
Radar	0.60	0.61	0.58	0.66	0.34	0.55	0.90
SG7	0.51	0.64	0.75	0.71	0.07	0.58	0.83
SG1	0.23	0.64	<0	0.83	<0	0.52	0.60
30-Jul-02							
Radar	0.75	0.85	0.54	0.55	0.74	<0	0.86
SG7	0.76	0.77	0.44	0.64	0.75	0.40	0.88
SG1	0.76	0.74	0.10	0.58	0.46	<0	0.78

Table 6.5 NSE_{obs} rural catchments

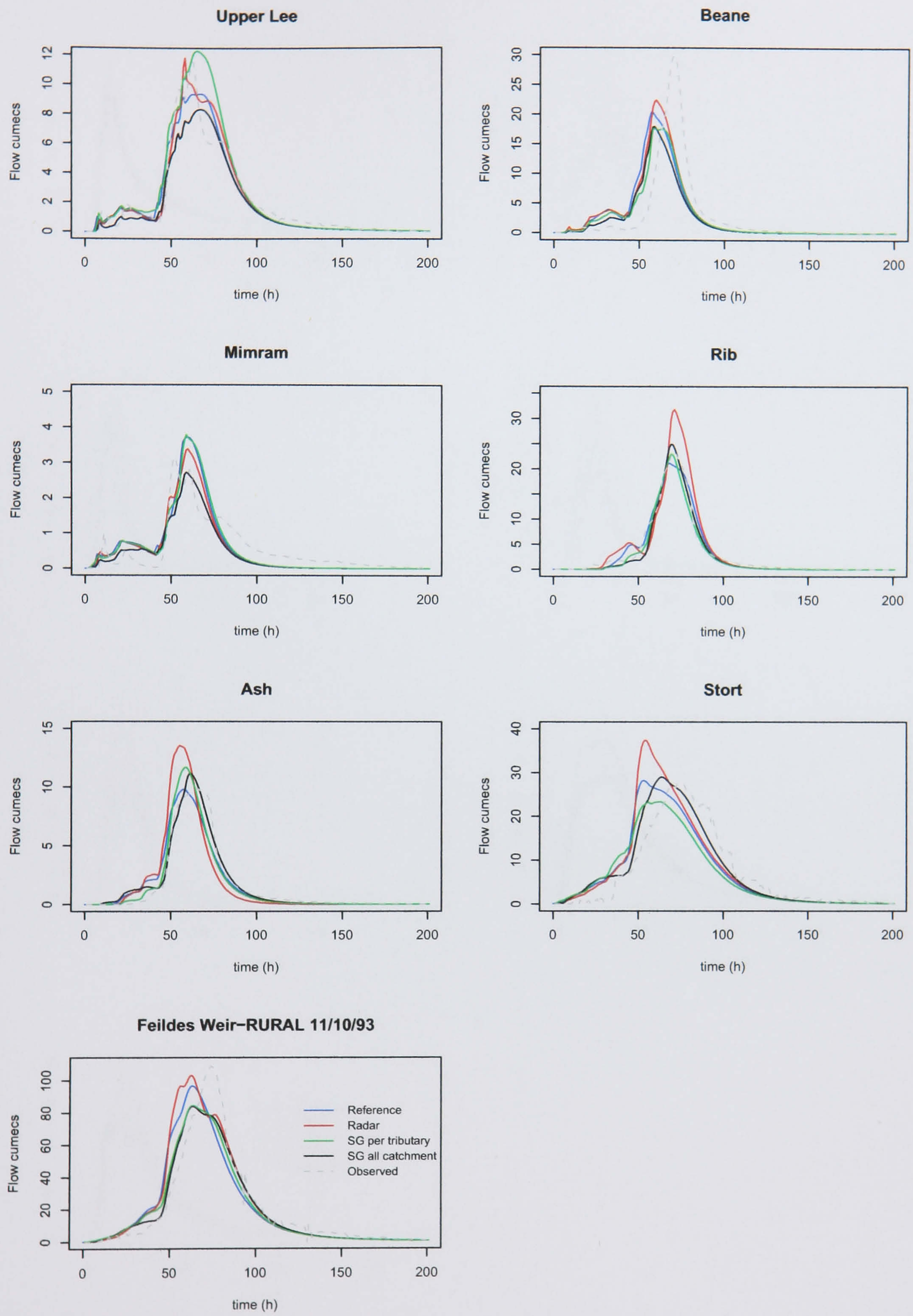

Figure 6.1 Observed, reference and simulated flows at catchment outlets on 11/10/93

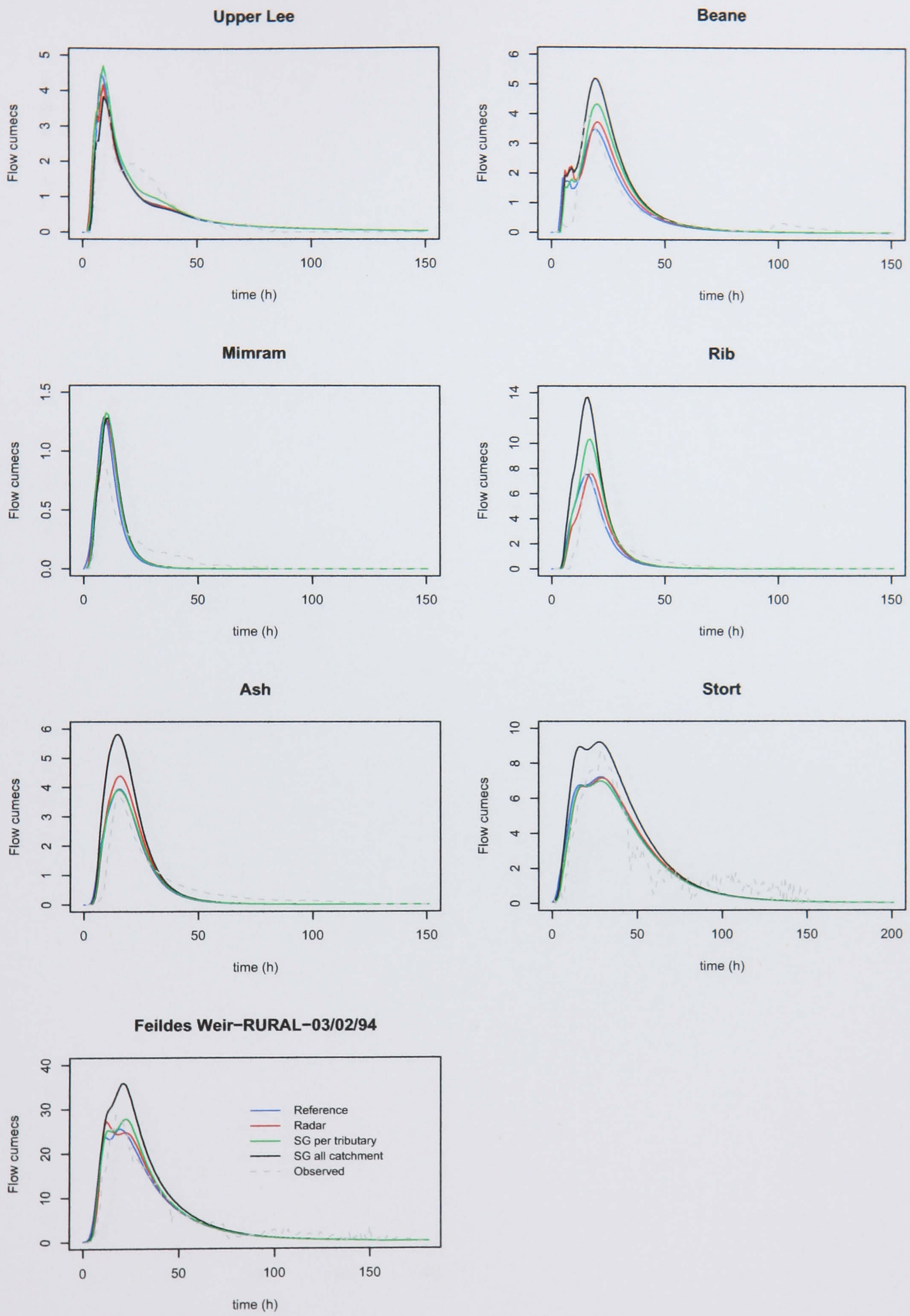

Figure 6.2 Observed, reference and simulated flows at catchment outlets on 03/02/94

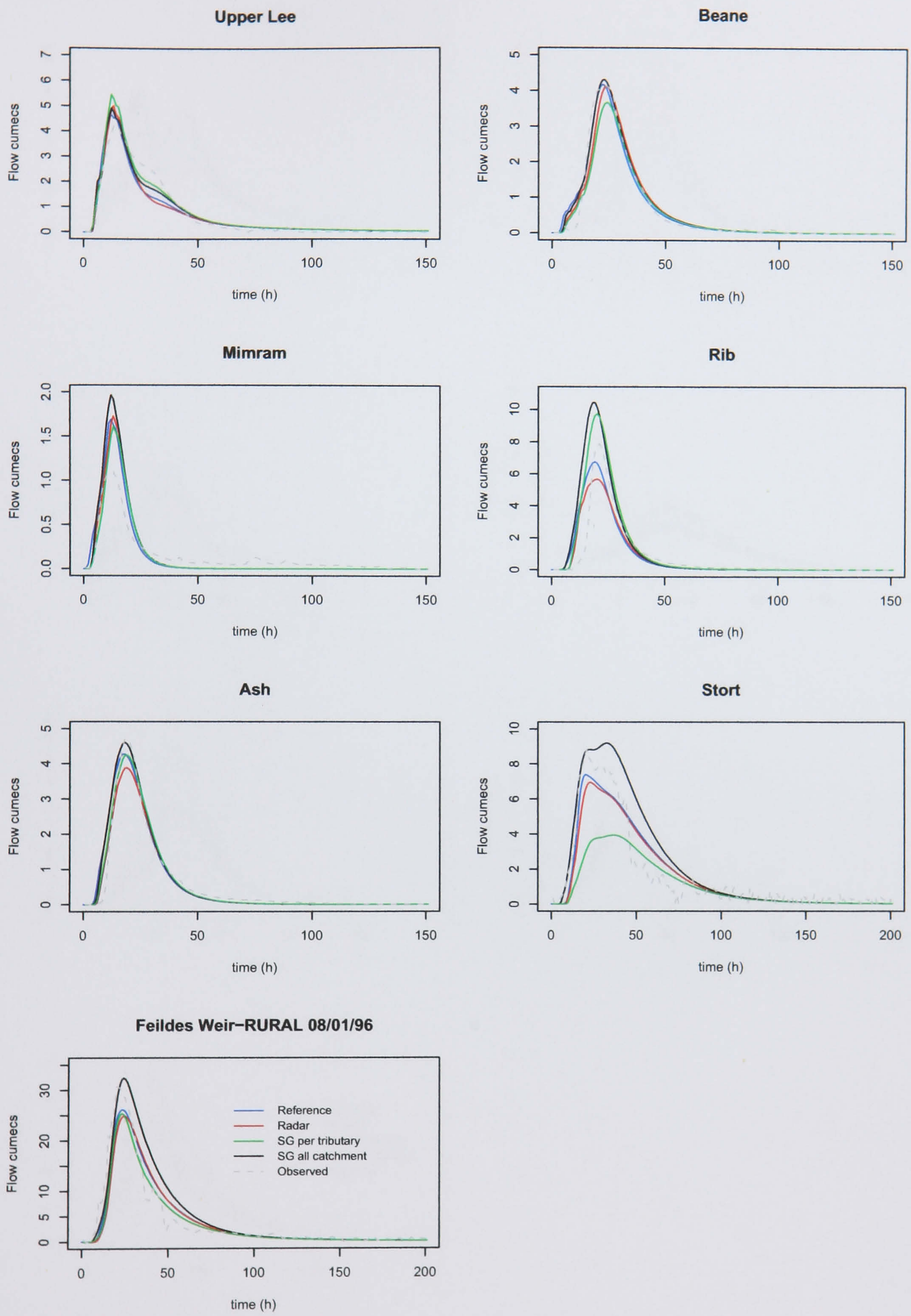

Figure 6.3 Observed, reference and simulated flows at catchment outlets on 08/01/96

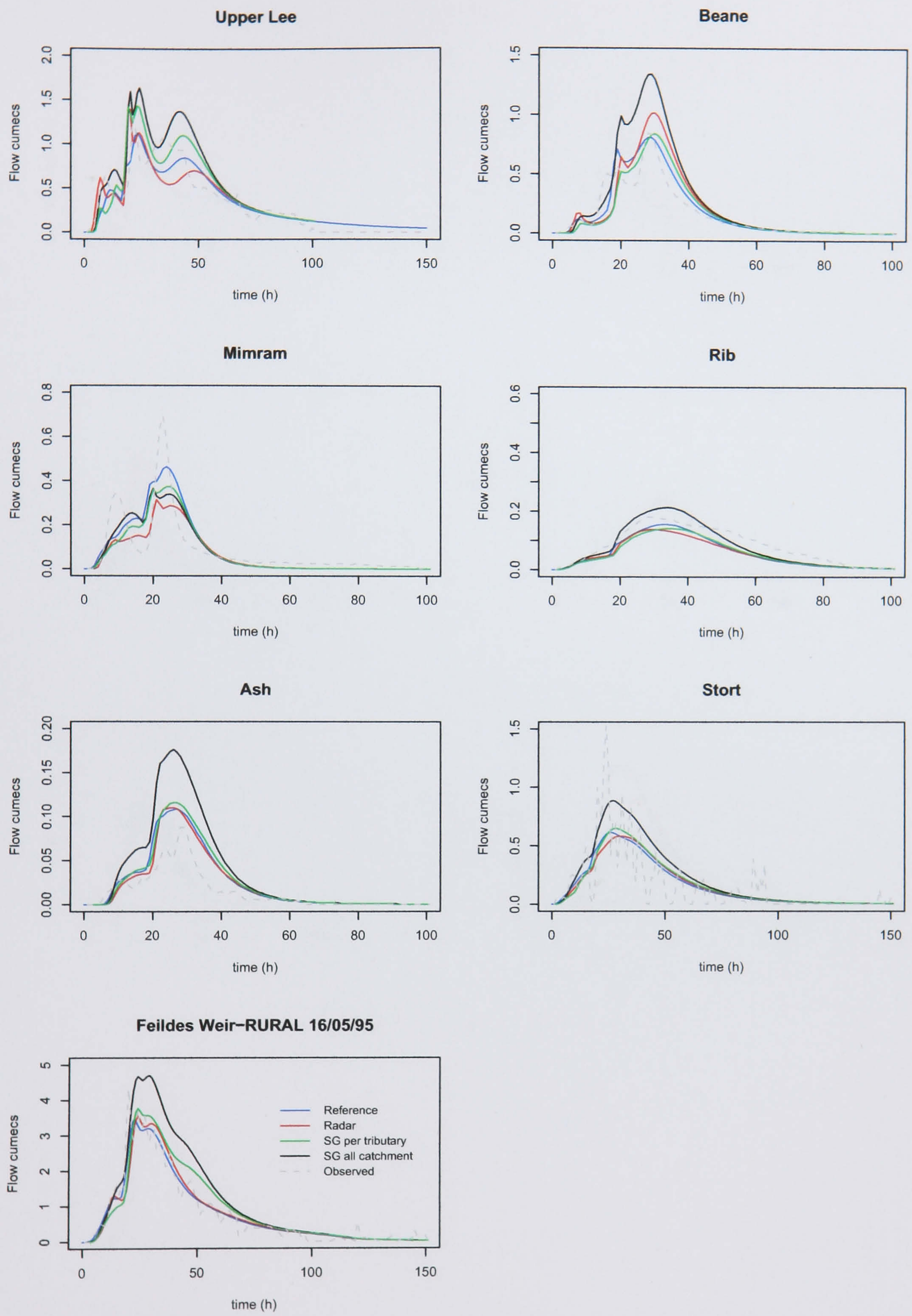

Figure 6.4 Observed, reference and simulated flows at catchment outlets on 16/05/95

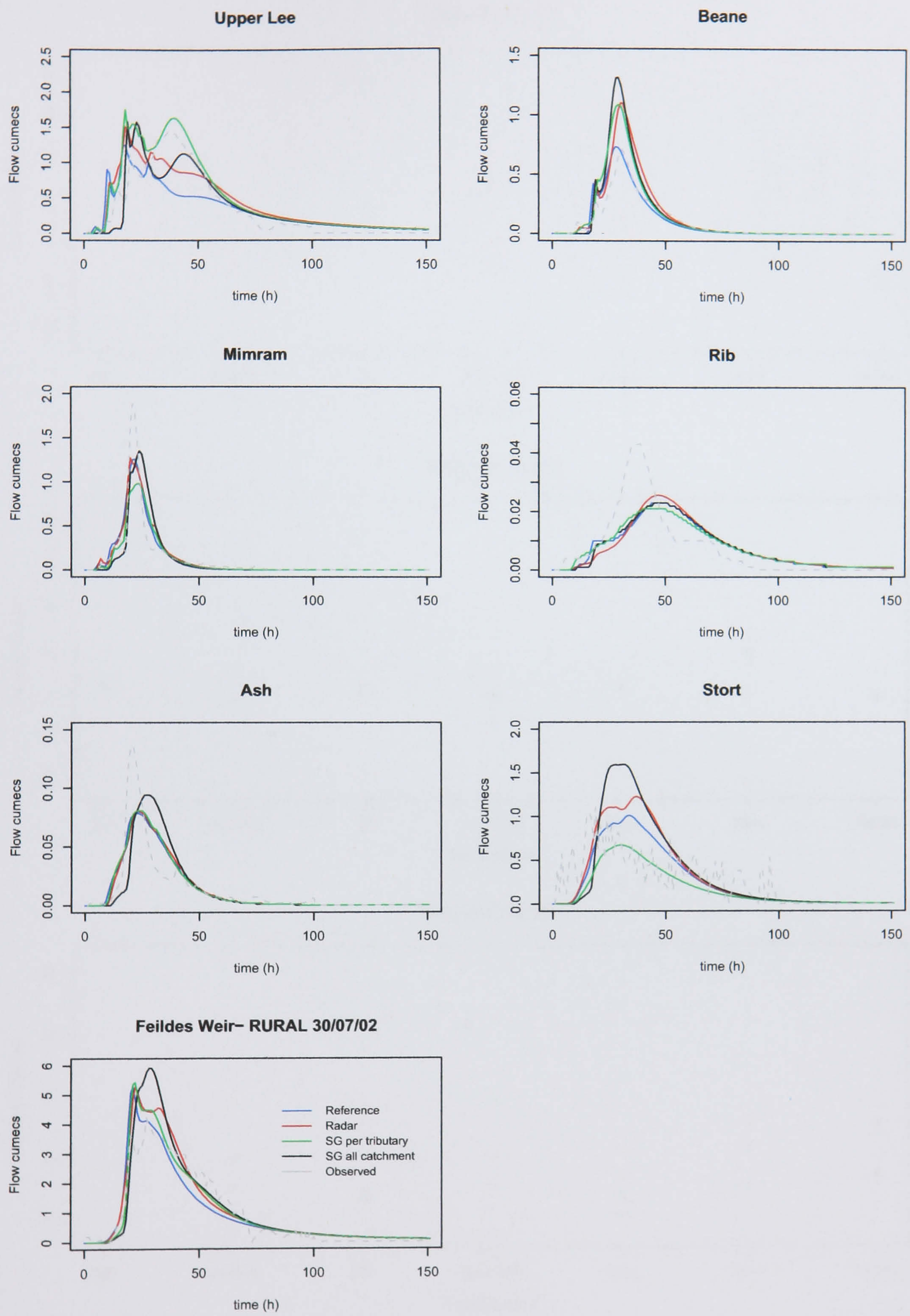

Figure 6.5 Observed, reference and simulated flows at catchment outlets on 30/07/02

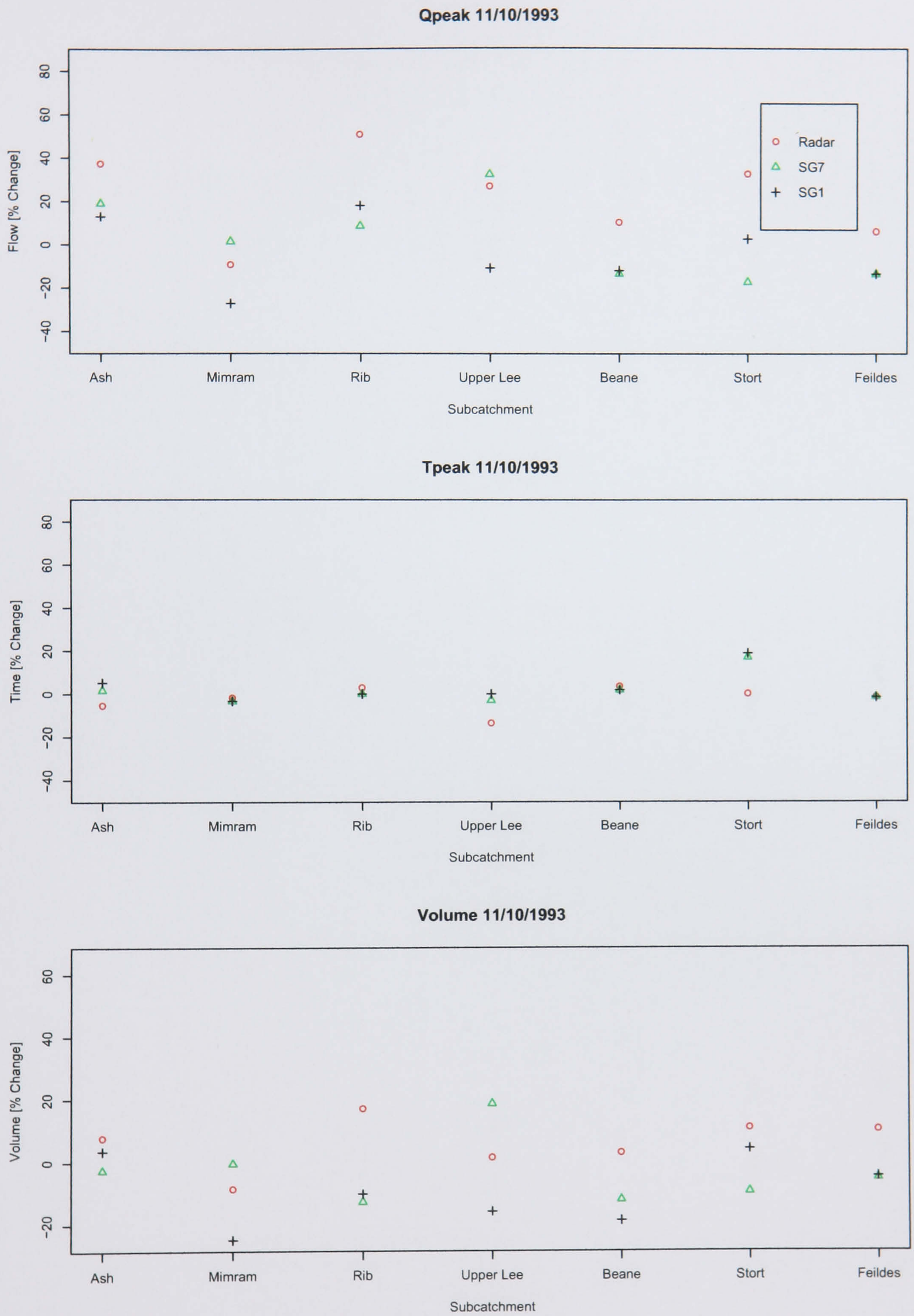

Figure 6.6 Percentage change in peak flow, time to peak and volume in comparison to the reference flow for the event of 11/10/93

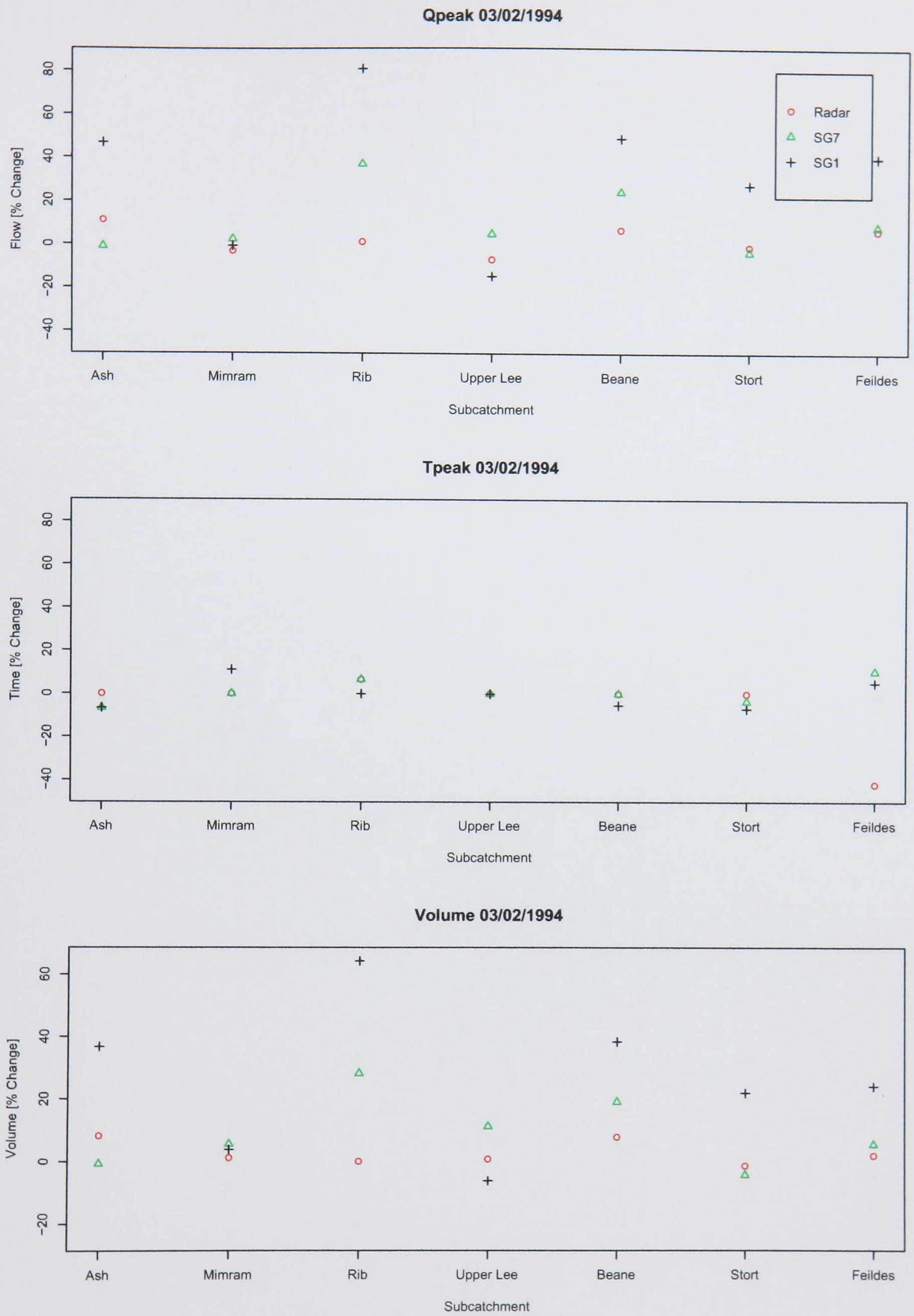

Figure 6.7 Percentage change in peak flow, time to peak and volume in comparison to the reference flow for the event of 03/02/94

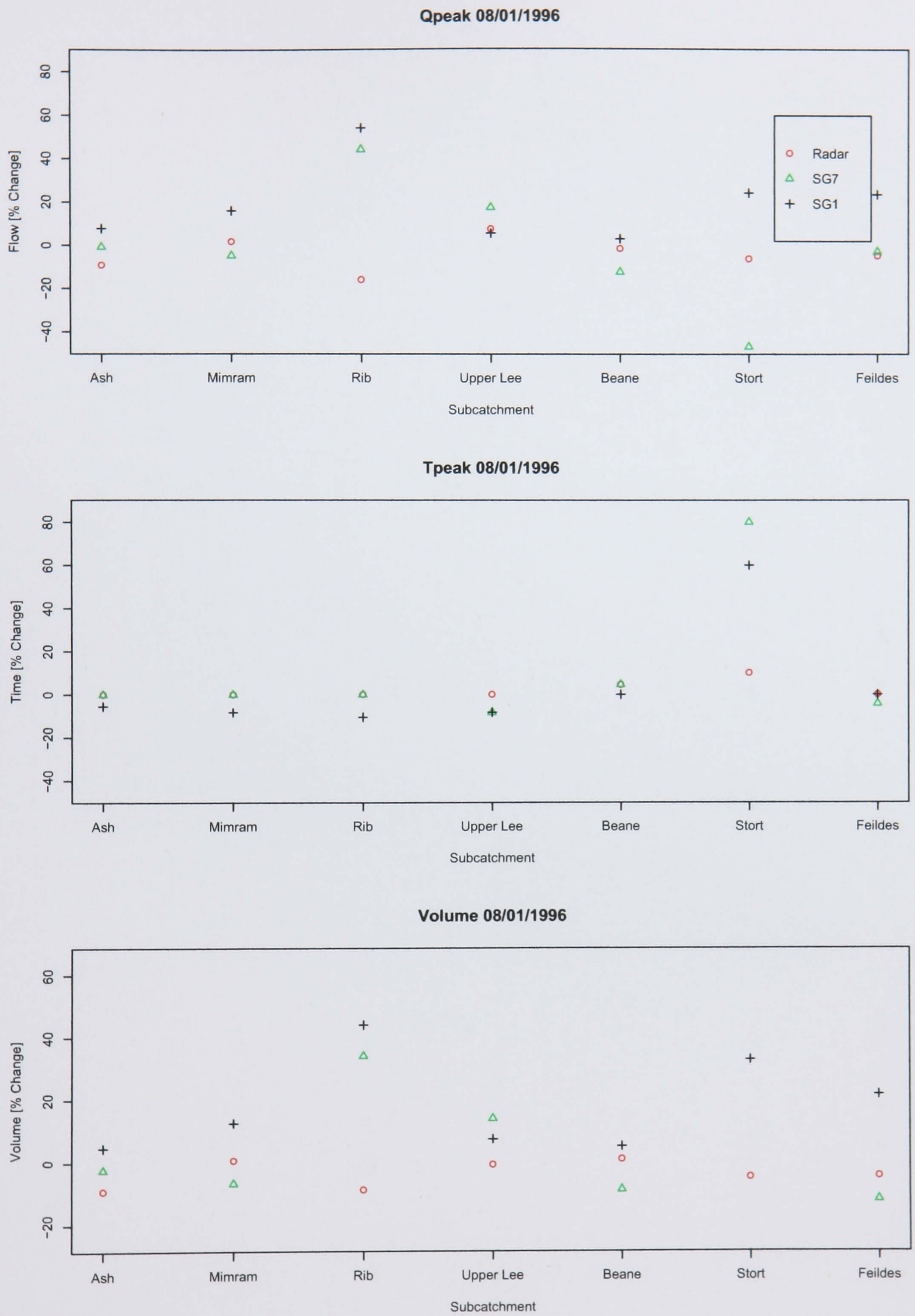

Figure 6.8 Percentage change in peak flow, time to peak and volume in comparison to the reference flow for the event of 08/01/96

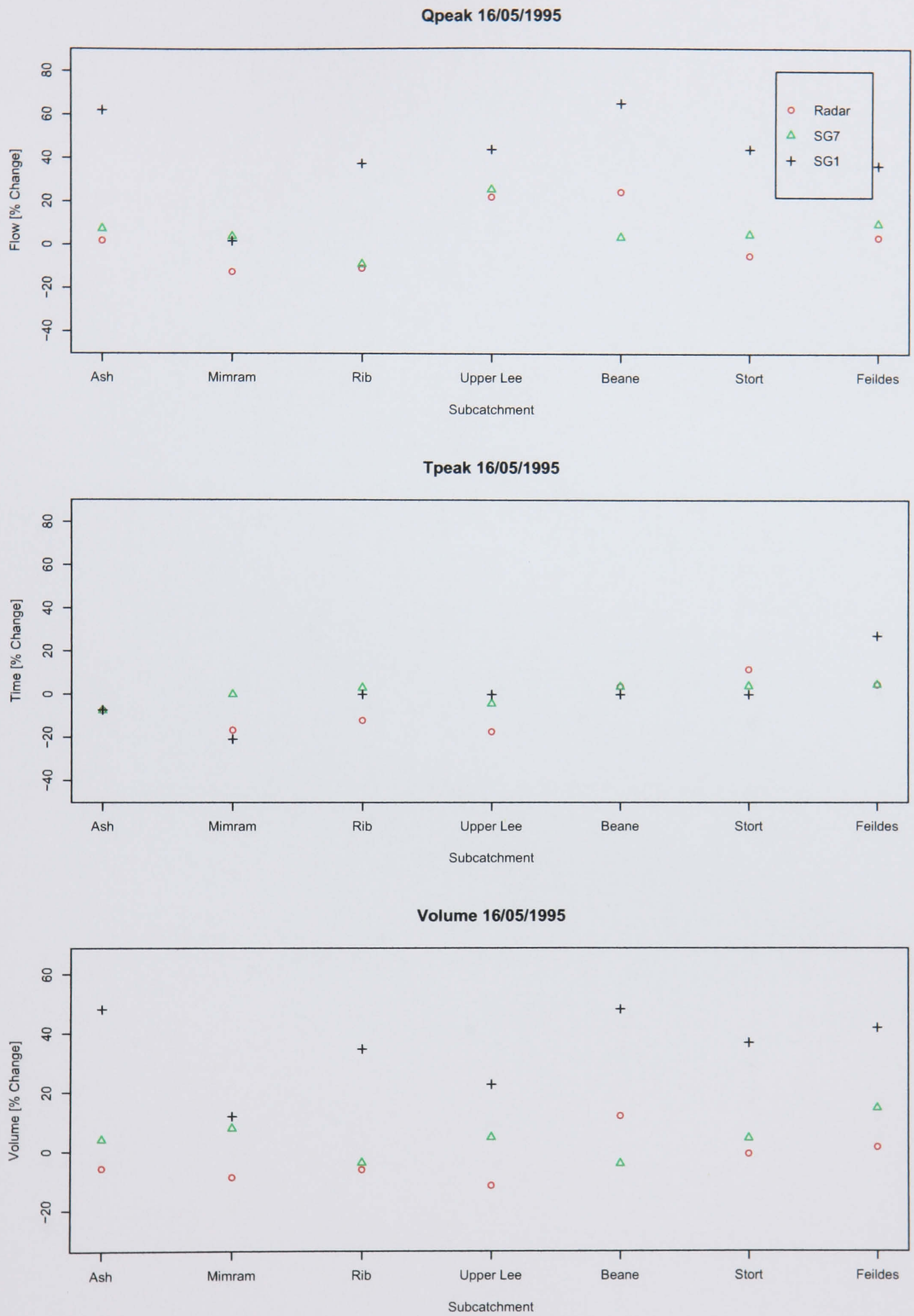

Figure 6.9 Percentage change in peak flow, time to peak and volume in comparison to the reference flow for the event of 16/05/95

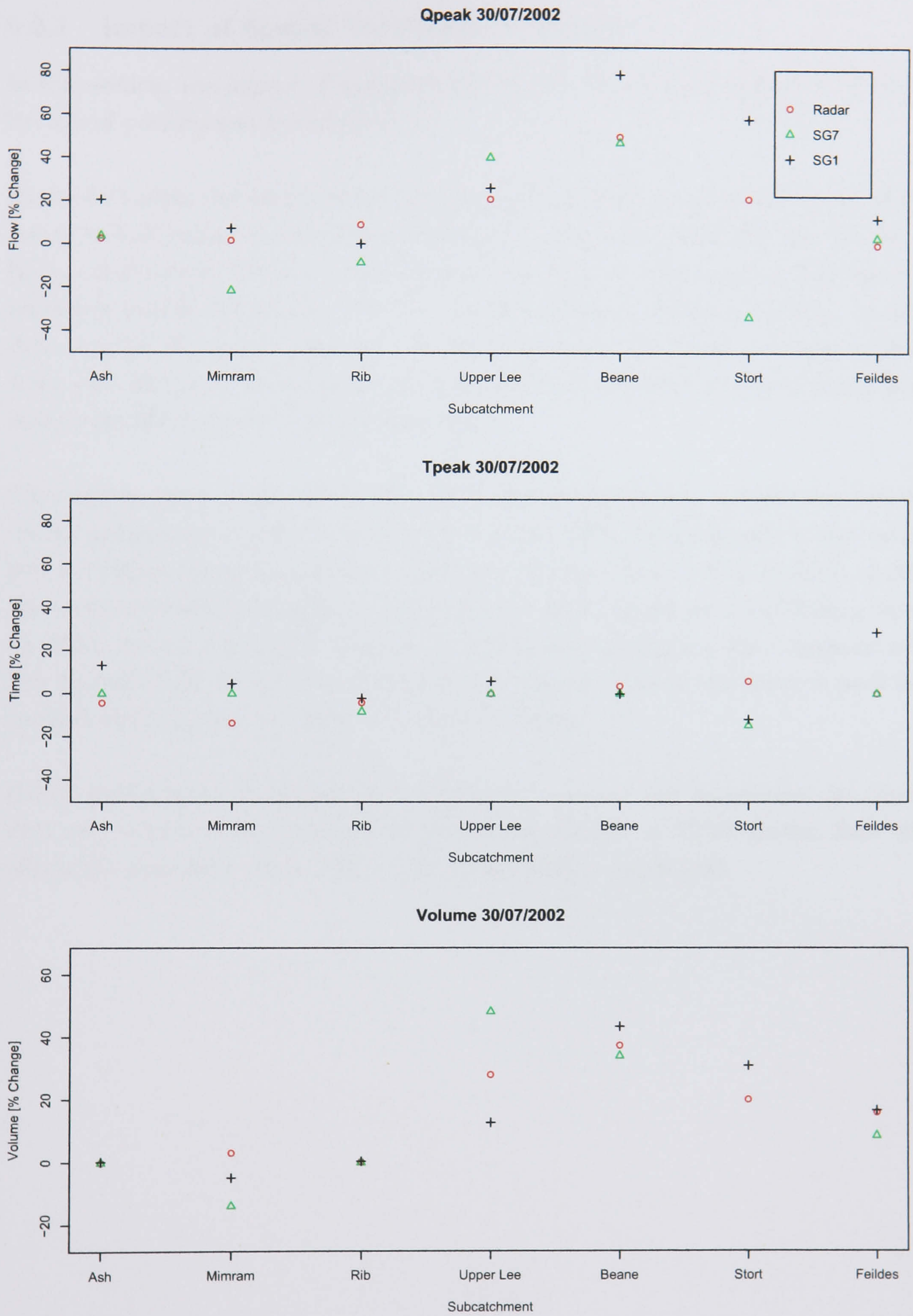

Figure 6.10 Percentage change in peak flow, time to peak and volume in comparison to the reference flow for the event of 30/07/02

6.2.1 Impact of Spatial Variability of Rainfall

In this section, the impact of spatial variability of rainfall, as measured by SDIR, on the model performance is evaluated.

Figure 6.11 plots the model performance in terms of NSE_{ref} against SDIR for all five events and all basins. A correlation between the increase in SDIR and the decrease in NSE_{ref} is observed. The top graph illustrates the impact of the three rainfall representations on model performance. Up to about 10% change in SDIR, the NSE_{ref} remains close to 1 for all rainfall scenarios. As SDIR increases, the NSE_{ref} remains high for radar data whereas it decreases for SDIR greater than 15% for SG7 and decreases more sharply for SDIR greater than 10% for SG1.

The bottom graph lumps all rainfall representations but makes a distinction between winter and summer events. It can be seen that the NSE_{ref} performance is high (above 0.9) for winter events up to SDIR of 20% and remains above 0.7 up to SDIR of 30%. For summer events, the results are less consistent with a larger spread of NSE_{ref} values for SDIR greater than 10%. The graph in Figure 6.12 displays the change in peak flow against SDIR. Overall for all three rainfall representations, the errors in peak flow increase as the spatial variability of rainfall increases.

Hence, precipitation dominates the hydrological response and its patterns are dependent on the type of rainfall representations and storms. A SDIR greater than 10% affects the peak flow, above 20% it reduces the NSE_{ref} below 0.80.

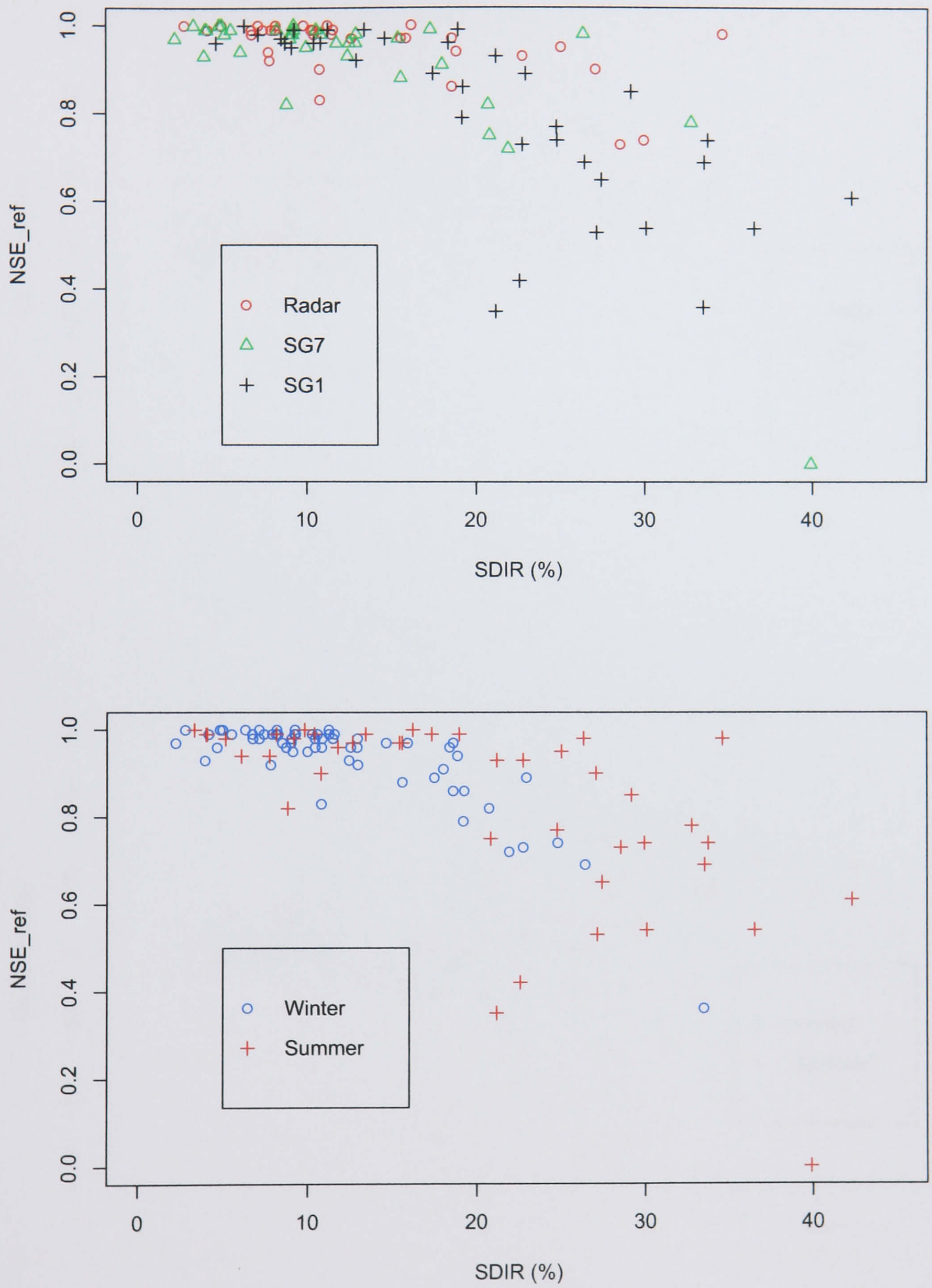

Figure 6.11 Impact of rainfall spatial variability on NSE_{ref}. Influence of rainfall estimators (Top) and type of rainfall events (Bottom).

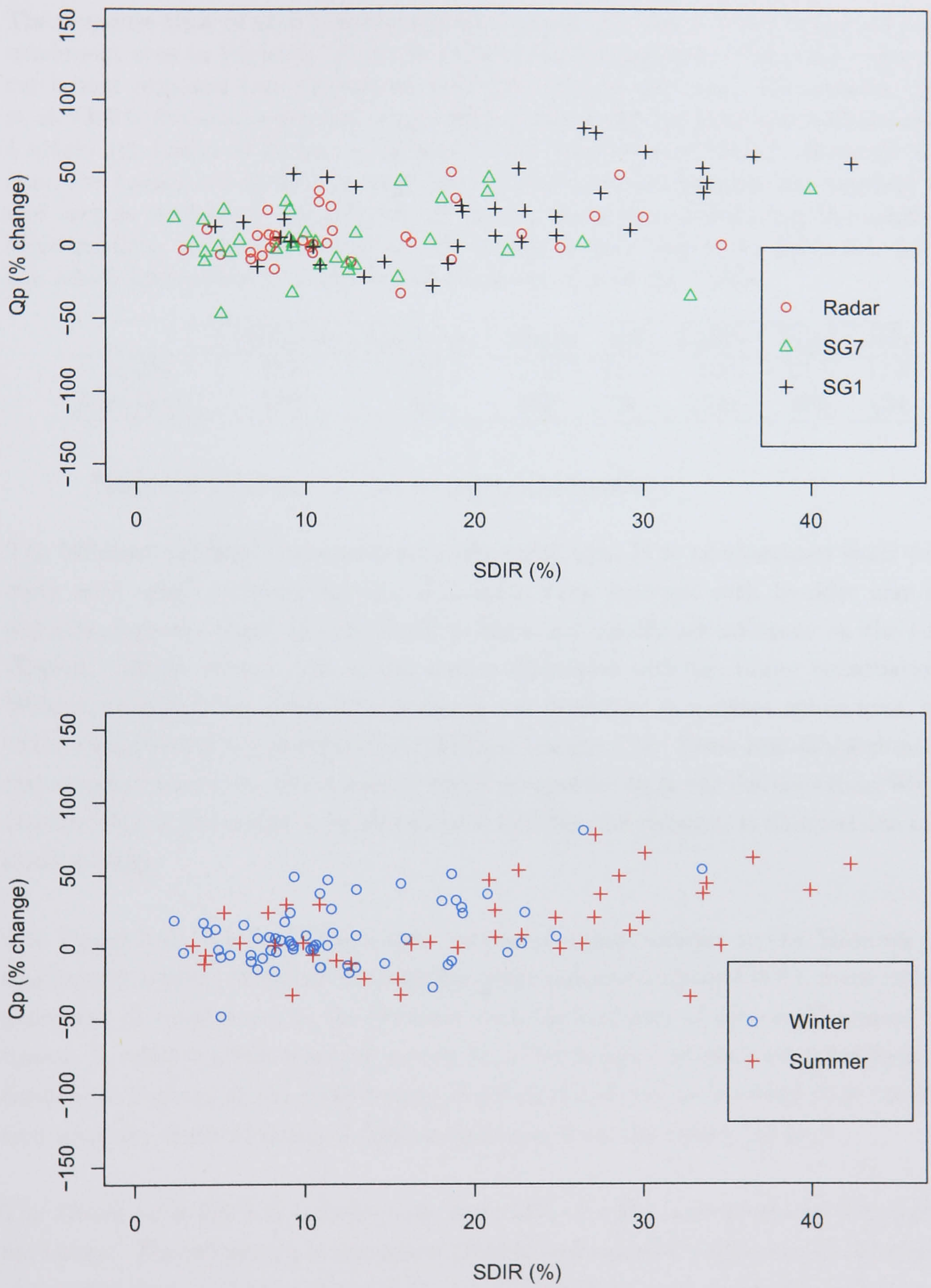

Figure 6.12 Impact of rainfall spatial variability on peak flow. Influence of rainfall estimators (Top) and type of rainfall events (Bottom).

6.2.2 Influence of Catchment Response Time

The response time of each (sub)catchment is given in Table 6.6 and is plotted against catchment area in Figure 6.13. If the basins were homogeneous, one would expect the catchment response time to increase with the scale of the basin. For instance, Berne et al. (2004) fitted a power law relationship between the lag time and surface area for 6 urban sub-basins of 38 ha to 105 km^2 in the Southwest of France. However in this case, the basins are distinct enough and no obvious trend between the response time and area is evidenced. Hypotheses to explain the drivers influencing the catchment response time are presented below. The reader is also referred to Table 3.1, 3.2 and 3.3, which present the hydrogeological characteristics of the basins.

	Mimram	Upper Lee	Beane	Ash	Feildes	Stort	Rib
t_c (h)	7.9	9.8	11.2	11.3	16.4	17.1	17.5
Area (km^2)	132	156	176	79	1033	278	134

Table 6.6 Mean lag time (t_c) for natural catchments

The Mimram (132km^2) is a predominantly rural area. It is an elongated chalk catchment with small outlying patches of London Clay bedrock with boulder clay drift deposits, however these are too small to have any significant influence on the runoff (Hawnt, 1987a). About 13% of the area is developed with the major conurbation of Welwyn Garden City. Even though this is not described as a dense urban area, most of the direct runoff is generated from Welwyn Garden City. From this subcatchment, a fast-response occurs (t_c of 7.9 hours), which is expected since the distance from Welwyn Garden City to the outlet is small (about 7 km) but the response is damped due to the chalk geology.

The Upper Lee (156 km^2) has similar geological characteristics to the Mimram (predominantly chalk). However because the urban extent is higher (35%), more runoff is generated in comparison to the Mimram with the majority of the runoff coming from Luton. A relatively fast response occurs (t_c of 9.8 hours), which is expected from this catchment because of the contribution of urban runoff, but it is slower than the Mimram since the town of Luton is further upstream from the outlet (23 km).

The Beane (176 km^2) is mainly rural with 13% of urban extent around the town of Stevenage. The catchment is comprised of chalk bedrock overlaid by superficial deposits of boulder clay. A slower response (t_c 11.2 hour) than that of the Upper Lee occurs and is expected since the urbanisation is less, but the larger extent of the impermeable clay layer may generate a higher amount of runoff

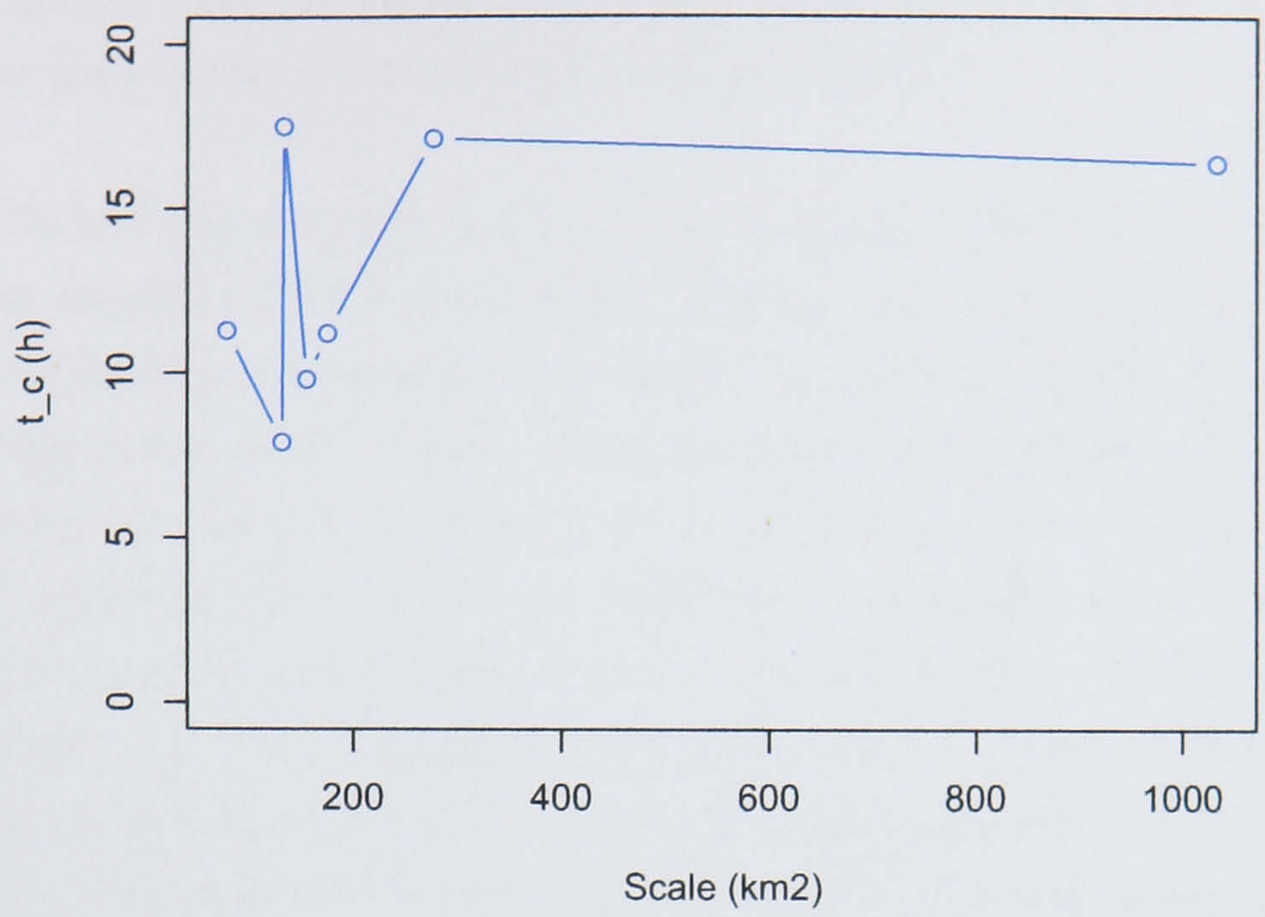

Figure 6.13 Catchment response time versus area

The 79 km^2 Ash catchment is characterised as rural (3.5% urban extent). It is predominantly chalk with the south eastern watershed boundary marking the interface with London Clay deposits (Hawnt, 1987b). It is overlaid by a particularly impermeable layer of boulder clay which generates significant runoff. Due to the small catchment size, a relatively fast-response (t_c of 11.3 hours) is expected from this catchment (but not as fast-responding as the above catchments with higher urban extent). A high response is expected due to the proportion of runoff generated from the clay contribution (i.e. not much water is absorbed into the chalk) .

The response at Feildes Weir outlet (1033 km^2) may be slightly faster than some of the more rural catchments (See the Rib below) as there is a higher area covered by urbanisation (15%) which would generate more runoff. However due to the larger size and the heterogeneity of the catchment, a relatively low response is expected.

The Stort catchment is more complex geologically. The underlying, or solid geology is composed mainly of London Clay with Chalk in the north-west part of the watershed and is overlaid by boulder clay drift deposits. 13% of the watershed is urbanised. The catchment area of the Stort is 278 km^2 which makes it the second largest of the catchments mentioned which increases the response time. It is more urban than the Rib so that might explain its quicker response. It may be slightly less than that at

Feildes Weir due to the influence of man made constructions (reservoir and navigation system). There is likely to be runoff in the south of the catchment where the chalk is confined but also in the north because of drift deposits.

The Rib (134 km^2) is a mixed chalk and boulder clay catchment, predominantly rural (3.5% urban extent). The impermeable boulder clay has a marked influence on the runoff characteristics and generates a significant amount of runoff. There is a major baseflow component to the runoff hydrograph due to percolation of effective rainfall falling directly on exposed (or relatively close to the surface) chalk surfaces. Direct runoff from upstream clay areas can infiltrate, for example when flowing over previously dry stream beds at the start of heavy rainfall (Hawnt, 1987b), (i.e. the water is absorbed, there is no runoff along the dry stream beds, initially, before a stream starts to flow). These location effects introduce a marked lag in the runoff response and high rainfall losses. Hence a slow response occurs (t_c of 17.5 hours) and a high response due to the extent of the impermeable boulder clay deposit.

Figure 6.14 displays the results in terms of NSE_{ref} (radar data, SG7 and SG1) for the five selected events and for each subcatchment ranked according to their characteristic time. The top graph presents the results for each rainfall representation whereas the bottom graph lumps all rainfall representations. In total, there are 15 observations per subcatchment. The boxplot represent the median, upper and lower quartile, the whiskers extend to the NSE value within 1.5 times the interquartile range from the box.

As highlighted in the review of the literature, contrasting observations arise from the studies in humid areas. No clear pattern emerges. It seems that the Mimram and the Lee catchment to Feildes Weir are less sensitive to spatial rainfall (see SDIR values in Table 6.2) with NSE values close to 1, which highlights the damping effect due to the chalk geology of the Mimram and the integrating effect at the large catchment scale for the Lee. This confirms that detailed knowledge of spatial rainfall is not required for basins characterised by a high level of dampening of the rainfall input signal (Obled et al., 1994; Smith et al., 2004; Woods and Sivapalan, 1999; Naden, 1992).

In conclusion, this case-study indicates that the dominant controls on the catchment response time are:

- The extent of runoff contributing areas (i.e. the extent of urbanisation and boulder clay drift)
- The location of these (urban) areas, with flow distance to the outlet

- The scale of the catchment

Attention should be focused on these interactions when modelling sub-humid basins in temperate regions. Altitude may be of importance in explaining runoff in areas with more relief.

Woods and Sivapalan (1999) proposed an analytical framework to assess the relative importance of these interactions. They defined the mean catchment runoff time (i.e. a characteristic catchment response time defined as the lag time between the beginning of the storm event to the centre of mass of the hydrograph) as folows:

$$E(T_q) = E(T_r) + E(T_h) + E(T_n) \tag{6.4}$$

where $E(T_q)$ is the mean catchment runoff times, $E(T_r)$ is the mean holding time for rainfall excess (i.e. the holding time for runoff to be generated), $E(T_h)$ is the mean holding time of hillslope travel and $E(T_n)$ is the mean holding time of network travel. An estimate of these holding times would give an insight and help quantifying the dominant controls on the mean runoff time.

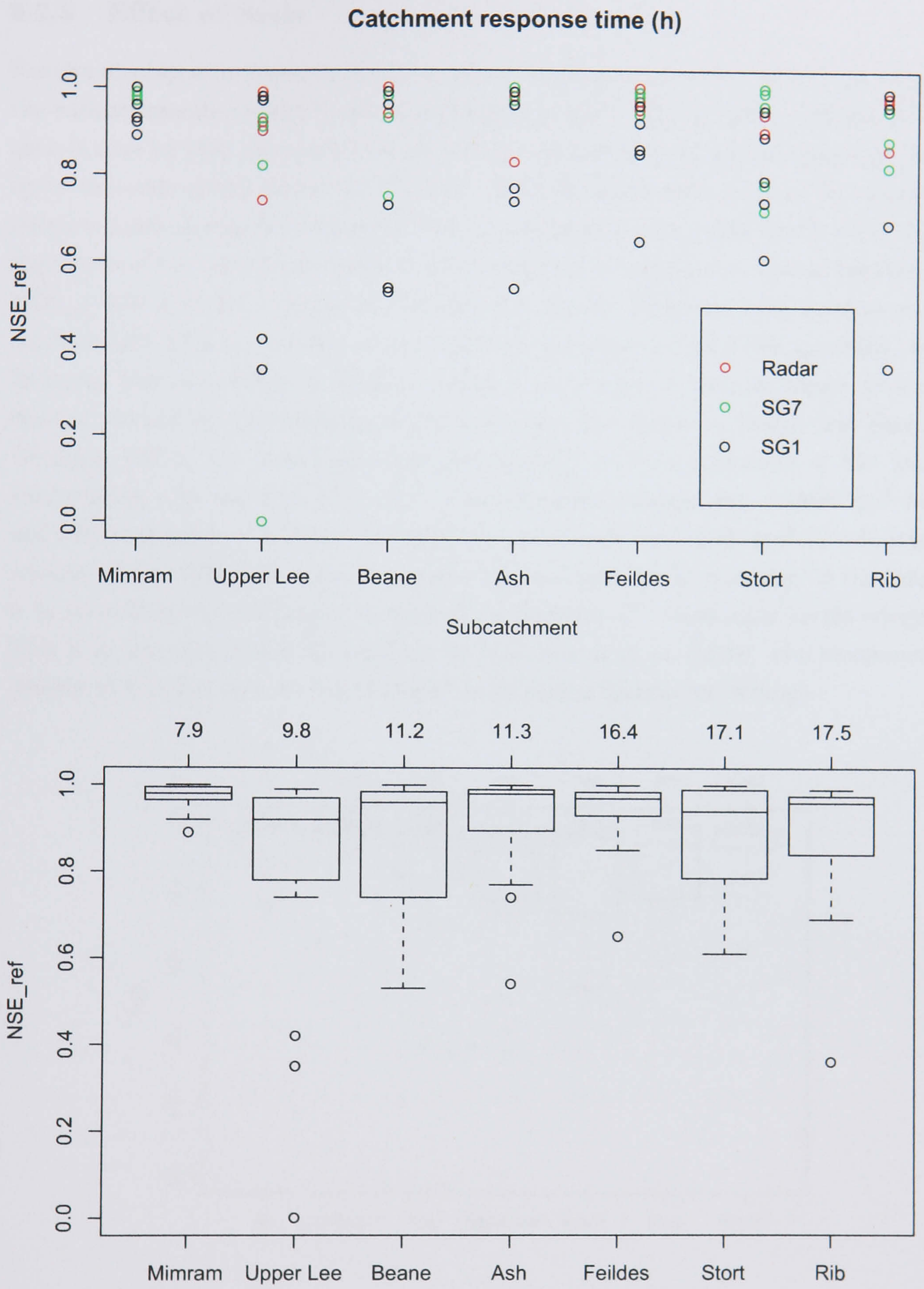

Figure 6.14 Boxplots of NSE criteria for each subcatchment ranked according to their catchment response time (expressed in hours on the upper axis)

6.2.3 Effect of Scale

Results displayed in Figure 6.15 are similar to those presented in Figure 6.14, but with the subcatchments ranked by size (upper axis in km^2). The graph is difficult to interpret; it may be that the sensitivity of the basin to variation in spatial rainfall increases up to the scale of the Beane ($\simeq$ 175 km^2), then decreases with scale as the catchment presents more spatial heterogeneity. At the catchment scale (1033 km^2), the integrating effects of the catchment result in less sensitivity to variation in spatial rainfall with NSE$_{ref}$ values mostly comprised between 0.8 and 1. However lower performance is reached with SG1 in the case of the convective summer event (NSE$_{ref}$=0.65), which indicates that knowledge of spatial rainfall is important at the catchment scale even though a detailed representation is not necessary. For instance, Dodov and Foufoula-Georgiou (2005) use catchment-averaged rainfall over subcatchments of 530 km^2 (9 subdivisions scheme) and 1600 km^2 (3 subdivisions scheme) for a 4800 km^2 basin, and subcatchments of 735 km^2 (10 subdivisions scheme) and 2450 km^2 (3 subdivisions scheme) for a 7300 km^2 basin in central North America. In our case, if the interest is in modelling the catchment outlet only, a network of 7 raingauges seems adequate. This is in agreement with the findings of Andréassian et al. (2001) who recommend a density of 8 raingauges at the 1120 km^2 scale (using lumped modelling).

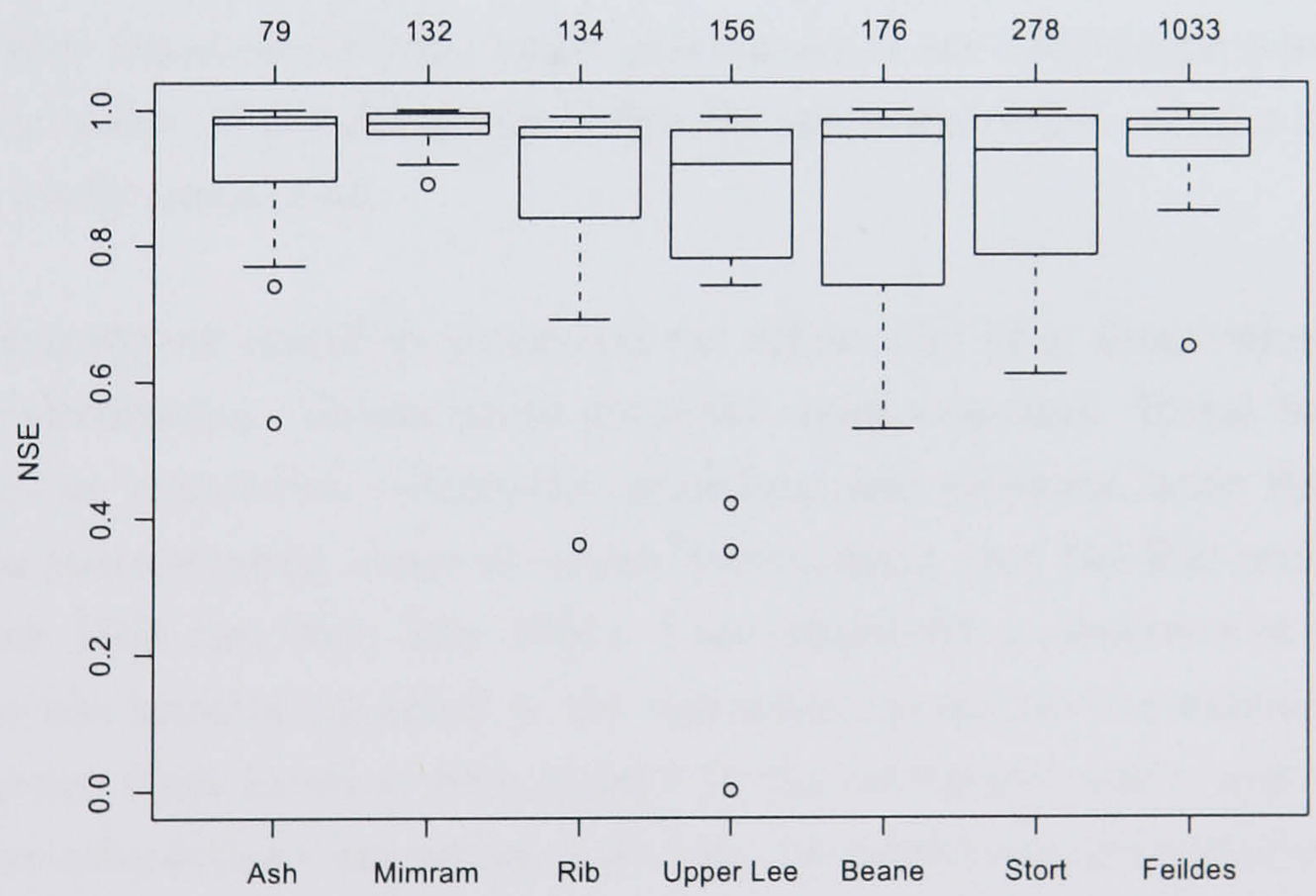

Figure 6.15 Boxplots of NSE$_{ref}$ criteria for each subcatchment ranked according to their size

6.2.4 Rainfall Variability, Catchment Characteristics and Model Performance

As the model performance is most sensitive with SG1, this rainfall representation is selected to emphasise and assess the relative importance of SDIR, catchment scale and catchment response time. Figure 6.16 represents NSE_{ref} versus SDIR for SG1. The top plot highlights the impact of catchment scale with light to dark colours representing small to large catchments. Similarly, the bottom plot highlights the impact of catchment response time with light to dark colours representing slow to fast catchments. These plots do not indicate any obvious relationships between catchment scale and response time on NSE_{ref}; however the relative importance of SDIR is confirmed with lower NSE_{ref} values as SDIR increases. As seen in Section 6.2.1, SDIR is a function of rainfall representation and storm type.

6.2.5 Conclusion

Results on existing, predominantly rural, catchments reveal that the basins are sensitive to the type of rainfall events, rainfall representation, catchment scale and catchment type. The findings show a clear relationship between the increase in spatial variability of rainfall and the decrease in model performance. More variability is introduced when extreme or summer events occur. Spatially variable rainfall and radar data lead to similar flow response whereas larger discrepancies are introduced when using input data from a subset of the raingauges. Results are worse when using a single gauge to model the whole catchment.

A higher amount of runoff is generated on urban and clay areas whereas the chalk is baseflow dominated. Urban areas generate rapid response. Rural basins are more sensitive to the antecedent catchment conditions and generate lower flows in summer than basins incorporating zones of urban development (see the Rib and Ash response on 16th May 1995 and 30th July 2002). Less sensitivity is observed at the catchment scale. Thus the integrating effect of the catchment is due to the extent of runoff contributing areas, their location with respect to the catchment outlet and the catchment scale. These interactions are incorporated in the catchment characteristic time: however it was not possible to assess their impact independently. This could be achieved using the analytical framework of Woods and Sivapalan (1999).

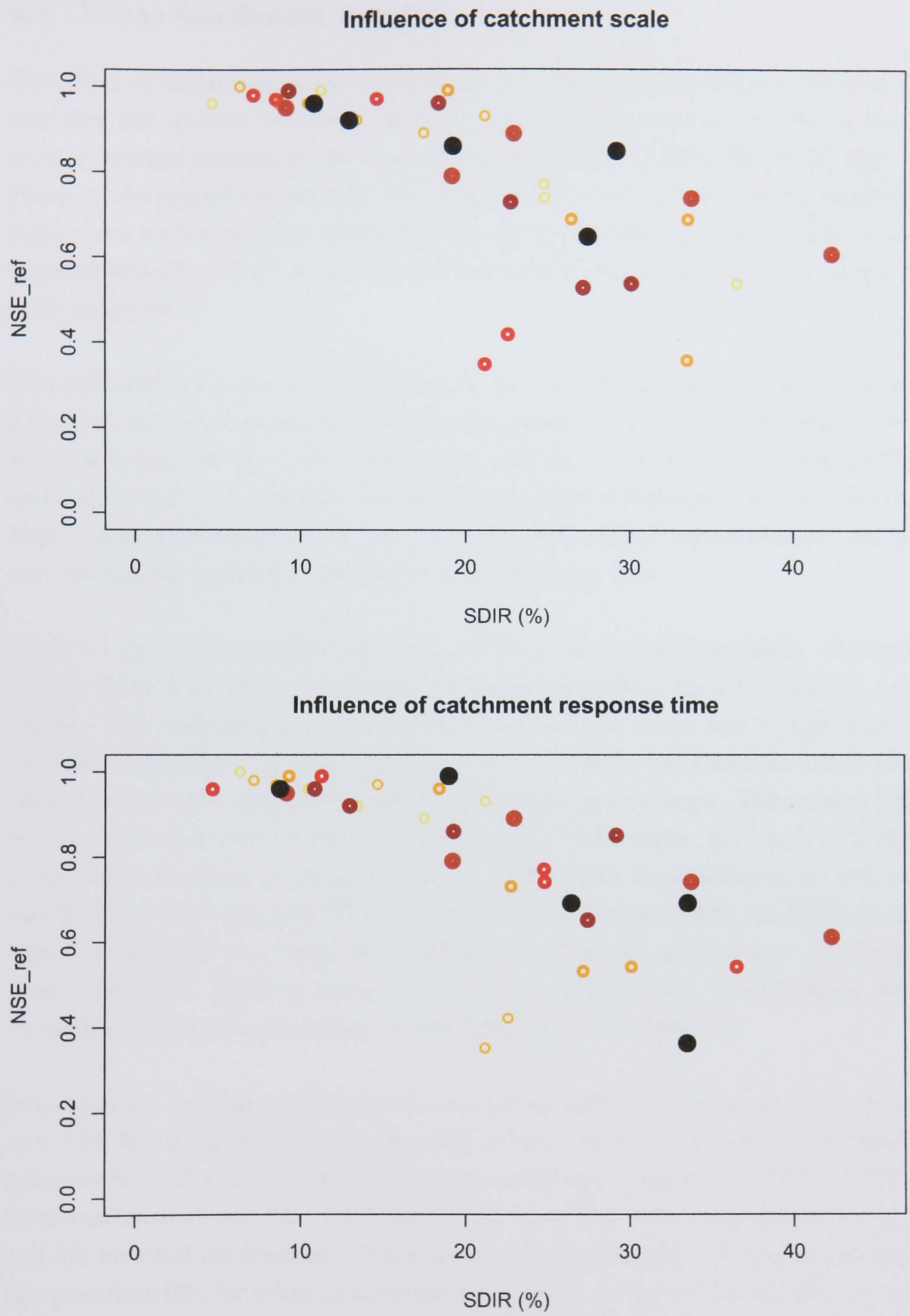

Figure 6.16 Model performance vs rainfall variability highlighting the effect of catchment scale (Top) and catchment response time (Bottom) for SG1 representation

6.3 Urban Catchment Results

The effect of urbanisation on runoff is due to (i) increase in impervious area which increases the amount of runoff, and (ii) hydraulic improvement of flow paths (e.g. roofs, roadways, gutters, pipes, channel) speeds up the response. RORB handles (i) by changing the percent impervious. The value input for each sub-area is the proportion of impervious surface which connects in some way to the drainage system. The hydraulic improvement (ii) is dealt with using the Reach Type Flag (Laurenson and Mein, 1988) as in Equation 5.7.

The subcatchments are turned artificially into completely urban basins by applying a fraction imperviousness of 30% to all subareas to ensure a faster response, and with the exception of the Stort, by changing the reach type from Natural to Lined (or Piped) and a slope of 0.1% is applied (following guidance from Example 8.4 in Laurenson and Mein, 1988) according to Equation 5.8. The same rainfall representations are tested and the simulated runoff is compared to the reference flow.

Table 6.7 presents the results in terms of NSE_{ref} for urban catchments. Figures 6.17 to 6.21 show that urban catchments are faster-responding than the existing natural basins. The hydrograph is characterised by a narrow shape and a high peak flow. Further, the response on urban catchments is sensitive to the temporal distribution of rainfall, with bursts of rainfall reflected in the hydrograph shape. The average NSE_{ref} for all catchments and events is 0.95, 0.92 and 0.73 for radar, SG7 and SG1, respectively. In comparison to rural basins, the performance is maintained for radar data and SG7 but decreases with SG1. As mentioned by Young (2005), the NSE statistic is biased towards the fit of high flows and tends to increase as the length of simulation period decreases. However these results serve as a first point of comparison and are complemented by the percentage change in Q_p, T_p, V in Table 6.8.

In comparison to rural catchments, the error in Q_p and T_p decreases for radar data (9.7 and 5.4% for urban catchments compared to 12.6 and 5.6% for rural catchments) and increases for SG7 (16.5 and 9.8% for urban catchments compared to 15.3 and 5.8% for rural catchments) and SG1 (38.5 and 12.7% for urban catchments compared to 28.1 and 8% for rural catchments). However errors in hydrograph volume increase slightly for radar data (8% for urban catchments compared to 7.4% for rural catchments) an decreases for SG7 (11.1% for urban catchments compared to 12.4% for rural catchments) and SG1 (18.4% for urban catchments compared to 21.6% for rural catchments).

Figure 6.22 to Figure 6.26 display the percentage change in Q_p, T_p and V for all

rainfall representations and all subcatchments ranked by size. The event of 30th July 2002 leads to more variation in the catchment response with a percentage peak change up to 120% compared to 80% for rural catchments.

	Upper Lee	Mimram	Beane	Rib	Ash	Stort	Feildes
11-Oct-93							
Radar	0.97	0.92	0.98	0.81	0.95	0.97	0.98
SG7	0.93	0.95	0.97	0.90	0.89	0.98	0.99
SG1	0.95	0.93	0.89	0.92	0.92	0.88	0.98
03-Feb-94							
Radar	0.97	0.97	0.99	1	1	1	1
SG7	0.95	1	0.96	0.94	0.98	1	0.99
SG1	0.98	0.98	0.83	0.62	0.86	0.86	0.93
08-Jan-96							
Radar	0.99	0.99	0.92	0.99	1	1	1
SG7	0.95	0.79	0.93	0.91	0.99	0.99	0.99
SG1	0.98	0.85	0.98	0.75	0.92	0.89	0.96
16-May-95							
Radar	0.98	0.99	0.98	0.93	0.99	0.97	0.99
SG7	0.93	0.99	0.96	0.97	0.96	0.94	1
SG1	0.82	0.77	0.69	0.66	0.40	0.81	0.83
30-Jul-02							
Radar	0.91	0.96	0.59	0.80	0.98	0.90	0.94
SG7	0.47	0.72	0.76	0.68	0.82	0.95	0.94
SG1	0.16	0.72	0.01	0.04	0	0.15	0.46

Table 6.7 NSE_{ref} for urban catchments

	Radar	SG7	SG1
Q_p (%)	9.7	16.5	38.5
T_p (%)	5.4	9.8	12.7
V (%)	8.0	11.1	18.4

Table 6.8 Percentage change of peak flow, time to peak and hydrograph volume

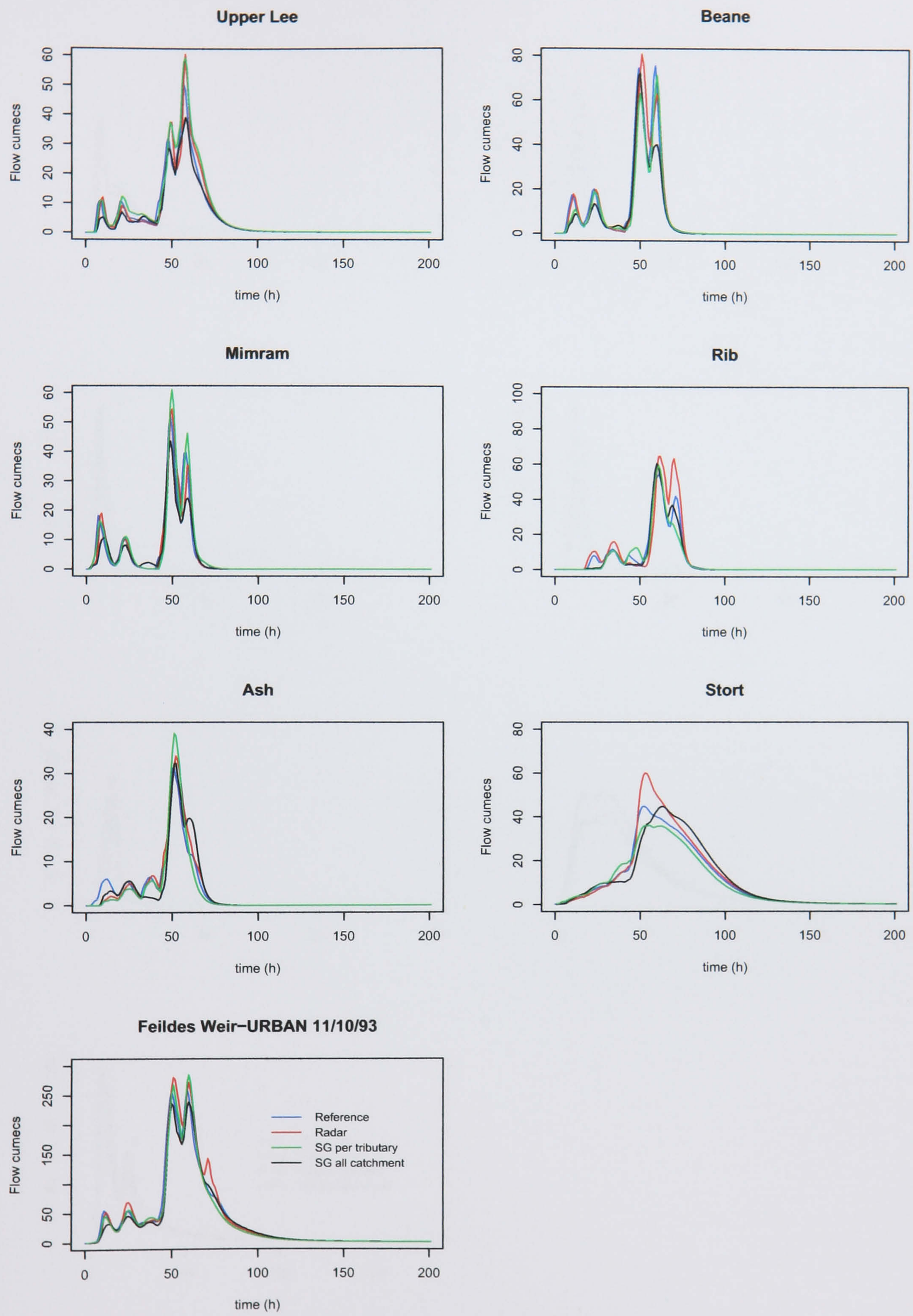

Figure 6.17 Reference and simulated flow at urban catchment outlets on 11/10/93

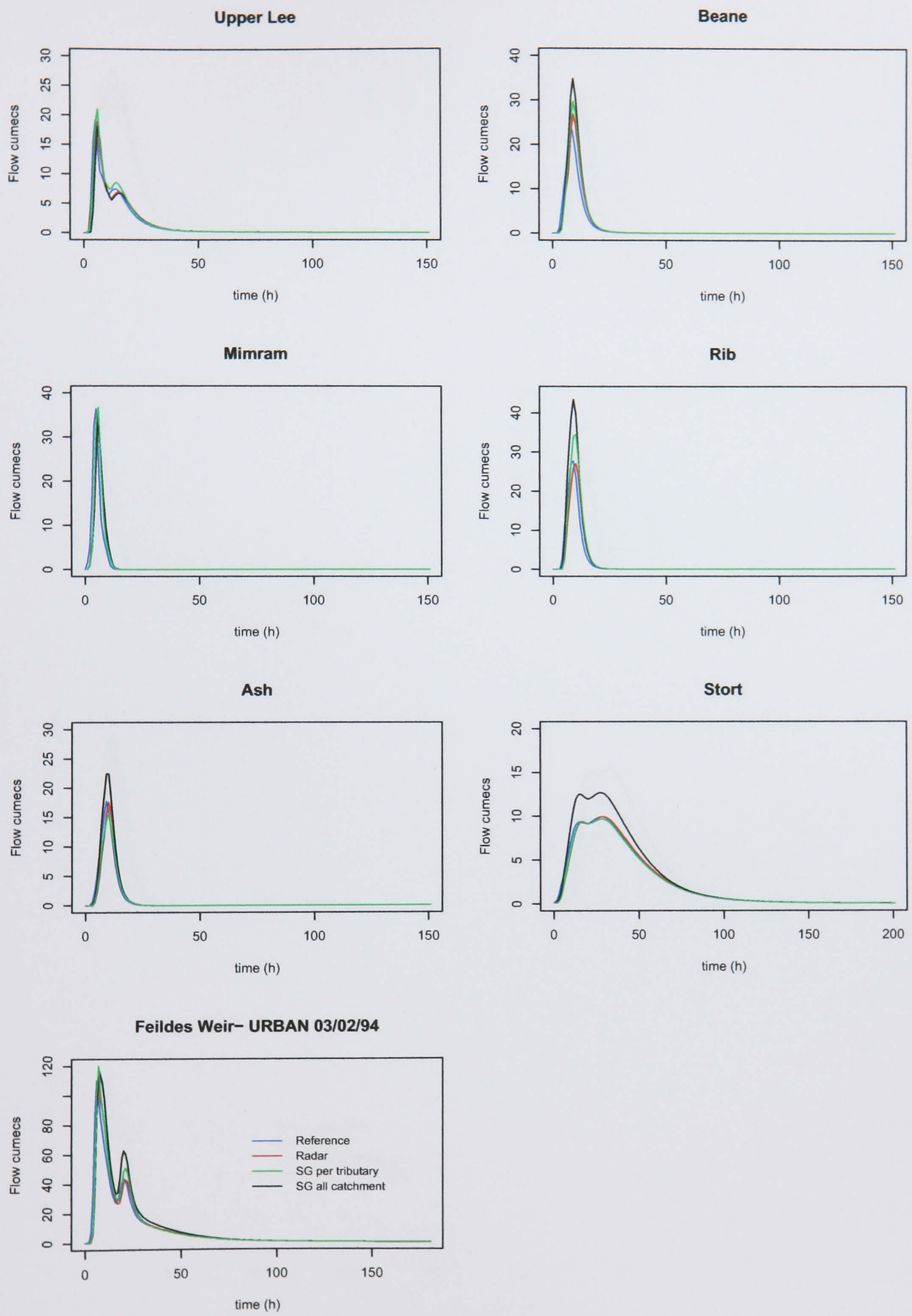

Figure 6.18 Reference and simulated flow at urban catchment outlets on 03/02/94

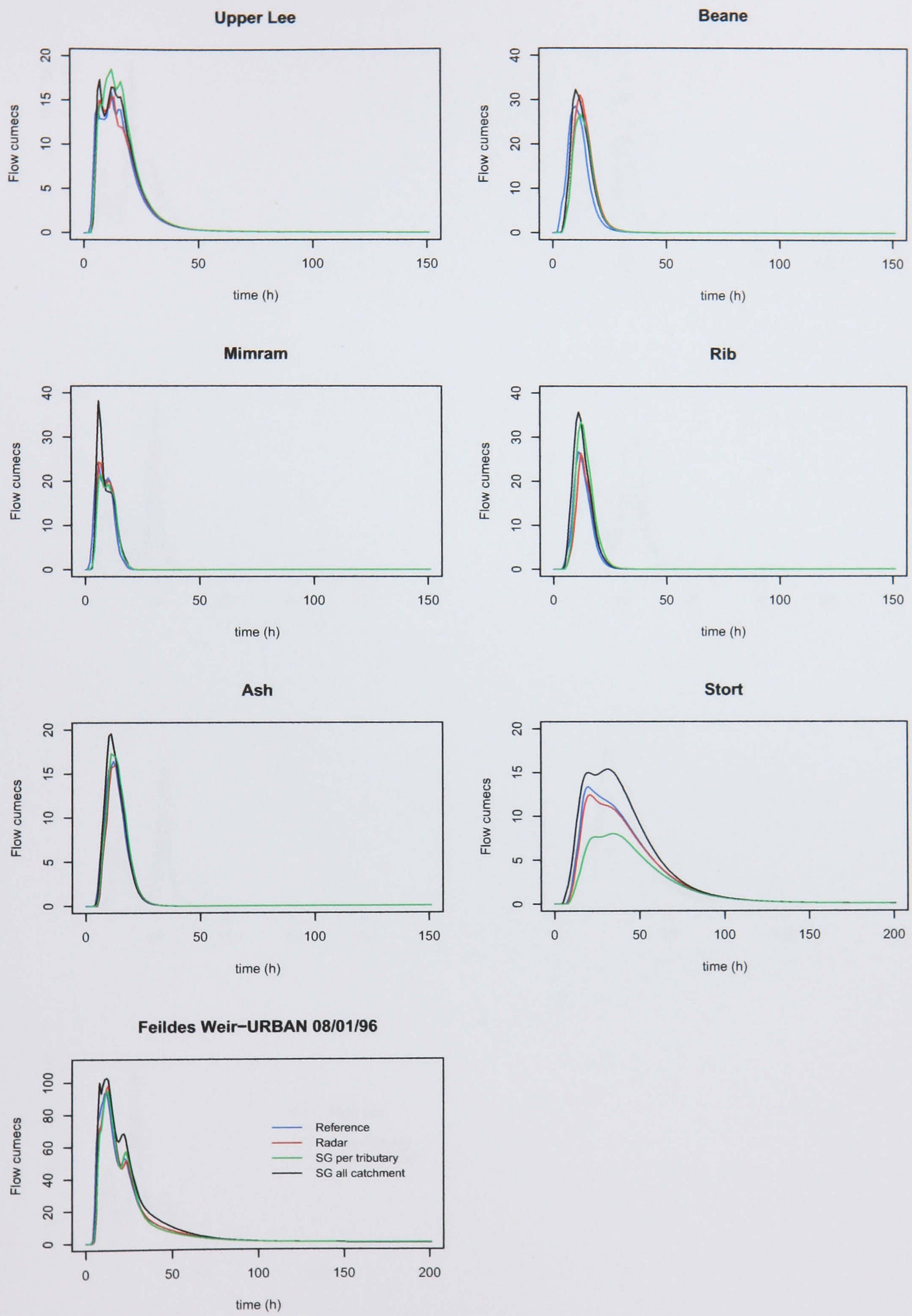

Figure 6.19 Reference and simulated flow at urban catchment outlets on 08/01/96

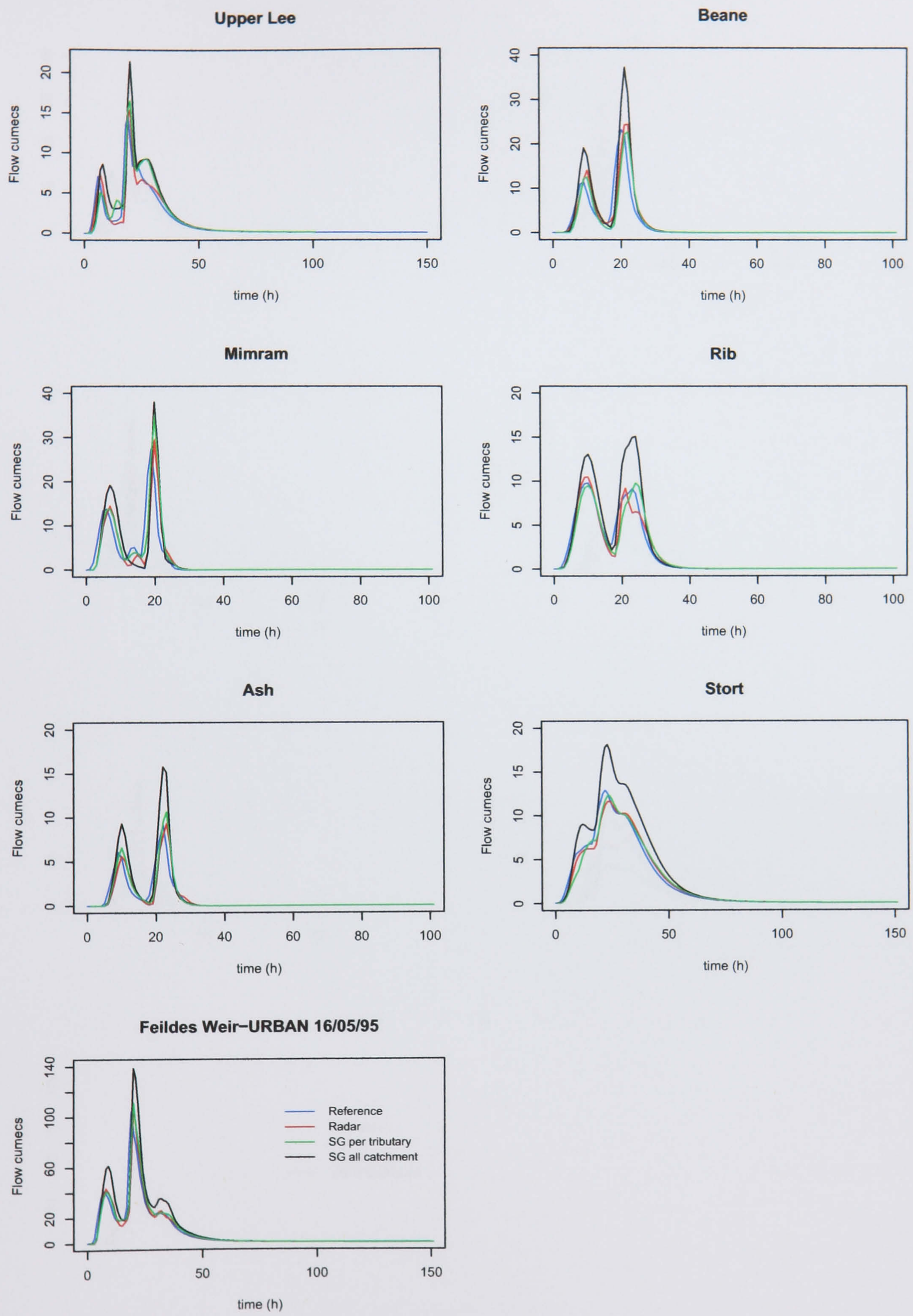

Figure 6.20 Reference and simulated flow at urban catchment outlets on 16/05/95

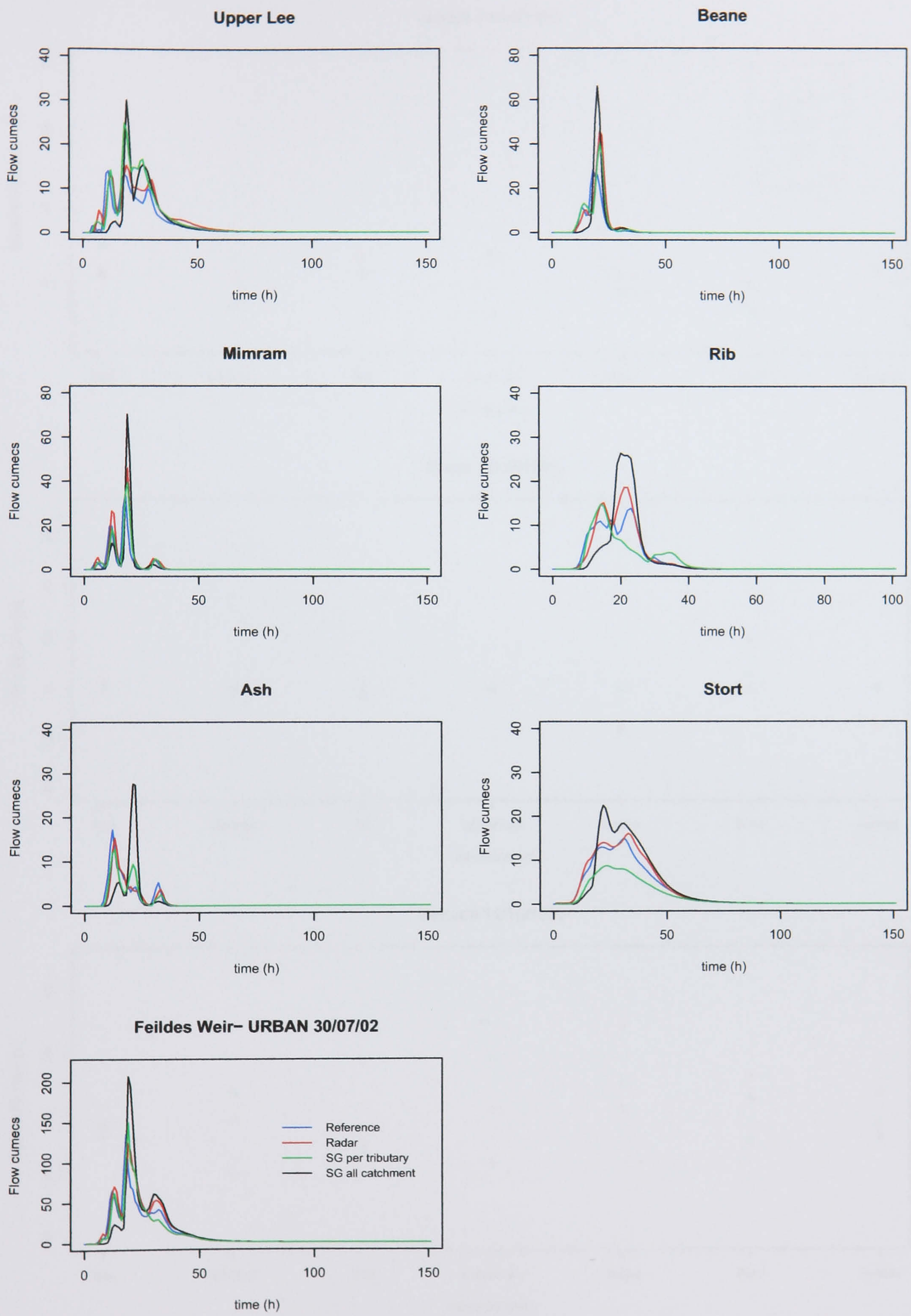

Figure 6.21 Reference and simulated flow at urban catchment outlets on 30/07/02

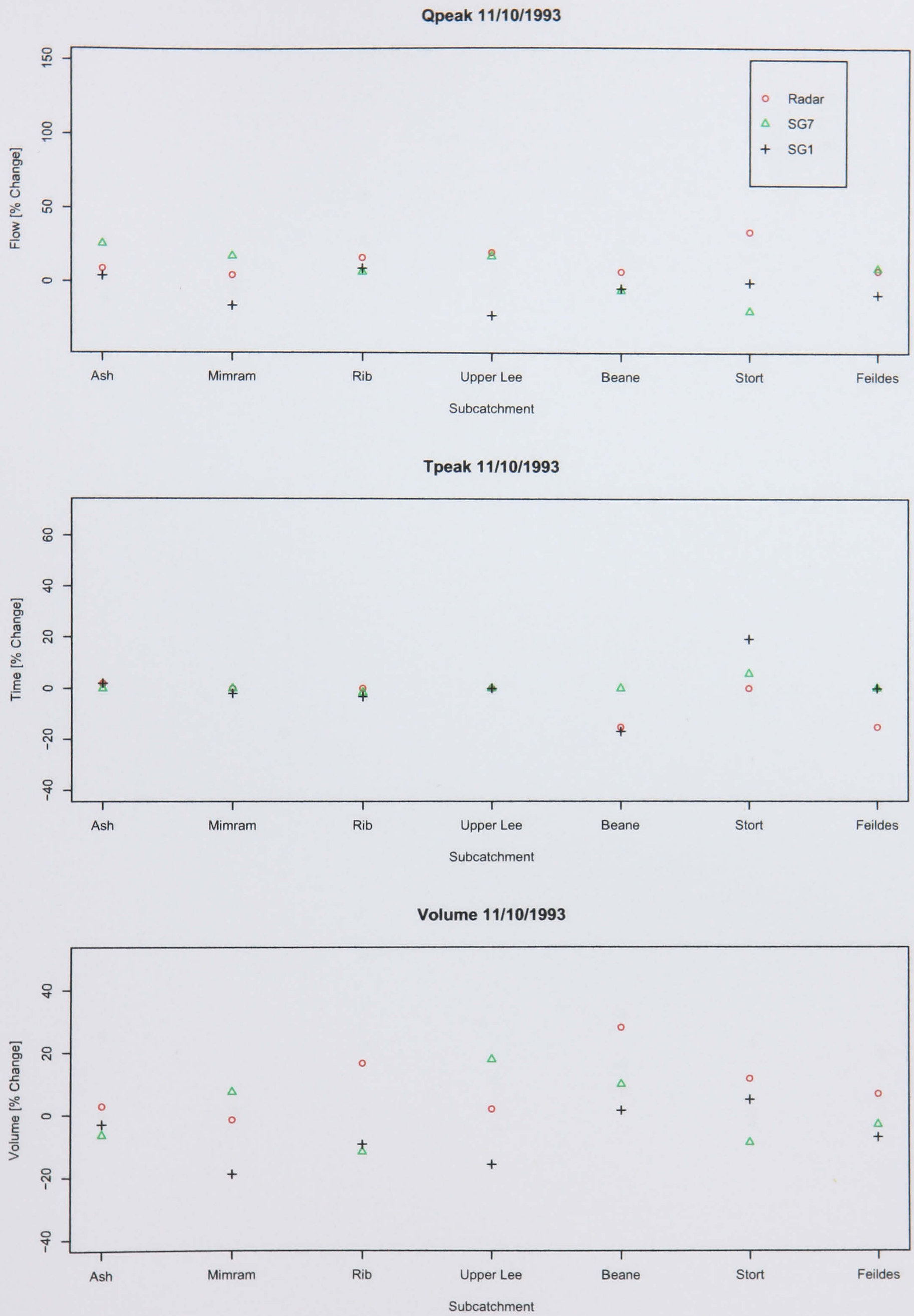

Figure 6.22 Relative change (%) in peak flow, time to peak and volume in comparison to the reference flow for the event of 11/10/93

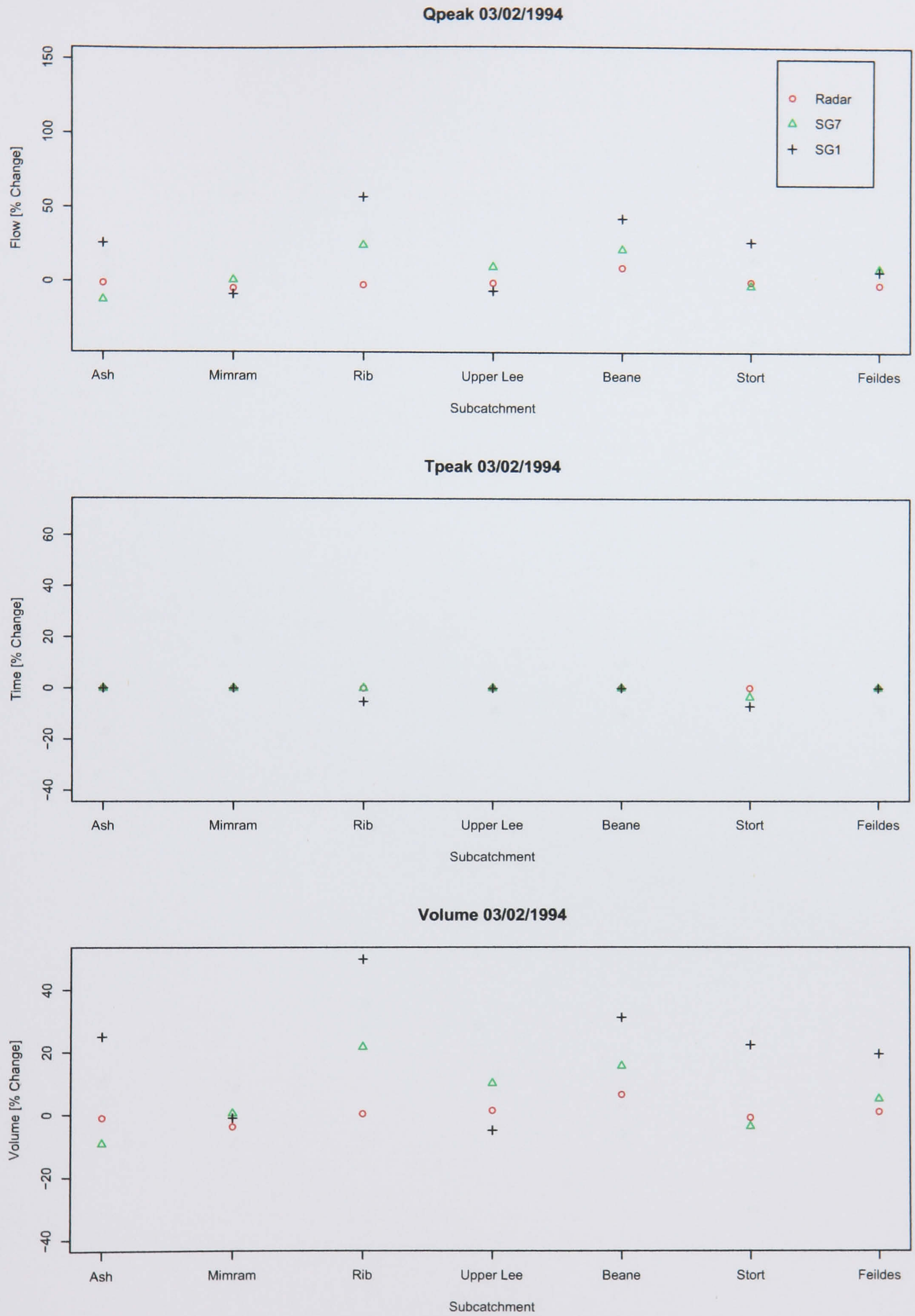

Figure 6.23 Relative change (%) in peak flow, time to peak and volume in comparison to the reference flow for the event of 03/02/94

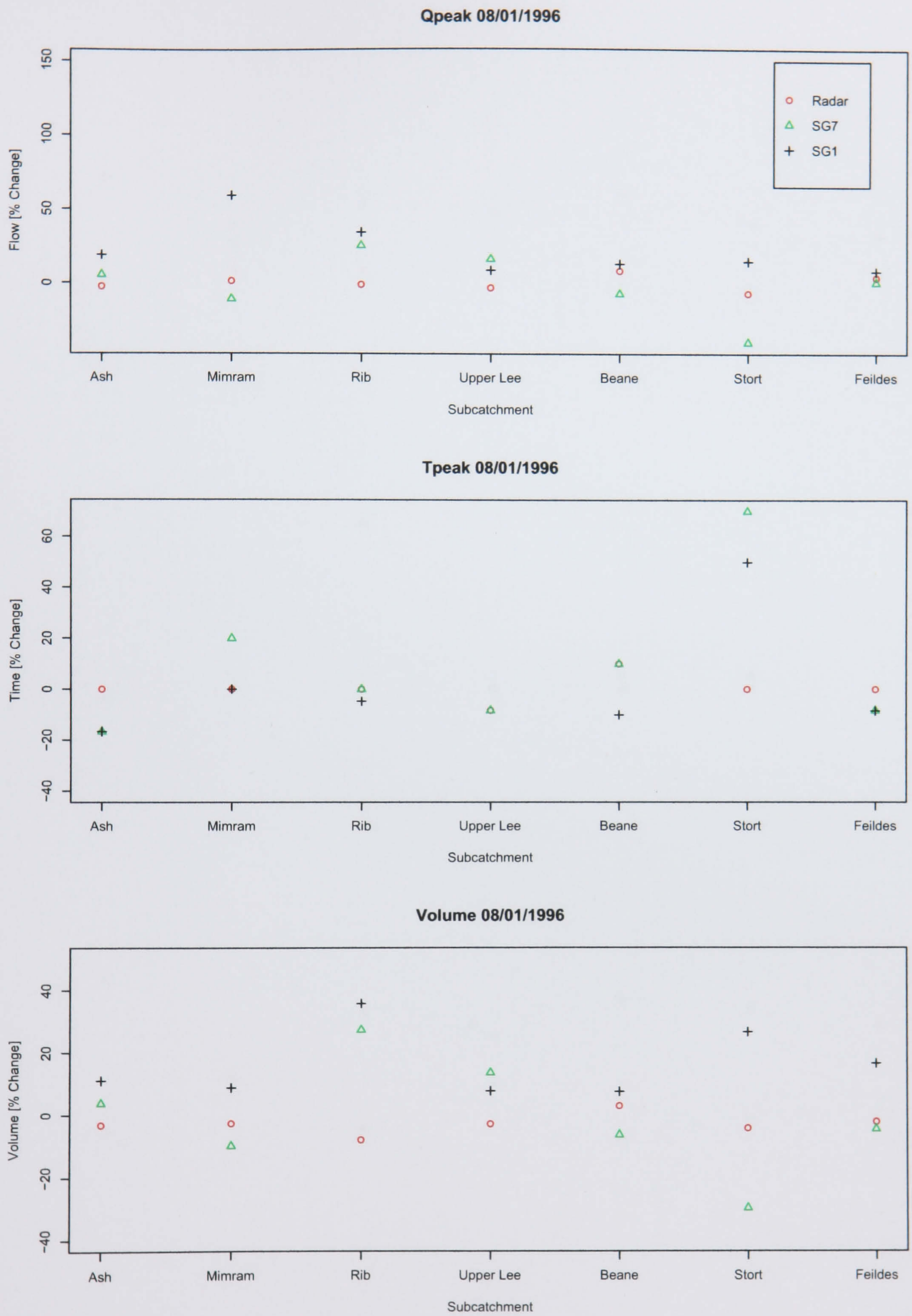

Figure 6.24 Relative change (%) in peak flow, time to peak and volume in comparison to the reference flow for the event of 08/01/96

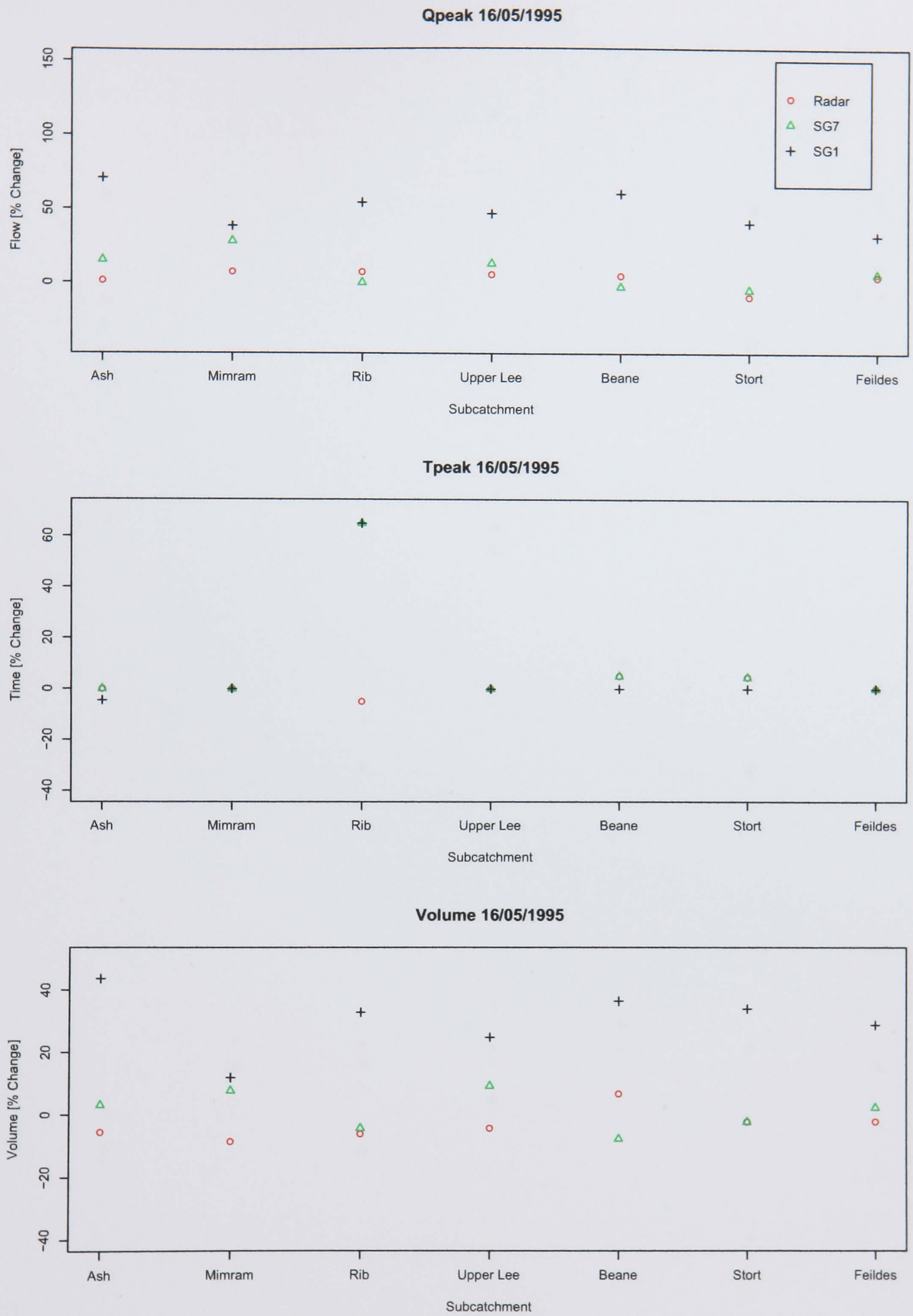

Figure 6.25 Relative change (%) in peak flow, time to peak and volume in comparison to the reference flow for the event of 16/05/95

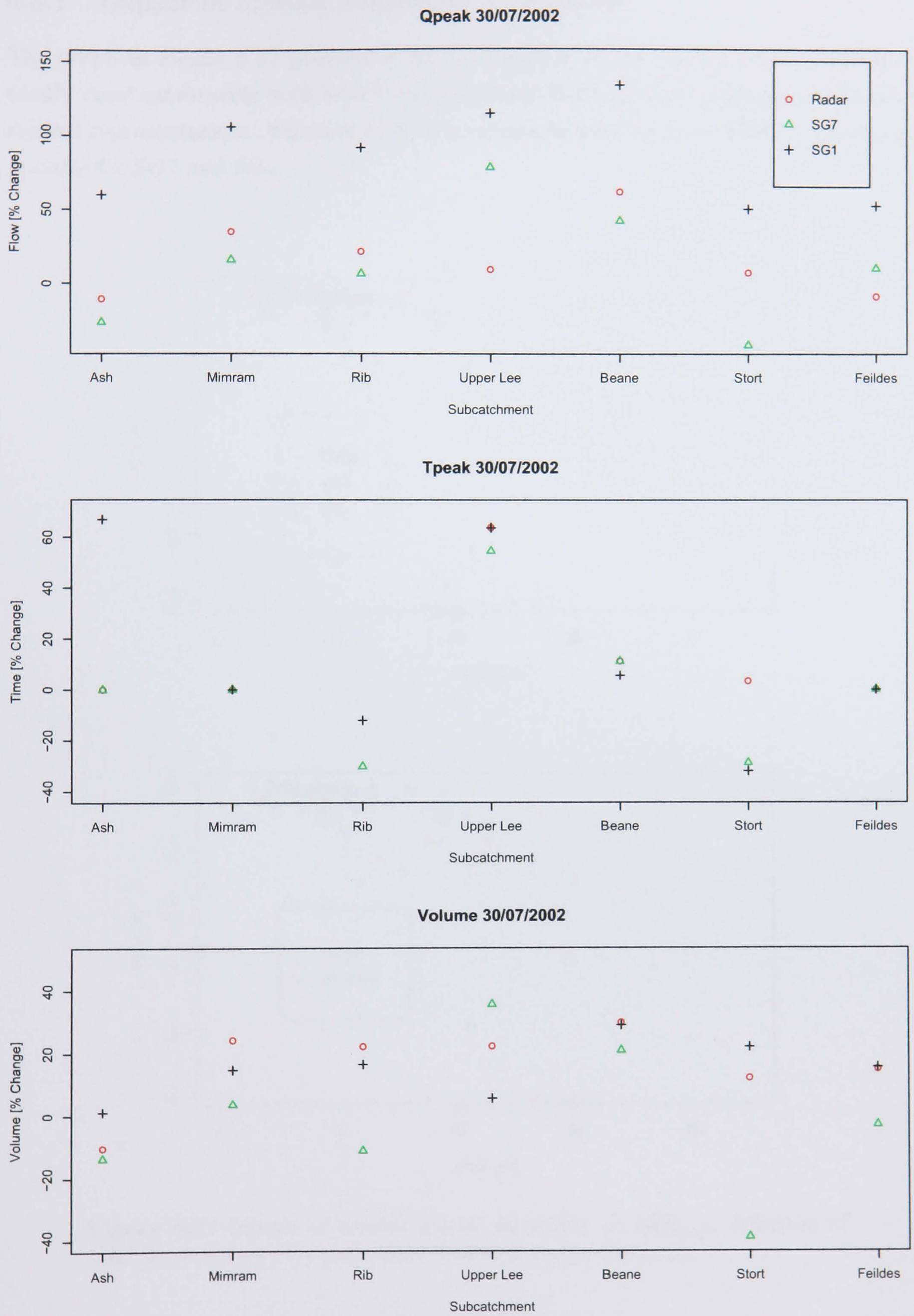

Figure 6.26 Relative change (%) in peak flow, time to peak and volume in comparison to the reference flow for the event of 30/07/02

6.3.1 Impact of Spatial Variability of Rainfall

The graph in Figure 6.27 presents a similar trend as in the case of existing predominantly rural catchments with SG1 leading to lower performance compared to the other rainfall representations. Summer events are characterised by lower NSE_{ref} values, expecially for SG7 and SG1.

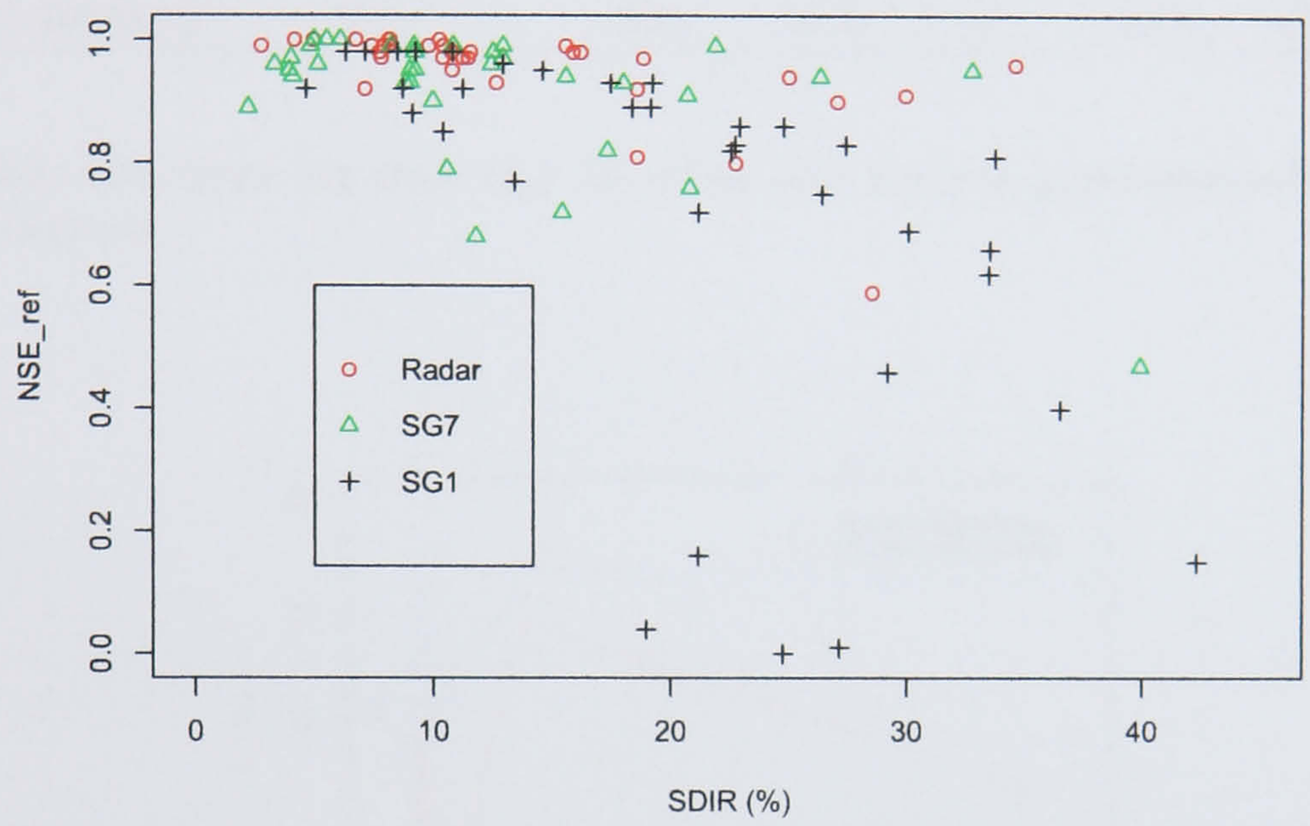

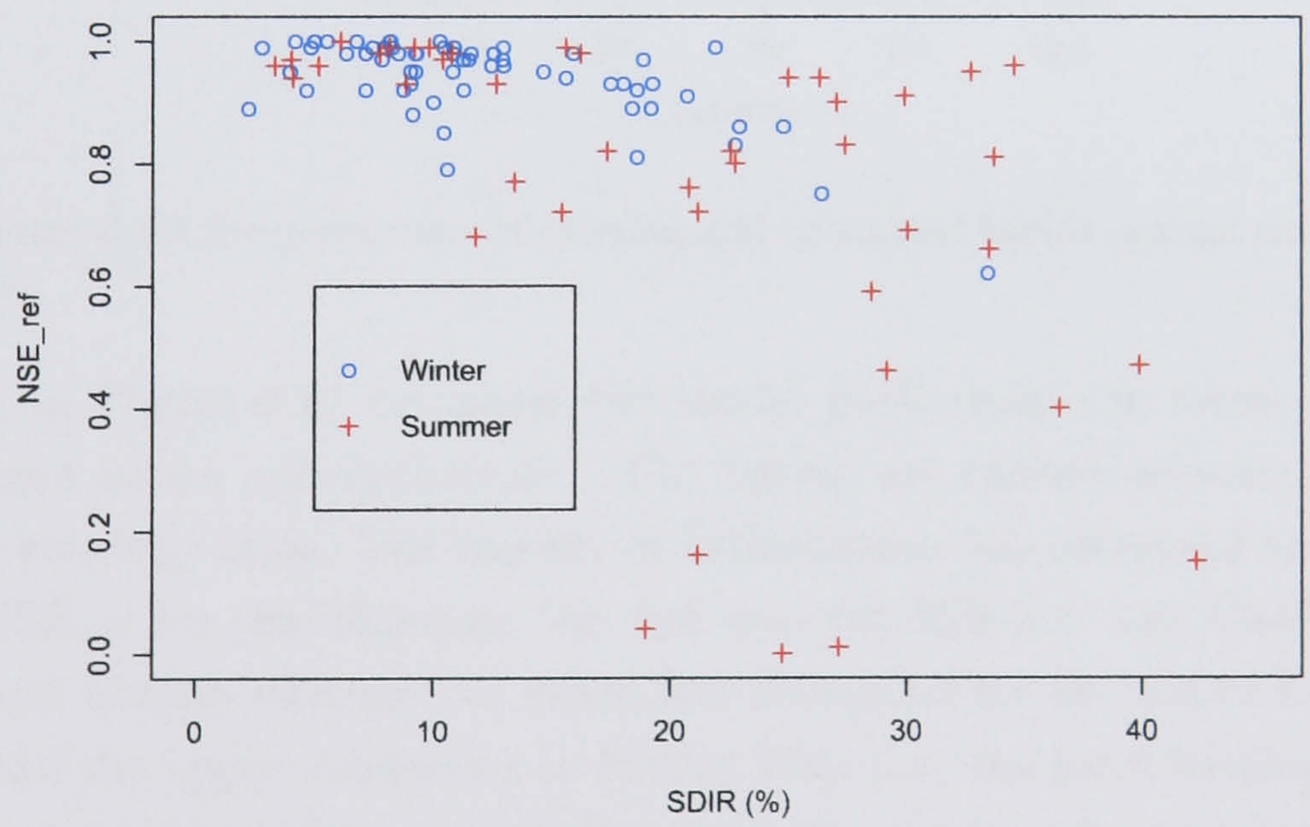

Figure 6.27 Impact of rainfall spatial variability on NSE_{ref}. Influence of rainfall estimators (Top) and type of rainfall events (Bottom).

6.3.2 Influence of Catchment Response Time and Catchment Scale

Table 6.9 presents the response time of the urbanised catchments. The response time of the existing and urbanised basins are plotted against catchment area in Figure 6.28. It can be seen that the impact of urbanisation decreases the catchment response time by about 50% on average across all basins.

	Mimram	Upper Lee	Beane	Ash	Feildes	Stort	Rib
t_c (h)-Urban	1.7	3.4	3.5	5	6.8	14.7	10.3
t_c (h)-Rural	7.9	9.8	11.2	11.3	16.4	17.1	17.5

Table 6.9 Mean lag time (t_c) for urban and natural (predominantly rural) catchments

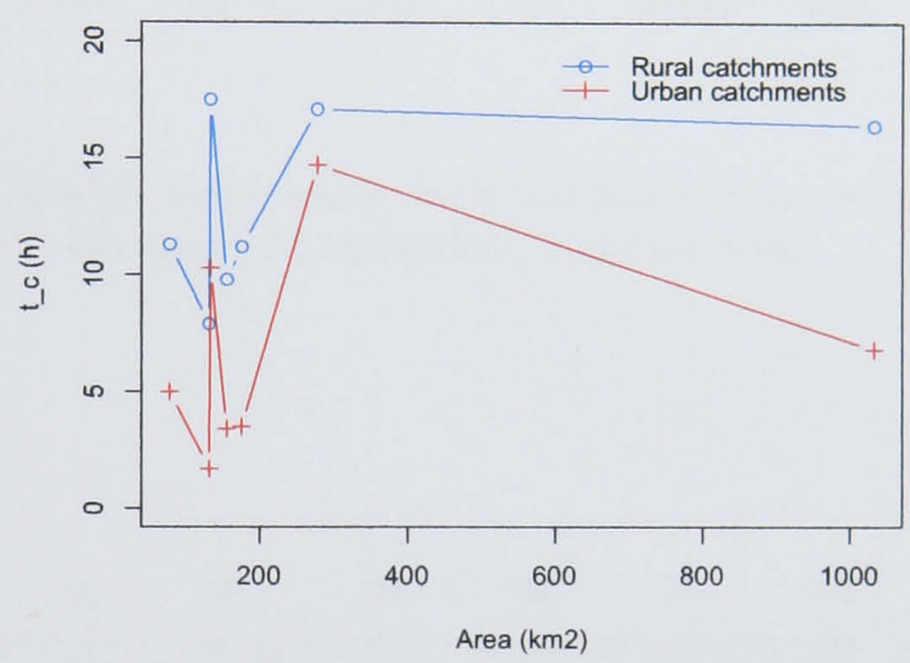

Figure 6.28 Response time of existing and urbanised basins against catchment area

The graph in Figure 6.29 compares the model performance in terms of NSE_{ref} for the rural and urban subcatchments. The basins are ranked according to the rural catchment response time. The impact of urbanisation has increased the interquartile range in NSE_{ref} for the Mimram, the Ash and the Rib (i.e. the Chalk and the two entirely rural basins) whereas the range has decreased for the upper Lee, the Beane, the Stort and the upper catchment to Feildes Weir (i.e. the more heterogeneous basins including a mixture of Clay and Chalk and zones of urban developments). Similarly, Figure 6.30 compares the performance of rural and urban catchments but ranked by size. The results confirm that urbanisation has an impact on the model performance at sub-basin scale. At catchment scale, the NSE_{ref} remains high using SG7 and radar data. Lower performance is observed using SG1 during summer events.

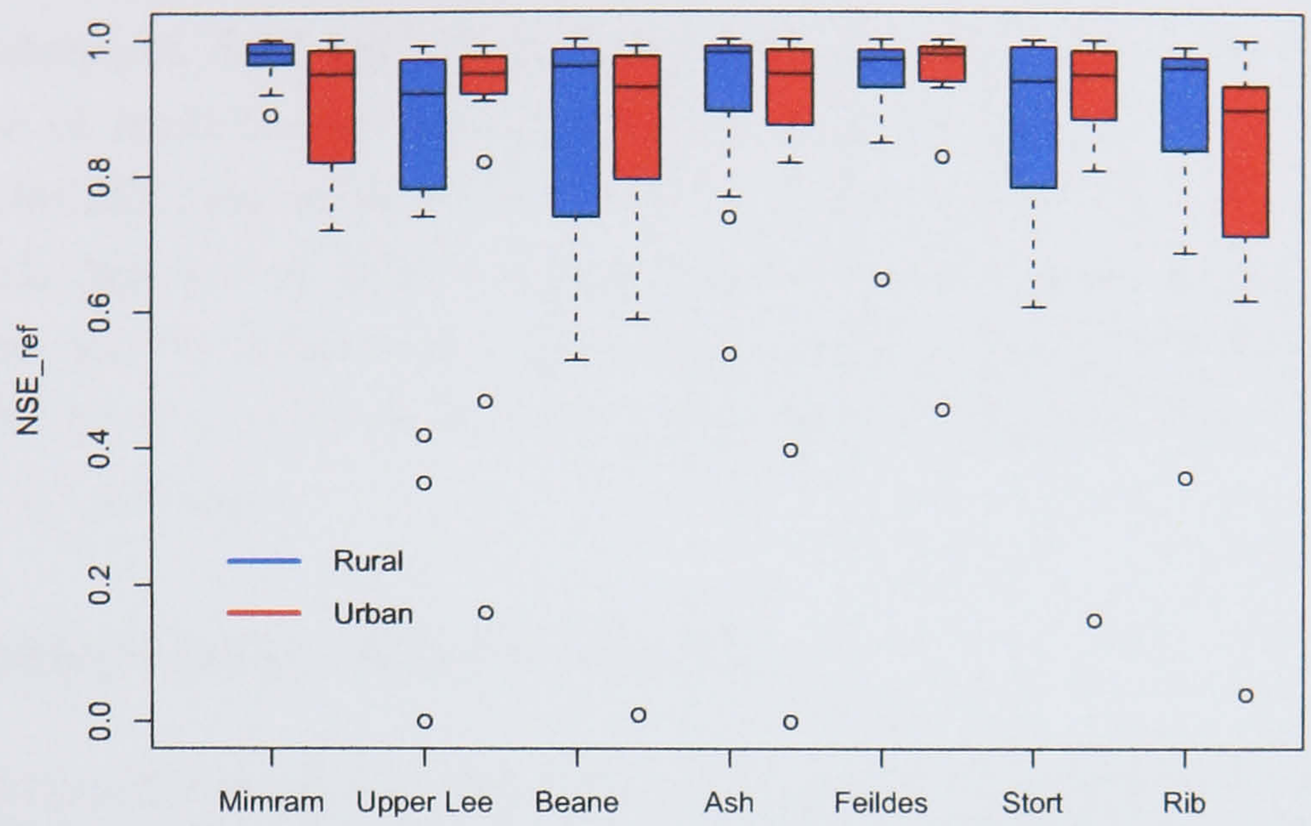

Figure 6.29 Model performance for rural and urban catchments ranked according to their catchment characteristic response time

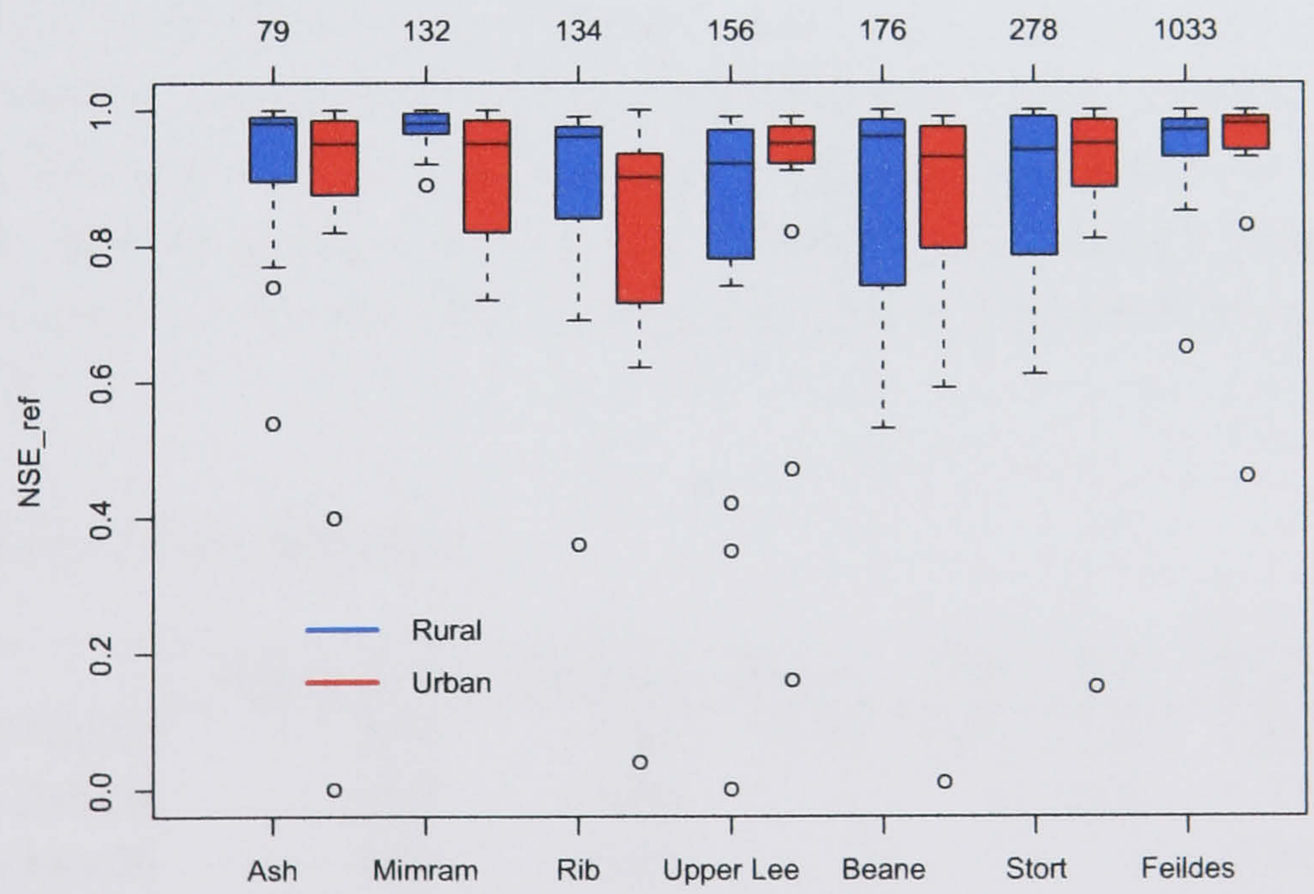

Figure 6.30 Boxplots of NSE$_r ef$ criteria for each urban subcatchment ranked according to catchment scale

6.3.3 Conclusion

In conclusion, results show that radar data lead to similar performance on rural and urban catchments. SG7 applied on urbanised basins leads to similar NSE_{ref} values as in the case of rural basins but to larger errors in Q_p and T_p. The discrepancies are enhanced for SG1, especially in the case of summer events. The effect of urbanisation decreases the lag time by 50% on average for all subcatchments. However the impacts of the lag time and the catchment scale on the runoff response were not clearly evidenced. Only at the whole catchment scale, less sensitivity to spatial rainfall (using radar data and SG7) is observed.

6.4 Disaggregation Scheme Results

So far, the rainfall-runoff investigation has focused on the impact of observed rainfall estimators. However it is common to have long records from raingauges at the daily time-scale but greater limitations at the hourly time-scale. Hence the spatial-temporal disaggregation scheme of Chapter 4 conditioned on observed daily data can be a useful alternative. In this section, a spatially-uniform temporal disaggregation of observed daily rainfall to hourly data is tested for validation of the methodology for hydrological applications. The sub-daily temporal profile of the raingauge closest to the centroid of the catchment (raingauge 163) is applied to disaggregate the daily values at the other sites. Spatial interpolation using Thiessen polygons is applied. In comparison to the reference rainfall, this rainfall estimator conserves the volume and the areal variability of rainfall but assess the impact of a single temporal distribution of rainfall over the catchment. The comparison between the simulated and reference flows are presented in Figures 6.31 to 6.35 for rural catchments and in Figures 6.36 to 6.40 for urban catchments.

6.4.1 Rural Catchments

	Upper Lee	Mimram	Beane	Rib	Ash	Stort	Feildes
11-Oct-93	0.99	0.98	0.98	0.99	0.98	0.98	0.97
03-Feb-94	0.97	0.99	1	1	0.98	1	1
08-Jan-96	0.98	0.99	1	1	1	0.96	0.99
16-May-95	0.97	1	1	1	1	1	0.99
30-Jul-02	0.92	0.96	0.95	0.99	0.94	0.98	0.96

Table 6.10 NSE_{ref} for the disaggregation scheme

Using this disaggregated scheme, the total areal rainfall variations are preserved, but a

	Radar	SG7	SG1	Dis
NSE_{ref}	0.95	0.91	0.80	0.98
Q_p (%)	12.6	15.3	28.1	6.6
T_p (%)	5.6	5.8	8.0	6.5
V (%)	7.4	12.4	21.6	4

Table 6.11 Summary performance on rural catchments

single hourly temporal profile of rainfall is applied to all subareas. Table 6.10 displays the NSE_{ref} results between the reference and simulated flow. Overall a close fit to the reference streamflow is obtained (NSE_{ref} about 1), the performance is slightly lower for the convective summer event of 30th July 2002 but still remains high ($NSE_{ref} >$ 0.92). A shift in the timing of the hydrograph is observed for the extreme event of 11th October 1993 and the convective event of 30th July 2002 as illustrated in Figure 6.31 and Figure 6.35. On the event of 16th May 1995, the disaggregation rainfall estimator does not reproduce the double-peaked hydrograph on the Upper Lee.

Table 6.11 summarises the model performance obtained for each rainfall scenario. Overall the model performance in terms of NSE_{ref} is higher using the disaggregated scheme (0.98), and decreases with radar data (0.95), SG7 (0.91) and SG1 (0.80). Since the areal variations are preserved using the disaggregation scheme, this rainfall scenario leads to smallest variations in Q_p and V but the percentage change in T_p is greater than when using radar data or SG7 (6.5% compared to 5.6 and 5.8%).

Since there is a trade-off between the rainfall variability and the integrating effect of the catchment, a simple disaggregation procedure can be applied with good modelling performance. This test also reveals that the impact of spatial variability of rainfall dominates the impact of temporal variability when modelling runoff on these catchments.

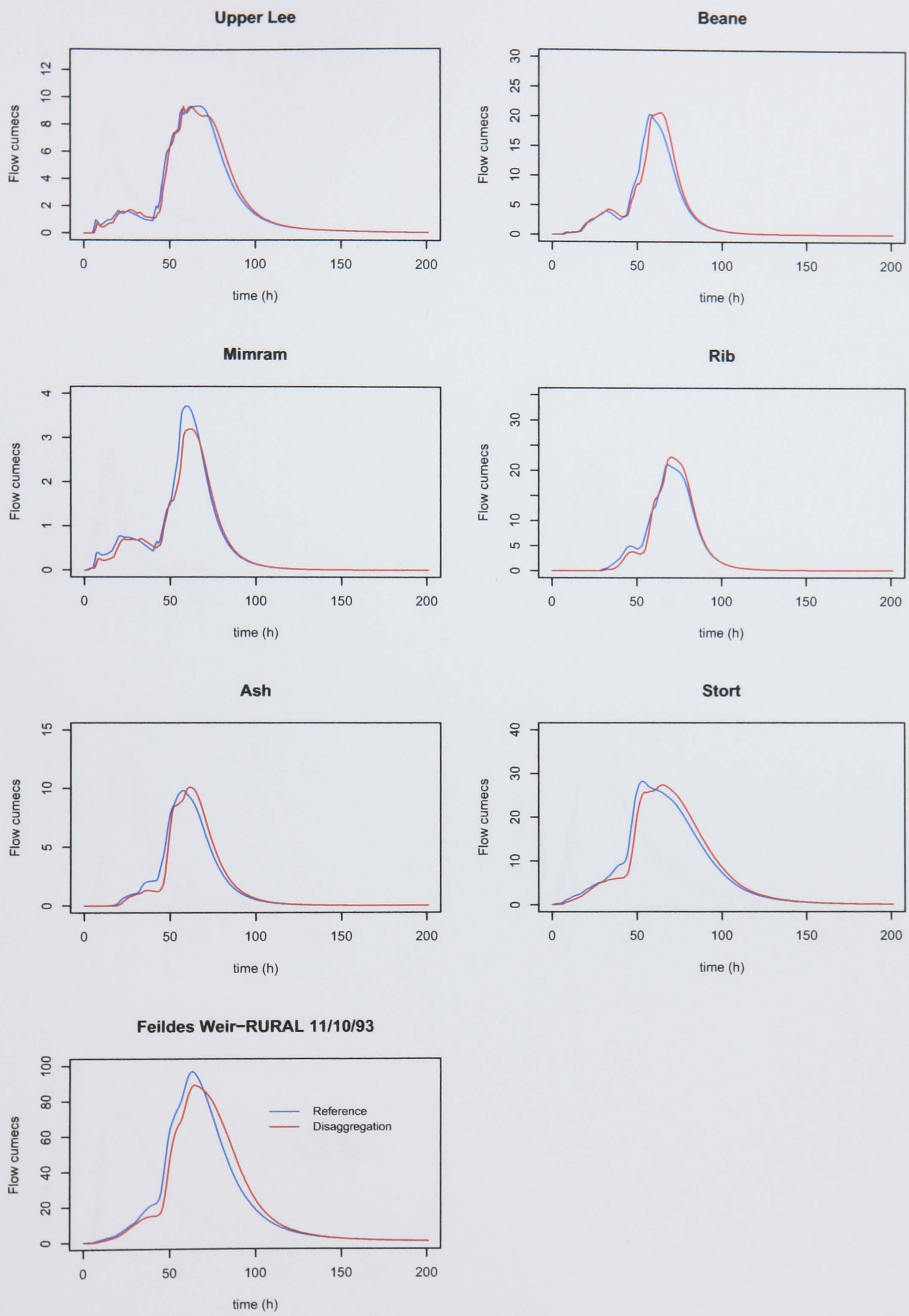

Figure 6.31 Simulated flow using disaggregated rainfall for the event of 11/10/93 (observed daily rainfall at all sites and hourly rainfall at master gauge, simulated hourly rainfall at other sites).

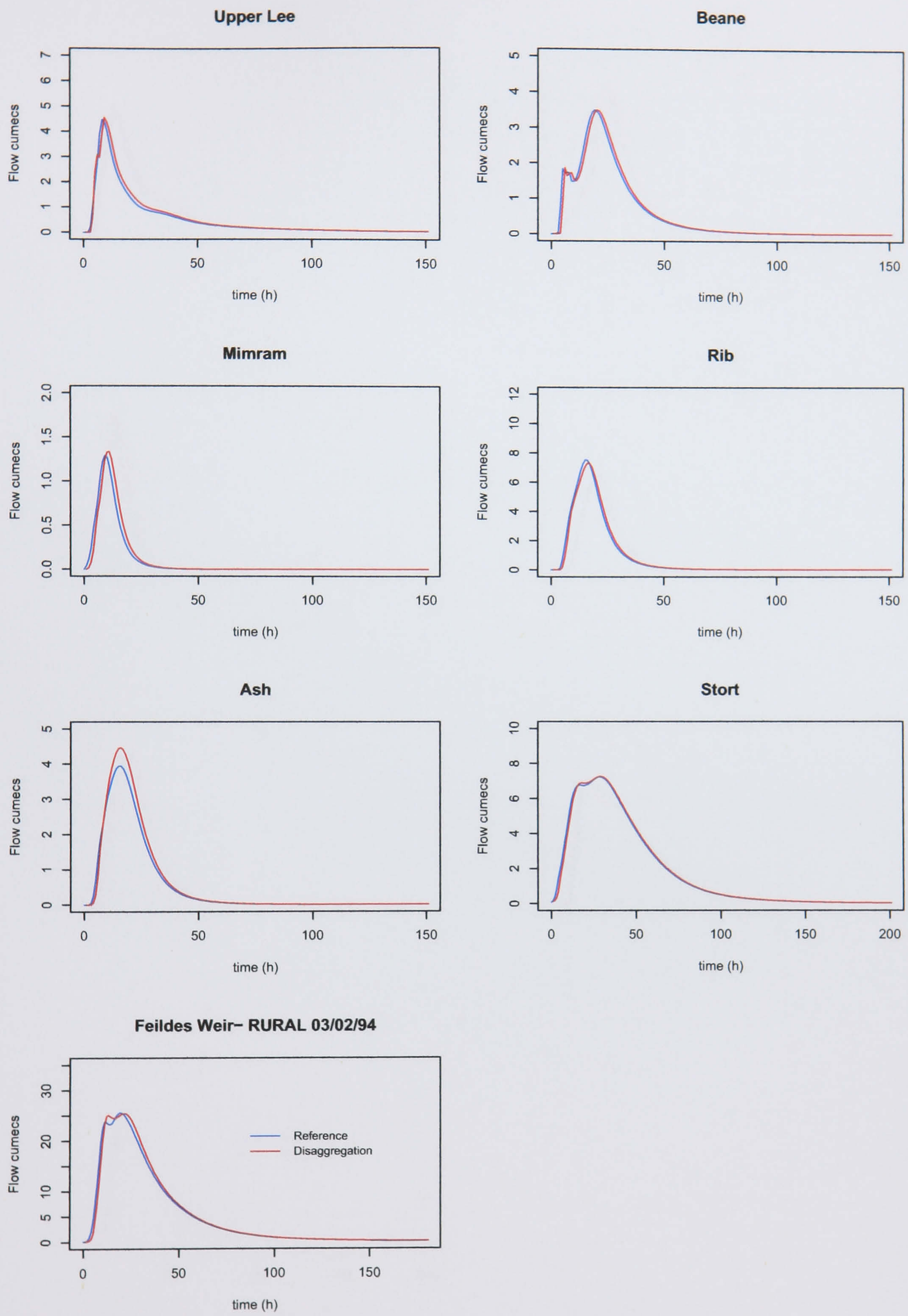

Figure 6.32 Simulated flow using disaggregated rainfall for the event of 03/02/94

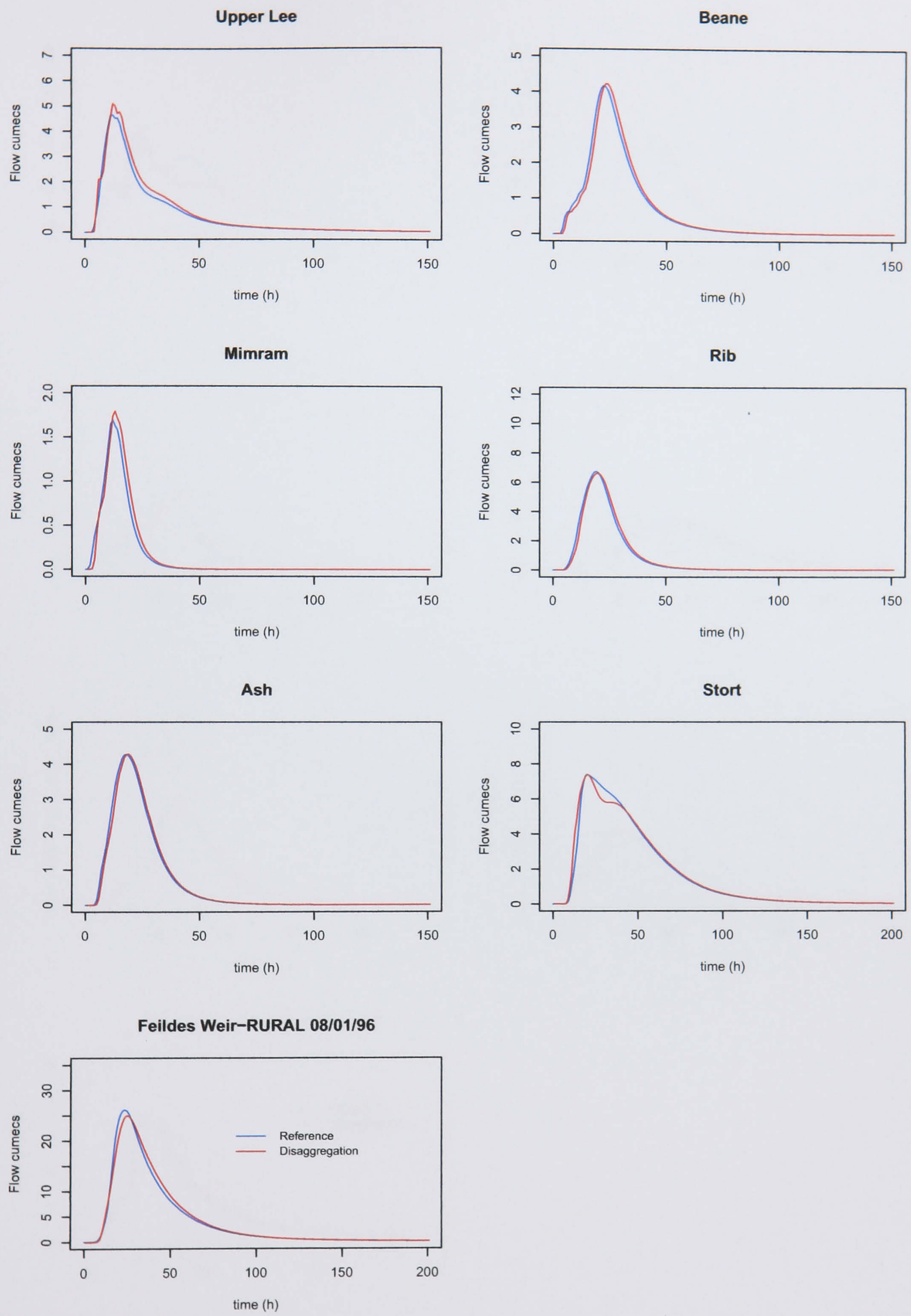

Figure 6.33 Simulated flow using disaggregated rainfall for the event of 08/01/96

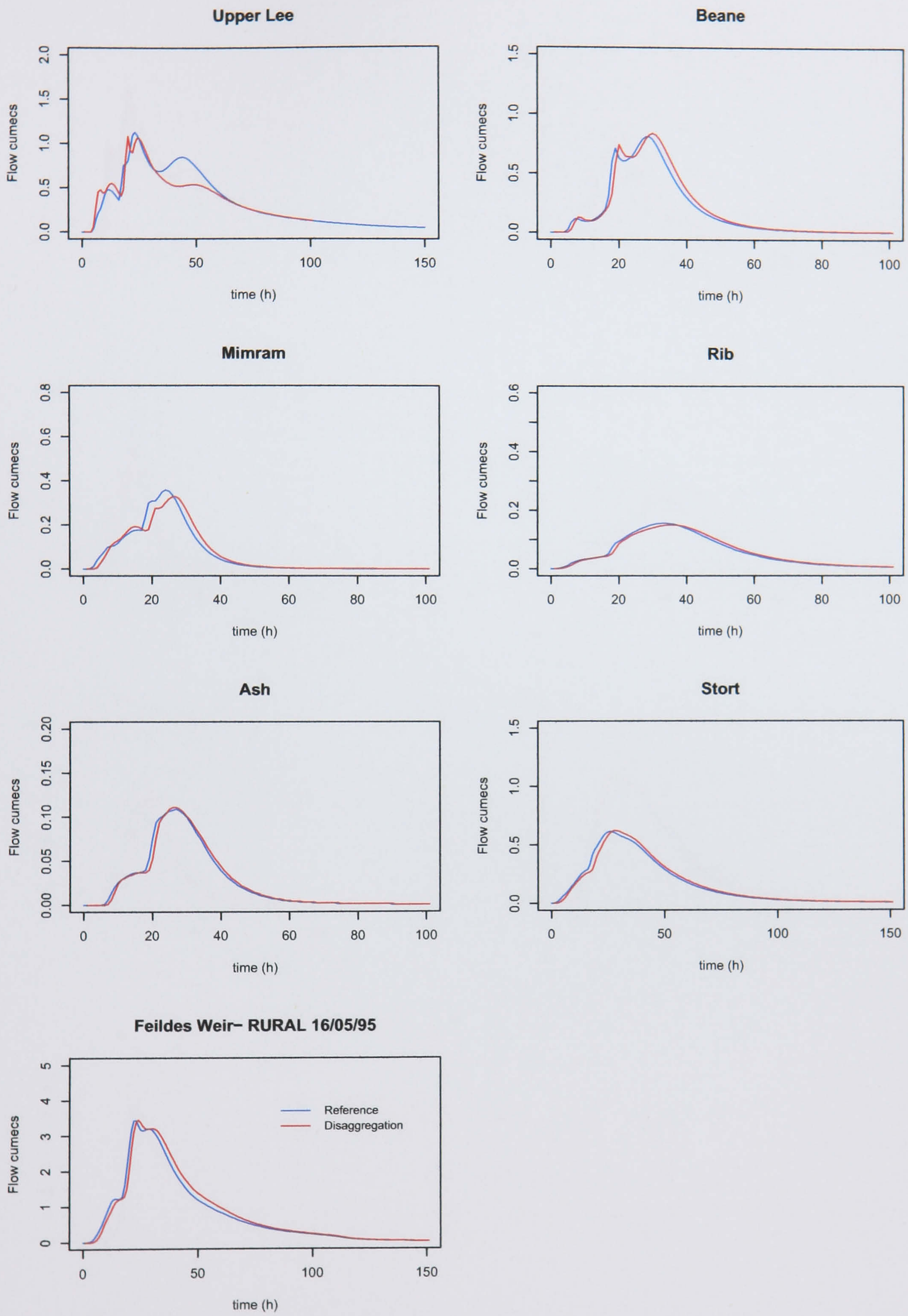

Figure 6.34 Simulated flow using disaggregated rainfall for the event of 16/05/95

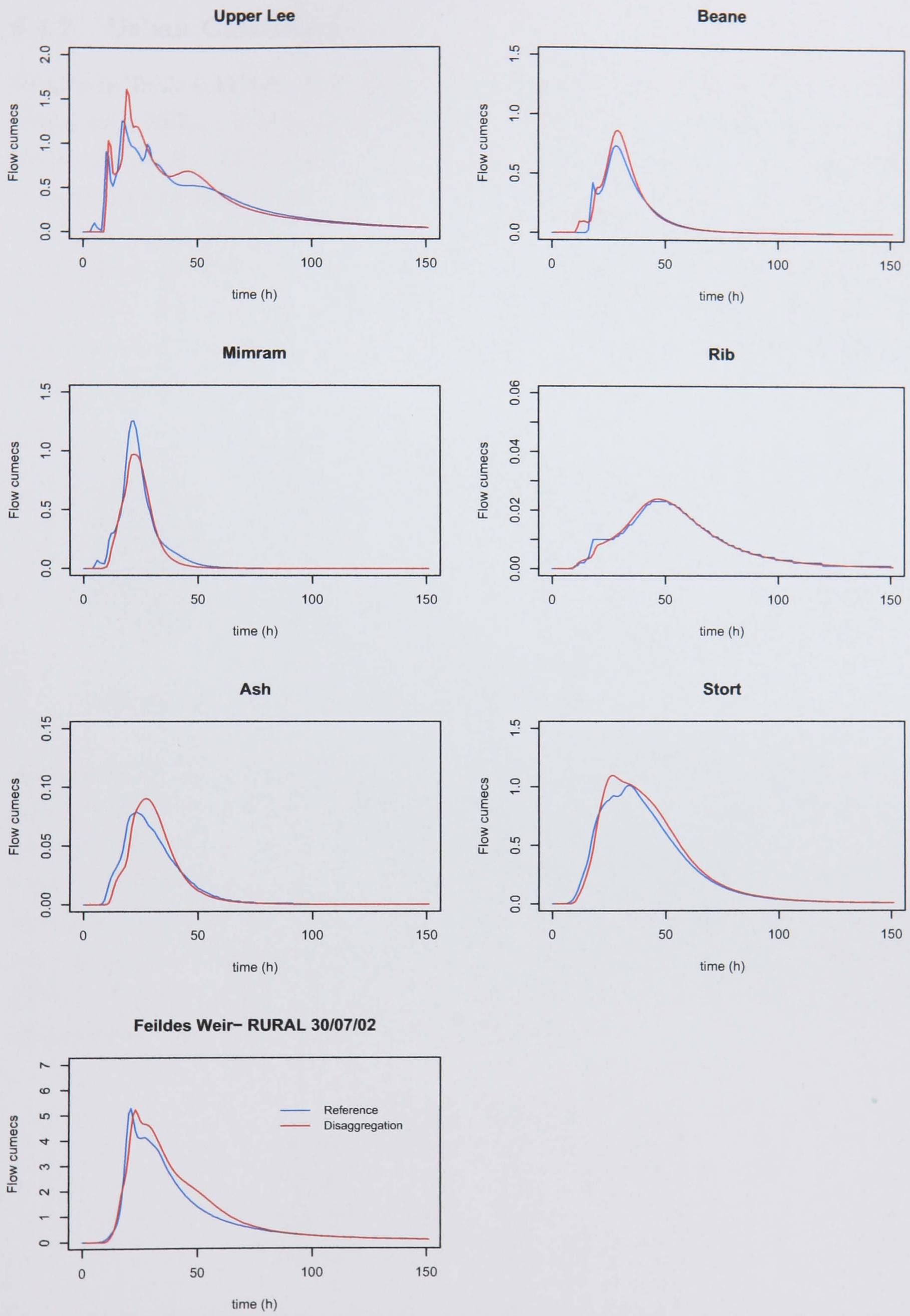

Figure 6.35 Simulated flow using disaggregated rainfall for the event of 30/07/02

6.4.2 Urban Catchments

As seen in Table 6.12, the model performance remains high for the artificially urbanised basins with NSE_{ref} of 0.94 on average for all events and (sub)catchments. Examining the results for the individual subcatchments, results show that the model performance is lower for the Mimram and the Ash on 30th July 2002 (NSE_{ref} of 0.71 and 0.33, respectively). In particular, the disaggregation rainfall estimator does not reproduce the double-peaked hydrograph on the Ash. Lower performance at the catchment scale is also observed (NSE_{ref} of 0.88). This indicates the limit of the disaggregation scheme which is not appropriate for temporally variable rainfall as in the case of localised convective storms.

	Upper Lee	Mimram	Beane	Rib	Ash	Stort	Feildes
11-Oct-93	0.98	0.94	0.99	0.93	0.90	0.97	0.97
03-Feb-94	0.98	0.98	1	0.99	0.99	1	1
08-Jan-96	0.98	0.97	0.93	1	1	0.97	0.99
16-May-95	0.93	0.83	0.96	0.96	0.97	0.99	0.96
30-Jul-02	0.92	0.71	0.93	0.88	0.33	0.98	0.88

Table 6.12 NSE_{ref} for the disaggregation scheme

A summary of the model performance characteristics obtained on average for all catchments and events and for all rainfall representations on urbanised catchments is presented in Table 6.13. Higher NSE_{ref} performance (0.95) and lower errors in Q_p (9.7%) and T_p (5.4%) are obtained with radar data. SG7 leads to high NSE_{ref} (0.92) but higher errors in Q_p (16.5%) and T_p (9.8%). The disaggregation scheme achieves the second best performance in terms of NSE_{ref} (0.94). It leads to similar change in Q_p (9%) as in the case of radar data but to larger errors in T_p (15.5%). Lowest model performance characteristics are obtained with SG1.

	Radar	SG7	SG1	Dis
NSE_{ref}	0.95	0.92	0.73	0.94
Q_p (%)	9.7	16.5	38.5	9
T_p (%)	5.4	9.8	12.7	15.5
V (%)	8	11.1	18.4	4.1

Table 6.13 Summary performance on urban catchments

6.4.3 Conclusion

Overall excellent performance of the disaggregation scheme is observed for all types of events and (sub)catchments when the basins are in natural condition (NSE_{ref} of 0.98 on average) even though the disaggregation rainfall estimator may not always reproduce double-peaked hydrographs. Some degradation in performance occurs although the high performance is maintained (NSE_{ref} of 0.94 on average) for the artificially urbanised basins. When there is a lack of available rainfall data, this simple disaggregation scheme conditioned on real or simulated daily rainfall can provide a useful alternative.

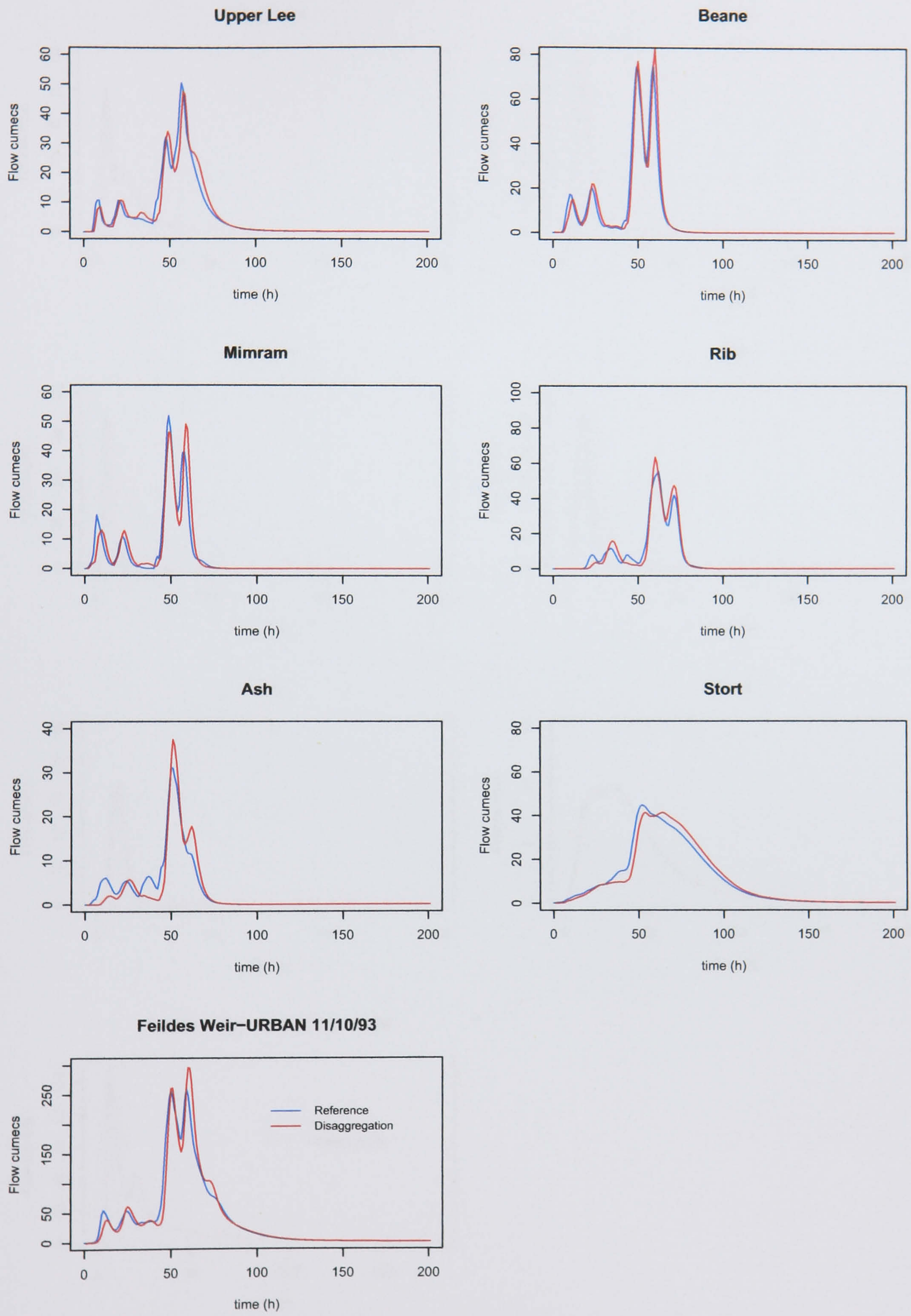

Figure 6.36 Simulated flow using disaggregated rainfall on urbanised catchments for the event of 11/10/93

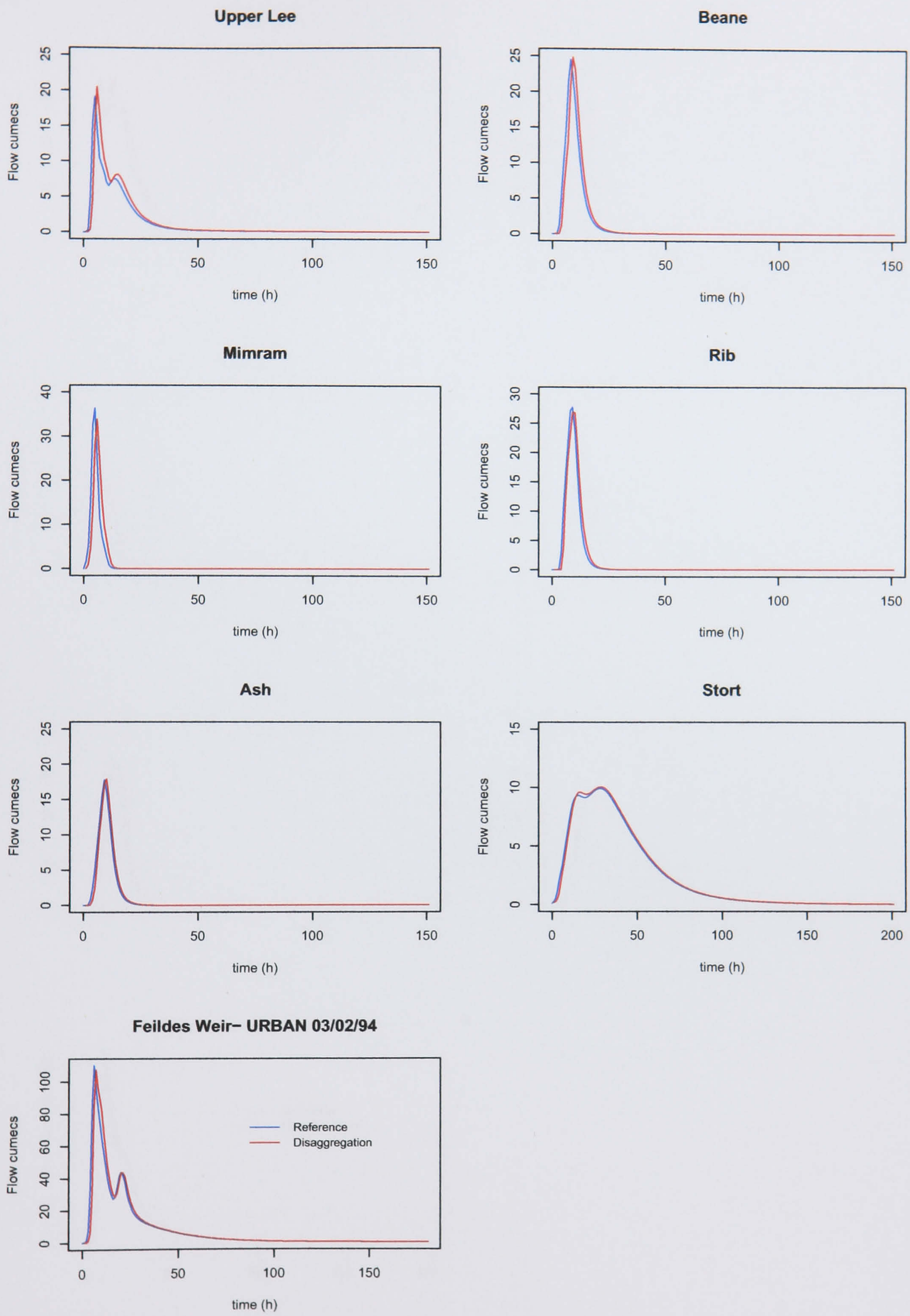

Figure 6.37 Simulated flow using disaggregated rainfall on urbanised catchments for the event of 03/02/94

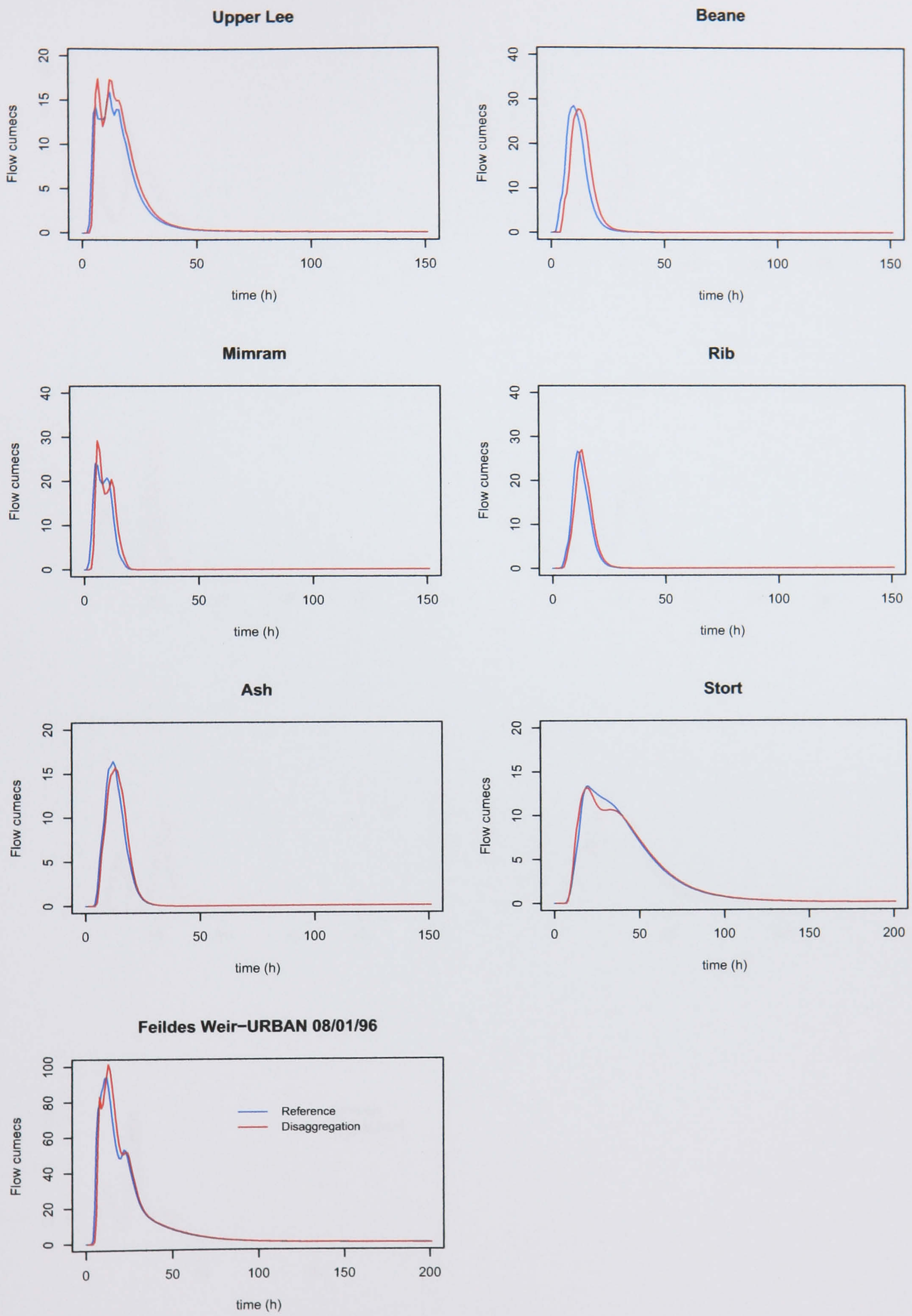

Figure 6.38 Simulated flow using disaggregated rainfall on urbanised catchments for the event of 08/01/96

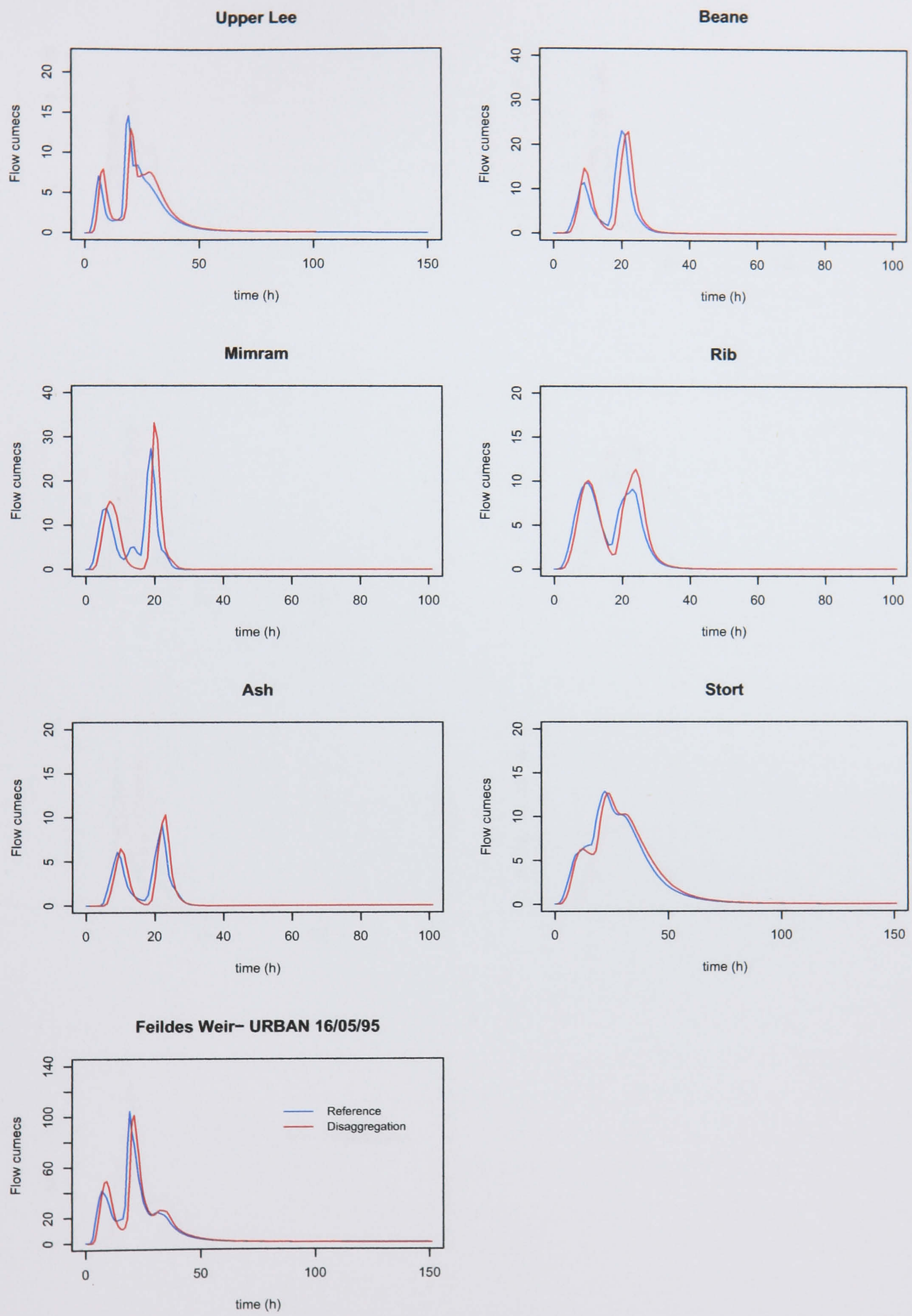

Figure 6.39 Simulated flow using disaggregated rainfall on urbanised catchments for the event of 16/05/95

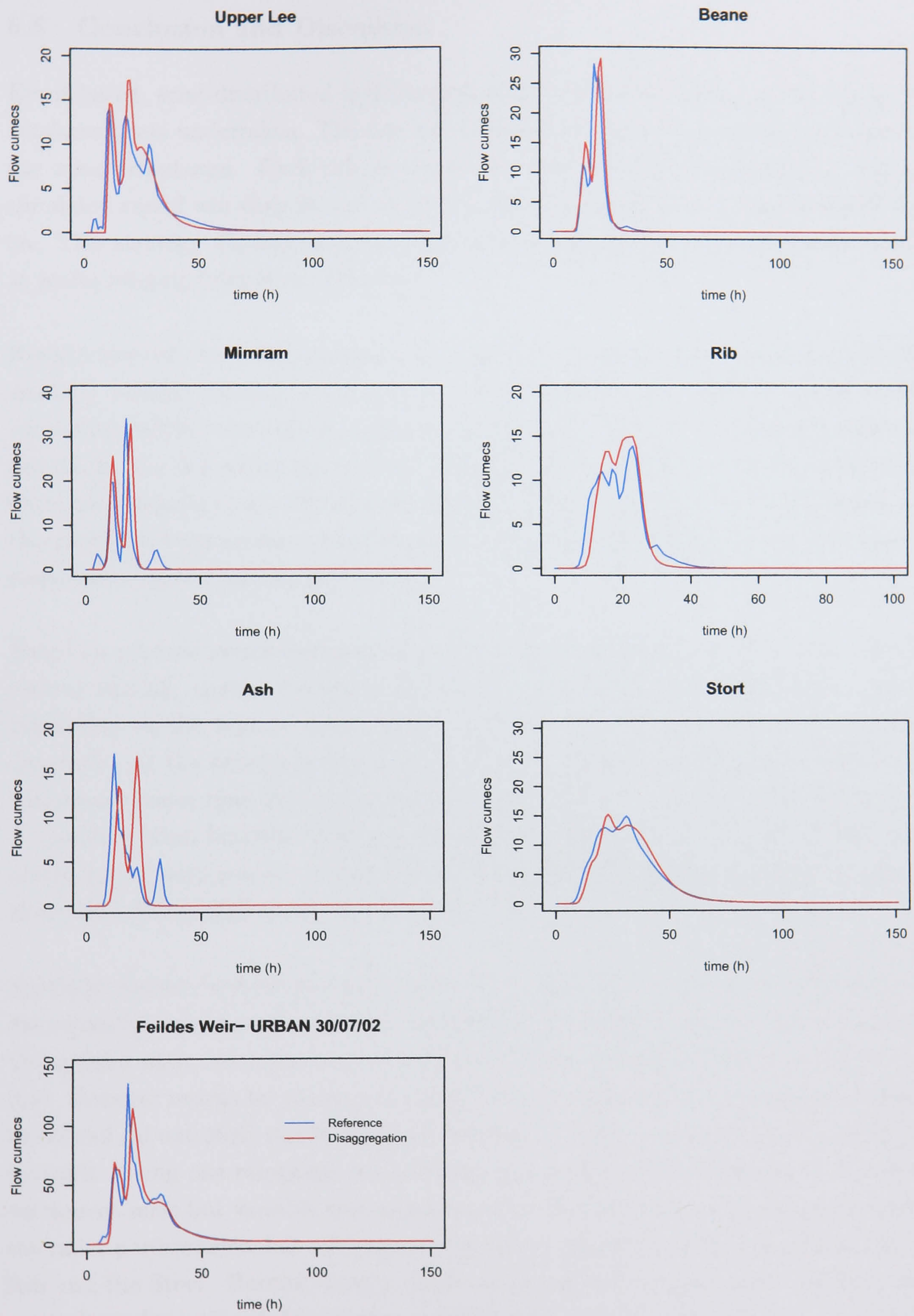

Figure 6.40 Simulated flow using disaggregated rainfall on urbanised catchments for the event of 30/07/02

6.5 Conclusion and Discussion

Event-based, semi-distributed hydrological rainfall-runoff modelling of the Upper Lee catchment was undertaken. The Lee was divided into six subcatchments, representing the main tributaries. Each subcatchment was first modelled independently and the simulated runoff was then routed into the total runoff generated at the watershed outlet. This strategy allowed analysis of the spatial structure of catchment-scale rainfall at scales ranging from 80 to 1000 km^2.

Results showed that the catchment response is a complex relationship between the spatially variable input and the watershed heterogeneity. An index of spatial rainfall variability (SDIR) was defined, based on the difference between the reference rainfall as defined by the full raingauge network and alternative rainfall estimators (using radar data, one raingauge per subcatchment and one raingauge for the whole catchment), and this proved to be the main controlling factor in determining the sensitivity of catchment response to spatial rainfall description.

Based on selected events representative of extreme and more common frontal and convective rainfall, spatial deviations in rainfall of up to SDIR of 40% were observed depending on the type of data available and this was reflected in the simulated hydrograph. At the subcatchment scale, spatial deviations in rainfall above 10% led to variations greater than 20% in the peak flow and 10% in the volume of the hydrograph. A modified Nash-Sutcliffe Efficiency criterion measured the performance of the simulated runoff with respect to reference simulated runoff. Spatial deviation in rainfall above 20% led to NSE values less than 0.8.

Spatially variable rainfall and radar data led to similar flow responses whereas larger discrepancies were introduced when using input data from a subset of the raingauges. Using radar data, results in terms of NSE were robust and remained high (usually above 0.9). However results for the largest summer event suggest that large spatial deviation in rainfall (about 30%) can be observed between the radar data and the full raingauge network. Using one raingauge per tributary achieved good performance at the whole catchment scale but variable performance at the subcatchment scale–generally close to the radar performance, but with some larger errors, particularly for some events on the Rib and the Stort. Results using a single raingauge for the catchment and subcatchment showed significant degradation in NSE values and also affected the reproduction of the peak hydrograph time.

Results were analysed to assess effect of catchment properties on runoff response. No

clear patterns emerged as a function of catchment area or catchment lag time. It was found that clay and/or partly urban subcatchments were more sensitive to the spatial distribution of rainfall, whereas the chalk rural subcatchment, the Mimram, exhibited a damping behaviour of the rainfall input. At a catchment scale of 1000 km^2, the impact of spatial variation of rainfall on runoff was less than at the subcatchment scale of 80 to 280 km^2. This underlines the integrating effect of the catchment as the size increases. When the existing subcatchments were artificially turned into fast-responding urban basins, a decrease in the catchment response time (about 50% on average for all subcatments) was observed and the discrepancies in terms of reproduction of peak flow and runoff volume were enhanced for the most variable events.

Hence these results demonstrate that spatial variability of rainfall is important, but that quantification depends in a complex manner on rainfall type, catchment properties and scale. For predominantly rural catchments, a network of 16 raingauges seems appropriate at 1000 km^2 scale, between 4 and 7 raingauges are required at 80-280 km^2. This recommendation may not be appropriate for summer convective events. As urbanisation increases, the requirements become greater. For the Mimram, a spatially averaged rainfall at the subcatchment scale seems sufficient due to the damping behaviour of the chalk geology.

The methodology of disaggregation of observed daily rainfall was also tested. Using this scheme, the spatial pattern of daily rainfall is preserved, but a single subdaily temporal profile of rainfall is applied uniformly in space. For the natural catchments, a close fit (NSE close to 1) between the simulated flow and the reference flow is obtained, suggesting that the damping effect of the catchments compensates for the lack of rainfall temporal variability at sub-daily scale. However for the artificially urbanised catchments, the peak flow performance is somewhat decreased (but is comparable to radar data) and larger errors in the timing of the peak are observed (15.5%). This confirms that urban catchments require a fine spatial and temporal resolution to adequately reproduce the streamflow. Berne et al. (2004) suggest a resolution of the order or minutes and kilometres for the modelling of urban catchments.

Chapter 7

Conclusions and Recommendations

This thesis has encompassed two themes across hydrology relating to the stochastic modelling of space-time rainfall and to the relative importance of spatial rainfall data for flood runoff generation. The use of the various types of observed rainfall data has been discussed together with their shortcomings (radar calibration issues, availability limitations). A new approach to spatial-temporal disaggregation of daily rainfall to obtain subdaily data at multiple sites has been presented. This can be applied to simulated daily rainfall at several sites on a catchment and simulated hourly data at one site. Alternatively the methodology can be used to disaggregate observed daily data, provided that the subdaily temporal profile is available at one of the gauges on the catchment. This simpler scheme was also validated with rainfall-runoff modelling procedures. In addition, the issue of the relative importance of spatial rainfall representation for flood runoff generation has also been investigated. To provide guidance on this issue, an extensive review of the international literature was undertaken and this was supplemented by a numerical investigation on the Lee catchment. This chapter summarises the main findings of this thesis, examines future directions of research and makes some recommendations.

7.1 Observed Data

This investigation stresses the need for rainfall data and emphasises the problems of availability and quality encountered with observed data. Calibration issues remain problematic for radar and long sequences are not yet routinely available. The choice of the events for the rainfall-runoff modelling study was partly constrained by the obligation to have all raingauges on a catchment operational. The problem was worse in the case of a sequence of radar images missing as no information on the space-time structure of rainfall was available for the entire region. Data quality and availability issues were also observed for the flow data, in particular with the Stort. Hence as an alternative, stochastic models of rainfall are developed to provide continuous spatial

data. In addition, rainfall-runoff studies are used for flow simulations to gain insights into catchment behaviour.

7.2 Stochastic Modelling of Space-Time Rainfall and Disaggregation

In the modelling of space-time rainfall, this thesis confirms that realistic multisite daily rainfall sequences can be generated using the GLMs of Chandler (2002) fitted to daily raingauge data even though the daily correlation in rainfall was underestimated in the case-study presented. Next, a simple disaggregation scheme can be applied if subdaily data are required. At a representative site on a catchment, a single-site disaggregation is performed using the HYETOS technique (Koutsoyiannis and Onof, 2001). The resulting profile is then linearly applied to all satellite gauges. Results are promising and suggestions for further development of the rainfall model include:

- Regarding the single-site disaggregation scheme
  - The estimation of the BLRPM parameters is delicate and further calibration of the model, possibly on a longer time-period, is required to find a parameter set that reproduces better the proportion of dry periods.
  - Bias in the standard deviation of hourly rainfall is introduced by the single-site disaggregation and this seems to be due to the empirical adjusting procedure which ensures that the hourly values are consistent with the daily rainfall depth.
- A refinement of the artificial profile algorithm is needed in the case where the daily rainfall depth falls in one hour. As a first approach, an upper limit on the hourly total could be set.
- The major limitation of the disaggregation scheme is the overestimation of the spatial correlation in rainfall due to a single temporal profile applied at all gauges. Further research is required to investigate how and at what scale allowance for spatial heterogeneity must be made. To address this issue, evaluation of the methodology could be extended to a larger region. Various options could be pursued for more complex procedures. One possible development would be to run independent disaggregation procedures for discrete sub-areas; another would be to build in spatial correlation to a multi-site procedure. More generally, continuous space-time models could be used for subdaily data, conditioned on daily GLM simulation.
- At the present stage, each step of the modelling procedure is done independently.

There is a need to develop the disaggregation methodology to automate the process.

Some testing was carried out to assess the suitability of the disaggregation scheme for use in rainfall-runoff modelling applications. When conditioned on observed daily rainfall, the rainfall-runoff investigation highlighted the excellent performance of the disaggregation scheme on natural catchments. However, some deterioration in performance occurred when the catchments were artificially urbanised. Further, in some cases, it was observed that double-peaked hydrographs were not adequately reproduced.

To validate the model, the full methodology (GLMs plus disaggregation) should be tested jointly with a rainfall-runoff model. This could be undertaken in the context of continuous simulation, generating an ensemble of rainfall realisations to assess the impact on the ensemble of simulated flow in comparison to the observed or reference flow. There is also a need to test the performance of the disaggregation scheme on a wider range of catchments.

7.3 The Significance of Spatial Rainfall Data for Runoff Estimation

The literature on the significance of spatial rainfall for runoff estimation is complex and sometimes contradictory. Effects can be expected to vary depending on the nature of the rainfall, the nature of the catchment, and the spatial scale of the catchment and rainfall. Runoff from urban areas is extremely sensitive to spatial rainfall, and the same is true for arid areas, where rapid flow response is generated from spatially-localised convective rainfall. This is problematic, since the required density of raingauges to capture the spatial variability exceeds that normally available from routine monitoring networks. In temperate regions, the review highlighted the trade-off in terms of catchment response between the impact of spatial variability of rainfall and the smoothing effect due to the heterogeneity of the catchment. Hence it was observed that as the scale increases, the importance of spatial rainfall decreases and there is a transfer from spatial variability of rainfall to catchment response time distribution as the dominant factor governing runoff generation.

Numerical experiments for the Lee catchment (1000 km^2 to Feildes Weir) showed a complex picture. The subcatchments varied greatly in geology and runoff response. Chalk catchments were less sensitive to spatial rainfall description than clay catchments or those with significant urban development. The dominant controls on the catchment response time were the extent of runoff contributing areas, the location of these areas with flow distance to the outlet, and the scale of the catchment. However

the catchments were too heterogeneous so that it was not possible to assess the relative importance of these interactions. As a result, no clear pattern emerged as a function of catchment scale, or response time, except that the effect of spatial variability was damped at the whole catchment scale of 1000 km^2. This is an interesting result which confirms the findings from the literature that as the scale increases, the impact of spatial rainfall decreases. The dominant effect was the variability of the rainfall; as this increased, so did the significance of appropriate rainfall characterisation. Spatially variable raingauge and radar data lead to similar flow response whereas larger discrepancies were introduced when using input data from a subset of the raingauges. When the catchments were numerically urbanised, the significance of spatial rainfall was enhanced.

It is concluded that, for largely rural catchments, a network of 16 raingauges seems appropriate at 1000 km^2 scale; between 4 and 7 gauges are required at 80 - 280 km^2, but this recommendation may not be appropriate for summer convective events. As urbanisation increases, the requirements become greater. This confirms that urban basins are sensitive to the spatial and temporal distribution of rainfall. It seems that subhourly data and a spatial resolution of the order of a few kilometers are required. The 5 min, 2 km radar data could be used to investigate the rainfall resolution needed for the modelling of urban catchments.

In order to reduce the impact of modelling discretisation, a small catchment subdivision (10 km^2) was applied. Therefore no spatial rainfall information was lost when using the raingauge network and radar pixel aggregation was done at small scale (average of 2-3 pixels per subarea). Further research to vary the subdivision scale and assess its impact on the flow could be undertaken. It is likely that the model performance would not vary much with a larger catchment subdivision and this would simplify the running of the rainfall-runoff model. A subjective manual calibration procedure was carried out and therefore some discrepancies were observed between the reference and the observed flow. In order to minimise the impact of this modelling error, the simulated flow driven by the rainfall estimators was compared to the reference flow so that only the effect of spatial rainfall was assessed.

Ideally, the whole catchment to Feildes Weir would have been modelled directly and the hydrograph at an interior point generated to evaluate the impact of scale. This option was not followed for two reasons, a) too large a number of subareas would have been generated, leading to computational problems, b) the subcatchments have very different behaviours that justify a spatial variation of model parameters. Improve-

ment in the modelling strategy would include automatic calibration, incorporation of a larger number of subdivisions in the model structure and the possibility of varying model parameters at subcatchment scale automatically. A simple spatial interpolation scheme based on Thiessen polygon method was used here to calculate the areal rainfall. Methods that take into account the distance between the estimation point and the observation stations such as inverse distance weighting and multiquadratics may be more suitable to model summer events.

Due to time constraints and calibration issues, in this investigation it was not possible to fully exploit the potential of radar data. Although a number of errors can be observed in the radar measurements, nevertheless radar data represent an important source of information, which allows the continuous spatial distribution to be studied. Records from the Chenies radar could be used for in-depth investigation of specific heavy rainfall and flood events, with particular attention to highly intense convective events giving rise to flash-floods in summer.

Possible extension of this work involves the use of continuous simulation to have a better understanding of the effect of antecedent conditions. For instance, a storm event even if not considered as an extreme rainfall, may produce serious flooding situations when the ground is wet from previous rainfall. In addition, sufficiently heavy rainfall in summer falling on dry ground may also generate a high amount of (fast) runoff. The use of continuous simulation to assess the sensitivity of the catchment response to the rainfall estimators under various catchment and storm conditions would also facilitate the derivation of flood frequency curves. This information would be useful for flood emergency planning and reservoir design for flood control.

Finally the results confirmed the findings of Naden (1992); Obled et al. (1994); Woods and Sivapalan (1999); Andréassian et al. (2001); Smith et al. (2004) and Dodov and Foufoula-Georgiou (2005) but further work involves analysing the impact of the rainfall estimators on a wide range of catchments.

7.4 Conclusions

In conclusion, this thesis addressed two themes with relevance to the hydrological community. These relate to the stochastic modelling of space-time rainfall and the importance of spatial rainfall data for runoff generation. In the context of multisite modelling of hourly rainfall, an approach for rainfall generation combined with a disaggregation procedure was proposed with potential applications. Results are promising and areas of further research are clearly defined. Besides, the scheme is readily applicable with

two main components of the procedure already available (GLIMCLIM, Chandler, 2002 and HYETOS, Koutsoyiannis and Onof, 2000).

This thesis assessed the importance of spatial rainfall representation and also gained knowledge into catchment behaviour. The importance of rainfall spatial variability was confirmed but further investigation on the impact of catchment scale on runoff generation should be undertaken. The catchments used in this investigation were very heterogeneous: thus the impact of catchment properties may have masked the impact of catchment scale. It would be interesting to redo the analysis on a more homogeneous catchment and run different rainfall scenarios at various subcatchment scales. Further, an analysis at an intermediate catchment scale ($\simeq 500km^2$) is required.

In the context of broad scale modelling, these two themes interrelate as rainfall simulations provide continuous input for hydrological models to support the planning of flood defences. The rainfall-runoff investigation presented in this thesis is instructive as the impact of the spatial structure of rainfall on runoff generation is now better understood. This gives feedback on the requirements in terms of modelling of spatial rainfall. For convective summer events, the spatial pattern of the storm totals is important: thus a model that represents the spatial variation of rainfall is required. The disaggregation scheme conditioned on simulated daily rainfall from a GLM is an alternative that needs to be tested. For urbanised catchments, the adequate spatial and temporal representation of subdaily rainfall is important. Therefore it is essential to better reproduce the spatial correlation of multisite rainfall at different time scales (here daily and hourly). Hence areas for further investigation are identified which include the adequate representation of spatial correlation in rainfall and the joint-testing of the rainfall model proposed here with a continuous hydrological model.

Bibliography

Ajami, N., Gupta, H., Wagener, T., and Sorooshian, S. (2004). Calibration of a semi-distributed hydrologic model for streamflow estimation along a river system. *Journal of Hydrology*, 298:112–135.

Andréassian, V., Perrin, C., Michel, C., Usart-Sanchez, I., and Lavabre, J. (2001). Impact of imperfect rainfall knowledge on the efficiency and the parameters of watershed models. *Journal of Hydrology*, 250:206–223.

Arnaud, P., Bouvier, C., Cisneros, L., and Dominguez, R. (2002). Influence of rainfall spatial variability on flood prediction. *Journal of Hydrology*, 260:216–230.

Aronica, G. and Cannarozzo, M. (2000). Studying the hydrological response of urban catchments using a semi-distributed linear non-linear model. *Journal of Hydrology*, 238:35–43.

Austin, G. (2001). Weather radar: theory and practice. In *Radar hydrology for real time flood forecasting*, pages 33–38. European Commission.

Bell, V. and Moore, R. (2000). The sensitivity of catchment runoff models to rainfall data at different spatial scales. *Hydrology and Earth System Sciences*, 4(4):653–667.

Bellone, E. (2003). Calibration of Chenies Data: Problems and changes, DEFRA project. Technical report, no. 10, Imperial College London and University College London.

Berne, A., Delrieu, G., Creutin, J.-D., and Obled, C. (2004). Temporal and spatial resolution of rainfall measurements required for urban hydrology. *Journal of Hydrology*, 299:166–179.

Bo, Z., Islam, S., and Eltahir, E. (1994). Aggregation-disaggregation properties of a stochastic rainfall model. *Water Resources Research*, 30(12):3423–3435.

Borga, M. (2002). Accuracy of radar rainfall estimates for streamflow simulation. *Journal of Hydrology*, 267:26–39.

Borga, M., Tonelli, F., Moore, R., and Andrieu, H. (2002). Long-term assessmen of bias adjustment in radar rainfall estimation. *Water Resources Research*, 38(11):1–10.

Brath, A., Montanari, A., and Toth, E. (2004). Analysis of the effects of different scenarios of historical data availability on the calibration of a spatially-distributed hydrological model. *Journal of Hydrology*, 291:232–253.

Buishand, T. and Brandsma, T. (2001). Multisite simulation of daily precipitation and temperature in the Rhine basin by nearest-neighbor resampling. *Water Resources Research*, 37(11):2761–2776.

Burgess, K., Deakin, R., Samuels, P., Chatterton, J., and Penning-Rowsell, E. (2000). Assessment of economic value of national assest at risk from flooding and coastal erosion. In *Proceedings of the DEFRA Conference of River and Coastal and Engineers*, pages 04.3.1–04.3.10, UK. MAFF.

Cameron, D., Beven, K., and Tawn, J. (2000). An evaluation of three stochastic rainfall models. *Journal of Hydrology*, 228:130–149.

Carpenter, T., Konstantine, P., and Sperfslagea, J. (2001). On the parametric and nexrad-radar sensitivities of a distributed hydrologic model suitable for operational use. *Journal of Hydrology*, 253:169–193.

Chandler, R. (2002). Generalized Linear modelling for daily climate time series (Software and Use guide). Technical report, n. 227, University College London. http://www.ucl.ac.uk/Stats/research/Resrpts/abstracts.html.

Chandler, R. and Wheater, H. (2002). Analysis of rainfall variability using Generalised Linear Models. a case study from the West of Ireland. *Water Resources Research*, 38(10).

Chaubey, I., Hann, C., Grunwald, S., and Salisbury, J. (1999). Uncertainty in the model parameters due to spatial variability of rainfall. *Journal of Hydrology*, 220:48–61.

Chow, V., Maidment, D., and Mays, L. (1988). *Applied Hydrology*. McGraw-Hill.

Cluckie, I., Tilford, K., Griffith, R., and Lane, A. (2000). Radar hydrometeorology using a vertically pointing radar. *Hydrology and Earth System Sciences*, 4:565–580.

Coe, R. and Stern, R. (1982). Fitting models to daily rainfall. *Journal of Applied Meteorology*, 21:1024–1031.

Collier, C. (1996). *Application of weather radar systems*. Wiley - Praxis.

Corral, C., Sempere-Torres, D., Revilla, M., and Berenguer, M. (2000). A semi-distributed hydrological model using rainfall estimates by radar. application to mediterranean basins. *Physics and Chemistry of the Earth*, 25(10–12):1133–1136.

Cowpertwait, P. (1994). A generalized point process model for rainfall: high-order. *Proceeding Royal Society London*, A447:23–37.

Cowpertwait, P. (1998). A poisson-cluster model of rainfall: high-order moments and extreme values. *Proceeding Royal Society London*, A454:885–898.

Cox, D. and Isham, V. (1980). *Point Processes.* Chapman and Hall, London.

Crees, M. (2003). CASCADE FLOOD WARNING SYSTEM Data for UCL - Statistical Sciences. Technical report, University College London.

De Lannoy, G., Verhoest, N., and De Troch, F. (2005). Characteristics of rainstorms over a temperate region derived from multiple time series of weather radar images. *Journal of Hydrology*, 307:126–144.

de Lima, J. and Singh, V. (2002). The influence of the pattern of moving rainstorms on overland flow. *Advances in Water Resources*, 25:817–828.

Dodov, B. and Foufoula-Georgiou, E. (2005). Incorporating the spatio-temporal distribution of rainfall and basin geomorphology inot nonlinear analyses of streamflow dynamics. *Advances in Water Resources*, 28:711–728.

Duan, Q., Sorooshian, S., and Gupta, H. (1992). Effective and efficient global optimization for conceptual rainfall-runoff models. *Water Resources Research*, 28(4):265–284.

EAE (2005). Encyclopedia of the Atmospheric Environment (Online). *http://www.ace.mmu.ac.uk/eae/english.html.*

Faulkner, D. (1999). *Flood Estimation Handbook, 2: Rainfall frequency estimation*, volume 3. Institute of Hydrology, United Kingdom.

Faulkner, D. and Wass, P. (2005). Flood estimation by continuous simulation in the Don catchment,. *Journal of the Chartered Institution of Water and Environmental Management*, In press.

Faurès, J., Goodrish, D., Woolhiser, D., and Sorooshian, S. (1995). Impact of small-scale spatial rainfall variability on runoff modeling. *Journal of Hydrology*, 173:309–326.

FLOODSITE (2005). Language of Risk Project Definitions, FLOODsite Consortium Report T32-04-01, available at www.floodsite.net.

Flynn & Rothwell (1991a). Report on Hydraulic Modelling (ONDA) of The River Stort. Technical report, Thames Region, National Rivers Authority.

Flynn & Rothwell (1991b). Report on Hydrologic Modelling (RORB) of Middle Lee, draft report. Technical report, Thames Region, National Rivers Authority.

Foufoula-Georgiou, E. and Krajewski, W. (1995). Recent advances in rainfall modelling, estimation, and forecasting. *Reviews in Geophysics*, 33:1125–1137.

Grayson, R. and Blöschl, G. (2000). Spatial modelling of catchment dynamics. In *Spatial patterns in catchment hydrology: observations and modelling*, pages 51–81, Cambridge press. Rodger Grayson and Günter Blöschl.

Gyasi-Agyei, Y. (2005). Stochastic disaggregation of daily rainfall into one-hour time scale. *Journal of Hydrology*, 309:178–190.

Halcrow (2001). The Lower Lee Flood Defence Strategy Study, Inception report. December, 2001.

Harrison, D., Driscoll, S., and Kitchen, M. (2000). Improving precipitation estimates from weather radar using quality control and correction techniques. *Meteorological Applications*, 6:134–144.

Hawnt, R. (1987a). Catchment runoff control study, Report on the evaluation of the hydrological response of the Mimram and Beane catchments. Technical report, Thames Water, Rivers Division.

Hawnt, R. (1987b). Catchment runoff control study, Report on the evaluation of the hydrological response of the catchments of the Rib and Ash. Technical report, Thames Water, Rivers Division.

Illingworth, A., Blackman, T., and Goddard, J. (2000). Improved rainfall estimates in convective storms using polarisation diversity radar. *Hydrology and Earth System Sciences*, 4:555–563.

Jensen, N. and Pedersen, L. (2005). Spatial variability of rainfall: variations within a single radar pixel. *Atmospheric Research*, In press.

Kitchen, M., Brown, R., and Davies, A. (1994). Real-time correction of weather radar data for the effects of bright band, range and orographic growth in widespread precipitation. *Quaterly Journal Royal Meteorological Society*, 120:1231–1254.

Koren, V., Finnerty, B., Schaake, J., Smith, M., Seo, D.-J., and Duan, Q.-Y. (1999). Scale dependencies of hydrologic models to spatial variability of precipitation. *Journal of Hydrology*, 217:285–302.

Kottegoda, N., Natale, L., and Raiteri, E. (2002). A parsimonious approach to stochastic multisite modelling and disaggregation of daily rainfall. *Journal of Hydrology*, 274:47–61.

Koutsoyiannis, D. and Onof, C. (2000). HYETOS - A Computer program for stochastic disaggregation of fine-scale rainfall. *http://www.itia.ntua.gr/e/softinfo/3/*.

Koutsoyiannis, D. and Onof, C. (2001). Rainfall disaggregation using adjusting procedures on a Poisson cluster model. *Journal of Hydrology*, 246:109–122.

Koutsoyiannis, D., Onof, C., and Wheater, H. (2003). Multivariate rainfall disaggregation at a fine timescale. *Water Resources Research*, 39(7):1173, doi:10.1029/2002WR001600.

Koutsoyiannis, D. and Pachakis, D. (1996). Deterministic chaos versus stochasticity in analysis and modeling of point rainfall series. *Journal of Geophysical Research*, 101(D21):26441–26451.

Laurenson, E. and Mein, R. (1988). RORB version 4 Runoff Routing program, User Manual. Technical report, Monash University, Department of Civil Engineering.

Lekkas, D. (2002). Review of single-site rainfall modelling, DEFRA project,Internal report no. 1. Technical report, Imperial College London and University College London.

Lekkas, D. and Onof, C. (2005). Introducing the variation of advective time delay (adt) to transfer function models. *Environmental Modelling & Software*, In press.

Lopes, V. (1996). On the effect of uncertainty in spatial distribution of rainfall on catchment modelling. *CATENA*, 28:107–119.

Lord, M. E. (1998). *An improved, adaptive calibration system for weather radar.* PhD thesis, University of Lancaster.

Lotufo Conejo, J. (1979). Hydrologic simulation and flood routing models: a case study. Technical report, Imperial College.

Marshall, J. and Palmer, W. M. (1948). The distribution of raindrops with size. *Journal of Meteorology*, 5:165–166.

Maskey, S., Guinot, V., and Price, R. (2004). Treatment of precipitation uncertainty in rainfall-runoff modelling: a fuzzy set approach. *Advances in Water Resources*, 27:889–898.

McCullagh, P. and Nelder, J. (1989). *Generalized Linear Models.* Chapman and Hall, London, second edition.

Mellor, D. (1996). The Modified Turning Bands (MTB) model for space-time rainfall. I. Model definition and properties. *Journal of Hydrology*, 175:113–127.

Michaud, J. and Sorooshian, S. (1994). Effect of rainfall-sampling errors on simulations of desert flash floods. *Water Resources Research*, 30(10):2765–2775.

Molnar, P. and Burlando, P. (2005). Preservation of rainfall properties in stochastic disaggregation by a simple random cascade model. *Atmospheric Research*, 77:137–151.

Moore, R.J.and May, B., Jones, D., and Black, K. (1994). Local calibration of weather radar over london. In *Advances in radar hydrology*, pages 186–195. European Commission.

Morin, E., Enzel, Y., Shamir, U., and Garti, R. (2001). The characteristic time scale for basin hydrological response using radar data. *Journal of Hydrology*, 252:85–99.

Naden, P. (1992). Spatial variability in flood estimation for large catchments: the exploitation of channel network structure. *Journal des Sciences Hydrologiques*, 37(1):53–71.

Nelder, J. and Mead, R. (1965). A simplex method for function minimization. *Computer Journal*, 7:308–313.

NERC (1975). *Flood Studies Report, Hydrological Studies*, volume 1. Natural Environment Research Council, United Kingdom.

NERC (1999). WINFAP-FEH CD-ROM version 1.0.

Ngirane-Katashaya, G. and Wheater, H. (1985). Hydrograph sensitivity to storm kinematics. *Water Resources Research*, 21(3):337–345.

Northrop, P. (1998). A clustered spatial-temporal model of rainfall. *Proceeding Royal Society London*, A454:1875–1888.

Obled, C., Wendling, J., and Beven, K. (1994). The sensitivity of hydrological models to spatial rainfall patterns: an evaluation using observed data. *Journal of Hydrology*. 159:305–333.

Ogden, F. and Julien, P. (1993). Runoff sensitivity to temporal and spatial rainfall variability at runoff plane and small basin scales. *Water Resources Research*, 29(8):2589–2597.

Ogden, F. and Julien, P. (1994). Runoff model sensitivity to radar rainfall resolution. *Journal of Hydrology*, 158:1–18.

Olsson, J. and Berndtsson, R. (1998). Temporal rainfall disaggregation based on scaling properties. *Water Science and Technology*, 37(11):73–80.

Onof, C. (2003). Mathematical expressions of generalised moments used in single-site models, DEFRA project, Internal report no. 8. Technical report, Imperial College London and University College London.

Onof, C., Chandler, R., Kakou, A., Wheater, H., and Isham, V. (2000). Rainfall modelling using Poisson-Cluster processes: a review of developments. *Stochastic Environmental Research and Risk Assessment*, 14:384–411.

Onof, C. and Lekkas, D. (2003). The calibration and validation of single-site models, DEFRA project,Internal report no. 3. Technical report, Imperial College London and University College London.

Onof, C., Townend, J., and Kee, R. (2005). Comparison of two hourly to 5-min rainfall disaggregators. *Atmospheric Research*, 77:176–187.

Onof, C. and Wheater, H. (1993). Modelling of british rainfall using a random parameter bartlett-lewis rectangular pulse model. *Journal of Hydrology*, 149:67–95.

Over, M. and Gupta, V. (1996). A space-time theory of mesoscale rainfall using random cascades. *Journal of Geophysical Research*, 101:26319–26332.

Over, T. (1995). *Modelling space-time rainfall at the mesoscale using random cascades.* PhD thesis, University of Colorado.

Porporato, A. and Ridolfi, L. (2001). Multivariate nonlinear prediction of river flows. *Journal of Hydrology*, 248:109–122.

Quasem, W. (2004a). Personal communication.

Quasem, W. M. (2004b). Effect of spatial variability of rainfall on runoff for the lee catchment. Master's thesis, Imperial College London.

Reed, S., Koren, V., Smith, M., Zhang, Z., Moreda, F., and Seo, D.-J. (2004). Overall distributed model intercomparison project results. *Journal of Hydrology*, 298:27–60.

Reefsgaard, J. and Knudsen, J. (1996). Operational validation and intercomparison of different types of hydrological models. *Water Resources Research*, 32(7):2189–2202.

Rodriguez-Iturbe, I., Cox, D., and Isham, V. (1987). Some models for rainfall based on stochastic point processes. *Proceeding Royal Society London*, A(410):269 288.

Rodriguez-Iturbe, I., Cox, D., and Isham, V. (1988). A point process for rainfall: further developments. *Proceeding Royal Society London*, A(417):283–298.

Rodriguez-Iturbe, I. and Eagleson, P. (1987). Mathematical models of rainstorm events in space and time. *Water Resources Research*, 23(1):181–190.

Rogers, J. (2005). (Editor) Research News. *Flood and Coastal Erosion Risk Management*, 8:1–16.

Schertzer, D. and Lovejoy, S. (1987). Physical modelling and analysis of rain and clouds by anisotropic scaling multiplicative processes. *Journal of Geophysical Research*, 92:9693–9714.

Schertzer, D., Tchiguirinskaia, I., Lovejoy, S., Hubert, P., Bendjoudi, H., and Larcheêque, M. (2002). Which chaos in the rainfall-runoff process? *Journal des Sciences Hydrologiques*, 47:139–148.

Shah, S., O'Connel, P., and Hosking, J. (1996a). Modelling the effects of spatial variability in rainfall on catchment response. 2. experiments with distributed and lumped models. *Journal of Hydrology*, 175:89–111.

Shah, S., O'Connel, P., and Hosking, J. (1996b). Modelling the effects of spatial variability in rainfall on catchment response. 1. formulation and calibration of a stochastic rainfall field. *Journal of Hydrology*, 175:67–88.

Shaw, E. (1994). *Hydrology in Practice*. Chapman and Hall, London, third edition.

Singh, V. (1997). Effect of spatial and temporal variability in rainfall and watershed characteristics on stream flow hydrograph. *Hydrological Processes*, 11:1649–1669.

Sivakumar, B., Sorooshian, S., Gupta, V., and Gao, X. (2001). A chaotic approach to rainfall disaggregation. *Water Resources Research*, 37(1):61–72.

Smith, M., Koren, V., Zhang, Z., Reed, S., Pan, J., and Moreda, F. (2004). Runoff response to spatial variability in precipitation: an analysis of observed data. *Journal of Hydrology*, 298:267–286.

Smith, M., Seo, D.-J., Koren, V., Reed, S., Zhang, Z., Duan, Q., Moreda, F., and Cong, S. (2003). The distributed model intercomparison project (dmip): motivation and experiment design. *Journal of Hydrology*, 298:4–26.

Smyth, G. (2006). Generalized Linear Models. available on 16/01/2006 at `http://www.statsci.org/glm/intro.html`.

Socolofsky, S., Adams, E., and Entekhabi, D. (2001). Disaggregation of daily rainfall for continuous watershed modeling. *Journal of Hydrologic Engineering*, 6:300–309.

Stern, R. and Coe, R. (1984). A model fitting analysis of rainfall data. *Journal of the Royal Statistical Society*, A147:1–34.

Sumbler, M. (1996). *British Regional Geology, London and the Thames Valley*. British Geological Survey, London, fourth edition.

Takens, F. (1981). Detecting strange attractors in turbulence. lecture notes in mathematics. In *Rand, D., Young, L.-S., (Eds.), Dynamical Systems and Turbulence, Springer Lecture Notes in Mathematics*, pages 366–381, Berlin.

Todini, E. (2001). A Bayesian technique for conditioning radar precipitation estimates to rain-gauge measurements. *Hydrology and Earth System Sciences*, 5(2):187–199.

Wheater, H., Chandler, R., Onof, C., Isham, V., Bellone, E., Yang, C., Lekkas, D., Lourmas, G., and Segond, M.-L. (2005a). Spatial-temporal rainfall modelling for flood risk estimation. *Stochastic Environmental Research and Risk Assessment*, 19(6):403–416.

Wheater, H., Isham, V., Chandler, R., Onof, C., Stewart, E., Bellone, E., Yang, C., Lekkas, D., Lourmas, G., Segond, M.-L., Frost, A., Prudhomme, C., and Crooks, S. (2005b). Improved methods for national spatial-temporal rainfall and evaporation modelling for BSM. R&D Technical Report F2105/TR, Imperial College London and University College London.

Wheater, H. and Lotufo Conejo, J. (1979). River Lea flood routing study. Technical report, Imperial College.

Wiggins, S. (1999). *Introduction to Applied Nonlinear Dynamical Systems and Chaos*. Springer, second edition.

Wilks, D. (1998). Multisite generalization of a daily stochastic rainfall generation model. *Journal of Hydrology*, 210:178–191.

Wood, S., Jones, D., and Moore, R. (2000). Static and dynamic calibration of radar data for hydrological use. *Hydrology and Earth System Sciences*, 4(4):545–554.

Woods, R. and Sivapalan, M. (1999). A synthesis of space-time variability in storm response: rainfall, runoff generation and routing. *Water Resources Research*, 35(8):2469–2489.

Yang, C., Chandler, R., Isham, V., and Weather, H. (2005). Spatial-temporal rainfall simulation using Generalized Linear Models,. *Water Resources Research*, 41:W11415, doi:10.1029/2004WR003739.

Young, A. (2005). Stream flow simulation within UK ungauged catchments using a daily rainfall-runoff model. *Journal of Hydrology*, In press.

Appendix A

Catchment descriptors

A brief description of each of the variables shown in Table A.1 is given below.

AREA	Catchment drainage area using an IHDTM-derived boundary (km^2)
BFIHOST	Base Flow Index derived using the HOST classification
DPLBAR	Mean of distance between each node (on regular 50 m grid) and the cathment outlet (km). Characterise the catchment size and configuration
DPSBAR	Mean of all the inter-nodal slopes for the catchment (m $km^{-}1$) Characterise the overall steepness.
FARL	Index of flood attenuation attributable to reservoirs and lakes.
PROPWET	Proportion of time when SMD was $\leq$6 mm during 1961-90.
SAAR	Standard period (1961-90) average annual rainfall (mm).
SPRHOST	Standard percentage runoff derived using the HOST classification.
$URBEXT_{1990}$	Extent of urban and suburban land cover (1990).

Name	AREA km^2	SAAR mm	BFIHOST	SPRHOST	FARL	PROPWET	DPLBAR km	DPSBAR mkm^{-1}	$URBEXT_{1990}$	Mean flow m^3s^{-1}	Number FEH	Number EA
Upper Lee at Luton Hoo	70.67	660	0.869	13.8	0.948	0.3	10.89	40.48	0.2785	0.23	38013	4640
Upper Lee at Water Hall	151.21	663	0.688	27.3	0.946	0.3	22.92	41.3	0.1636	1.3	38018	4690
Mimram at Whitwell	39.1	651								0.09	38017	4730
Mimram at Fulling Mill	98.9	658	0.741	25.9	0.982	0.3	11.56	43.88	0.0287	0.22	38011	4770
Mimram at Pashanger	130.53	656	0.72	27.4	0.986	0.3	16.74	45.03	0.0424	0.54	38003	4790
Beane at Stevenage	634	36								0.1	38012	4827
Beane at Hertford	175.1	631								0.59	38030	4890
Quin at Griggs Bridge	50.4	625								0.15	38029	4939
Rib at Wadesmill	136.55	625	0.469	38	0.999	0.3	18.64	39.03	0.0126	0.51	38004	4980
Ash at Mardock	78.23	619	0.505	35.8	1.000	0.31	12.81	35.04	0.0134	0.3	38002	5080
Stort at Mountfichet	20.5	622								0.06	38016	5106
Stort at Gypsy Lane	25.9	609								0.08	38028	5129
Stort at Sheering	54.6	599								0.32	38026	5169
Stort at Elisabeth Way	136.55	625	0.469	38	0.999	0.3	18.64	39.03	0.0126	0.18	38007	5189
Stort at Glen Faba	280.2	605								1.46	38027	5190
Lee at Rye Bridge	758.3	640								3.61	38031	5280
Lee at Feildes Weir	1040.78	630	0.565	34.0	0.954	0.29	29.64	37.1	0.0579	4.44	38001	5290
Cobbins brook at Sewarsdone rd	38.81	617	0.223	49.5	0.997	0.29	7.09	45.36	0.0376	0.22	38020	5329
Small river Lee at Ordnance rd	41.5	643								0.31	38024	5339
Turkey brook at Albany Park	41.55	666	0.243	47.9	0.950	0.29	9.32	56.33	0.0439	0.21	38021	5349
Salmons brook at Edmonton	33.9	658								0.14	38019	5359
Pymmes brook at Silver street	40.71	672	0.243	48.0	0.982	0.29	8.08	41.15	0.4239	0.49	38022	5369
Lee flood channel at Low Hall	1243	632								2.31	38023	5380
Lee at Lee bridge	1369.88	632	0.510	36.7	0.897	0.29	49.69	36.6	0.101	5.5	38032	5390

Table A.1 Lee Catchment descriptors

Source: Flood Estimation Handbook, volume 5 (Bayliss, 1999)

http://www.nerc-wallingford.ac.uk/ih/nrfa/station_summaries/op/EA-Thames1.html

Appendix B

Spatial Extent of Selected Events

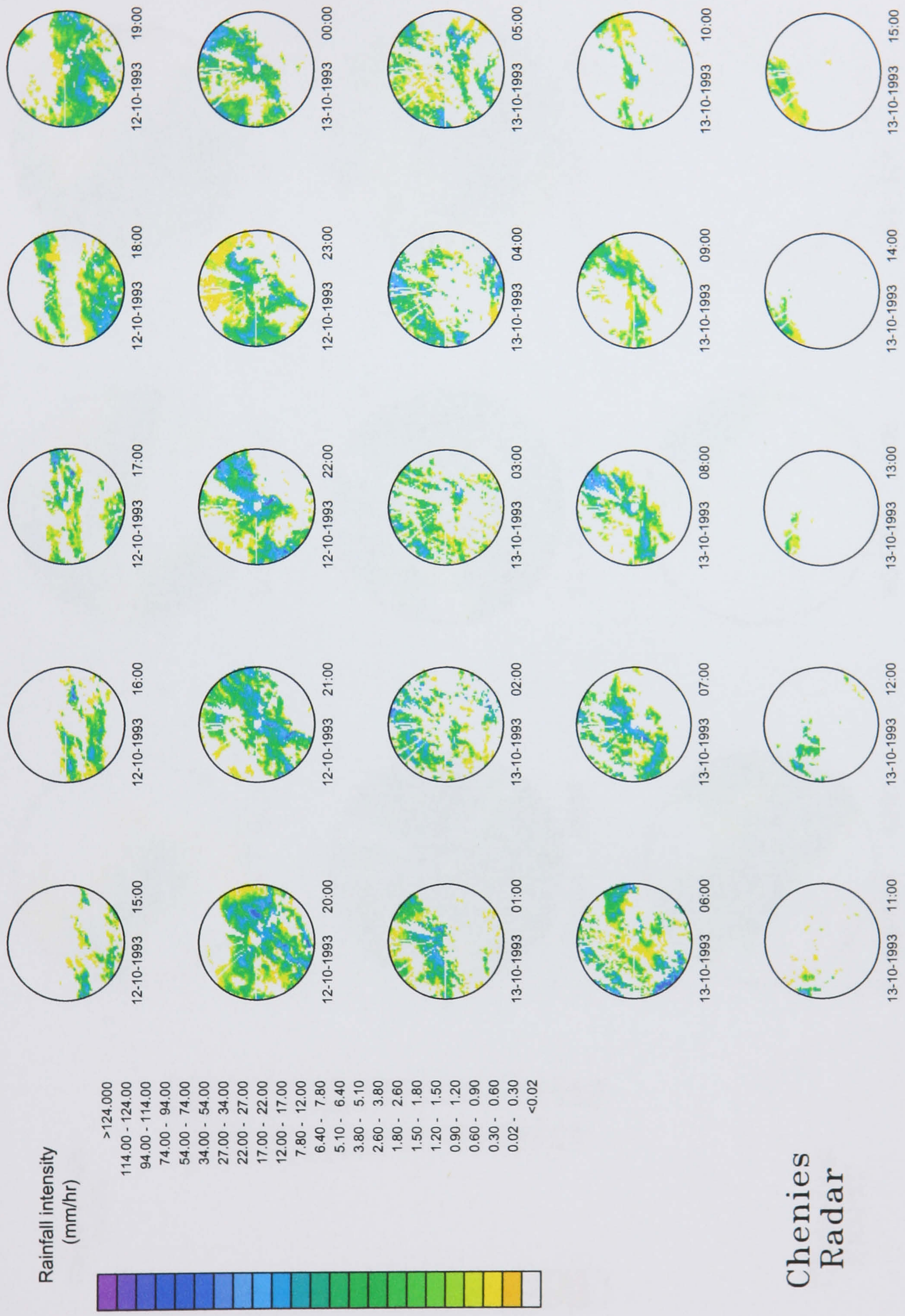

Figure B.1 Radar images for the event of 11th October 1993

Chenies
Radar

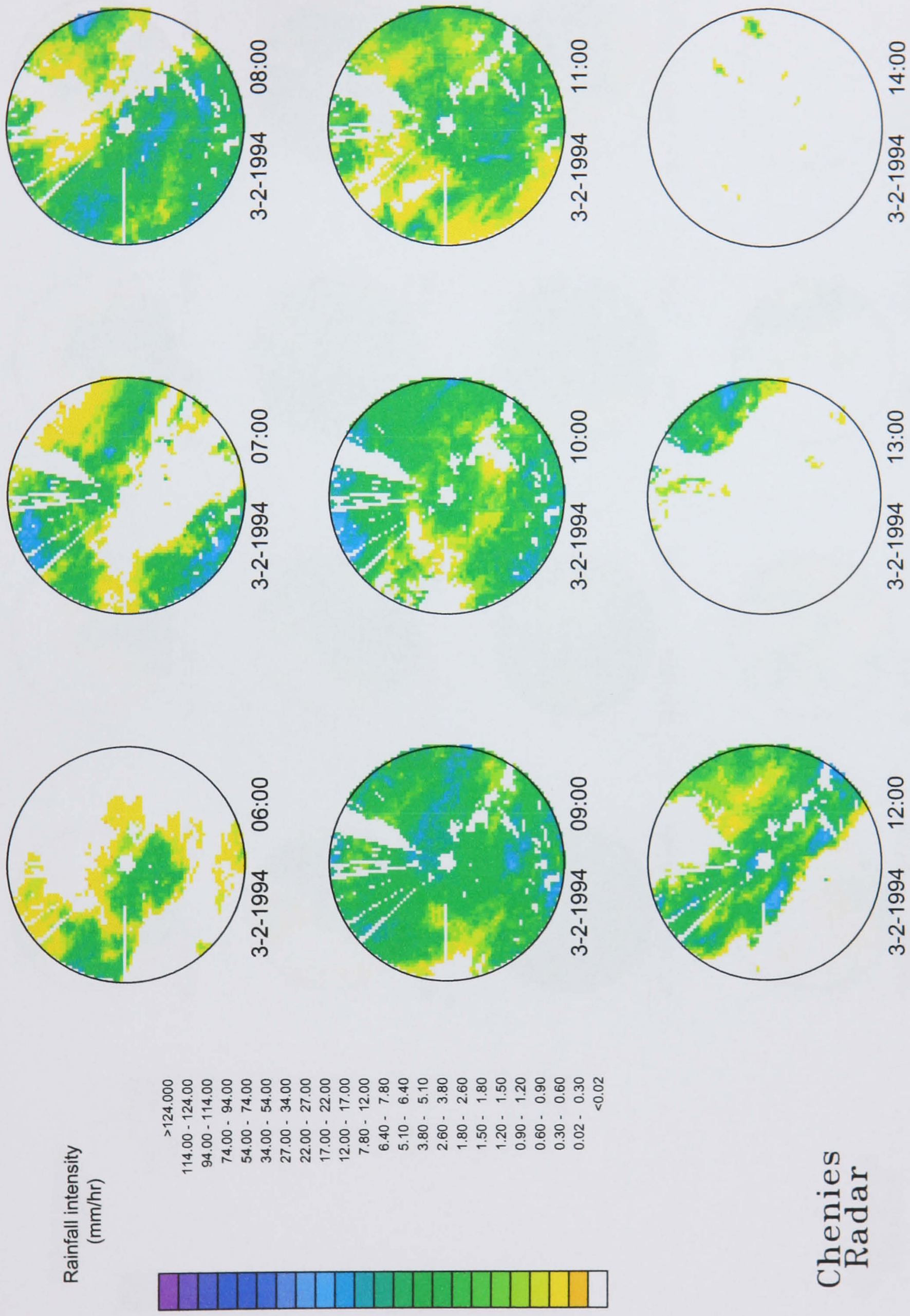

Figure B.2 Radar images foe the event of 3rd February 1994

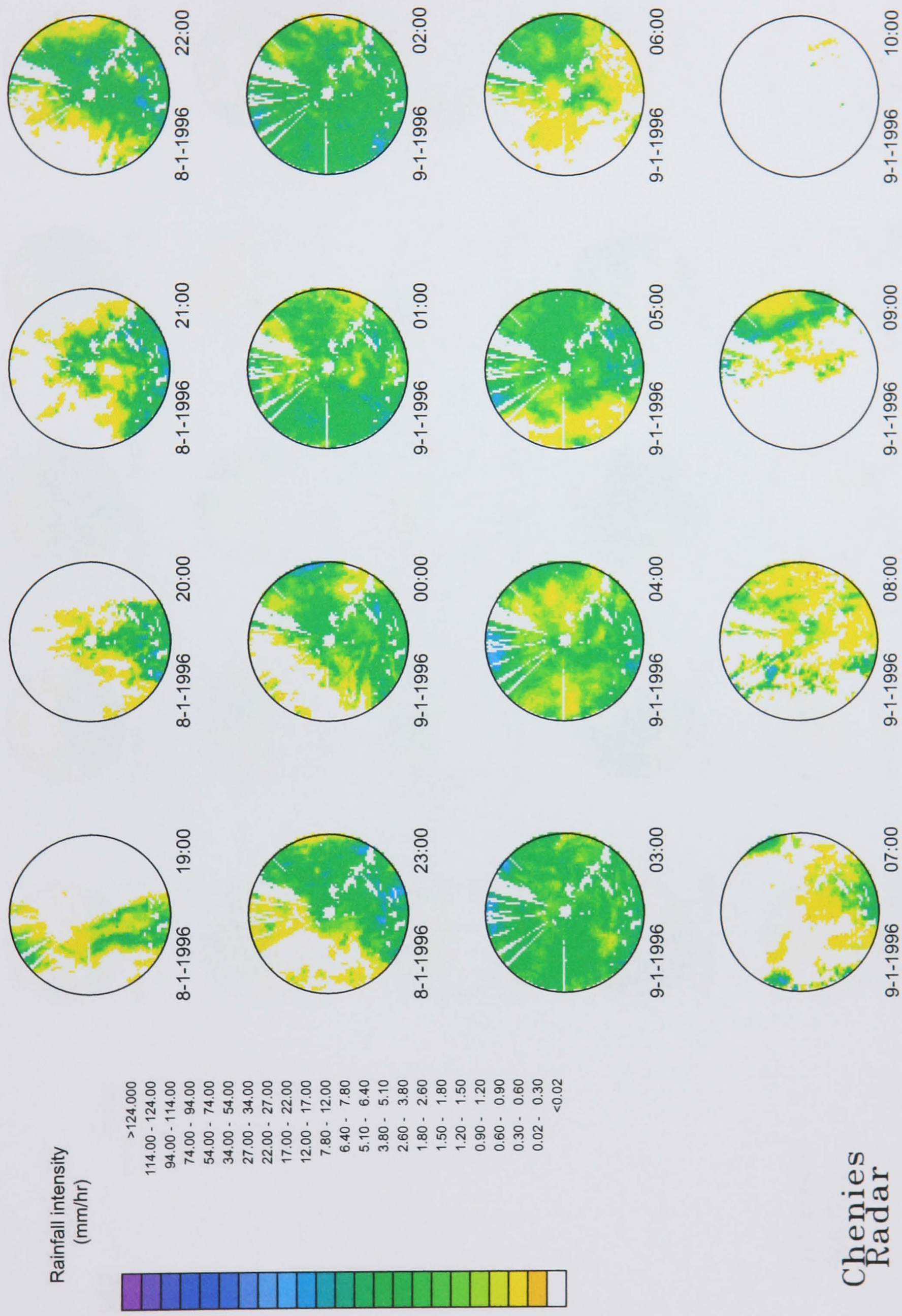

Figure B.3 Radar images for the event of 8th January 1996

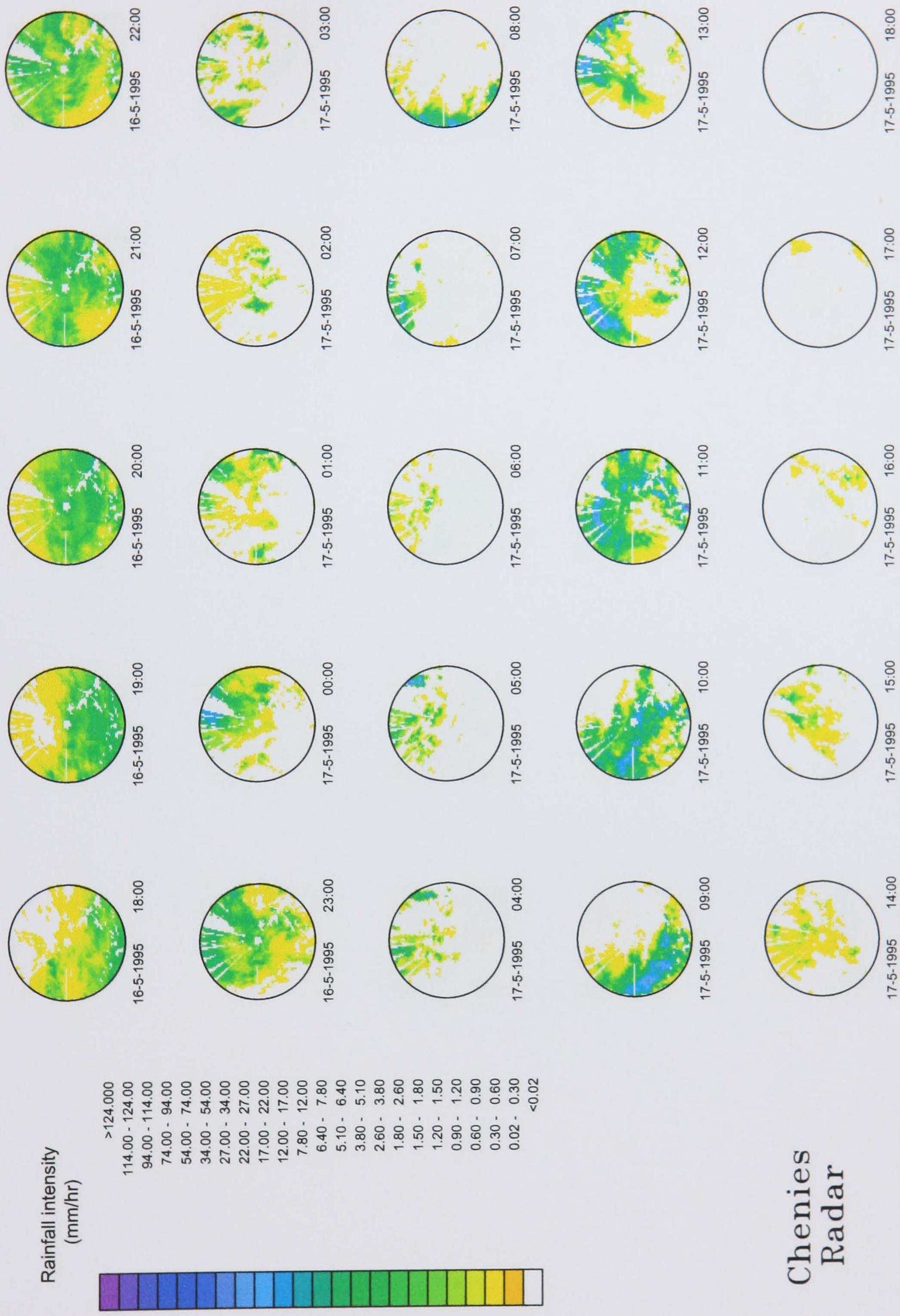

Figure B.4 Radar images for the event of 16th May 1995

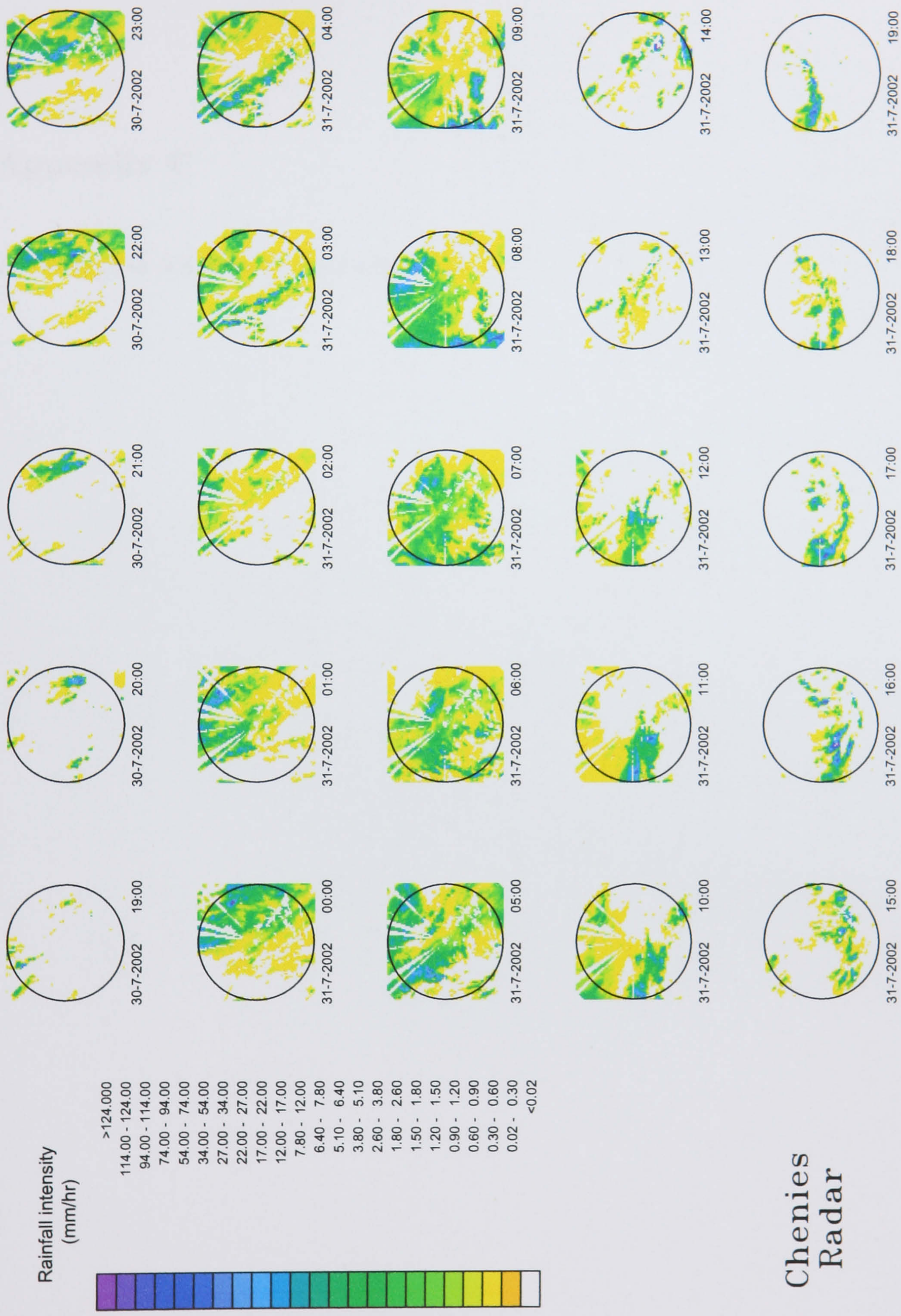

Figure B.5 Radar images for the event of 30th July 2002

Chenies
Radar

Appendix C

Averaged rainfall time-series

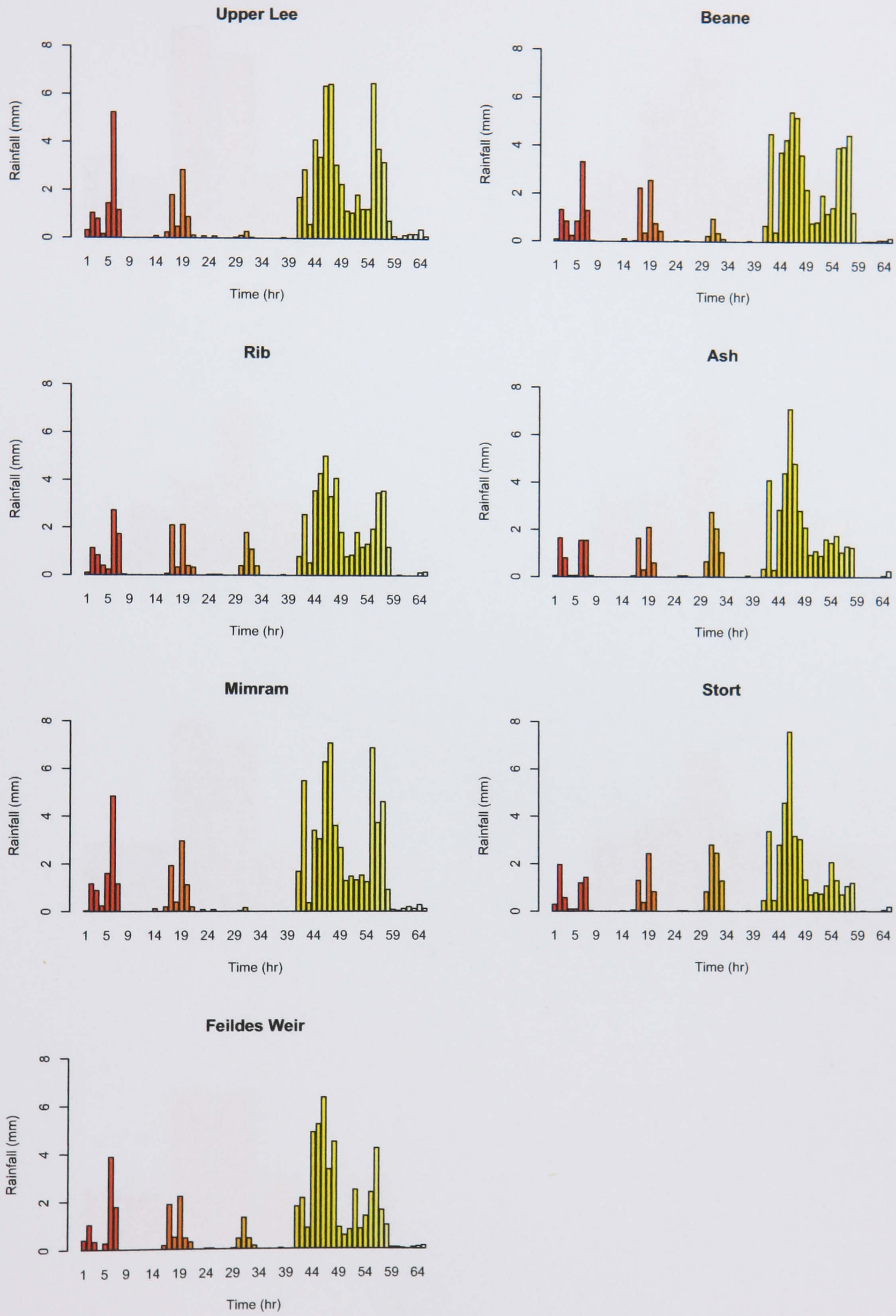

Figure C.1 Hourly averaged rainfall time-series for the even of 11th October 1993

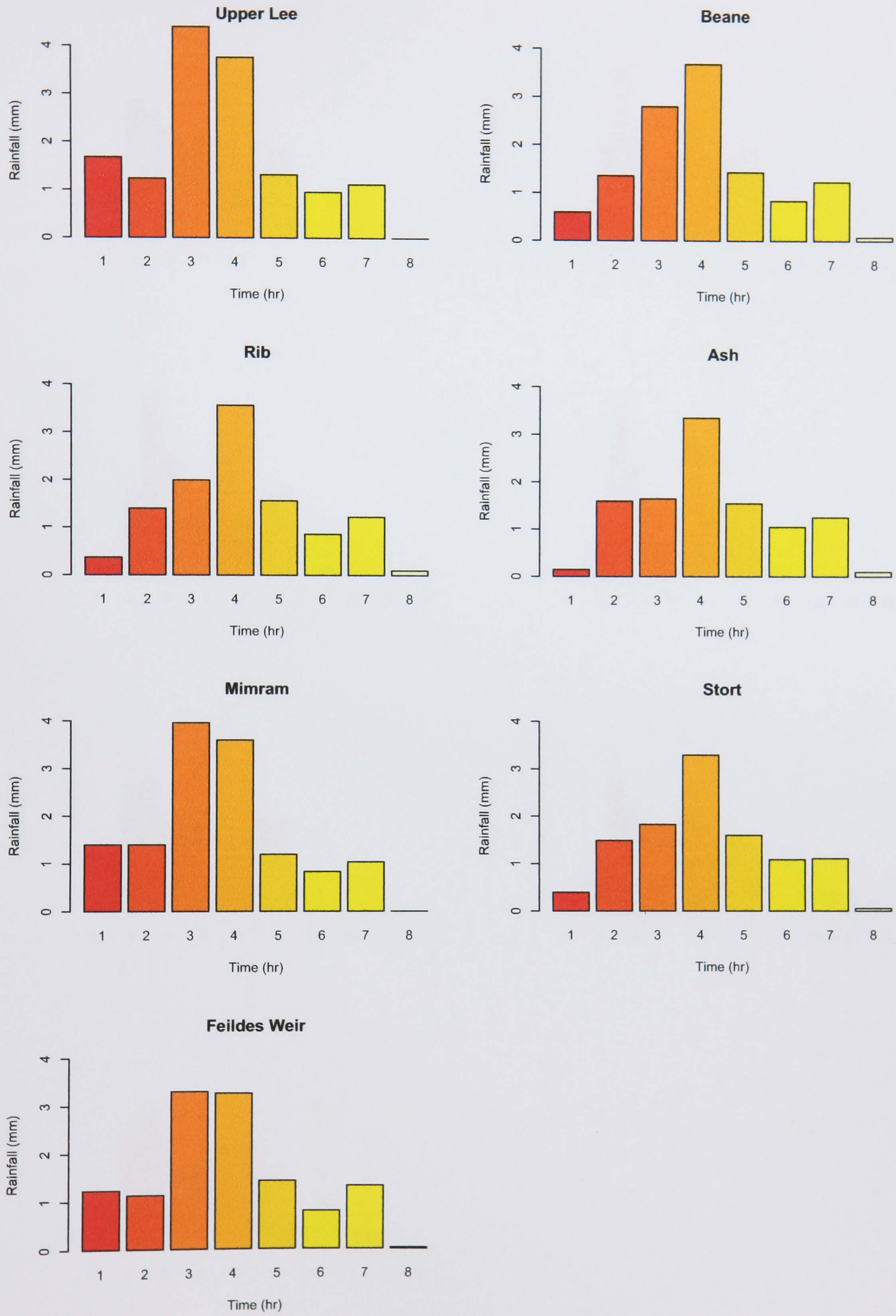

Figure C.2 Hourly veraged rainfall time-series for the event of 3rd February 1994

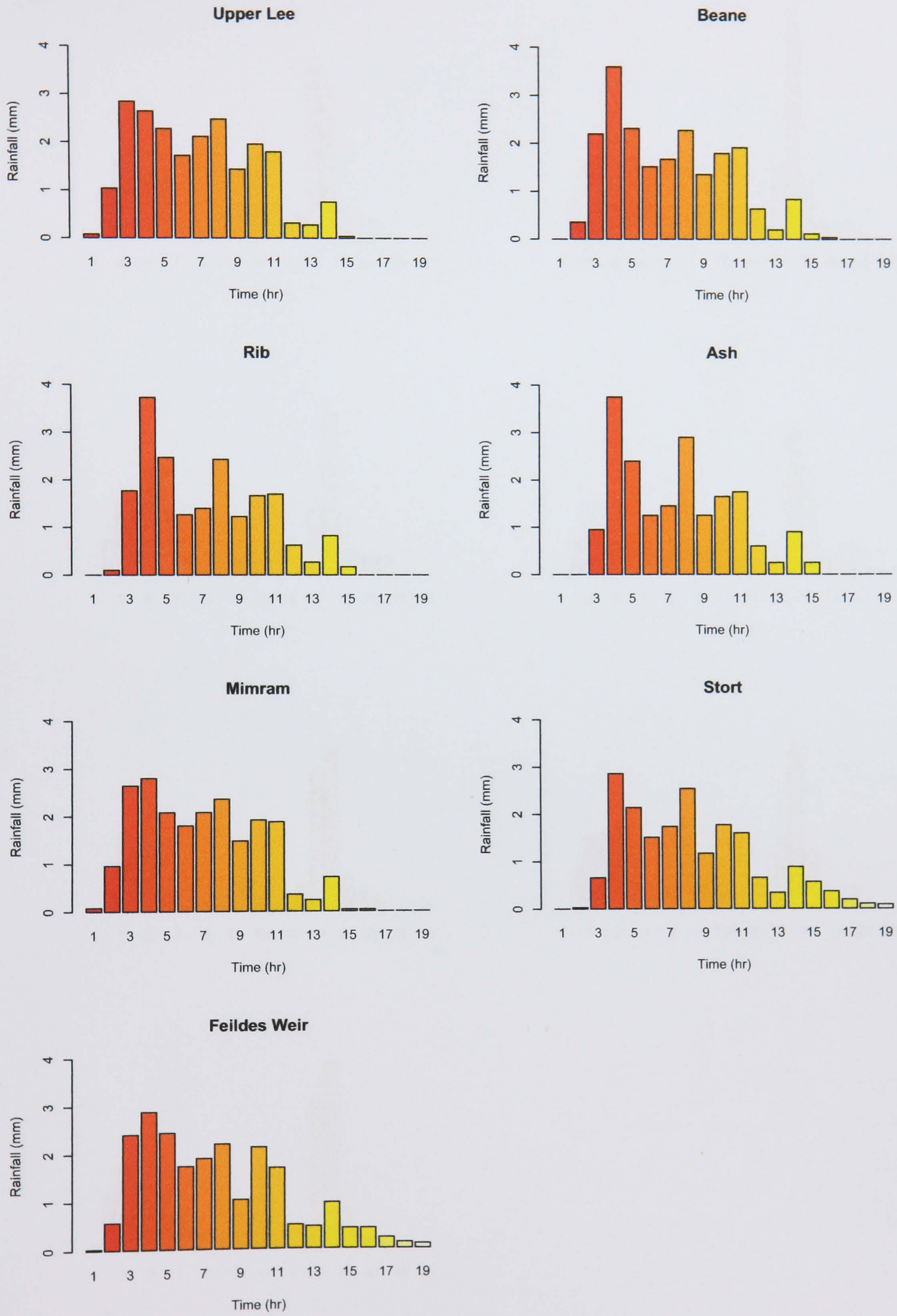

Figure C.3 Hourly averaged rainfall time-series for the event of 8th January 1996

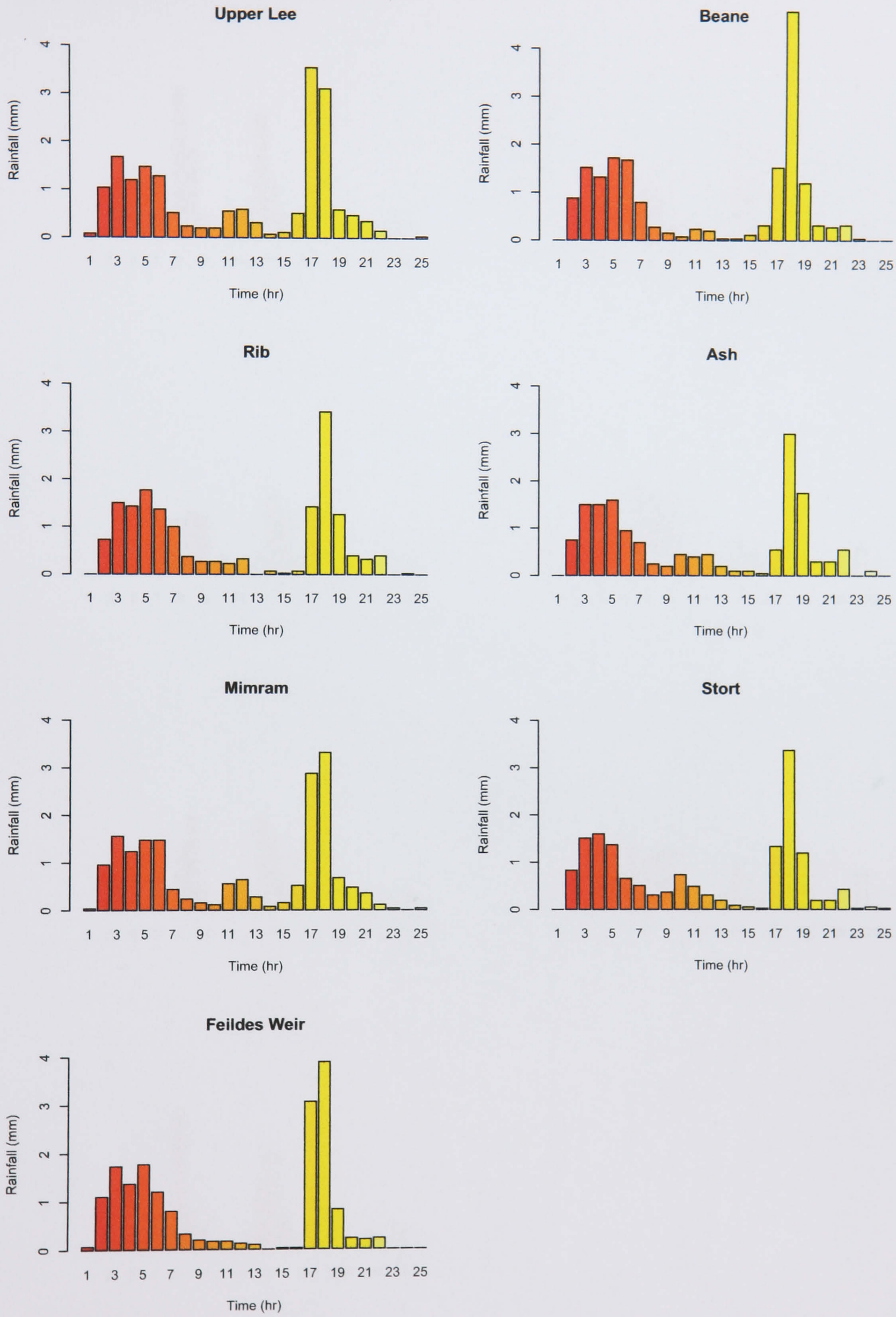

Figure C.4 Hourly averaged rainfall time-series for the event of 16th May 1995

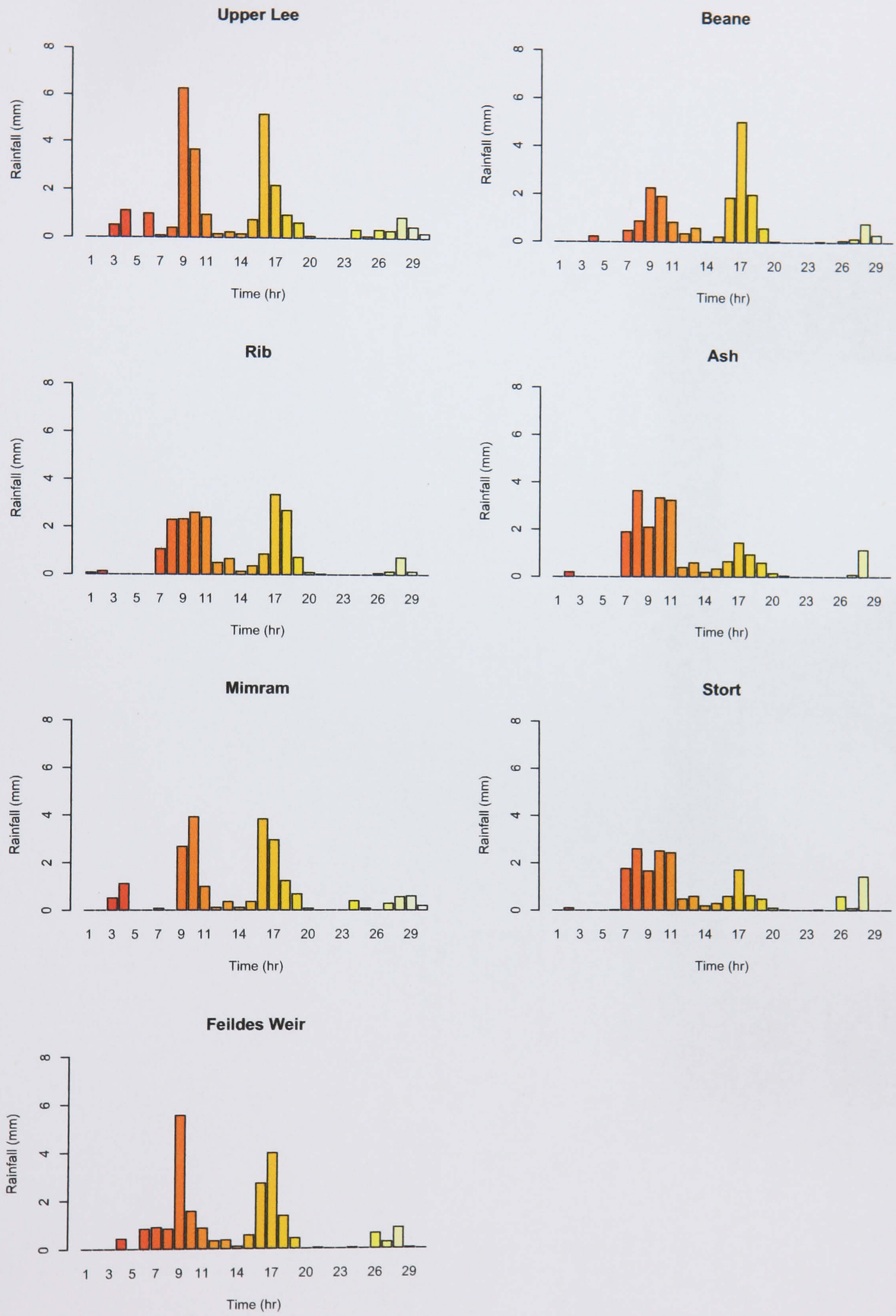

Figure C.5 Hourly averaged rainfall time-series for the event of 30th July 2002

BIBL. LONDIN. UNIV.